Aircraft Trajectory Optimization for a Cruise Segment with Imposed Flight Time Constraint

by

Radu Ioan DANCILA

MANUSCRIPT-BASED THESIS PRESENTED TO ÉCOLE DE TECHNOLOGIE SUPÉRIEURE IN PARTIAL FULFILLEMENT OF THE REQUIREMENTS FOR THE DEGREE OF DOCTOR OF PHILOSOPY
Ph.D.

MONTRÉAL, JANUARY 27TH, 2021

ÉCOLE DE TECHNOLOGIE SUPÉRIEURE
UNIVERSITÉ DU QUÉBEC

BOARD OF EXAMINERS

THIS THESIS HAS BEEN EVALUATED

BY THE FOLLOWING BOARD OF EXAMINERS

Ms. Ruxandra Mihaela Botez, Thesis Supervisor
Systems Engineering Department at École de technologie supérieure

Ms. Lyne Woodward, President of the Board of Examiners
Electrical Engineering Department at École de technologie supérieure

Mr. Marc Paquet, Member of the jury
Systems Engineering Department at École de technologie supérieure

Mr. Adrian Hiliuta, External Evaluator
CMC Electronics

THIS THESIS WAS PRENSENTED AND DEFENDED

IN THE PRESENCE OF A BOARD OF EXAMINERS AND PUBLIC

ON JANUARY 18, 2021

AT ÉCOLE DE TECHNOLOGIE SUPÉRIEURE

ACKNOWLEDGMENTS

First and foremost, I would like to express my gratitude and to thank my advisor, Professor Ruxandra Botez, for the opportunity to be part of her team and to conduct my M.Sc. and PhD research in her laboratory, the Research Laboratory in Active Controls, Avionics and Aeroservoelasticity (LARCASE), for her constant guidance, motivation, and support throughout this entire period. I would also like to thank her for her constant and tireless efforts to support her students, to provide top-notch equipment, to establish collaborations with industrial partners, and make it possible to conduct research in areas that are at the forefront of aeronautical research.

I would also like to thank the Green Aviation Research and Development Network (GARDN) and CMC Electronics for their partnership and collaboration with LARCASE in the field of flight trajectory optimization, which led to this research. In particular, I would like to thank Messrs. Sylvain Cofsky, Rex Hygate, Claude Provencal, Yvan Blondeau, Dominique Labour, and Oussama Abdul-Baki.

I would like to express my gratitude to Ministère de l'Éducation et de l'Enseignement supérieur du Québec for selecting my candidature to participate at the Munich Aerospace Summer Summit on Green Aerospace. Also, I would like to thank the Fonds de développement de l'ÉTS (FDÉTS) for their recognition of my academic achievements, and the financial support, through an internal scholarship.

Many thanks are due to my colleagues at LARCASE, for their friendship and collaboration: Bogdan, Oscar, Georges, Marine, Manuel, Tica, Maxim, Nicoleta, Magdalena, Andreea, Oliviu, Alejandro, and so many others.

Special thanks to my family for their constant and unwavering support, for their motivation and encouragement to pursue the PhD studies.

Optimisation des trajectoires de vol pour un segment ayant une contrainte de temps de vol

Radu Ioan DANCILA

RÉSUMÉ

Les investigations présentées dans cette thèse concernent le domaine d'optimisation des trajectoires de vol, traité de point de vue de la planification du vol. L'objectif de l'optimisation est de trouver le plan de vol optimal qui minimise la fonction coût sélectionnée et respecte les contraintes imposées. L'optimisation prend en compte les performances de vol de l'avion, la configuration de l'avion (charge, quantité de combustible, etc.), les conditions atmosphériques au long de la trajectoire de vol, et les contraintes imposées. La composante latérale du plan de vol est composée par des segments obtenus suite à la sélection des nœuds adjacents d'une grille de routage. La grille de routage est construite à partir de la route orthodromique entre le point de début et la fin du segment à optimiser, d'une déviation maximale relative à la route orthodromique, et d'une distance au sol maximale entre deux nœuds de la grille.

La première direction de recherche a été l'investigation d'un nouveau modèle d'atmosphère, décrivant la variation des paramètres atmosphériques dans des points sélectionnés au long de la composante latérale de la trajectoire de vol ou dans les nœuds d'une grille de routage, à une altitude sélectionnée, en fonction du temps. Ce modèle est créé à partir des prédictions fournies par les organisations météorologiques dans les nœuds d'une grille 4D (coordonnées géographiques, altitude, et temps). La valeur d'un paramètre de l'atmosphère dans un point de définition des paramètres atmosphériques (point géographique et altitude), à un instant de temps voulu, est calculée par une interpolation linéaire. Les tests ont révélé que les valeurs des paramètres atmosphériques calculés avec la méthode proposée ont le même niveau de précision (des différences d'ordre 10^{-14}) et, en moyenne, sont obtenues six fois plus rapidement que celles obtenues à partir du modèle classique et des interpolations quadridimensionnelles. Ainsi, le processus d'optimisation est plus rapide, ou donne la possibilité d'évaluer plus des plans de vol dans un temps donné, ce qui peut conduire à l'obtention des meilleurs résultats d'optimisation. Le modèle d'atmosphère proposé peut être élargi en créant des instances du modèle pour un ensemble d'altitudes d'intérêt.

La deuxième investigation évalue la performance d'une nouvelle méthode d'optimisation, basée sur des algorithmes génétiques, où l'optimisation est appliquée autant sur la composante latérale du plan de vol que sur la composante verticale. La grille de routage pour la composante latérale du plan de vol a été construite en utilisant la méthodologie décrite dans la première ci-haut direction de recherche. Les composants verticaux de la famille des plans de vol ont été construits à partir d'un modèle choisi de structure et de topologie. La performance du profil optimal, obtenue suite à l'optimisation, a été comparée avec celle d'un

plan de vol de référence, obtenus suite à une optimisation du profil de vitesses au long d'une trajectoire (plan de vol latéral et profil d'altitude) d'un vol réel, trouvé sur le site «FlightAware». Une investigation additionnelle a évalué les effets sur la performance de l'optimisation et le temps de calcul, découlant de la correction des paramètres des plans de vol (le profil d'altitudes et vitesses) par rapport aux limites de l'enveloppe de vol de l'avion. Des tests ont été effectués pour six valeurs d'indice du coût, et dix essais pour chaque valeur d'indice du coût. Les résultats des tests effectués ont montré que la correction des plans de vol par rapport à l'enveloppe de vol de l'avion a résulté dans une réduction de la performance de l'optimisation et une augmentation de plus de deux fois du temps d'exécution. Par rapport au plan de vol de référence, la méthode d'optimisation proposée a produit une diminution des coûts totaux entre 1.598% et 3.97% lorsque les plans de vol n'étaient pas corrigés.

Dans la troisième investigation, une nouvelle méthode / une nouvelle approche a été étudié pour l'optimisation des plans de vol, dérivé de la méthode Non-dominated Sorting Genetic Algorithm II utilisée dans les optimisations multi-objectifs. La méthode proposée traite le cas où le temps de passage au point final du segment à optimiser est un instant préféré par le planificateur ou le résultat d'une négociation avec le système de gestion du trafic aérien. La méthode proposée identifie, en parallèle, un ensemble des plans de vol optimaux, qui correspondent à un ensemble des contraintes d'heure d'arrivée requise (fenêtres de temps) contigües imposées au point final du segment à optimiser. L'avantage de cette méthode est que le décideur peut sélectionner le plan de vol qui correspondant au mieux à ses critères et, si le plan de vol est rejeté par le système de gestion du trafic aérien, alors il peut sélectionner le suivant meilleur plan de vol sans nécessiter d'effectuer une nouvelle optimisation. L'étude a investigue sept variantes de la méthode proposée et 10 tests ont été effectués pour chaque variante. Les tests ont évalué le cas où l'ensemble des contraintes d'heure d'arrivée a été constitué par 31 valeurs (fenêtres de temps contigües). Les résultats des tests ont montré une très bonne convergence des solutions. Pour cinq variantes de la méthode proposée, la différence maximale entre la consommation de combustible pour une solution et le minimum «global» pour la même valeur de la contrainte de temps d'arrivée (pout toutes les variantes de la méthode et tous les tests) a été inférieure à 90 kg de combustible (0.14%). Pour la variante la moins performante, les plans de vol optimaux ont donné une consommation de combustible avec moins que 321 kg (0.56%) au-dessus du minimum «global».

Mots-clés : trajectoire de vol, plan de vol, optimisation des trajectoires de vol, contraintes d'optimisation, heure d'arrivée requise (RTA), système de gestion du vol (FMS), système de gestion du trafic aérien (ATM), performance de vol de l'avion, modèle de performance de l'avion, Base of Aircraft Data (BADA), données atmosphériques, modèle des données atmosphériques, modèle des données d'atmosphère GRIdded Binary (GRIB), algorithmes d'optimisation, optimisation multi-objectifs, algorithmes génétiques, Non-dominated Sorting Genetic Algorithm-II (NSGA-II).

Aircraft trajectory optimization for a cruise segment with imposed flight time constraint

Radu Ioan DANCILA

ABSTRACT

The work presented in this thesis is applied in the field of aircraft flight trajectory optimization, approached as a flight-planning problem. The objective of the optimization is to determine an optimal flight plan, which minimizes a selected cost function and satisfies all the imposed constraints. The optimization takes into account the particular aircraft performance data and flight configuration (load, fuel quantity, etc.), initial and final points (latitudes, longitudes, and altitudes) of the flight segment to be optimized, atmospheric conditions along the flight trajectory, as well as optimization and navigation constraints. It was assumed in this work that the lateral component of a flight plan was composed by a set of sub-segments, constructed by selecting adjacent nodes from a routing grid. The routing grid was constructed based on the orthodromic route between the initial and final points of the segment to be optimized, a selected maximum lateral deviation from the orthodromic route, and a maximum sea level distance between the grid nodes.

The first research subject concerned a new atmospheric data model that defines the variation of the atmospheric parameters as functions of time in selected points along the lateral flight trajectory or in the nodes of a routing grid, at a selected altitude. The model was constructed based on the forecast data provided by the Meteorological Agencies, in GRIB2 data format, and defined in the nodes of a 4D grid (geographic location, altitude, and time). As a result, an atmospheric parameter value in an atmospheric data definition point (geographic location and altitude), at the time instance of interest, was obtained by a one-dimensional linear interpolation. Test results showed that, compared with the classic four-dimensional linear interpolation from the GRIB forecast data, the proposed model yielded identical atmospheric parameters values (differences of the order of 10^{-14}) and, on average, it was six times faster. Therefore, by using the proposed atmospheric data model it would be possible to perform an optimization faster or to evaluate more candidate flight plans during the allotted execution time, which would yield better optimization results. The proposed model can be extended by generating the model data for each altitude from a set of altitudes of interest.

The second investigation evaluates the performance of a new optimization method, based on genetic algorithms, where both the lateral and the vertical components of the flight plan are subjected to optimization. In this study, the routing grid for the lateral component of the candidate flight plans was constructed according to the methodology presented in the first investigation. The family of vertical flight plans was constructed according to a selected structure and topology. The results were compared with a reference flight plan, obtained as the optimal profile (speed optimization) for a flight along the flight track and altitude profile of a real flight, retrieved from the FlightAware website. Subsequently, another investigation analyzed the effects of performing flight plan corrections (altitude – speed profile) relative to the aircraft flight envelope (correction of the candidate flight plan parameters, so that the

aircraft flight parameters would remain within the flight envelope limits), on the optimization results and execution time. A total of 60 tests were performed, composed of 10 test runs for each of the six cost index values considered in the evaluation. The results showed that, by performing the flight plan corrections relative to the aircraft flight envelope, the computation times increase by a factor larger than two and the results are less optimal. Relative to the reference flight plan, the proposed optimization method, in which the candidate flight plans were not corrected, yielded a total cost reduction between 1.598% and 3.97%.

The third investigation evaluates a new flight plan optimization method / approach, derived from the Non-dominated Sorting Genetic Algorithm II multi-objective optimization method. The proposed method applies to the case where a crossing time is desired / expected to be imposed at the final point of the segment under optimization (Required Time of Arrival). The time constraint value could be a preferred crossing time instance selected by the flight planner or, it could result from a negotiation with the Air Traffic Management System. The proposed method identifies, in parallel, a set of optimal flight plans corresponding to a set of selected contiguous flight time constraints ("windows") imposed at the final point of the flight segment to be optimized. The advantage of the proposed method is that decision makers can select the flight plan that best suits their criteria and, if rejected by the Air Traffic Management system, they can select the next best flight plan from the set of solutions without having to perform a new optimization. Seven method variants were evaluated, and 10 test runs were performed for each variant. The tests considered the case where 31 contiguous time constraint windows were imposed at the final point of the segment under optimization. Test results showed a very good convergence of the solutions. For five method variants the maximum fuel burn differences relative to the "global" minimum for a time constraint value (for all the method variants and all the test runs) were less than 90 kg of fuel (0.14%). The worst optimization method found optimal flight plans that yielded fuel burns with a maximum of 321 kg (0.56%) more than the "global" optimum.

Keywords: flight trajectory, flight plan, flight trajectory optimization, constrained optimization, Required Time of Arrival (RTA), Flight Management System (FMS), Air Traffic Management (ATM), aircraft flight performance, aircraft performance model, Base of Aircraft Data (BADA), atmospheric data, atmospheric data model, Gridded Binary atmospheric data model (GRIB), optimization algorithm, genetic algorithm, multi-objective optimization, Non-dominated Sorting Genetic Algorithm (NSGA-II).

TABLE OF CONTENTS

LIST OF TABLES

Page

LIST OF FIGURES

Page

LIST OF ABREVIATIONS

1D	One-dimensional
2D	Two-dimensional
3D	Three-dimensional
4D	Four-dimensional
AAL107	Flight 107 of American Airlines
ACARS	Aircraft Communications Addressing and Reporting System
ADM	Atmospheric Data Model
ADS-B	Automatic Dependent Surveillance - Broadcast
APM	Aircraft Performance Model
ASL	Above Sea Level
ATM	Air Traffic Management System
BADA	Base of Aircraft Data
CAS	Calibrated Air Speed
CDO	Continuous Descent Operations
CFP	Corrected Flight Plan
CI	Cost Index
C_{LFPL}	Child Lateral Flight Plan
DM	Decision Maker
ECON	Economic speed
EDT	Eastern Daylight Time
EOC	End of Cruise
EST	Eastern Standard Time

ETA	Estimated Time of Arrival
ETE	Estimated Time En-route
FAA	Federal Aviation Administration
FCU	Flight Control Unit
FMS	Flight Management System
FPL	Flight Plan
FRA	Free Route Airspace
GA	Genetic Algorithms
GARDN	Green Aviation Research and Development Network
GDPS	Global Deterministic Prediction System
GHG	Green House Gas
GRIB	Atmospheric data model extracted from the GRIB2 files
GRIB2	GRIdded Binary 2 data file format
GS	Ground Speed
IAS	Indicated Air Speed
IATA	International Air Transport Association
ICAO	International Civil Aviation Organization
IDLE	Idle TLA setting
ISA	International Standard Atmosphere
JFK	John F. Kennedy Airport, New York
kn	knots [n.m. / h]
LARCASE	Research Laboratory in Active Controls, Avionics and Aeroservoelasticity
LAX	Los Angeles International Airport

LFPL	Lateral Flight Plan component
LHR	London Heathrow Airport
MCMB	Maximum Climb TLA setting
MCRZ	Maximum Cruise TLA setting
MMO	Maximum Operational Mach speed
MOGA	Multi-Objective Genetic Algorithm
MOO	Multi-Objective Optimization
n.m.	Nautical Miles
NAT-OTIS	North Atlantic Organized Track System
NCFP	Non Corrected Flight Plan
NextGen	Next Generation Air Transport System
NG-FMS	New Generation Flight Management System
NSGA-II	Non-dominated Sorting Genetic Algorithm II
NWP	Numerical Weather Prediction
ORT	Orthodromic Route
PDB	Performance DataBase
P-ORT	Perpendicular to the Orthodromic Route
$P_{\_extended}$	Extended population
RDPS	Regional Deterministic Prediction System
RGRID	Routing Grid
RTA	Required Time of Arrival
RUC	Rapid Update Cycle
SESAR	Single European Sky ATM Research

SLA	Sea Level Altitude
SLL	Sea Level Length
SWR40	Flight 40 of Swiss Air
T	Air temperature
TAS	True Air Speed
TAP	Traffic Aware Planner
TBO	Trajectory Based Operations
TC	Total cost
TEM	Total Energy Model
TLA	Thrust Lever Angle
TOC	Top of Climb
TOD	Top of Descent
TS	Tentative Solutions set
TSC601	Flight 601 of Air Transat
UAS	Unmanned Aerial Systems
UTC	Universal Coordinate Time
uint8	8 bits unsigned integer
uint16	16 bits unsigned integer
VFPL	Vertical Flight Plan Component
VMO	Maximum Operational IAS speed
WGS84	World Geodetic System 1984
WPT	Waypoint
W_U	Wind component along the Geographic North axis

W_V	Wind component along the Geographic East axis
ZHR	Zurich Airport

LIST OF SYMBOLS

alt_{CRZi}	Cruise altitude for cruise segment i (ft)
alt_{CRZ_INIT}	Initial cruise altitude (ft)
alt_{CRZ_FINAL}	Cruise altitude for the last cruise section (ft)
alt_{FINAL}	Aircraft altitude at the final WPT of the flight trajectory (ft)
alt_{INIT}	Initial aircraft altitude (ft)
a_0	Speed of sound at sea level in ISA conditions (kn or m/s)
c_{f_dist}	Segment length correction factor function of the aircraft altitude (-)
$C_{(ijkm)}$	Generic coefficients for computing the ADM model
CAS_{CLIMB}	Climb phase CAS speed (kn)
$CAS_{DESCENT}$	Descent phase CAS speed (kn)
CAS_{INIT}	Aircraft CAS speed in WPT_{init} (kn)
CAS_{FINAL}	Aircraft CAS speed in WPT_{final} (kn)
CI	Cost index value (kg of fuel / min)
d_{MAX}	Maximum distance deviation from ORT (n.m.)
d_{STEP}	Distance between two consecutive WPTs along the ORT of the RGRID (n.m.)
D	Coefficients of a generic ADM atmospheric parameter
D_0	Generic reference parameter value for an ADM element
D_m	Generic parameter variation slope for an ADM element
D_{0_T}	Reference value for the air temperature of an ADM element (ºK)
D_{0_WU}	Reference value for the North wind component of an ADM element (kn)
D_{0_WV}	Reference value for the East wind component of an ADM element (kn)

D_{m_T}	Air temperature variation slope for an ADM element (ºK / s)
D_{m_WU}	North wind component variation slope for an ADM element (kn / s)
D_{m_WV}	East wind component variation slope for an ADM element (kn / s)
D_V	Generic coefficients for the ADM model point
D_{V_0}	Generic reference parameter value for an ADM element
D_{V_m}	Generic parameter variation slope for an ADM element
flight_time	Flight time (h)
fpm	feet per minute (ft/min)
fuel_burn	Fuel burn (kg of fuel)
ft	feet
ft_{domain}	Time span for the atmospheric data (h)
ft_{RTAn}	total flight time corresponding to constraint RTA_n
FT_TO_NM	Feet to n.m. conversion factor (n.m. / ft)
GS	Ground speed (kn)
hPa	100 Pa
idx_t	ADM data time domain index
idx_WPT_{ij}	Routing grid index for the WPT_{ij}
IAS	Indicated air speed (kn)
h_{geom}	Aircraft altitude above sea level (ft)
kn	Knots
ºK	Kelvin
lat	Latitude (deg)
lon	Longitude (deg)

m_i	Number of updated Tentative Solution elements at iteration i
M	Mach number (-)
$MACH_{CLIMB}$	Climb phase Mach speed (-)
$MACH_{CRZ\_FINAL}$	Mach speed for the final cruise section (-)
$MACH_{CRZ\_INIT}$	Initial cruise Mach speed (-)
$MACH_{CRZi}$	Mach speed on cruise segment i
$MACH_{DESCENT}$	Descent phase Mach speed (-)
MMO	Maximum operational Mach speed (-)
M_i	Number of non-empty Tentative Solutions elements at iteration i
N_{LAT}	Number of GRIB data latitude domains
N_{LON}	Number of GRIB data longitude domains
N_M	Position along the routing grid's orthodromic route where the mutation is performed
N_{ORT}	Number of WPTs along the orthodromic route
N_{PS}	Number of GRIB data pressure altitude domains
N_R	Number of elements remaining to be copied from the extended population to the new population
N_{STEP}	Number of lateral steps relative to the ORT
N_T	Number of GRIB data time domains
N_V	Number of atmospheric parameters
N_W	Maximum number of steps along P-ORT
N_{WPT}	Number of WPTs in the routing grid
p	Probability for performing a mutation after the crossover
ps	Static air pressure / isobaric level (Pa)

ps_0	Static air pressure at sea level in ISA conditions (Pa)
Pa	Pascal (kg m^{-1} s^{-2})
P_i	Parent lateral flight plan i
P_{ix}	Section x of parent lateral flight plan i
P_0	Initial population
P_{i+1}	Population of generation i + 1
q_c	Dynamic pressure (Pa)
R	Universal gas constant for dry air (J/kg/ºK)
RTA_0	Reference RTA constraint (s)
RTA_n	n^{th} RTA constraint (s)
R_{earth}	Earth radius (n.m.)
S_j	Step j in the crossover transition segment construction of a child lateral flight plan
t	time (h)
t_{ref}	Reference time value for the GRIB domain (h)
$t_{WPTfinal}$	Aircraft crossing time at WPT_{final} (h)
$t_{WPTinit}$	Aircraft crossing time at WPT_{init} (h)
T	Air temperature (ºK)
TAS	True air speed (kn)
T_0	Air temperature at sea level in ISA conditions (ºK)
TC	Total cost (kg of fuel)
TS_i	Tentative Solutions set at iteration i
V	GRIB data atmospheric parameter value. Could be wind speed (kn) or air temperature (K)

VMO	Maximum operational IAS speed (kn)
WPT_{final}	Last WPT of the flight trajectory
WPT_{init}	First WPT of the flight trajectory
WPT_{ij}	Routing grind WPT situated in the node [i, j]
W_U	Wind speed along the geographic North axis (kn)
W_V	Wind speed along the geographic East axis (kn)
α_{CD}	Aircraft climb / descent angle (deg)
α_{CRB}	Aircraft crabbing angle relative to the flight trajectory segment heading (deg)
α_{Segm}	Flight segment heading at the aircraft location, relative to the geographic North (deg)
γ	Adiabatic index for air (-)
θ	Air temperature ratio relative to sea level altitude in ISA conditions (-)
ΔRTA	RTA constraint window size (s)

INTRODUCTION

The aviation industry strives to improve their operations, individually and globally, as a result of two converging necessities: on one hand is the need to reduce costs, to increase economic performance, and on the other hand to reduce polluting emissions, in order to protect the environment and observe the environmental regulations.

One way to reduce the costs is to minimize them for each flight, by selecting/flying along a flight profile that would be best fit for the aircraft load and flight performance, route, atmospheric conditions, etc. The optimal flight profile must observe all aircraft performance limitations, navigation regulations and policies, all imposed constraints, and minimizes a selected cost function.

The optimal flight profile is defined as a flight plan. As a flight planning problem, the optimization objective is to identify the lateral and vertical flight profile components (the projection of the trajectory on the Earth's surface and the altitude speed profile) that offer the "best" atmospheric conditions along the flight path and the "best" altitude–speed profile for the specific aircraft performance and load.

An optimal flight plan is obtained as a result of search conducted over a set of candidate flight plans. Generally, this search requires a large number of flight plan performance evaluations (simulations of the flight along the selected candidate flight plans). In order to improve the performance of the optimization, it is necessary to increase the precision of the input data (aircraft performance model and atmospheric data model) and of the flight performance calculations / flight trajectory simulations. In addition, it is necessary to improve the methods used for generating and selecting the candidate flight plans (optimization methods and algorithms), and reduce the computational complexity so that a maximum number of flight profiles can be evaluated in a time interval and/or reduce the optimization execution time. As some requirements for the optimization methods/algorithms are contradictory (e.g. increased precision versus reduced computational complexity), the

adopted optimization methods are specific for the particular optimization problem, and represent a tradeoff between the contradictory requirements.

The research presented in this thesis addresses the following main subjects:

1. The development and evaluation of a new atmospheric data model appropriate for constant altitude cruise flight trajectory performance calculations and optimization algorithms. This model defines the atmospheric parameters variation as functions of time, in selected points along the trajectory or in the nodes of a routing grid, at the selected altitude. The first hypothesis is that the proposed atmospheric data model would generate the atmospheric parameter values in a node of the routing grid faster and with the same precision, relative to the case where they are calculated based on the data format provided by the meteorological agencies and 4D linear interpolations. The second hypothesis is that for a constant altitude flight trajectory calculation (the longest section of a flight) the proposed model would yield important computation time reductions. This would be particularly true when the lateral flight plan is constructed based on a routing grid having a distance between the grid nodes smaller or equal to the integration step used in the flight trajectory performance calculation;
2. The development and evaluation of an optimization method based on genetic algorithms, in which both the lateral and the vertical components of a candidate flight plan are subject to optimization. A structure for the lateral and vertical components of the candidate flight plans, as well as methods to construct the candidate flight plan components and to perform the genetic operations are proposed. The routing grid used in the construction of the candidate flight plans and in the flight performance calculations is similar to that proposed in the first research. The genetic operations (crossover and mutation) applied during the optimization are specific for each component of the candidate lateral flight plan, due to the differences between the structures and the assumptions / construction rules / limitations considered for each component. The first hypothesis is that the proposed optimization method converges to a solution that is better (has a lower total cost) than that of a flight plan obtained by optimizing the speed profile along an imposed lateral and altitude flight plan

components. The second hypothesis is that if the invalid flight plans (which result in aircraft flight parameters outside the flight envelope) would be corrected (the flight plan parameters are modified so that the aircraft flight parameters are within the flight envelope limits) it would improve the optimization results (lower total cost). However, the consequence would be a longer execution time due to the additional computations required by the flight plan correction process;

3. The development and evaluation of an optimization method capable to identify a set of optimal flight plans, corresponding to a flight segment with a set of contiguous Required Time of Arrival (RTA) constraints at the final point. The structures and construction of the flight plan components and the atmospheric data model are similar to those used in the previous investigation. The proposed optimization method is derived from the NSGA-II (Deb, Pratap, Agarwal & Meyarivan, 2002) method used in multi-objective optimizations. The first hypothesis is that the method can find solutions for all the RTA constraint set values. The second hypothesis is that by performing flight plan corrections (relative to the aircraft's flight envelope) for the initial generation of candidate flight plans, more initial tentative flight plan solution (which satisfy an RTA constraint from the set) would be identified in the first iterations of the optimization. The third hypothesis is that by performing a local search (in each iteration adding mutated versions of the tentative solution flight plans) the quality of the solutions would be improved. The fourth hypothesis was that, for a sufficiently large number of iterations, the optimization method (the search conducted in the objective space) converges to "globally optimum" solutions.

The structure of this thesis and the research methodologies used in each of the investigations are presented in CHAPTER 2 (APPROACH AND ORGANIZATION OF THE THESIS).

CHAPTER 1

LITERATURE REVIEW

1.1 Aircraft flight trajectory

An aircraft flight trajectory represents the 3D path (geographical locations and altitude) followed by an aircraft between the departure and arrival airports. The flight trajectory is the result of the aircraft executing a flight plan (FAA, n.d.a). An aircraft's flight evolution, and thus its flight trajectory, is limited by its flight envelope (specific for the aircraft model), flight rules and regulations (FAA, n.d.d; FAA, n.d.c), and specific navigation rules and regulations.

At an airspace level, the air traffic is managed by the Air Traffic Management System (ATM), which monitors all aircraft flights within its area of control in order to detect and avoid flight trajectory conflicts, and to increase throughput. Before the flight, each aircraft's flight plan must be submitted for validation by the ATM, which analyzes it for conflicts with all active (already validated) flight plans, and compliance with navigation rules and regulations. New initiatives, like the Next Generation Air Transport System (NextGen) in US (FAA, 2020) and Single European Sky ATM Research (SESAR) in Europe (European Commission, 2020) aim to increase the airspace flexibility by allowing aircraft to fly along more efficient routes, that would be better adapted to their specific operational needs and to aircraft's capabilities. For example, by 2022, it is expected that a large part of the European airspace would implement the Free Route Airspace (FRA) concept (Eurocontrol, 2020) where an aircraft no longer has to follow predetermined air corridors. Trajectory Based Operations (TBO) (Cate, 2013; Torres & Delpome, 2012) is a 4D air traffic management concept where the aircraft fly along 4D routes that are better adapted for their needs.

A flight plan (Altus, 2009; FAA, n.d.a) defines the intended aircraft flight trajectory in a compact form, which can be evaluated by the ATM to validate it relative to conflicts with

already approved flight plans, and by aircrew to program it into aircraft's Flight Management Systems (FMS).

1.2 Flight trajectory performance calculation

An aircraft's flight trajectory and flight performance parameters, used by the ATM for flight plan validation, and by flight planners for flight trajectory planning / optimization, are determined following an "accelerated" simulation of the planned flight. The results of the simulation are the lateral flight path (succession of geographic points) overflown by the aircraft, the altitude and speed profile along the lateral flight profile, the crossing time and aircraft weight / fuel burned to / fuel available at points along the lateral profile, etc. These calculations are performed based on the aircraft's weight and flight performance data, atmospheric conditions, flight plan, flight and navigation rules and regulations, etc.

The accelerated flight simulation is performed by first decomposing the flight plan in phases, and then by decomposing each phase into segments on which the mathematical model describing the aircraft's evolution and performance parameters does not change. Each segment is further decomposed in sub-segments (integration steps). The accelerated simulation is done by successively evaluating the flight performance parameters and aircraft evolution on each sub-segment; the aircraft position, flight parameters, and configuration at the end of a sub-segment are the input data for the flight simulation / calculations along the following sub-segment. For flight planning / optimization applications and in FMS platforms, the accelerated flight simulation is performed according to a specific methodology (Schreur, 1995), described in sub-sections 4.2.5 and 5.3.4.

The aircraft performance model used in the accelerated flight simulation calculations differs as a function of the platform on which the simulations are performed (ATM, FMS, research environment) and on the intended application. In FMS platforms, where the computational power and memory resources are limited, the aircraft performance model is defined by interpolation tables (Performance DataBase – PDB) (Murrieta-Mendoza & Botez, 2015a;

Sibin, Guixian & Junwei, 2010; Murrieta-Mendoza, Demange, George & Botez, 2015b), which are less accurate but less computationally complex than aero-propulsive models.

In research and ATM context, where the computations are performed on more powerful systems or where the computation time is not of strict concern, the aircraft performance calculations are performed using more complex and more precise aircraft models, such as Base of Aircraft Data (BADA) (Eurocontrol, n.d; Eurocontrol, 2010; Nuic, Poles & Mouillet, 2010a; Nuic, 2010b). Other aircraft performance models are specific for particular phases of the flight / flight segment types, or for aircraft performance elements. Dancila, Botez & Labour (2013) have proposed an aircraft performance model for the cruise phase, which allows to compute the fuel burn for a selected flight time, at a specific speed, on a constant altitude cruise segment, or the time necessary to burn a selected fuel quantity. Ghazi, Botez & Achigui (2015a) developed a method to create an engine performance model from flight tests executed on a level D flight simulator. Ghazi & Botez (2015b) developed a high-fidelity aircraft performance model, intended for use in research environment, which uses non-linear models for aerodynamic coefficients and actuators.

1.3 Atmospheric data in flight trajectory performance calculations

The atmospheric data used in flight trajectory performance calculations are based on atmospheric data forecast models issued regularly by meteorological agencies, in a GRIdded Binary format (GRIB2) (Environment Canada, n.d.g; NOAA, n.d.a). The GRIB2 data define the atmospheric parameter values in the nodes of a 4D grid (latitude, longitude, pressure altitude, and time). Each environmental agency may issue the atmospheric forecast data in various forecast models. These forecast models differ in terms of geographic region covered by the forecast, grid type (latitude-longitude or polar stereographic) and resolution, interval for which the predictions are made, and update rate. The wind prediction data may be provided in terms of speeds and angles, wind components along the North and East geographic axes, or both. Global scale forecast models, such as Global Deterministic Prediction System (GDPS) (Environment Canada, n.d.a; Buehner et al., 2015) provide the

forecast data that cover the entire globe surface. The regional forecasts cover a smaller specific area. Examples of regional prediction systems are the Regional Deterministic Prediction System (RDPS) (Caron et al., 2015; Environment Canada, n.d.e) and the Rapid Update Cycle (RUC) (Schwartz, Benjamin, Green & Jardin, 2000; Cole, Green, Jardin, Schwartz & Benjamin, 2000). The RUC forecasts cover a smaller geographic area, are more accurate, and are updated more frequently.

Various studies analyzed the accuracy of the atmospheric data predictions. Schwartz et al. (2000) performed an analysis of the RUC forecasts by comparing the forecasted data with the real atmospheric conditions encountered by aircraft, retrieved from Aircraft Communications Addressing and Reporting System (ACARS). They have found that the forecast errors vary function of the difference between issuing time and the instance for which the atmospheric parameter is evaluated (increases when the difference increases), increases when the forecasted wind is larger or the altitude is higher, and varies function the time of the day and period of the year. In a similar study conducted by Cole et al. (2000), the wind error probability distribution and the percentage of instances when the error surpassed 10 m/s were analyzed. The authors found that the wind errors are larger during the Winter season, when the winds are stronger; they also noted that there are spatio-temporal regions where errors are large, but not shown in the statistical analysis data due to the small region where they occur.

Stohl, Wotawa, Seibert & Kromp-Kolb (1995) analyzed the precision of various interpolation methods (linear weighted distance, nearest neighbor, bilinear, cubic) to compute the atmospheric data in a point; they concluded that the higher order methods (bicubic interpolation) gave the best accuracy, however they have the disadvantage to be the most computationally intensive and to require the highest execution time. The authors noted that, in strong wind fields, the time interpolation results were more affected by the interpolation method and, thus, required a higher order interpolation method to reduce the errors. Fukuda, Shirakawa & Senoguchi (2010) compared the ground speed recorded by aircraft with its value computed using atmospheric data computed by spline interpolation from the forecast data. The authors concluded that the ground speed estimation error due to the atmospheric

parameter estimation error was smaller than the ground speed estimation error resulted from aircraft speed error (scheduled versus real speed). In flight trajectory simulations and flight planning applications, the atmospheric parameters are computed by use of multi-dimensional linear interpolations from the forecast data (Rubio & Kragelund, 2003; De Smedt & Berz, 2007; Zhang & McGovern, 2008; Bronsvoort, McDonald, Potts & Gutt, 2011; Wickramasinghe, Harada & Miyazawa, 2012; Wynnyk, 2012), as a tradeoff between accuracy and computational complexity.

The atmospheric data can be considered as having both deterministic and stochastic components. Depending on the platform (ATM, FMS, research) and context (flight plan validation, flight trajectory optimization, etc.) the atmospheric data is considered having only a deterministic component or both components (deterministic and stochastic). In current FMS and ATM / flight planning / optimization applications, the atmospheric data is considered as having only a deterministic component.

The atmospheric data model used in FMS platforms defines the atmospheric parameters as deterministic and stationary, at selected locations along the flight trajectory (Waypoints – WPT), at a limited set of altitudes. The atmospheric parameters in other locations than the WPTs and/or the altitudes where they were defined are computed by linear interpolations (De Smedt & Berz, 2007; Stell, 2010a; Stell, 2010b; Bronsvoort et al., 2011).

Bronsvoort et al. (2011) present a wind model, generated on ground-based platforms, tailored for the descent phase of the flight. The wind model, adapted for specific FMS platform atmospheric data calculations, is generated based on high resolution forecast data, aircraft flight plan and landing procedure, so that the interpolation errors are minimized during the descent phase.

Vaddi, Tandale & Cheng (2011) present a wind model that considers both the deterministic and stochastic components. The stochastic component is constructed using an autoregressive

model based on forecast data and aircraft flight data from the same airspace, and a time lag smaller than 15 min.

1.4 Flight trajectory optimization

A flight trajectory optimization can be performed at airspace level, in order to ensure the safe operations and increase the aircraft throughput, or at aircraft level, to minimize / maximize an objective function. An aircraft trajectory optimization can be performed on ground-based platforms, in the planning phase, or, to a limited extent, on the FMS platforms.

The high-level flight trajectory optimization is performed by ATM systems. The ATM performs accelerated simulations of the flight along the submitted flight plans in order to detect flight trajectory conflicts and to ensure minimum lateral, vertical, and time separations between aircraft.

The objective of an aircraft trajectory optimization problem, defined as a flight-planning problem, is to identify an optimal flight plan. The flight trajectory resulted from the "flight plan execution" must observe aircraft's flight envelope limitations and flight and navigation regulations and rules (FAA, n.d.b; FAA, n.d.c; FAA, n.d.d).The optimization can be conducted only along the lateral flight plan component (the projection of the flight trajectory on the Earth's surface), along the vertical flight plan component (the "altitude – speed" profile), or along both the lateral and vertical flight plan components.

A review of the on-board flight trajectory optimization algorithms, strategies, and patents, performed on FMS platforms, conducted by Di Vito, Corraro, Ciniglio & Verde (2009), presents an analysis of proposed optimization methods, their features, advantages, and disadvantages.

Zillies et al. (2014) studied the efficiency increase to be obtained if the flight trajectories are optimized for the atmospheric conditions. The study performed the optimization of constant

altitude and speed cruise segments, by use of a Dijkstra algorithm. In each iteration, a new point is added at the half point along the orthodromic route between the aircraft location at the current iteration and the final point, until a minimum distance between the current and final point is reached. The new point is selected among five equally spaced nodes across the orthodromic route. The optimized routes resulted in fuel and flight time reductions relative to the orthodromic route.

Dancila & Botez (2016a) proposed a method to select the maximal optimal geographic area for flight trajectory routing, with a limit on maximum ground distance. The selected area is an ellipsoid with parameters computed based on the departure and the arrival points, placed in its focal points. A method for reducing the vertical flight profile calculations is proposed by Dancila & Botez (2018). The authors constructed and computed, in advance, based on the specific optimization problem data (departure and destination points, aircraft load, set of considered speeds, set of estimated landing weights, etc.), a set of vertical flight segments for each flight phase, that cover the entire aircraft flight envelope.

Zhou, Duan, Li & Di (2013) developed a flight planning method based on differential evolution, where in each iteration a chaotic search is performed in the vicinity of the best solution identified so far (up to that iteration) in order to escape local minima and improve the results by increasing the probability to find the global minima.

Patrón, Berrou & Botez (2015b) proposed an optimization method based on genetic algorithms, where the lateral flight profiles are constructed by selecting nodes from a routing grid formed by a planned track and four parallel tracks; each track was divided in n sub-segments. The optimization is performed in three steps. First, the optimal climb vertical profile, along the planned track, was identified by evaluating all possible speed values. Then, a genetic algorithm identified the optimum cruise track for the planned vertical profile. Finally, the descent phase was optimized by an exhaustive evaluation of the descent for all scheduled speed combinations.

Murrieta-Mendoza, Beuze, Ternisien & Botez (2017b) presented a vertical flight profile optimization using a Beam Search Algorithm, where the optimization problem was defined as a discrete optimization problem modeled as a “decision tree”. The tree nodes are visited successively and, in each node, non-optimal branches are determined using an optimistic cost heuristic and are pruned in order to reduce the number of profile calculations.

Gardi, Sabatini & Ramasamy (2016) presented a review of flight trajectory optimization approached as a control problem with multiple and conflicting objectives. These conflicting objectives could be operational (costs, fuel burn, airspace congestion) and environmental (noise, contrails, polluting emissions). An example of flight trajectory optimization approached as control problem could be the optimization (to minimize the fuel burn) of a cruise flight trajectory at constant altitude, in the presence of winds, where the control variables are the aircraft heading and speed.

Ramasamy, Sabatini, Gardi & Kistan (2014) presented a concept of operations for the next generation FMS, that was developed for 4D Intent Base Operatations / Trajectory Based Operations. The optimization algorithm uses a point of mass aircraft model with 3 degrees of freedom and variable mass. The optimization is performed as a “control problem”, where the control variables are the engine power, load factor, and bank angle. The authors perform an evaluation of the errors impacting the trajectory calculations and their magnitudes.

Hagelauer & Mora-Camino (1998) presented an optimization method based on dynamic programming, that identifies an optimal cruise flight profile for a flight with multiple time constraints, in various points along the flight trajectory.

1.5 Multi-objective optimization

Multi-objective optimization algorithms identify solutions that represent a tradeoff between competing and contradictory objectives. A survey of the multi-objective optimization methods used in Engineering is presented by Marler & Arora (2004). Miettinen (2001)

presents various concepts, approaches, and methods for conducting multi-objective optimizations.

Fonseca & Fleming (1993) present an analysis of multi-objective optimization methods based on genetic algorithms. Methods for conducting multi-objective optimizations for problems with multiple constraints, by use of evolutionary algorithms, are proposed by Fonseca & Fleming (1998a) and Fonseca & Fleming (1998b). Examples of multi-objective optimization methods based on genetic algorithms are Multi-Objective Genetic Algorithm (MOGA) (Murata & Ishibuchi, 1995) and local search methods (Ishibuchi & Murata, 1996; Ishibuchi & Murata, 1998).

An elitist multi-objective optimization method, called Non-dominated Sorting Genetic Algorithm II (NSGA-II), was proposed by Deb et al. (2002). This method performs the optimization using genetic algorithms and non-dominated population sorting. Jensen (2003) proposes a new non-dominated population sorting that is more efficient. This method reduces the number of comparisons between the population members and, thus, reduces the computation time.

CHAPTER 2

APPROACH AND ORGANIZATION OF THE THESIS

The research presented in this thesis, pertaining to the field of flight planning / flight trajectory optimization, was conducted in the following sequence of steps / phases:

1. A literature review in which were analyzed existing methods for performing atmospheric data and flight trajectory performance calculations, and flight trajectory optimization. This research identified areas in which improvements / new approaches could be considered;
2. Statement of the objectives to be addressed in the research;
3. Investigation of a new atmospheric data model for constant altitude cruise segments;
4. Investigation of a new flight plan / flight trajectory optimization method based on genetic algorithms, in which the lateral flight plan components are defined by nodes of a routing grid, and where the vertical flight plan components have a selected structure (set of altitude-speed segments types, construction rules, and constraints). The genetic operations (crossover and mutation) performed during the optimization are specific for each flight plan component; and
5. Investigation of a new flight plan / flight trajectory optimization method that identifies a set of optimal flight plans for a flight segment. Each flight plan is determined as the optimal solution for a particular RTA constraint value from a set of selected contiguous RTA constraints imposed at the final point of the segment.

Following the first research phase, two main directions of investigation were considered. The first direction concerned the improvement of the atmospheric data model used in flight trajectory performance calculations for the cruise phase, in order to reduce the computational complexity and the execution time. The second direction was related to the flight trajectory optimization, considered as a flight-planning problem.

In the third phase, a new atmospheric data model was proposed. The new atmospheric data model defines the atmospheric parameters variation as a function of time in points

(geographic locations) along the cruise segment and at the selected cruise altitude. This investigation evaluated the performance of the model when it is used in the context of flight trajectory optimization, in which the lateral component of the candidate flight trajectory is constructed based on a routing grid. The model for the atmospheric parameter variation as functions of time, as well as the construction and the parameters of the routing grid, were developed following a research regarding the methodologies used for the atmospheric parameters calculations in flight trajectory performance calculations, and the methodologies used for constructing candidate flight trajectories in flight trajectory optimization algorithms. The atmospheric data and computation time using the new proposed method were compared with their values obtained by four-dimensional interpolation from the forecast data. Another analysis evaluated the memory requirements of the proposed model, and the computational time reduction for a flight profile performance parameters calculation.

The fourth phase consisted in the development and analysis of a new flight trajectory optimization method based on a genetic algorithm, which identified the optimal flight plan that minimizes the total cost for the flight. The novel elements of this investigation were:

1. The construction of the candidate lateral flight plan segments according to the methodology and based on the routing grid devised in the first investigation;
2. The proposed structure of the vertical component of the candidate flight profiles; and
3. The genetic operators (crossover and mutation) specific for each flight plan component.

Ten tests were performed for each of six Cost Index (CI) values; for each test, the total cost of the optimal flight plan identified by the proposed method was compared with the total cost of a reference flight plan, that was created based on a real flight trajectory. The set of tests were performed twice, in order to investigate the effects of correcting invalid flight plans, with respect to the altitude – speed flight envelope, on optimization performance.

In the fifth phase, a new approach and method for optimizing the flight plan of a flight trajectory segment were presented. The optimization method / approach considers the case

where the time of arrival at the final point of the optimized segment is the result of a negotiation between the flight planner and the ATM. The optimization method, derived from the NSGA-II method used in multi-objective optimization, identifies a set of optimal flight plans corresponding to a set of contiguous RTA constraints (domains), selected by the flight planner. The lateral and vertical flight plan components, as well as the atmospheric data model, are similar with those used in the previous two phases. Seven variants of the proposed optimization method were evaluated in order to investigate the influence of different procedures employed during the optimization.

These investigations resulted in a set of three papers written as main author, presented in Chapters 3 to 5. The three papers were submitted for publication in peer-reviewed journals, and the first paper was already published. Dr. Ruxandra Botez, Ph.D. advisor and co-author of the papers, supervised the research.

The first research paper was published in the “Proceedings of the Institution of Mechanical Engineers, Part G: Journal of Aerospace Engineering”, in August 2020: “New Atmospheric Data Model for Constant Altitude Accelerated Flight Performance Prediction Calculations and Flight Trajectory Optimization Algorithms” (Dancila & Botez, 2020a). This paper presents a method for constructing an atmospheric data model, adapted for use in constant altitude cruise segment calculations, that reduces the atmospheric parameters calculation complexity and time. This new atmospheric data model provides the same data accuracy as when calculated by four-dimensional interpolation from GRIB forecast data. The proposed atmospheric data model was conceived based on the GRIB forecast data model and on the associated mathematical equation used for computing an atmospheric parameter in a geographical location, at a selected altitude and time. A new method is proposed for constructing an orthogonal routing grid between the initial and final points of the segment; the main axis of the routing grid is the direct route (orthodrome) between the two points. The grid node locations, along the two axes, are selected so that the distance between two adjacent nodes would be smaller than the integration step used in the flight trajectory performance calculation. Tests were performed using four routing grids (grid node step

distances along the two axes, and maximum node deviations from the main axis) and an atmospheric data time domain of 12 hours. The memory space requirements (for the same geographic area, altitude, and time domain), and the computation time for an atmospheric parameter in a grid node, were compared with those obtained under same conditions (for an identical geographic location, altitude, and time) using the GRIB forecast data model. Another test evaluated the flight trajectory performance computation time reduction obtained when the atmospheric data in the nodes of the routing grid were computed using the proposed method relative to the case where they were computed by four-dimensional interpolation from the GRIB data.

The second research paper, called “New Flight Trajectory Optimization Method using Genetic Algorithms”, was accepted for publication in “The Aeronautical Journal” on November 15, 2020. This paper proposes a new methodology for constructing the flight plan candidates, where their lateral and vertical components are constructed based on the routing grid presented in the first research paper. The paper also proposes a template / structure for the vertical and lateral flight plan candidates, as well as specific crossover / mutation operations adapted for the structure of the lateral and vertical flight plan components. A subsequent investigation evaluates the influence of performing flight plan parameters (altitude and speed) corrections, relative to the aircraft’s flight envelope, on the optimization performance. The performance of the optimization method was evaluated using a set of 12 tests: for six CI values, with and without flight plan corrections. The optimal profiles identified by the proposed method were compared with their corresponding reference profiles. The reference profiles were obtained through a speed optimization of a lateral flight plan and an altitude profile of a real flight, retrieved from FlightAware (www.flightaware.com), under identical conditions (aircraft weight, fuel quantity, CI value, etc.).

The third research paper, “New Fight Plan Optimization Method Utilizing a Set of Alternative Final Point Arrival Time Targets (RTA Constraints)”, was submitted for publication to “The Aeronautical Journal”, in November 2020. First, the paper presents the

context and statement of the optimization problem, and defines its assumptions and limitations. Then, it describes the methodology used to construct the candidate flight plans and to perform the crossover and mutation operations, as well as the atmospheric data used in the calculations, which are similar with those presented in the first two papers. Next, the paper presents an overview of the methodology used to perform the accelerated flight simulation and to compute the performance parameters for a flight along a flight plan candidate. Then, an analysis of the relationship between the dependent variables of interest (fuel burn and flight time) and the independent variables (flight plan parameters, initial aircraft weight and fuel, atmospheric conditions, etc.) is performed, and an optimization method derived from the NSGA-II multi-objective optimization method is presented. Seven variants of the proposed method were considered in order to evaluate different strategies (e.g. local search, initial population flight plan correction, population members fitness assignment methods, etc.) employed during the optimization. Finally, 70 test runs were performed (10 identical test runs for each method) to evaluate and compare the performance of the method variants. The test scenario was constructed based on a real flight track data, that was retrieved from the site FlightAware.

CHAPTER 3

NEW ATMOSPHERIC DATA MODEL FOR CONSTANT ALTITUDE ACCELERATED FLIGHT PERFORMANCE PREDICTION CALCULATIONS AND FLIGHT TRAJECTORY OPTIMIZATION ALGORITHMS

Radu Ioan Dancila[a] and Ruxandra Mihaela Botez[b]

[a,b]École de Technologie Supérieure, Université du Québec
LARCASE Laboratory of Research in Active Controls, Aeroservoelasticity and Avionics
1100 rue Notre Dame Ouest, Montréal, H3C1K3, Québec, Canada

This article was published[1] in Proceedings of the Institution of Mechanical Engineers, Part G: Journal of Aerospace Engineering, August 14, 2020
Paper No. 945555, DOI: 10.1177/0954410020945555

Résumé

Cet article présente une nouvelle méthode pour stoker dans la mémoire et calculer les données atmosphériques utilisées dans des calculs de performance pour des segments de vol en croisière, à une altitude constante. Cette méthode a été conçue pour les applications avec contraintes de temps de calcul, tels que les calculs de prédiction des paramètres de performance dans les systèmes de gestion du vol et/ou optimisation des trajectoires de vol. Le modèle proposé a été construit à partir des prédictions atmosphériques fournies par les services météorologiques, dans un format GRIB2, ainsi qu'un ensemble des points de cheminement qui définissent la composante latérale du (des) profil(s) de vol évalué(s). Le modèle de données atmosphériques peut être construit/mis au jour en arrière-plan ou hors-ligne, lorsque des nouvelles prédictions atmosphériques sont disponibles. Les résultats obtenus en utilisant le modèle proposé ont montré que les valeurs des paramètres atmosphériques sont identiques (des différences d'ordre 10^{-14}) aux celles calculées par une interpolation linéaire quadridimensionnelle et en moyenne les calculs sont six fois plus

[1] The paper presented in this chapter contains minor modifications relative to the version printed in Proceedings of the Institution of Mechanical Engineers, Part G: Journal of Aerospace Engineering, Paper No. 945555, DOI: 10.1177/0954410020945555, on August 14, 2020. These modifications were made at the request of the members of the Board of Examiners.

rapides. Des tests ont montré aussi une réduction importante du temps de calcul des paramètres de performance des trajectoires de vol quand le modèle d'atmosphère proposé est utilisé dans les calculs. Le modèle proposé peut-être étendu pour un ensemble d'altitudes (habituellement un multiple de 1,000 ft).

Abstract

This article presents a new method for storing and computing the atmospheric data used in time-critical flight trajectory performance prediction calculations, such as flight performance prediction calculations in flight management systems and/or flight trajectory optimization, of constant altitude cruise segments. The proposed model is constructed based on the forecast data provided by Meteorological Service Agencies, in a GRIB2 data file format, and the set of waypoints that define the lateral component of the evaluated flight profile(s). The atmospheric data model can be constructed/updated in the background or off-line, when new atmospheric prediction data are available, and subsequently used in the flight performance computations. The results obtained using the proposed model show that, on average, the atmospheric parameter values are computed six times faster than through 4D linear interpolations, while yielding identical results (value differences of the order of 10^{-14}). When used in flight trajectory performance calculations, the obtained results show that the proposed model conducts to significant computation time improvements. The proposed model can be extended to define the atmospheric data for a set of cruise levels (usually multiple of 1,000 ft).

3.1 Introduction

The large number of aircraft in operation today, combined with the forecasted air traffic increase (EEA, 2018) strengthen the necessity to identify new means and methods to increase the levels of air traffic safety and efficiency. A larger number of aircraft will determine an increase in fuel consumption and, as a consequence, in green house gas (GHG) emissions, with a negative impact on the environment. From the point of view of air traffic security and

efficiency, a larger number of aircraft, within the same airspace, will require new and better flight planning and flight performance estimation methods, in order to increase the airspace throughput while maintaining the required level of separation and reducing the potential of flight trajectory conflicts.

One of the means to improve the aircraft operations efficiency is to improve the aircraft performance characteristics: better engines that use less fuel and generate fewer polluting emissions, better airframes with lighter materials and structures, and better aerodynamic characteristics. For example, current research in the field of structures and aerodynamics investigate new methods and techniques that could allow in-flight shape modification for elements of the aircraft's structure (morphing structures) (Koreanschi et al., 2016a; Koreanschi et al., 2016b; Koreanschi et al., 2016c; Grigorie, Botez & Popov, 2016) in order to obtain the optimal profile for each phase of the flight (reduce the drag without affecting the lift) and to improve the stall characteristics. The result is a reduction of the required thrust and, thus, a reduction of fuel burn and GHG emissions.

In the field of aircraft model development, the focus is on methodologies that can identify high fidelity engine (Ghazi et al., 2015a) and aircraft (Ghazi & Botez, 2015b) performance models from flight data. These models are intended for use as research tools, for aircraft performance evaluation, and in-flight trajectory optimization algorithms.

Another important reduction of the fuel consumption and the GHG emissions can be obtained by implementing a new operational paradigm, known as trajectory-based operations (TBO), where each aircraft flies along an optimal flight trajectory, adapted to the specific flight (route, load, aircraft performance, and company operational criteria) and atmospheric conditions (winds and air temperature profile). The flight trajectory optimization can be performed on-ground, by the operational department of aircraft operators, or, to a limited extent, on-board by flight management system (FMS). Herndon, Cramer & Nicholson (2009) analyzed the differences between the implementation of the navigation procedures in several FMS platforms produced by different manufactures, and the effects that these differences

have on the air traffic management, predictability of the air traffic, and the execution of navigation procedures.

The FMS computes the various aircraft flight performance parameters (fuel burn, climb/descent horizontal distance, optimal altitude, optimal speed, etc.) using an aircraft performance model based on performance tables (Murrieta-Mendoza et al., 2015b) and multi-dimensional linear interpolations. New aircraft performance models can add new capabilities and functionalities. For example, the constant altitude and speed cruise flight fuel burn model, presented in Dancila et al. (2013) provides a means to compute, faster and with more precision, the fuel burned in a given flight time and the flight time necessary to burn a given fuel quantity. This functionality is very helpful when evaluating, for example, the earliest moment when the aircraft can initiate a step climb.

Both the FMS platforms and the flight trajectory optimization algorithms perform, iteratively, accelerated simulations of the flight:

1. Along the programmed flight trajectory (and the programmed alternate flight route), from the current aircraft location to destination (in the case of FMS);
2. Along the set of candidate flight profiles (in the case of flight trajectory optimization).

in order to determine, among others, the estimated time of arrival (ETA), estimated time en-route (ETE), fuel burn to (available fuel at) different points along the route, verify that the aircraft flight parameters do not exceed the flight envelope limits, and that navigation constraints, such as required time of arrival (RTA), imposed for points along the flight trajectory are observed. In flight trajectory optimization algorithms, the results of the iterative accelerated flight performance prediction calculations are used to determine the best solution among the candidate flight profiles (the flight profile that minimizes the selected cost function).

Faster flight performance prediction calculations will determine an increase of the number of flight profiles evaluated per allotted time and/or less time required for the evaluation of a given number of flight profiles. In the FMS platform, the flight performance prediction

calculations are time-critical: they are performed repeatedly, according to a schedule, and within an imposed time window. In flight trajectory optimization algorithms, faster flight performance prediction calculations would result in a faster optimization process and/or better optimization solutions.

The accelerated flight performance prediction calculations are performed progressively, step by step, by decomposing the flight profile in small sub-segments (integration steps) and, then, on each sub-segment the performance data are computed considering that the parameters that intervene in the calculations are constant (e.g. air temperature, wind, speed/acceleration, aircraft weight, fuel burn rate, etc.). This decomposition into sub-segment is done using a heuristic method that offers a trade-off between the computation time and precision. As a result, during each flight performance evaluation, the atmospheric parameters need to be evaluated at multiple points along the flight trajectory.

The moment when the aircraft reaches a geographic location and altitude is function of the trajectory followed by the aircraft (speed and altitude profiles, and flight track) from the departure point to that location. Therefore, for better flight performance estimations, the atmospheric parameters data model should take into account the variation function of time. In the traditional implementation of FMS platforms, the atmospheric parameters are associated to waypoints (WPTs) along the flight profile. In each WPT, the atmospheric parameters are considered stationary (defined as pre-set values that do not vary as a function of time), at a selected set of altitudes (Bronsvoort et al., 2011). The atmospheric parameters in points situated on a segment determined by two WPTs and/or altitudes different that those where they were defined are computed through linear interpolation.

The aircraft's avionics system can determine, based on the data acquired from the aircraft's sensors and navigation systems, the difference between the estimated and the real atmospheric conditions at the current location (dead reckoning). The differences are considered stochastic components of the atmospheric parameters, and can be used to correct the forecasted atmospheric data, to a limited extent, as the chaotic nature of the atmospheric

flows and atmosphere's anisotropy make it irrelevant for locations situated far away and/or reached much later.

National meteorological service agencies create and publish analyses and forecasts, for a set of atmospheric parameters, at specific geographic locations, pressure altitudes, and time instances. These forecasts are numerical models (Numerical Weather Prediction [NWP]), provided in a gridded binary (GRIB2) (Environment Canada, n.d.g; NOAA, n.d.a) file format, and describe the atmosphere at various scales (global (Environment Canada, n.d.a; Buehner et al., 2015) or regional (Environment Canada, n.d.e; Caron et al., 2015)), map projections (polar-stereographic or latitude-longitude), resolutions (map grid sizes), time frames, and with specific forecast refresh rates. For each forecast type (defined by the prediction scale, map projection and grid resolution), the forecast provides the atmospheric parameter values at the nodes of a 4D grid - at a predetermined set of latitude and longitude locations, pressure altitudes (isobaric levels), and forecast time instances. The forecast data files are retrieved using specific software tools (wget (Environment Canada, n.d.f) and wgrib2 (NOAA, n.d.b)), which provide the means to select the types of atmospheric parameters, geographic area, isobaric altitudes, and time domain for which the data are imported, and to perform grid size changes (regrid). A regional scale forecast is issued for a reduced geographic area, on a more refined grid and with a higher refresh rate than the global scale forecasts. An example of regional scale forecast is the regional deterministic prediction system (RDPS) (Environment Canada, n.d.d), issued by Environment Canada Meteorological Service.

Due to the chaotic nature of the atmosphere, forecasts issued by the meteorological agencies are subject to errors and do not necessarily reflect the real conditions encountered at the prediction points (location and time). The magnitude of the errors varies function of the time of the year, time of day (day or night), region, how long ahead in time is the prediction made for, etc. This impacts the accuracy of the atmospheric parameter estimations, relative to what an aircraft will encounter, and, as a result, the flight trajectory and flight performance parameters' (flight time, fuel burn, etc.) estimations.

A study of the air particle trajectory computation models from wind observations and predictions, the error sources and the accuracy for different forecast data sources, models and interpolation methods are presented in Stohl (1998). The authors found that the most accurate wind predictions are the NWP. An analysis of the nearest neighbour, linear weighted distance, bilinear, quadratic, and bicubic interpolation methods applied to wind interpolation, presented in Stohl et al. (1995), concludes that, for the horizontal wind components, the higher order methods are more precise: among the evaluated methods the bicubic interpolation is the most precise, but the most computing intensive. Regarding the time interpolation, the authors conclude that the linear interpolation yields the best results when the wind forecast time resolution is 6 h or less, and that the precision of the time interpolation is affected more when performing the calculations in strong wind fields, thus, it is necessary to employ a higher wind forecast temporal resolution to compensate this effect.

In Schwartz et al. (2000), 13 months of real atmospheric conditions encountered by aircraft, reported through the Aircraft Communications Addressing and Reporting System (ACARS), were compared with atmospheric data predictions generated by 4D linear interpolations, from rapid update cycle (RUC) forecasts. Based on the prediction accuracy for 20 min ahead forecast, the authors noted that the forecast error varies function of the time of the year, time of the day, and increases with forecast time increase, when the forecasted wind is larger and/or altitude is higher.

Different authors evaluated the incertitude associated with the atmosphere data prediction. Vaddi, Tandale & Lin (2013) present a method to create an uncertainty model for the wind forecasts based on the difference between the forecast data and the real wind encountered by aircraft, retrieved from ACARS data. The model has realistic spatio-temporal correlations and can be used in stochastic analysis of flight trajectories, to generate random wind predictions for Monte Carlo simulations. In Lee, Weygandt, Schwartz & Murphy (2009), the uncertainty for each of the North and East wind component predictions are considered to be the standard deviations from the average of the set of forecasted values in a given location and altitude. The authors note that the uncertainty decreases when the forecast lag time

decreases. A study regarding the magnitude and source of wind prediction errors, presented in Cole et al. (2000), analyzed the difference between RUC predictions and actual wind data encountered by aircraft. The study evaluated the percentage of wind speed error larger than 10 m/s, the wind error probability distribution, and the time domains when most of the large wind prediction errors occur. It was noted that the rate of wind prediction error increases during winter, when the winds are stronger. Another observation was that there are small spatio-temporal regions where the errors are important; however, due to the domain's small size, they are not reflected in the statistical analysis of the forecast accuracy.

The atmospheric parameters can be considered as having two components: one deterministic and the other stochastic, accounting for the chaotic nature of the atmosphere/prediction incertitude. A review of the literature showed that the atmospheric data model used in flight trajectory performance calculations varies function of the context in which the flight trajectory performance calculations are performed: FMS, air traffic management system (ATM), flight planning, flight trajectory simulation, or control law/guidance algorithms.

The more complex atmospheric models are used in studies regarding flight planning/trajectory optimization strategies, optimal flight control/guidance, conducted offline, on computer platforms, where there are limited or no calculation time constraints. The flight planning and optimization problems presented in literature (Soler-arnedo, Olivares & Staffetti, 2010; Soler, Olivares, Staffetti & Bonami, 2011; Soler, Olivares & Staffetti, 2015) consider the wind components (North and East) stationary, deterministic, and computed through polynomial regression from RUC predictions. In Vaddi, Sweriduk, Tandale & Cate (2012), closed-loop tests evaluate the robustness of a descent guidance algorithm to atmospheric data uncertainties. The wind is considered to have two components: a deterministic component, obtained from the forecast data and assumes it only has a linear variation with altitude, and a stochastic component constructed using an autoregressive model (Vaddi et al., 2011) based on forecast data and flight data from the same airspace and a lag of no more than 15 min. A trajectory prediction model presented in Fukuda et al. (2010) computes the ground speed using atmospheric parameters calculated by spline interpolation

from prediction data. A comparison with the ground speed computed based on the atmospheric data recorded by the aircraft showed that the ground speed error due to the atmospheric parameter estimation error is smaller than the error due to the difference between the aircraft's scheduled speed and real speed.

In ATM and online flight planning applications, the atmospheric data models consider only the deterministic components. Other flight trajectory simulations/flight planning studies use a simplified atmospheric model, where the atmospheric parameters are considered stationary and are computed using multi-dimensional linear interpolations (3D and 4D) based on the forecast data (Rubio & Kragelund, 2003; Zhang & McGovern, 2008; Wynnyk, 2012; Wickramasinghe et al., 2012; Jensen, Tran & Hansman, 2015).

In FMS platforms, the atmospheric data model is simplified, only a deterministic component is considered. The wind is considered stationary and, depending on the platform, the wind value can be defined as constant for the flight phase or segment, or as a set of constant values at specific altitudes in WPTs along the flight trajectory and computed by linear interpolations (De Smedt & Berz, 2007; Stell, 2010a; Stell, 2010b; Bronsvoort et al., 2011). During the flight, the stochastic components of the atmospheric conditions are calculated as the difference between the values computed based on the forecast data and the values measured by the avionics. A heuristic method (wind blending) applies the wind differences as corrections to the predicted values, to estimate the wind values to be used in the performance calculations (Stell, 2010a; Stell, 2010b). In order to improve the predictability of continuous descent arrival flight trajectories computed in FMS platforms, a tailored descent forecast wind approach is proposed in Bronsvoort et al. (2011). The tailored wind forecast is computed by an on-ground platform, based on the aircraft's flight plan, the landing procedure for the selected runway, and updated high resolution forecasts, and then uploaded into FMS. The tailored winds are a representation of the wind structure along the descent profile, in FMS specific model format, computed so that it minimizes the descent profile interpolation error. Methods as the one presented in Bronsvoort et al. (2011) can be used for increasing the

atmospheric data precision only for the case when there is a short lag between the forecast and the times instance of the wind prediction used in the flight profile calculation.

3.2 Methodology

The research presented in this article investigates a new dynamic atmospheric data model suitable for use in time-critical tasks, such as accelerated flight trajectory performance prediction calculations and/ or optimization of constant altitude cruise segments, in the FMS platforms and in flight trajectory optimization algorithms.

The proposed model is derived from, and based on, the atmospheric forecast data published by the meteorological agencies. The advantage of the proposed atmospheric data model is that it computes the atmospheric data, in the selected set of WPTs, with the same accuracy as when:

1. Computed by 4D linear interpolation, using the original (GRIB) data; or
2. Computed through linear time interpolation, based on the atmosphere parameter values calculated in the set of WPTs, at time instances that encompass the time instance of interest.

while requiring fewer computations.

The atmospheric data for a specific flight trajectory performance prediction and/or optimization problem can be precompiled offline or in the background, each time a new forecast data is available, and uploaded/updated in the target platform. The proposed model can be extended to define the atmospheric data for a set of cruise altitude of interest, generally a multiple of 1,000 ft.

This section is structured as follows: the first sub-section analyzes the forecast data issued by the meteorological service agencies, the second sub-section describes the 4D linear interpolation method that is the basis for the proposed atmospheric data model and, finally, the last sub-section presents the new atmospheric data model, the methodology used to

generate it, and its typical utilization to compute an atmospheric parameter in a node of a flight profile routing grid.

3.2.1 The GRIB atmospheric data forecast mode

This research was conducted using the forecast data provided by Environment Canada Meteorological Service. The article presents the methodology for the case when the data model is constructed based on a global deterministic prediction system (GDPS) (Buehner et al., 2015) forecast. GDPS is a global level forecast that uses a latitude – longitude map projection, and is available for two grid resolutions: 0.25º x 0.25º (Environment Canada, n.d.b) and 0.6º x 0.6º (Environment Canada, n.d.c). The GDPS forecasts are issued twice a day, at 00h and 12h universal coordinate time (UTC), with predictions made at 3 h intervals, up to 240 h for the 0.25º x 0.25º grid, and 144 h for the 0.6º x 0.6º grid. For both grids, the atmospheric parameters are provided at a fixed set of 27 isobaric levels. From hereon, in this article, GRIB designates the atmospheric data model containing the data extracted from these forecast data files. The proposed methodology can also be applied for RDPS forecast data, when the geographic area of interest is completely within the geographic area covered by the specific RDPS.

Figure 3.1 and Figure 3.2 are an illustration of a wind profile and air temperature GDPS forecast, with a 0.6º x 0.6º grid resolution, issued by Environment Canada on 14 June 2016 at 00 h UTC, for 03 h UTC and isobaric level 275 hPa (approx. 32,000 ft). The plots present the atmospheric data cropped to a region covering a large part of the North Atlantic (between longitudes W78 and E1.8, and latitudes N22.8 and N67.2). It can be noted that the atmospheric parameters have a complex variation as function of the geographic location (and altitude and time, not illustrated in Figure 3.1 and Figure 3.2), which cannot be globally described using simple mathematical models. The GRIB format forecasts are reduced complexity models that approximate the atmospheric parameters values and their space–time evolution.

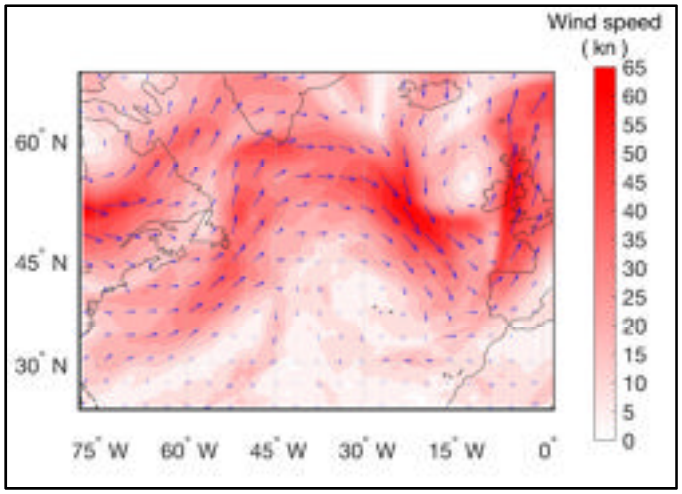

Figure 3.1 Wind forecast over the North Atlantic for 14 June 2016 at 03 h UTC and isobaric level 275 hPa, issued by Environment Canada on 14 June 2016 - 00 h UTC, in a GDPS forecast with a 0.6º x 0.6º grid resolution

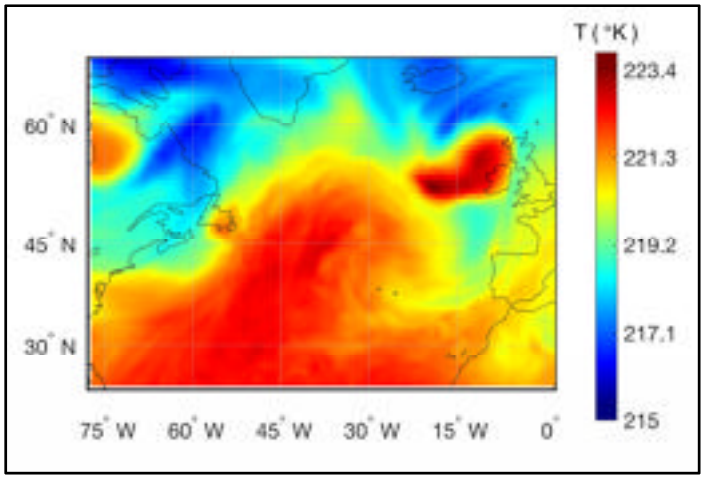

Figure 3.2 Air temperature forecast over the North Atlantic for 14 June 2016 at 03 h UTC and isobaric level 275 hPa, issued by Environment Canada on 14 June 2016 – 00 h UTC, in a GDPS forecast with a 0.6º x 0.6º grid resolution

The size of the GRIB atmospheric model data used in the calculations is a function of the selected geographic domain (latitude and longitude), isobaric levels, and time domains that

cover the range of possible geographic coordinates, altitudes, and flight times encountered along the evaluated flight trajectory. Even for constant altitude flight profiles, except the case when the altitude of interest corresponds to one of the atmospheric data isobaric levels, the atmospheric data model must contain at least two isobaric levels.

Let N_{LAT}, N_{LON}, N_{PS}, and N_T be the number of latitude, longitude, isobaric level, and time domain intervals of the GRIB data that cover the range of data necessary for a flight trajectory performance calculation, respectively. Let N_V be the number of atmospheric parameter data types of interest. In this study $N_V = 3$, the atmospheric parameters of interest are the air temperature (T), and the wind expressed as speed components along the geographic axes (North wind component W_U and East wind component W_V). Based on set of data provided in the GDPS GRIB files (the set of latitude, longitude, isobaric level, and time instances where the atmospheric data is defined and the resolution of atmospheric parameter values) the amount of memory necessary to store the data can be computed as follows:

1. (N_{LAT} + 1) single precision values for the latitude domain limits;
2. (N_{LON} + 1) single precision values for the longitude domain limits;
3. (N_{PS} + 1) 16 bit unsigned integer (uint16) values for the isobaric level domain limits;
4. (N_T + 1) 8 bit unsigned integer (uint8) values for the time domain limits;
5. N_V x (N_{LAT} +1) x (N_{LON} + 1) x (N_{PS} + 1) x (N_T + 1) single precision values for the atmospheric parameter values.

In the case where the GRIB atmospheric data model is defined in points that have the same value (constant) along a GRIB data grid axis, and the constant value is equal with a domain limit along that axis, the corresponding N value is equal to 0. For example, if the isobaric level is constant and equal with a GRIB grid node definition isobaric level then N_{PS} equals to 0.

3.2.2 Four-dimensional linear interpolation

The GRIB data model defines the atmospheric parameters' values in the nodes of a 4D grid, where the four axes are the latitude (lat), longitude (lon), isobaric level (ps), and time (t). A parameter value in a point other than a grid node is computed through interpolation.

Given the increasing incertitude of the forecast atmospheric data as a function of time, and the large time span generally covered by a flight profile relative to the forecast issue time, it is difficult to determine if the more complex and computationally intensive interpolation methods (such as polynomial, bicubic, spline, and kriging (Li & Heap, 2008) interpolations), theoretically more precise, are justified by the increase in precision relative to 4D interpolation, especially for time instances very far from the prediction issue time.

Although polynomial, bicubic, spline, and kriging interpolation are theoretically more precise than a 4D linear interpolation, in this case, they are impractical for the applications envisaged in this article due to:

1. Computational complexity/execution time constraints;
2. A larger number of forecast data points/model parameters that need to be used in the computations for (especially for an accurate kriging interpolation);
3. The chaotic nature of the atmospheric flows, with local anisotropies that change with time and location, and, as a result, requiring different interpolation models as a function of time and location domain where the interpolation is performed;
4. The large span of the time and geographic location domains covered by the evaluated flight profiles(s).

The 4D linear interpolation is an extension of the bilinear interpolation, used in current FMS platform to compute the atmospheric parameters, to a 4D domain.

Let the point of interest be $P(lat, lon, ps, t)$, situated at latitude *lat*, longitude *lon*, isobaric level *ps*, and at moment *t*. Let V be the atmospheric parameter value computed in the point P.

The first step of the 4D linear interpolation is to identify the 4D GRIB data domain, delimited by [lat_i lat_{i+1}], [lon_j lon_{j+1}], [ps_k ps_{k+1}], and [t_m t_{m+1}], containing the point *P*.

Then, linear interpolations are performed iteratively, along each axis. In each of the iterations, the interpolations are performed along a selected axis, and the resulted number of values (thus, linear interpolations to be performed in the next step) is halved (see in the paragraph below). Therefore, the total number of linear interpolations required to compute an atmospheric parameter in a point that is not a grid node are:

$$N_I = 2^4 - 1 = 15 \tag{3.1}$$

These calculations are based on the parameter's values defined in *n* GRIB data grid nodes, where *n* is:

$$n = 2^4 = 16 \tag{3.2}$$

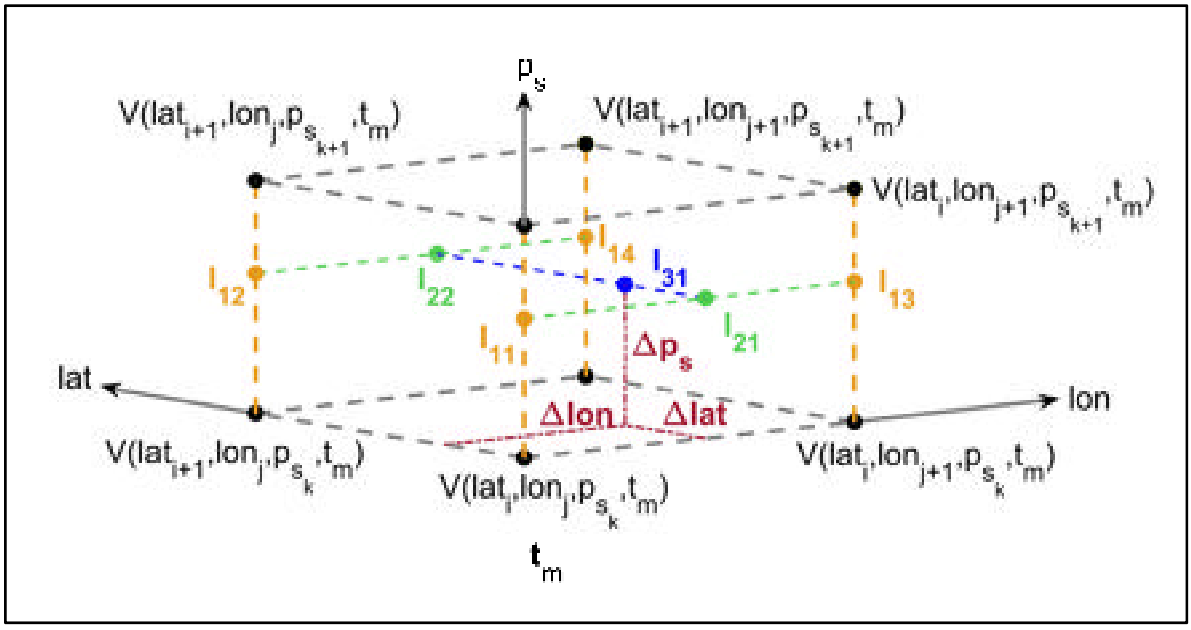

Figure 3.3 Illustration of the first set of 4D linear interpolation steps required for computing an atmospheric parameter - interpolation over latitude, longitude, and isobaric altitude at the moment t_m

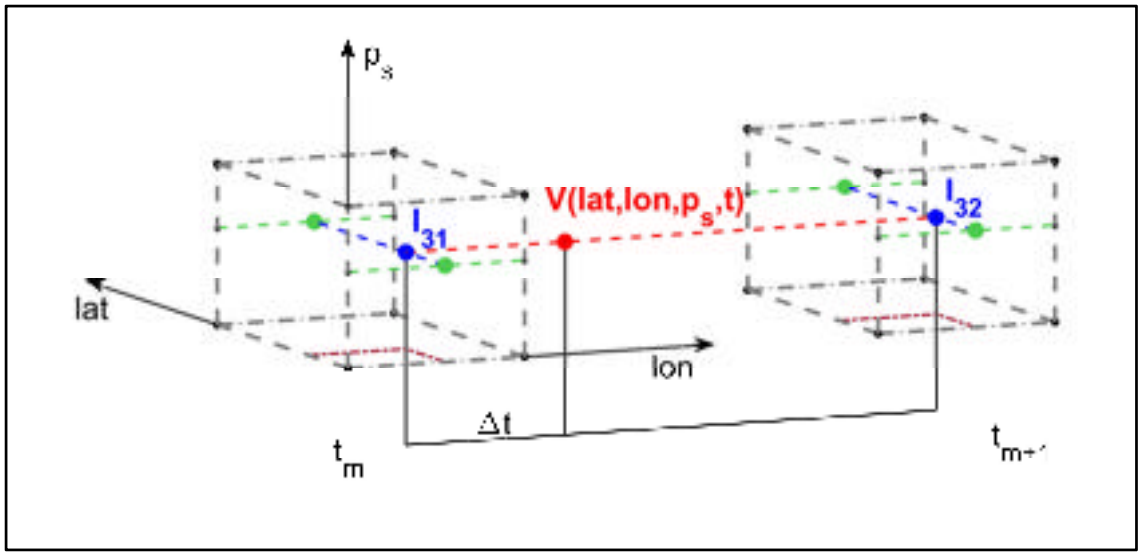

Figure 3.4 Illustration of the last step of the 4D linear interpolation - the interpolation along the time axis

A graphical illustration of the 4D linear interpolation process is presented in Figure 3.3 and Figure 3.4.

In this example, the first set of interpolations is performed along the isobaric level axis, between pairs of nodes with the same latitude, longitude and time grid coordinates (the vertical edges in Figure 3.3). The resulting intermediary points (designated in Figure 3.3 as I_{11} to I_{14}) correspond to the parameter's value at the set of latitude, longitude, and time combination that delimit the grid domain in which the point of interest is located, and at the isobaric level of interest.

If $V_{i,j,k,m}$ denotes a parameter value in the GRIB data node [lat_i, lon_j, ps_k, t_m], then the parameter's value calculated by linear interpolation in point I_{11} (Figure 3.3) can be expressed as:

$$\begin{aligned} I_{11} &= V(lat_i, lon_j, ps, t_m) = V_{i,j,k,m} + \frac{V_{i,j,k+1,m} - V_{i,j,k,m}}{ps_{k+1} - ps_k}(ps - ps_k) \\ &= V_{i,j,k,m} + \frac{V_{i,j,k+1,m} - V_{i,j,k,m}}{ps_{k+1} - ps_k}\Delta ps \end{aligned} \tag{3.3}$$

where Δps is the isobaric pressure difference between the pressure altitude (ps) for which the parameter is calculated, and the GRIB domain reference pressure level value (ps_k).

In the second iteration, the interpolations are performed along the longitude axis, between the points with the atmospheric parameter values I_{11} to I_{14}, and produce the values corresponding to the points I_{21} and I_{22}. In the third step, the interpolation is performed along the latitude axis, between the values I_{21} and I_{22}. It produces I_{31}, the atmospheric parameter value at the latitude, longitude, and the isobaric altitude of interest. However, this value does not correspond to the time instance of interest. Figure 3.3 illustrates the interpolation process for one of the two time instances that bracket the time interval where the atmospheric parameters are calculated. The three interpolation steps presented in the previous paragraph are repeated, and produce I_{32}, the atmospheric parameter values into the other time instance that defines the forecast domain containing the point of interest. The last interpolation step, illustrated in Figure 3.4, performs the interpolation along the time axis, between the values I_{31} and I_{32}, the parameter's values computed for (lat, lon, ps, t_m) and (lat, lon, ps, t_{m+1}) - the blue dots in Figure 3.4. The resulting value (the red point in Figure 3.4) is the parameter value in the point of interest: *V(lat, lon, ps, t)*.

By performing the 4D linear interpolation and, at each step, by replacing the interpolated values with their expressions relative to the GRIB domain's grid reference values, it results:

$$\begin{aligned} V(lat, lon, ps, t) &= V\left(lat_i + \Delta lat, lon_j + \Delta lon, ps_k + \Delta ps, t_m + \Delta t\right) \\ &= V_{i,j,k,m} + C_i\,\Delta lat + C_j\,\Delta lon + C_k\,\Delta ps + C_m\,\Delta t + \\ &\quad C_{ij}\,\Delta lat\,\Delta lon + C_{ik}\,\Delta lat\,\Delta ps + C_{im}\,\Delta lat\,\Delta t + \\ &\quad C_{jk}\,\Delta lon\,\Delta ps + C_{jm}\,\Delta lon\,\Delta t + C_{km}\,\Delta ps\,\Delta t + \\ &\quad C_{ijk}\,\Delta lat\,\Delta lon\,\Delta ps + C_{ijm}\,\Delta lat\,\Delta lon\,\Delta t + \\ &\quad C_{ikm}\,\Delta lat\,\Delta ps\,\Delta t + C_{jkm}\,\Delta lon\,\Delta ps\,\Delta t + \\ &\quad C_{ijkm}\,\Delta lat\,\Delta lon\,\Delta ps\,\Delta t \end{aligned} \tag{3.4}$$

where:

1. The C coefficients (their expressions are summarized in Table 3.1) are functions only of the 4D grid domain limits and the parameter's values in these nodes; and

2. The Δ values are the offsets of the calculation point's coordinates (latitude, longitude, isobaric level or time) relative to the reference point of the GRIB domain P(lat_i, lon_j, ps_k, t_m) - e.g. $\Delta ps = ps - ps_k$.

Table 3.1 4D linear interpolation coefficients

4D linear interpolation coefficient expressions	
First order coefficients	$C_i = \frac{V_{i+1,j,k,m} - V_{i,j,k,m}}{lat_{i+1} - lat_i}$ $\quad C_k = \frac{V_{i,j,k+1,m} - V_{i,j,k,m}}{ps_{k+1} - ps_k}$ $C_j = \frac{V_{i,j+1,k,m} - V_{i,j,k,m}}{lon_{j+1} - lon_j}$ $\quad C_i = \frac{V_{i,j,k,m+1} - V_{i,j,k,m}}{t_{m+1} - t_m}$
Second order coefficients	$C_{ij} = \frac{\begin{pmatrix} V_{i+1,j+1,k,m} - V_{i+1,j,k,m} \\ -V_{i,j+1,k,m} + V_{i,j,k,m} \end{pmatrix}}{(lat_{i+1} - lat_i)(lon_{j+1} - lon_j)}$ $\quad C_{ij} = \frac{\begin{pmatrix} V_{i+1,j,k+1,m} - V_{i+1,j,k,m} \\ -V_{i,j,k+1,m} + V_{i,j,k,m} \end{pmatrix}}{(lat_{i+1} - lat_i)(ps_{k+1} - ps_k)}$ $C_{im} = \frac{\begin{pmatrix} V_{i+1,j,k,m+1} - V_{i+1,j,k,m} \\ -V_{i,j,k,m+1} + V_{i,j,k,m} \end{pmatrix}}{(lat_{i+1} - lat_i)(t_{m+1} - t_m)}$ $\quad C_{jk} = \frac{\begin{pmatrix} V_{i,j+1,k+1,m} - V_{i,j+1,k,m} \\ -V_{i,j,k+1,m} + V_{i,j,k,m} \end{pmatrix}}{(lon_{j+1} - lon_j)(ps_{k+1} - ps_k)}$ $C_{jm} = \frac{\begin{pmatrix} V_{i,j+1,k,m+1} - V_{i,j+1,k,m} \\ -V_{i,j,k,m+1} + V_{i,j,k,m} \end{pmatrix}}{(lon_{j+1} - lon_j)(t_{m+1} - t_m)}$ $\quad C_{km} = \frac{\begin{pmatrix} V_{i,j,k+1,m+1} - V_{i,j,k+1,m} \\ -V_{i,j,k,m+1} + V_{i,j,k,m} \end{pmatrix}}{(ps_{k+1} - ps_k)(t_{m+1} - t_m)}$
Third order coefficients	$C_{ijk} = \frac{\begin{pmatrix} V_{i+1,j+1,k+1,m} - V_{i+1,j+1,k,m} - V_{i+1,j,k+1,m} + V_{i+1,j,k,m} \\ -V_{i,j+1,k+1,m} + V_{i,j+1,k,m} + V_{i,j,k+1,m} - V_{i,j,k,m} \end{pmatrix}}{(lat_{i+1} - lat_i)(lon_{j+1} - lon_j)(ps_{k+1} - ps_k)}$ $C_{ijm} = \frac{\begin{pmatrix} V_{i+1,j+1,k,m+1} - V_{i+1,j+1,k,m} - V_{i+1,j,k,m+1} + V_{i+1,j,k,m} \\ -V_{i,j+1,k,m+1} + V_{i,j+1,k,m} + V_{i,j,k,m+1} - V_{i,j,k,m} \end{pmatrix}}{(lat_{i+1} - lat_i)(lon_{j+1} - lon_j)(t_{m+1} - t_m)}$ $C_{ikm} = \frac{\begin{pmatrix} V_{i+1,j,k+1,m+1} - V_{i+1,j,k+1,m} - V_{i+1,j,k,m+1} + V_{i+1,j,k,m} \\ -V_{i,j,k+1,m+1} + V_{i,j,k+1,m} + V_{i,j,k,m+1} - V_{i,j,k,m} \end{pmatrix}}{(lat_{i+1} - lat_i)(ps_{k+1} - ps_k)(t_{m+1} - t_m)}$ $C_{jkm} = \frac{\begin{pmatrix} V_{i,j+1,k+1,m+1} - V_{i,j+1,k+1,m} - V_{i,j+1,k,m+1} + V_{i,j+1,k,m} \\ -V_{i,j,k+1,m+1} + V_{i,j,k+1,m} + V_{i,j,k,m+1} - V_{i,j,k,m} \end{pmatrix}}{(lon_{j+1} - lon_j)(ps_{k+1} - ps_k)(t_{m+1} - t_m)}$
Fourth order coefficient	$C_{ijkm} = \frac{\begin{pmatrix} V_{i+1,j+1,k+1,m+1} - V_{i+1,j+1,k+1,m} - V_{i+1,j+1,k,m+1} + V_{i+1,j+1,k,m} \\ -V_{i+1,j,k+1,m+1} + V_{i+1,j,k+1,m} + V_{i+1,j,k,m+1} - V_{i+1,j,k,m} \\ -V_{i,j+1,k+1,m+1} + V_{i,j+1,k+1,m} + V_{i,j+1,k,m+1} - V_{i,j+1,k,m} \\ +V_{i,j,k+1,m+1} - V_{i,j,k+1,m} - V_{i,j,k,m+1} + V_{i,j,k,m} \end{pmatrix}}{(lat_{i+1} - lat_i)(lon_{j+1} - lon_j)(ps_{k+1} - ps_k)(t_{m+1} - t_m)}$

To summarize, for each atmospheric parameter calculation it is necessary to perform:

1. Four data domains limit list searches, in order to identify the latitude, longitude, isobaric level, and time values that bound the atmospheric data grid domain where the point of interest is situated;
2. Four subtractions to compute the domain value span along each GRIB axis;
3. Fifteen linear interpolations - each interpolation requires a subtraction, a multiplication, and a division.

3.2.3 The proposed new dynamic atmospheric data model

The proposed Atmospheric Data Model, from here on designated as ADM, is intended for time-critical flight performance prediction calculations, which perform accelerated simulations of the flight along the flight profile.

In order to conduct efficient accelerated flight trajectory prediction calculations and/or flight trajectory optimizations (fast and accurate), it is essential to use an atmospheric data model with a low computational workload, and that would be the most precise possible.

The ADM is derived from and computed based on the GRIB data model, and is adapted for constant pressure altitude (isobaric level) flight trajectories performance calculations, where the flight profile definition parameters are the sub-segment speeds and the lateral flight profile. However, the model can be easily extended to define the atmospheric data for a set of cruise altitudes by instantiating it for each altitude of interest.

The ADM can be computed/updated offline or in the background, when new GRIB prediction data are available, and stored in memory. The proposed model will be analyzed to evaluate the computational workload necessary to compute the atmospheric parameters, precision relative to a 4D linear interpolation, the memory storage requirements, and the computational workload required to generate the model.

This ADM was developed for the case where a lateral profile is constructed as a succession of sub-segments, where each sub-segment connects two adjacent WPTs from a grid (routing grid) - similar with the model presented in Rodionova, Delahaye, Sbihi & Mongeau (2014). The grid of WPTs is constructed in such a way that, for each segment, the performance parameters are calculated in a single integration step (do not require further decomposition in sub-segments): the segment lengths are smaller than a selected threshold. The segment lengths are selected to be smaller or equal to the integration step size used in accelerated flight simulation of the cruise phase. The integration step size is selected as a tradeoff between the accuracy of the results and the computation time. Small integration steps (e.g. 1 n.m.) would yield more accurate estimations of the aircraft flight performance, however, in this case, a higher number of segment calculations will be performed and, thus, the computation time will increase.

The ADM defines the atmospheric parameter data in the nodes (WPTs) of the routing grid, at the selected cruise altitude (pressure altitude), as a function of time. An atmospheric parameter's value in a routing grid node (WPT) and time instance is calculated through linear interpolation, based on the parameter values defined for the WPT at predetermined instances of time. This article presents the case when the ADM data for the set of WPTs and reference times are computed based on the 4D linear interpolation method. However, the model data (coefficients) can be computed offline using other, more complex and computationally intensive interpolation methods (e.g. polynomial, bicubic, spline, kriging, etc.).

This section presents case when the model is constructed and used in flight trajectory optimization algorithms. The case when the model is used for in-FMS flight profile performance prediction is an equivalent case, where the atmosphere definition points (the routing grid) are a set of points defined so that they comprise the active lateral flight profile and the possible/selected alternate route(s).

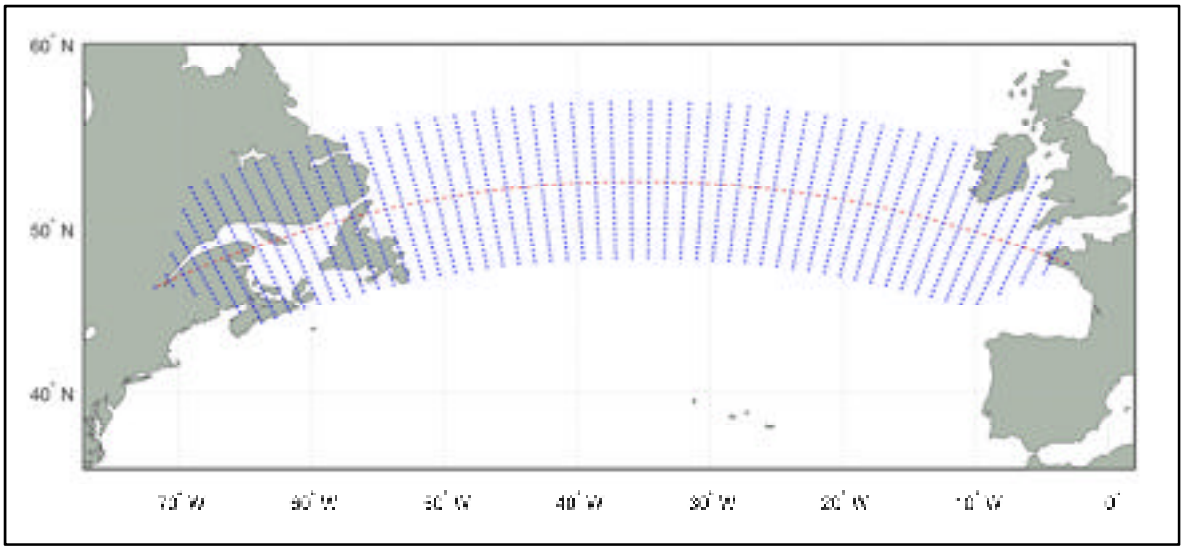

Figure 3.5 Example of a grid of waypoints that can be used in candidate creation

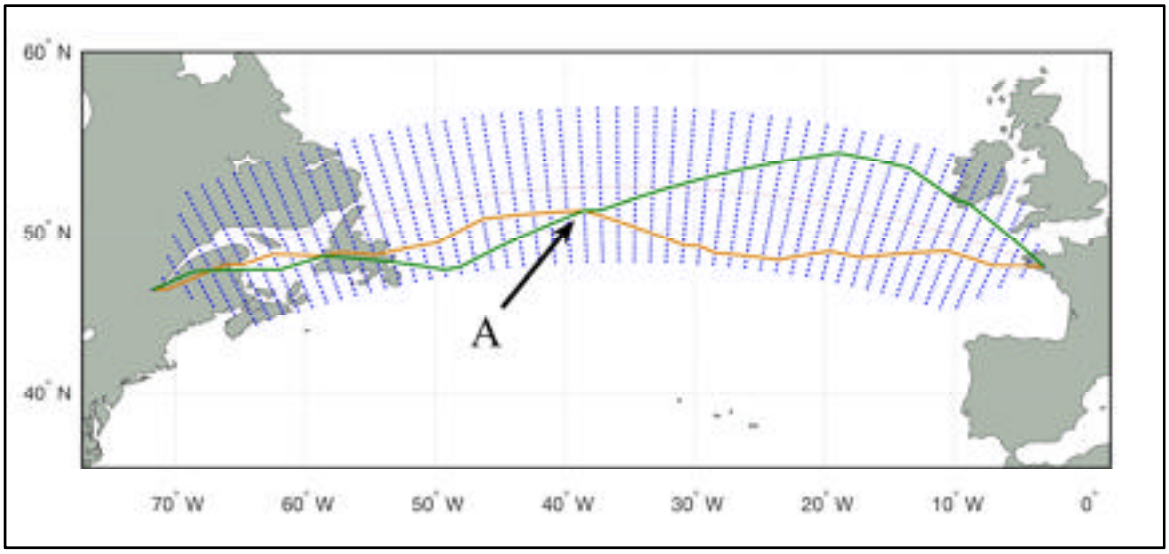

Figure 3.6 Example of two lateral profile trajectories that can reach a geographic location at different times

In the example presented in Figure 3.5, the grid is constructed based on the orthodromic route between the initial and final WPTs of the cruise segment under optimization. First, the orthodrome is decomposed in equal sub-segments of a selected length. Then, from each WPT

on the orthodrome, a perpendicular great circle is constructed and WPTs are placed at a selected constant distance from each other, up to a selected maximum deviation from the orthodrome.

The time instance when an aircraft reaches a WPT (e.g. point A in Figure 3.6) depends on the path (set of sub-segments) taken to that WPT and the aircraft's speed on each previous sub-segment. Given that the locations of each WPT (latitudes and longitudes) are fixed, and that the pressure altitude is also constant, the atmospheric data model needs only to describe the atmospheric parameter's variation with time at each WPT location.

For simplicity, in this section, the ADM model's coefficients denoted as D_V (with components D_{V_0} and D_{V_m}) and the atmospheric data parameter denoted as V are used as generic designations. An ADM that models three atmospheric parameters, such as T, W_U, and W_V, will have three sets of D coefficients: D_T (with components D_{0_T} and D_{m_T}), D_{WU} (with components D_{0_WU} and D_{m_WU}), and D_{WV} (with components D_{0_WV} and D_{m_WV}).

It can be noted that, when a coordinate of the 4D point where the atmospheric parameter is calculated does not change, its corresponding Δ value in equation (3.4) is constant. The expression of the atmospheric parameter value V can therefore be simplified by factoring the elements of equation (3.4).

The new expression for V is given in equation (3.5). The expressions for the coefficients D_V are summarized in equation (3.6).

$$V(lat, lon, ps, t) = D_{V\_0} + D_{V\_m}\Delta t, \quad where \begin{cases} lat = lat_i + \Delta lat = ct \\ lon = lon_j + \Delta lon = ct \\ ps = ps_k + \Delta ps = ct \\ t = t_m + \Delta t \end{cases} \tag{3.5}$$

Another method to compute the D_V coefficients is to compute the atmospheric parameter values, through 4D interpolation, for the time domain limits and then use these values to compute the D_V coefficients using equation (3.7):

$$\begin{cases} D_0 = V_{i,j,k,m} + C_k\,\Delta ps + C_i\,\Delta lat + C_j\,\Delta lon + \\ \quad C_{ik}\,\Delta lat\,\Delta ps + C_{jk}\,\Delta lon\,\Delta ps + C_{ij}\,\Delta lat\,\Delta lon + \\ \quad C_{ijk}\,\Delta lat\,\Delta lon\,\Delta ps \\ D_m = C_m + C_{km}\,\Delta ps + C_{im}\,\Delta lat + C_{jm}\,\Delta lon + \\ \quad C_{ikm}\,\Delta lat\,\Delta ps + C_{jkm}\,\Delta lon\,\Delta ps + C_{ijm}\,\Delta lat\,\Delta lon + \\ \quad C_{ijkm}\,\Delta lat\,\Delta lon\,\Delta ps \end{cases} \tag{3.6}$$

$$\begin{cases} D_{V\_0} = V(lat, lon, ps, t\_m) \\ D_{V\_m} = \dfrac{V(lat, lon, ps, t_{m+1}) - V(lat, lon, ps, t_m)}{t_{m+1} - t_m} \end{cases} \tag{3.7}$$

However, this method of computing the D_V coefficients requires two 4D interpolations and, therefore, is slower than the proposed method - equation (3.6). As a result, the ADM creation/update time when the coefficients are computed using equation (3.7) is longer than when computed using equation (3.6).

Since the ADM defines the atmospheric parameter values at given grid WPTs, the atmospheric data can be organized in the same way as the WPT data grid or stored as part of the WPT data. This way, the retrieving of the atmospheric information can be done without any overhead - based on information already available (e.g. selected WPT indexes or WPT data).

Further a WPT is from the initial (starting) WPT, the later is the earliest time and the larger is the time window when the aircraft can reach the WPT. The range of possible crossing times for the set of WPTs of the routing grid, and therefore the range of time for which the model should be defined, can be estimated using a heuristic. The stored data and the computation time (model data instance generation and parameters calculations) would be thus reduced.

Let N_{WPT} be the number of WPTs in the grid, N_V the number of atmospheric parameters of interest, and N_T the number of GRIB time domain intervals that span the possible flight times between the initial and final WPT. The amount of memory necessary to store the atmospheric data is:

1. (N_T + 1) uint8 values, for the time domain limit values - unique for all WPTs atmospheric data;
2. 2 x N_{WPT} x N_V x N_T double precision values, for the two coefficients (D_{V_0} and D_{V_m}) stored for each WPT, each atmospheric parameter, and each time domain, organized as follows:
    a. N_{WPT} data structures, where each structure stores the atmospheric data for a WPT;
    b. Each WPT data structure contains N_V data structures, corresponding to the N_V atmospheric parameters;
    c. Each atmospheric parameter data structure contains two vectors of length N_T, one for each of the D coefficients that defines the parameter's time variation.

A graphical description of the method used to compute the atmospheric parameter value V in an ADM grid WPT WPT_{ij} and a time instance t is presented in Figure 3.7.

An atmospheric parameter calculation is performed in four steps:

1. From the list of ADM time domain limits, find the index (idx_t) of the time domain containing the time instance (t) of interest and the reference time value (t_{ref}) for the ADM time domain (the inferior time value delimiting the ADM time domain);
2. Compute the time offset (Δt) between the time instance of interest (t) and the ADM time domain reference value (t_{ref}): $\Delta t = t - t_{ref}$;
3. From the ADM data corresponding to the WPT of interest (identified by idx_WPT_{ij}), retrieve the D_V coefficients for the time domain (idx_t) that contains the time instance (t), for which the calculation is performed: $D_{V\_0}(idx\_WPT_{ij}, idx\_t)$ and $D_{V\_m}(idx\_WPT_{ij}, idx\_t)$. This step is a memory data read since the waypoint index(es)

is(are) known from the flight trajectory WPT selection phase, and the time domain index has been determined in the first step of the calculation;

4. Compute the atmospheric parameter value using equation (3.5): a multiplication and a summation.

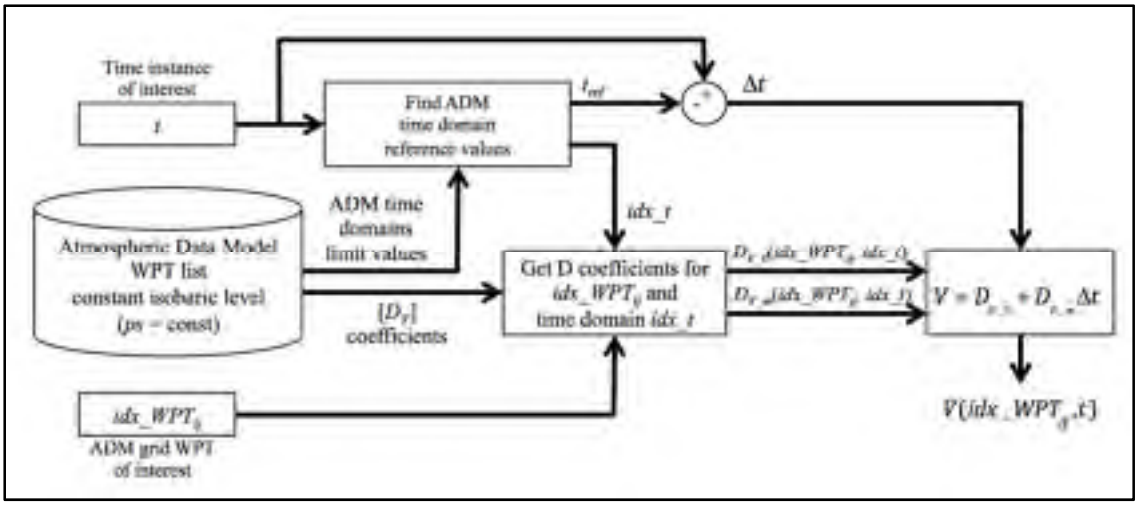

Figure 3.7 Atmospheric parameter calculation in a waypoint identified by index idx_WPT_{ij}, at a constant isobaric level, and at time instance t

The atmospheric parameter values calculated using ADM should be as precise as those calculated through 4D linear interpolation from GRIB data. In fact, from the point of view of data processing (from forecast data to the atmospheric parameter's value at a certain geographic location, altitude and time), the two are equivalent. The only source of difference is the precision of the data type used for storing the model's D_V coefficients.

The methodology used to construct the ADM is presented in Figure 3.8 and Figure 3.9. In order to construct the ADM, it is necessary to:

1. Retrieve and store the vector containing the GRIB data time domain limits that encompass the maximum range of flight times between the initial and final WPT of the flight trajectory;
2. For each WPT:

a. Identify the GRIB data domains that correspond to WPT's latitude, longitude, isobaric level, and time range of interest;
b. For each of the GRIB data domains, compute and store the D_{V_0} and D_{V_m} coefficients (using the formulas presented in equation (3.6) and Table 3.1).

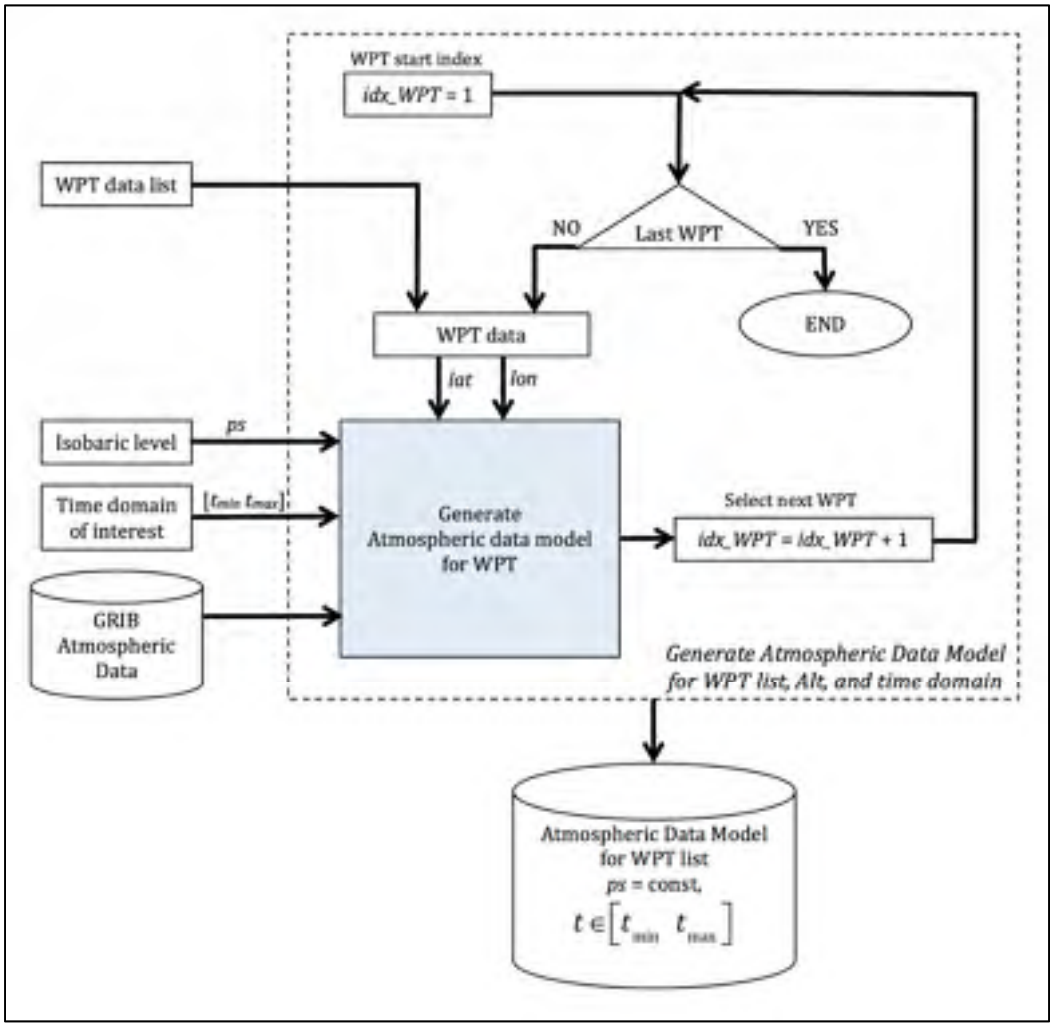

Figure 3.8 ADM construction workflow for constant isobaric altitude and for a set of fixed waypoints: global level (for the set of waypoints)

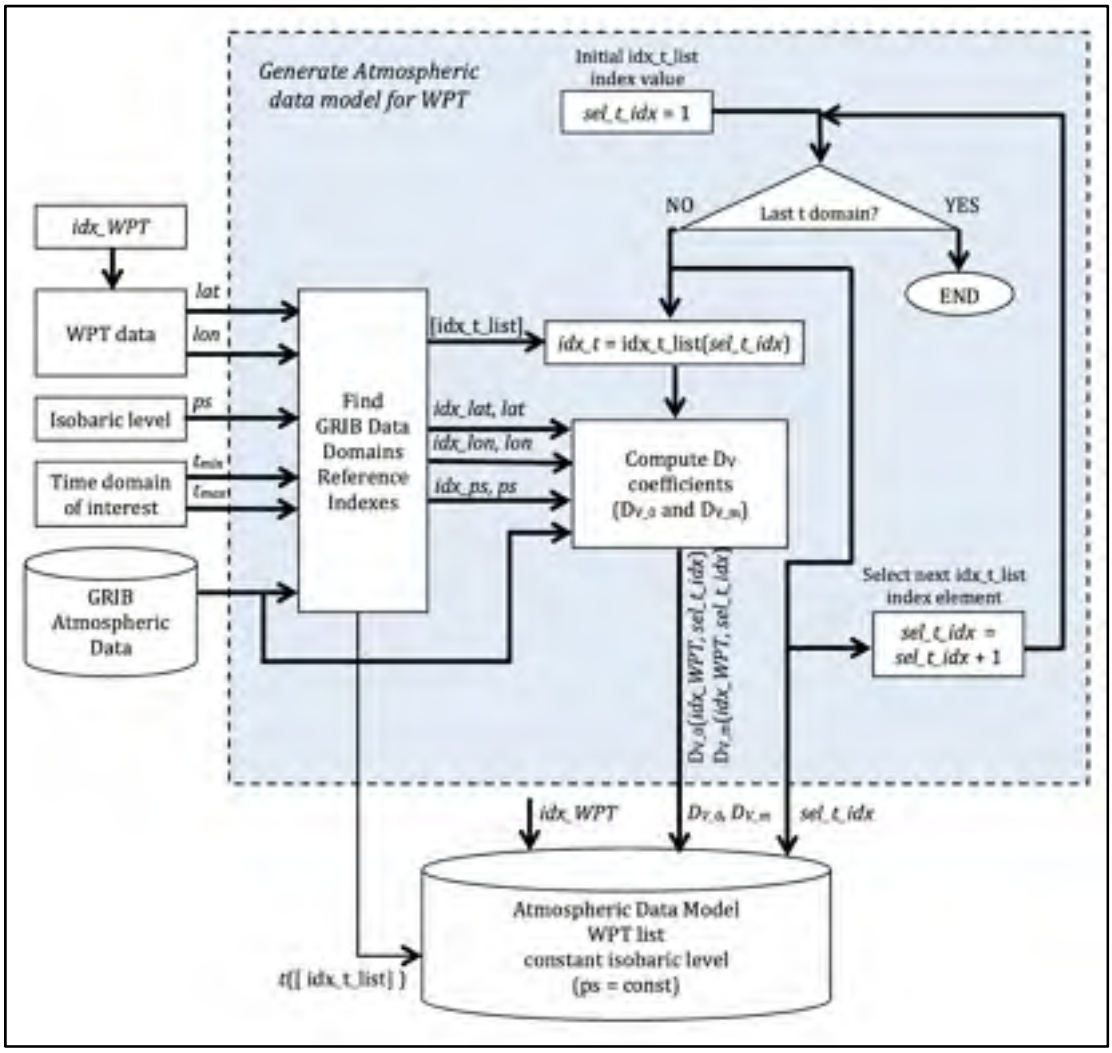

Figure 3.9 ADM construction workflow for constant isobaric altitude and for a set of fixed waypoints: (detailed workflow for a waypoint

3.3 Results

This section presents the results of a comparison between the performances of the proposed ADM, in terms of speed, precision and required memory, and the performance of the GRIB data model.

The ADM evaluation considers the case of a constant altitude cruise segment optimization, for which the candidate lateral flight profiles are constructed as a succession of sub-segments

that connect adjacent WPTs from a grid (see sub-section 3.2.3). First, the flight profile of a real flight was retrieved from FlightAware - chosen to be the flight TSC601 (FlightAware, 2016) Nantes to Montreal, flown on 14 June 2016. The cruise altitude, the locations (latitude and longitude coordinates), and flyover times for the initial and final positions of the cruise phase were retrieved from the flight track data (Table 3.2). The atmospheric data forecasts issued by Environment Canada are referenced to UTC. Therefore, the flyover times at the initial and final cruise WPTs (referenced to Eastern daylight time - EDT) were converted to UTC (EDT + 4), and added to the reference data in Table 3.2. It should be noted that the cruise phase of the real flight included a step climb later during the cruise, and a step descent back to 30,000 ft before the end of the cruise. The cruise altitude was retained as the initial cruise altitude of 30,000 ft in order to evaluate the time requirement for data model generation for a long cruise segment and, as a consequence, a large routing grid (number of WPTs).

Table 3.2 Reference data for the cruise phase of the flight TSC601 of 14 June 2016 (retrieved from FlightAware (2016))

Waypoint	Reference data				
	Latitude	Longitude	Altitude (ft)	Time (EDT)	Time (UTC)
Initial cruise WPT	N47 55’40.80”	W003 06’28.80”	30,000	09:39:39	13:39:39
Final cruise WPT	N46 32’3.480”	W071 45’32.940”	30,000	15:47:06	19:47:06

Next, the orthodromic route between the initial cruise WPT and the final WPT was generated, and divided in 55 equal length segments (56 WPTs). The locations of the WPTs along the orthodrome were chosen so that they yield the minimum number of equal length segments that are shorter or equal to 50 n.m. Then, in each WPT along the orthodrome a great circle was generated, perpendicular to the orthodrome in that WPT, and a set of WPTs, situated at a distance d_{STEP} of each other, were placed on both sides of the orthodrome (similar with the grid presented in Figure 3.5). It was assumed that the aircraft always moves forward along the grid, to a WPT situated one step forward along the orthodrome, at the same deviation on the perpendicular great circle, or up to N_{STEP} grid node (WPTs) lateral deviations (on either side) relative to the current deviation from the orthodrome. Therefore,

the grid started with one point, the initial cruise WPT, and increased by N_{STEP} WPTs on each side of the orthodrome as we travel along the great circle, up to a maximum distance deviation d_{MAX}. At the other end, the number of offset WPTs started to decrease by up to N_{STEP} WPTs on each side of the orthodrome until it ended with only one WPT - the final cruise WPT.

In order to evaluate the time necessary to generate the atmospheric data for various grid complexities, four grids were generated as a combination of two lateral step values (d_{STEP}), number of lateral deviations N_{STEP}, and maximum lateral deviations (d_{MAX}). Table 3.3 contains the characteristics for each of the four grids constructed for a flight trajectory between the WPTs given in Table 3.2. Grids 1 and 3 correspond to higher resolution grids, which allow a more refined evaluation of the optimal lateral profile.

Table 3.3 Selected routing grid characteristics

Grid	Routing grid characteristics								GRIB data	
	d_{MAX} (nm)	d_{STEP} (nm)	N_{STEP}	Total number of grid WPTs	Geographic area covered by the grid				Number of GRIB domains covering the grid	
					Min LAT	Max LAT	Min LON	Max LON	Lat	Lon
1	250	10	2	2,180	N46 32'3.480”	N56 48'44.835636 "	W071 45'32.940”	W003 06'28.80”	18	115
2	250	20	1	1,148	N46 29'59.845”	N56 58'44.408577 "	W071 45'32.940”	W003 06'28.80”	18	115
3	500	10	2	3,056	N44 12'8.510617"	N60 58'34.15914"	W071 45'32.940”	W003 06'28.80”	29	115
4	500	20	1	1,556	N44 12'8.510617"	N60 58'34.15914"	W071 45'32.940”	W003 06'28.80”	29	115

The forecast time interval for the GRIB data was determined based on the real track flyover time at the initial and final WPTs of the cruise segment. A buffer was added to the two limits in order to cover for all the possible flight time variations due to the lateral profile and ground speed differences along the various selected flight trajectories. It was estimated that the time interval 12 to 24h UTC covers the range of flight times for the cruise segment along any possible lateral flight profile based on the selected grids. The isobaric level for an

altitude of 30,000 ft is 300.77 hPa. This isobaric level is not a GRIB file data pressure altitude domain limit.

Based on the determinations presented in the previous paragraph, the GDPS GRIB files with a resolution of 0.6º x 0.6º, issued on 14 June 2016 at 12h UTC for the forecast period 12 to 24h UTC, isobaric levels 350 and 300 hPa, were imported from the Environment Canada website. They contain the forecasts for air temperature and wind (W_U and W_V components). The data in the imported files were cropped to the latitude and longitude domains that covered the geographic area containing the grid (Table 3.3). The resulted GRIB model data have one isobaric level domain ($N_{PS} = 1$), four time domains ($N_T = 4$), 115 longitude domains ($N_{LON} = 115$) and, function of the selected grid, 18 latitude domains ($N_{LAT} = 18$) for grids 1 and 2 (see Table 3.3) and 29 latitude domains ($N_{LAT} = 29$) for grids 3 and 4. The structure of the GRIB model data is described in sub-section 3.2.1. The GRIB data model for three atmospheric parameters (air temperature, and wind components - $N_V = 3$) was implemented in MATLAB R2018a, and its structure is described in Table 3.4.

The amount of data occupied in the memory by the cropped GRIB data is 530,049 bytes for the grids 1 and 2, and 836,377 bytes for grids 3 and 4.

Table 3.4 GRIB data structure implementation in MATLAB: structure elements and size for the selected geographic area

GRIB data structure element	Data type	Number of elements	Number of bytes function of the grid type	
			Grids 1 & 2	Grids 3 & 4
TimeDomainLimitValues	uint8	$N_T + 1$	5	5
IsobaricLevelDomainLimitValues	Single-precision (floating-point)	$N_{PS} + 1$	4	4
LatDomainLimitValues		$N_{LAT} + 1$	152	240
LonDomainLimitValues		$N_{LON} + 1$	928	928
AtmosphereData		$N_V * (N_T + 1) * (N_{PS} + 1) * (N_{LAT} + 1) * (N_{LON} + 1)$	528,960	835,200

For the proposed ADM (sub-section 3.2.3), the vector containing the time domain limit values is stored only once, for the entire set of WPTs. The ADM data structure, its elements and the memory occupied in a MATLAB 2018.a implementation are presented in Table 3.5:

Table 3.5 ADM data structure elements implementation in MATLAB (time domain limits and waypoint data) and size

ADM data structure element	Data type	Number of elements	Number of bytes
TimeDomainLimitValues	uint8	$N_T + 1$	5
WPT_AtmosphereData	Structure with double-precision (floating-point) elements	$2 * N_T$	416

The amount of memory occupied by the proposed model for the four grid types (grids 1 to 4 in Table 3.3) are presented in Table 3.6.

Table 3.6 Memory used by the proposed Atmosphere Data Model

Grid	Number of WPTs	Total data size for grid (Number of WPTs * 416) (bytes)	Total used memory (Memory for WPTs + memory for TimeDomainLimitValues) (bytes)
1	2,180	906,880	906,885
2	1,148	477,568	477,573
3	3,056	1,271,296	1,271,301
4	1,556	647,296	647,301

As expected, for the same covered geographic area, the memory used by the proposed model is a function of the routing grid size and resolution. It can be noted that, for grids with low resolution (grids 2 and 4), the proposed model requires less memory than the memory used by the GRIB data model.

As previously mentioned, the proposed ADM is generated based on the GRIB data model, offline or in the background, before its use in accelerated flight profile performance calculations. In order to evaluate the computational workload and the time necessary to generate the ADM, the ADM was generated for the four grids described in Table 3.3. Two

methods for generating the ADM were compared. The first method generated the ADM based on the proposed methodology (sub-section 3.2.3, Figure 3.8 and Figure 3.9). In the second method, the atmospheric parameters for the time domain were computed through 4D linear interpolation: the atmosphere parameters were computed for each routing grid WPT and time domain limit value, and then the D coefficients were computed for each time domain using equation (3.7). The results of the comparisons for the time necessary to create the ADM and the model precision are presented in Table 3.7. The time values represent the total time (computed using the MATLAB functions tic and toc) necessary to generate the ADM's three tables: temperature and wind components (W_U and W_V).

Table 3.7 ADM creation method performance

Grid	ADM creation Execution time (s)		Execution time difference (s)	Maximum coefficient value difference (absolute value) (4D interpolation – ADM)					
	Proposed method	Based on 4D Interpolation		Temperature		Wind North (W_U)		Wind East (W_V)	
				D_{0_T} (K)	D_{m_T} (K/h)	D_{0_WU} (kn)	D_{m_WU} (kn/h)	D_{0_WV} (kn)	D_{m_WV} (kn/h)
1	1.483117	2.863120	1.380003	8.5265×10^{-14}	2.20448×10^{-14}	2.13162×10^{-14}	6.43929×10^{-15}	2.13162×10^{-14}	6.66133×10^{-15}
2	0.935013	1.534994	0.599980	8.5265×10^{-14}	1.98174×10^{-14}	2.13162×10^{-14}	5.32907×10^{-15}	1.42108×10^{-14}	6.66133×10^{-15}
3	1.877345	4.521300	2.643955	8.5265×10^{-14}	2.20448×10^{-14}	2.13162×10^{-14}	6.43929×10^{-15}	2.13162×10^{-14}	6.66133×10^{-15}
4	1.780533	2.506082	0.725549	8.5265×10^{-14}	2.02893×10^{-14}	2.13162×10^{-14}	5.32907×10^{-15}	1.42108×10^{-14}	6.66133×10^{-15}

It can be observed that the proposed method to create the ADM is much faster than when the coefficients are calculated through 4D linear interpolation from the GRIB data. The differences between the values of the coefficients computed using the two methods are very small.

Next, the computational workload and the precision of atmospheric parameter calculations were evaluated by comparing the three atmospheric parameters (air temperature and wind components), and the time necessary to compute them by using ADM, with those obtained using the classical method (4D linear interpolation from the GRIB data). For this purpose, the

atmospheric parameters were computed in every node of the routing grid, for each time domain limit value, and for 10 equidistant intermediate time values within each time domain. Given the fact that a GRIB time interval span is 3 h, the resulting time step used for the performance assessment is 16’21.81’’ (3 h divided in 11 equal intervals). Table 3.8 presents the results of the comparison between the two methods (ADM versus 4D linear interpolation), expressed in terms of minimum and maximum parameter value differences, for the entire set of parameter evaluations performed in this study. Table 3.9 presents a comparison between the computation times evaluated using the MATLAB function ‘‘timeit’’.

Table 3.8 Comparison between the atmospheric parameters computed with the ADM model and 4D linear interpolation

GRID	Atmosphere parameters difference (ADM - 4D linear interpolation)					
	T(K)		W_V (kn)		W_U (kn)	
	Min	Max	Min	Max	Min	Max
1	-8.5265×10^{-14}	8.5265×10^{-14}	-2.8421×10^{-14}	2.1316×10^{-14}	-2.1316×10^{-14}	2.1316×10^{-14}
2	-8.5265×10^{-14}	8.5265×10^{-14}	-1.7763×10^{-14}	2.1316×10^{-14}	-2.1316×10^{-14}	2.1316×10^{-14}
3	-8.5265×10^{-14}	8.5265×10^{-14}	-2.8421×10^{-14}	2.84217×10^{-14}	-2.1316×10^{-14}	2.1316×10^{-14}
4	-8.5265×10^{-14}	8.5265×10^{-14}	-2.8421×10^{-14}	2.1316×10^{-14}	-2.1316×10^{-14}	2.1316×10^{-14}

Table 3.9 Comparison between the atmospheric parameters computation times for the ADM model and 4D linear interpolation

GRID	Computation time ratio (4D linear Interpolation/ADM)				
	Min	Mean	Max	Median	Standard deviation
1	2.664491	6.545356	2.15763e+01	5.9502	1.4318
2	2.596380	6.650567	1.75927e+01	6.0338	1.5144
3	1.957937	6.602139	2.706310e+01	6.0226	1.4360
4	1.788913	6.512603	1.989292e+01	5.9374	1.4163

It can be noticed that, on average, the ADM yields the atmospheric parameter values six times faster than a 4D linear interpolation. These results are confirmed by the histogram presented in Figure 3.10, which shows that for a majority of the evaluated cases the computations using ADM are about six times faster. The differences between the values calculated with the ADM and those computed through a 4D linear interpolation are very

small (of the order of 10^{-14}), many orders of magnitude better than the precision of the GRIB forecast data issued by the environment agencies (Schwartz et al., 2000; Cole et al., 2000; Lee et al., 2009; Vaddi et al., 2013). The results are practically identical.

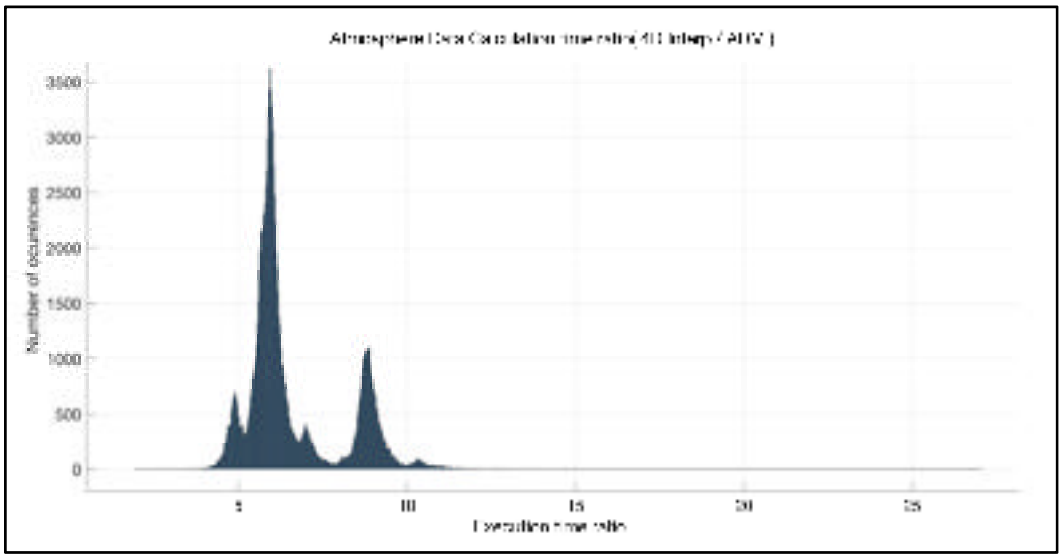

Figure 3.10 The distribution of the computation time ratios
(4D linear interpolation/ADM) for grid 3 and atmospheric data
from 14 June 2016 issued at 12h UTC, for 12 to 24h UTC

A final evaluation was conducted in order to compare the difference in computation times for flight profile calculations. This evaluation was performed using the grid 3 and the atmospheric data for 14 June 2106, for the period 12 to 24h UTC, a flight altitude of 30,000 ft, and an initial time (the time when the aircraft is at the initial point of the cruise segment) of 13:30 UTC. The aircraft performance data were computed for a long-range transport aircraft for which the BADA 4.0 model was available at LARCASE. BADA provides a methodology for calculating the aero propulsive forces acting on the aircraft, the aircraft motion as a result of these forces (equations based on the Total Energy Model - TEM), and the associated fuel burn. The aircraft's configuration parameters (e.g. zero-fuel weight, fuel quantity and speed) at the beginning of the evaluated flight profile were chosen within the range specified in the BADA model. The evaluation was performed at a constant

speed (MACH 0.8), and for two random flight tracks (Figure 3.11) defined by choosing WPTs from grid 3.

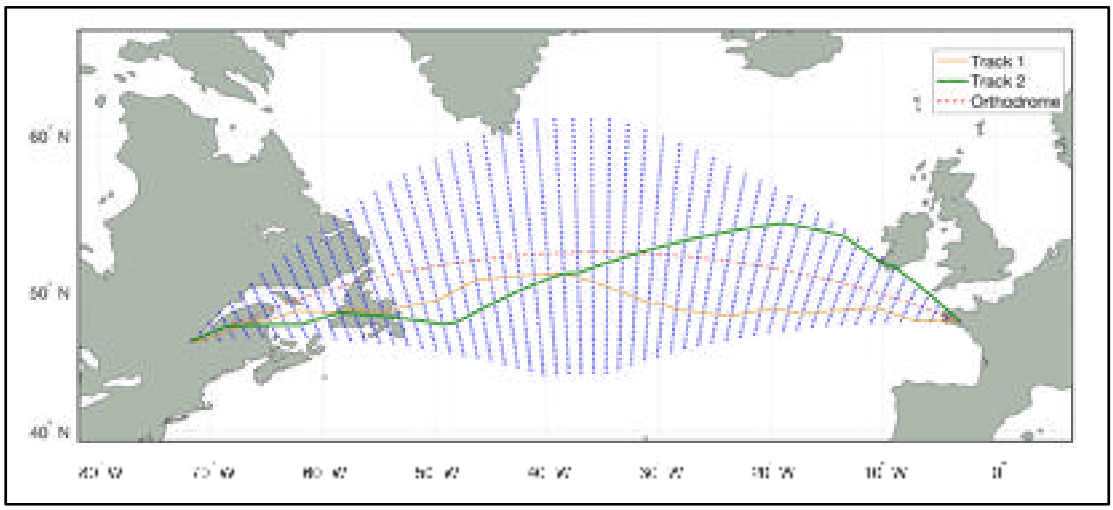

Figure 3.11 The flight profiles chosen to evaluate the computation times for flight trajectory performance evaluation using ADM (grid 3, max deviation 500 nm, deviation step 10 nm, up to 2 deviation steps at each waypoint)

The two evaluated flight tracks (Figure 3.11) are defined by the set of WPTs selected from the ADM / routing grid. At each flight track step, the aircraft advances to a new WPT situated one grid step ahead along the orthodrome, and up to N_{STEP} grid step deviations ([$-N_{STEP}$ N_{STEP}]) on the direction normal to the orthodrome (according to the assumptions made when constructing the ADM/routing grid - please see the third paragraph, at the beginning of this section).

Therefore, the number of WPTs that define a trajectory is equal to the number of grid WPTs along the orthodromic route. A flight trajectory can be thus defined by a set of WPT's, ordered as function of their positions along the orthodromic route grid axis, and their grid position deviations relative to the orthodromic route. Table 3.10 shows the set of WPTs that define the test flight tracks, and their offsets relative to the orthodromic grid route.

Table 3.10 Test flight tracks defined as number of grid step deviations from the orthodromic route, at each waypoint along the track

WPT number (position along the orthodromic route grid axis)	Track 1 WPT offset (relative to the orthodromic route grid axis)	Track 2 WPT offset (relative to the orthodromic route grid axis)	WPT number (position along the orthodromic route grid axis)	Track 1 WPT offset (relative to the orthodromic route grid axis)	Track 2 WPT offset (relative to the orthodromic route grid axis)	WPT number (position along the orthodromic route grid axis)	Track 1 WPT offset (relative to the orthodromic route grid axis)	Track 2 WPT offset (relative to the orthodromic route grid axis)
1	0	0	20	22	-8	39	14	22
2	2	-2	21	22	-6	40	14	20
3	4	-4	22	20	-4	41	14	18
4	6	-6	23	20	-2	42	14	16
5	6	-8	24	18	0	43	12	14
6	6	-10	25	16	2	44	10	12
7	6	-12	26	14	4	45	10	10
8	8	-12	27	12	6	46	8	10
9	10	-14	28	10	8	47	6	10
10	12	-16	29	8	8	48	4	10
11	14	-18	30	8	10	49	4	8
12	16	-18	31	8	12	50	4	6
13	16	-18	32	8	14	51	2	4
14	16	-18	33	8	16	52	2	2
15	18	-18	34	8	18	53	2	0
16	20	-16	35	8	20	54	2	0
17	22	-14	36	10	22	55	2	0
18	22	-12	37	12	24	56	0	0
19	22	-10	38	14	24			

For each of the two tracks, full trajectory performance calculations were performed: successive calculation of the atmospheric parameters, flight time, and fuel burn for each sub-segment of the flight profile. The flight track performance calculations were performed once with the atmospheric data computed using the ADM and a second time with the atmospheric parameters computed using the 4D linear interpolation.

The atmospheric data computed by 4D interpolation of GRIB data and by the ADM model are identical. Therefore, for identical flight trajectories, aircraft model (performance characteristics), and initial aircraft weight, the results of the flight trajectory performance calculations (fuel burn, flight time, total cost) using the two atmospheric data models (GRIB and ADM) are also identical.

Algorithm 3.1 Pseudo code for the evaluation and comparison of flight trajectory performance calculation times when the atmospheric parameters are calculated using ADM and 4D linear interpolation

```
load ADM data
load GRIB data
load Grid data
load track data
load altitude, initial time
load aircraft configuration
load aircraft performance model

for idx_track = 1 : 1 : 2
    for counter = 1 : 1 : 10
        position aircraft at the initial waypoint
        set aircraft initial configuration (altitude, weight, cg...)
        set initial time

        tic
            compute track flight profile performance using ADM
        time_ADM(counter) = toc

        position aircraft at the initial waypoint
        set aircraft initial configuration (altitude, weight, cg...)
        set initial time
        tic
            compute track flight profile performance using 4D linear interpolation
        time_4D(counter) = toc
    end
end
```

The flight profile computation times for the two calculations were compared in order to determine the possible advantages and time calculation reductions made possible by using the ADM. The time necessary to compute the flight track performance parameters was evaluated using the Matlab functions *tic* and *toc*. The code execution times evaluated with *tic* and *toc* vary function of the tasks scheduling executed by the operating system. Therefore, in order to have a good evaluation of the method's performance, the flight performance calculation code was executed and timed 10 times for each track and atmospheric calculation

method (ADM and 4D linear interpolation). Since for each of the 10 instances of flight profile performance calculations using an atmospheric calculation method the code and the input data are the same, the code execution time should be identical. Therefore, the execution time differences should be attributed to the processor time allocation performed by the operating system. The pseudo code for the time performance evaluation test is presented in Algorithm 3.1.

The results of the computation time evaluations are presented in Table 3.11. It was noted that the execution times reported by *tic*/*toc* for the first execution of the flight trajectory calculation using the ADM (the first call in the evaluation loop – Track 1, iteration 1, in Table 3.11) were very large in comparison with the other execution times and were attributed to the operating system/Matlab. A possible explanation could be that the time difference was caused by a Matlab or Windows thread launched at the beginning of the test script execution. Therefore, the computation time for this first flight trajectory performance calculation was discarded.

Table 3.11 Flight trajectory performance calculation times when the atmospheric parameters are calculated using ADM and 4D linear interpolation (Grid 3, Atmospheric data for June 14, 2016, 12h to 24h UTC)

		Iteration										Min
		1	2	3	4	5	6	7	8	9	10	
Track 1	ADM (s)	0.3308	0.0994	0.0999	0.1024	0.1024	0.0926	0.0910	0.0887	0.0954	0.0973	0.0887
	4D Interp (s)	0.1964	0.1289	0.1157	0.1117	0.1136	0.1139	0.1074	0.1056	0.1027	0.1195	0.1027
	Diff (s) (ADM – 4D)	0.1344	-0.0294	-0.0158	-0.0092	-0.0112	-0.0213	-0.0163	-0.0168	-0.0072	-0.0222	-0.0139
	ADM vs 4D (Diff / 4D) [%]	68.4317	-22.8376	-13.6783	-8.2714	-9.8750	-18.6962	-15.2299	-15.9280	-7.0663	-18.6303	-13.5876
Track 2	ADM (s)	0.1043	0.0964	0.0967	0.1006	0.0963	0.0961	0.0890	0.0839	0.0905	0.0938	0.0839
	4D Interp (s)	0.1160	0.1098	0.1164	0.1150	0.1138	0.1116	0.1018	0.1035	0.1122	0.1038	0.1018
	Diff (s) (ADM – 4D)	-0.0117	-0.0134	-0.0197	-0.0144	-0.0174	-0.0154	-0.0128	-0.0196	-0.0217	-0.01	-0.0179
	ADM vs 4D (Diff / 4D) [%]	-10.0973	-12.2000	-16.9694	-12.5564	-15.3623	-13.8595	-12.5880	-18.9931	-19.3532	-9.6320	-17.6415

It can be noted that the computation time for the flight trajectory performance calculations using the GRIB data atmospheric model and 4D linear interpolation is significantly larger than in the case when the ADM model is used.

3.4 Conclusions

This article presented a new atmospheric data model (ADM) and methodology for storing the atmospheric data and computing the atmosphere parameters in a set of fixed WPTs situated at the same constant pressure level. This model was developed based on the GDPS GRIB atmospheric data model published by the Meteorological Service Agencies. The ADM can be created off-line or in the background, and subsequently be used by the FMS or ATM platforms to compute the atmosphere parameters necessary for the flight trajectories accelerated simulation or optimizations. The proposed methods for creating, storing and use of the ADM are much faster than using the 4D linear interpolation methods.

For the evaluated cases, the ADM creation time using 4D linear interpolations is between 1.4 and 2.4 times slower than the proposed method. The time necessary to compute the air temperature and wind values using ADM is, on average, six times shorter than when they are computed by 4D linear interpolation, while the differences between the atmospheric parameter values computed with the two methods are negligible (of the order of 10^{-14}). When used in flight trajectory calculation algorithms, the ADM resulted in a significant reduction (more than 10%) in the time necessary to perform the calculations. Since the flight trajectory calculation algorithms and the input data are identical, and the atmospheric parameters calculated by the two methods (ADM and 4D linear interpolations) are identical, the results of the flight trajectory performance calculations are identical.

For small sets of WPTs (small size grids or lower resolution WPT grids), it was shown that ADM has a smaller memory footprint than the equivalent GRIB data model. Since each atmospheric data element is associated with a WPT, it makes it easier to store it in a structure associated to the WPT or identify it based on the information identifying the WPT - without additional overhead. The proposed atmospheric model can be extended to define the atmospheric data at a set of cruise altitudes.

Although the forecasts issued by the meteorological agencies become more precise, they are subject to incertitude. Therefore, the estimated atmospheric parameters do not necessarily reflect the actual conditions encountered by the aircraft. For critical applications, such as accelerated flight performance estimation for flight profiles with navigation time (RTA) constraints, statistical information regarding the forecast data error (published by the meteorological agencies, research data and/or heuristics) should be used to generate worst-case scenarios - the most unfavorable atmospheric conditions along the flight profile - in order to ensure that the navigation constraints are met with the required level of confidence. When used in flight trajectory optimization algorithms, the atmospheric data incertitude will result in near-optimal flight profile solutions.

Future work could investigate the possible advantages and improvements, in terms of computation time and flight trajectory performance parameters accuracy gains, when the ADM is used in conjunction with the algorithm for predicting an aircraft's fuel burn on constant speed and altitude flight trajectories (Dancila et al., 2013).

Other studies could:

1. Evaluate an extension and improvement of the ADM in order to consider different atmosphere definition altitudes at the WPT locations;
2. Perform a comparison of the ADM model's precision relative to the precision obtained when other interpolation methods are employed, more complex and more computing intensive than 4D linear interpolation and the ADM, and compare with the precision of the atmospheric prediction data issued by the meteorological agencies;
3. Compare the atmospheric parameters computed using 4D linear interpolation, ADM, and other (more complex) interpolation methods, with the real atmospheric data (recorded during flight).

CHAPTER 4

NEW FLIGHT TRAJECTORY OPTIMIZATION METHOD USING GENETIC ALGORITHMS

Radu Ioan Dancila[a] and Ruxandra Mihaela Botez[b]

[a,b]École de Technologie Supérieure, Université du Québec
LARCASE Laboratory of Research in Active Controls, Aeroservoelasticity and Avionics
1100 rue Notre Dame Ouest, Montréal, H3C1K3, Québec, Canada

This article was accepted for publication[2] in The Aeronautical Journal,
on November 15, 2020

Résumé

Cet article présente une nouvelle méthode d'optimisation des trajectoires de vol, basée sur des algorithmes génétiques, où le critère d'optimisation est la minimisation des coûts totaux. Les trajectoires de vol évaluées dans l'optimisation sont définies en tant que plans de vol et elles ont deux composants : le plan de vol latéral (les points géographiques qui définissent les segments de la projection en plan horizontal de la trajectoire de vol), et le plan de vol vertical (l'ensemble des données qui décrivent le profil d'altitude et vitesse et les points géographiques où leurs changements sont initiées). Les composants latéraux du plan de vol sont construits en sélectionnant des nœuds adjacents d'une grille de routage. Les nœuds de la grille de routage sont générés à partir de la route orthodromique entre le point initial et le point final de la trajectoire de vol, ainsi que les valeurs sélectionnées pour les pas de la grille au long de ses axes. Deux stratégies sont investiguées par rapport au traitement des cas où un plan de vol est invalide (par rapport à l'enveloppe de vol de l'avion). Une première stratégie est d'assigner une valeur très grande (une pénalité) pour le coût total d'un tel plan de vol. La deuxième stratégie est de corriger le plan de vol : ajuster les paramètres de vol (altitude et/ou vitesse) pour le rendre dans les limites de l'enveloppe de vol. Les tests effectués ont montré

---

[2] The paper presented in this chapter contains minor modifications relative to the version accepted for publication in The Aeronautical Journal, on November 15, 2020. These modifications were made at the request of the members of the Board of Examiners.

que la deuxième stratégie est plus couteuse du point de vue computationnel (le temps d'exécution a plus que doublé) et la qualité des résultats a diminué par rapport à la première stratégie. Les paramètres de performance des profils optimaux identifiés par la méthode proposée, dans les deux approches relatives aux plans de vol invalides, ont été comparés avec les paramètres de performance des plans de vol de référence qui ont été obtenus dans les mêmes conditions : poids initial de l'avion, points géographiques initial et final et les altitudes et les vitesses de l'avion dans ces points, indice de coût, et conditions atmosphériques. Les coordonnées géographiques et les altitudes dans les points initial et final, ainsi que les données pour le profil de vol de référence, ont été récupérées à partir du site FlightAware. Ces données correspondent aux celles d'un vol réel, effectué avec le même type d'avion que celui utilisé dans cette étude. Plusieurs tests ont été effectués pour six valeurs d'indice de coût. Étant donnée la nature aléatoire des algorithmes génétiques, leur convergence vers une solution optimale n'est pas garantie, ainsi la solution peut être non-optimale ou localement optimale (optimum local). Pour une meilleure évaluation de la performance de la méthode proposée, 10 essais ont été effectués pour chaque valeur d'indice de coût. La réduction du coût total pour le plan de vol optimal obtenu avec la méthode proposée par rapport au plan de vol de référence a été entre 0.822% et 3.042% pour les cas où les plans de vol invalides ont été corrigés, et entre 1.598% et 3.97% pour les cas où une valeur représentant la pénalité a été assignée au coût total des plan de vol invalides.

Abstract

This paper presents a new flight trajectory optimization method, based on genetic algorithms, where the selected optimization criterion is the minimization of the total cost. The candidate flight trajectories evaluated in the optimization process are defined as flight plans with two components: a lateral flight plan (the set of geographic points that define the flight trajectory track segments), and a vertical flight plan (the set of data that define the altitude and speed profiles, as well as the points where the altitude and/or speed changes occur). The lateral components of the candidate flight plans are constructed by selecting a set of adjacent nodes from a routing grid. The routing grid nodes are generated based on the orthodromic route

between the flight trajectory's initial and final points, a selected maximum lateral deviation from the orthodromic route, and a selected grid node step size along and across the orthodromic route. Two strategies are investigated for the handling of invalid flight plans (relative to the aircraft's flight envelope) and to compute their flight performance parameters. A first strategy is to assign a large penalty total cost to the invalid flight profiles. The second strategy is to adjust the invalid flight plan parameters (altitude and/or speed) to the nearest limit of the flight envelope, with priority being given to maintaining the planned altitude. The tests performed in this study have shown that the second strategy is computationally expensive (more than double the execution time relative to the first strategy), and yields less optimal solutions. The performances of the optimal profiles identified by the proposed optimization method, using the two strategies regarding invalid flight profile performance evaluation, were compared with the performance data of a reference flight profile, using identical input data: initial aircraft weight, initial and final aircraft geographic positions, altitudes and speed, cost index, and atmospheric data. The initial and final aircraft geographic positions, and the reference flight profile data, were retrieved from the FlightAware web site. This data corresponds to a real flight, performed with the aircraft model used in this study. Tests were performed for six Cost Index values. Given the randomness of the genetic algorithms, the convergence to a global optimal solution is not guaranteed (the solution may be non-optimal or a local optima). For a better evaluation of the performance of the proposed method, ten test runs were performed for each Cost Index value. The total cost reduction for the optimal flight plans obtained using the proposed method, relative to the reference flight plan, were between 0.822% and 3.042% for the cases when the invalid flight profiles were corrected, and between 1.598% and 3.97% for the cases where the invalid profiles were assigned a penalty total cost.

4.1 Introduction

According to ICAO forecasts (ICAO, 2018; ICAO, n.d.a), the future annual growth of passenger and cargo traffic, up to 2035, is estimated to be approximately 4.3% and 3.9%, respectively, which will result in a doubling of the number of passengers by 2037 (IATA,

2018). This reality requires better flight planning, navigation and airspace management strategies and tools in order to facilitate the safe and efficient routing of aircraft through the increasingly crowded airspace.

The expected air traffic increase highlights the need to identify optimal flight trajectories that are adapted for each origin-destination pair, aircraft model (performance) and load, atmospheric conditions, and navigation constrains (restricted areas, altitude and/or speed constraints, time constraints, etc.). Better flight planning would result not only in a better use of the airspace, but also in a reduction of fuel consumption, with a direct impact on the greenhouse gas emissions and, therefore, on the environment. Additionally, the resulted operational cost reductions would benefit aircraft operators, and the economy in general.

An improvement of flight planning performance could be achieved by several methods, individually or in combination, such as:

1. Better aircraft performance models, which would allow a better and a quicker estimation of an aircraft's flight trajectory (space and time evolution) and fuel consumption. For example, a new fuel burn model for constant altitude and speed flight, proposed by Dancila et al. (2013), computes the fuel burned in a selected flight time, and the flight time necessary to burn a selected fuel quantity, faster and with greater precision than the existing methods. This model can be used, for example, to determine the earliest moment when a step climb is possible;
2. Better atmospheric data forecasts, which would yield atmospheric data closer to that encountered by an aircraft during flight. For example, the tailored descent forecast wind method, proposed in Bronsvoort et al. (2011), was designed to improve the predictability of Continuous Descent Operations (CDO) flight trajectories computed by Flight Management System (FMS) platforms. This method generates tailored wind forecasts based on the selected landing procedure, and on high resolution regional forecasts;
3. New navigation strategies, which could yield more flexibility in selecting a flight trajectory that is better adapted for the flight mission. By implementing the

Trajectory-Based Operations (TBO) paradigm (Torres & Delpome, 2012; Cate, 2013), it would be possible for each aircraft to fly along a flight trajectory that is adapted to the specific flight and atmospheric conditions; and

4. New optimization strategies, which would identify faster, and more precisely, globally optimal or near-optimal flight plans/trajectories.

The flight trajectory optimization process can be approached from two main directions as function of the objective of the optimization. In a first approach, the optimizations can be performed at a global level (airspace), in Air Traffic Management System (ATM) platforms. In this case, the main focus is to increase the airspace throughput while maintaining safe operations: ensure the minimum space and time separation between aircraft (Rodionova, Sibihi, Delahaye & Mongeau, 2012; Chaimatanan, Delahaye & Mongeau, 2012), and eliminate or reduce the potential of flight trajectory conflicts (Matsuno & Tsuchiya, 2014). The optimality of a flight trajectory, at aircraft level, is not considered or is secondary to the main objective stated above.

A second approach concerns the optimization of a flight trajectory at the aircraft level, according to a selected criterion (e.g. fuel burn, flight time, or operational costs minimization) and the imposed navigation constraints (e.g. altitude and/or speed constraints along the flight track, time constraints, etc.). An aircraft flight trajectory optimization can be conducted on-board (during the flight), in an FMS platform, or on the ground, in the flight-planning phase (before the flight). The requirements for the on-board optimization methods are stricter, due to the limited computational power available, and to the standards for on-board equipment certification (deterministic algorithms).

Generally, a flight trajectory optimization problem can be defined as an optimal control/guidance problem, where the objective is to identify the control law that will guide the aircraft along the optimal flight trajectory (Soler-arnedo et al., 2010; Soler, Olivares & Staffetti, 2010; Jardin & Bryson, 2012; Park & Clarke, 2012; Bonami, Olivares, Soler &

Staffetti, 2013; Soler et al., 2015; Villaroel & Rodrigues, 2016), or as a search problem, where the optimal flight profile is obtained using search algorithms.

In a study presented in Di Vito et al. (2009), the authors conducted a review of on-board flight trajectory optimization algorithms, strategies, and patents for 2D, 3D and 4D trajectory optimizations. The analysis focuses on identifying the features of the proposed methods, their strengths and weaknesses, and suggests new directions of investigation based on the analyzed solutions. Yu & Zhang (2015) present an extensive survey of the path planning methods, with an accent on flight planning for Unmanned Aerial Systems (UAS).

Multidisciplinary optimization methods (Ceruti, Voloshin & Marzocca, 2014; Ceruti, Fiorini, Boggi & Mischi, 2018) can be applied when the trajectory optimization is part of a higher level ("system") optimization, where part of the optimization process are the selection of the aircraft performing the mission (as a function of capacity, flight performance, and operational costs) and the payload (function of the volume, weight, delivery constraints, premium paid for delivery, delivery penalties, etc.).

Zillies et al. (2014) analyze the achievable improvement in flight efficiency in European airspace if the flight trajectories are optimized for the actual atmospheric conditions (air temperature and winds). Their study considers a flight at constant altitude and speed, where the "candidate" routes are constructed based on the orthodromic route between the limits of the segment to be optimized. A route is composed by a limited number of waypoints (a maximum of six). A Dijkstra search algorithm is applied iteratively in order to identify the best node among five equally spaced nodes constructed at the halfway point between the current node (at the current iteration) and the destination, until the remaining segment length is less than 100 n.m. The authors observed that the detours resulted from following better wind conditions led to savings in fuel and time compared to the orthodromic routes.

Ceruti & Marzocca (2017) devised a method for optimizing the flight trajectory of two airships, modeled by Bezier curves, using a Particle Swarm Optimization algorithm. The two

airships, where one airship is cruising (denoted “cruiser”) and the other is climbing from the ground (denoted “feeder”), must perform an in-flight docking. The optimization algorithm identifies the parameters of the Bezier curves and the target speed at the docking point so that, at the docking point, the two trajectories are tangent, the two airships have identical speeds, and the total energy required for the maneuver is minimal.

Qu, Zhang & Zhang (2014) propose a novel two-step flight path optimization method for Unmanned Aerial Vehicles (UAVs) that fly in a hostile airspace. In a first step, a Dijkstra search algorithm identifies the shortest route through the airspace, determined by selecting nodes of a grid obtained by 3-D Delaunay triangulation of the airspace. In a second step, the shortest route identified in the first step is optimized using an artificial potential field method in order to take into account the weather, aircraft dynamics, and the threats.

Casado, Vilaplana & Goodchild (2013) studied the influence of the uncertainty of aircraft performance parameter estimation for the climb, cruise and descent phases of the flight on the ATM system’s safety, efficiency and capacity. They used a stochastic aircraft performance model generated based on an aircraft performance degradation model, in conjunction with Monte Carlo simulations, to determine the sensitivity of the trajectory prediction error to the aircraft performance model uncertainty for each phase of the flight, and the parameters that are most influenced by these uncertainties.

An aircraft behavioral model (Gillet, Nuic & Mouillet, 2010) based on analysis of historical flight data addresses the need to use realistic aircraft behavior in ATM flight simulations in order to better predict the air traffic conditions.

A method to generate estimations of wind prediction uncertainties, presented by Lee et al. (2009), analyzed each forecast data point of a Rapid Update Cycle (RUC) forecast, and computed their average wind components values as well as the standard deviations (considered as wind uncertainty). This work analyzed the effects of wind uncertainties on aircraft trajectory predictions by comparing the along-track differences between a simulated

flight with predicted winds, and a simulated flight where the uncertainties were added to the forecasted winds.

Dancila & Botez (2016a) addresses the problem of selecting the maximal optimal geographic area for flight trajectory routing, while bounding the maximum total ground distance to a selected value. The authors present a new method for selecting an ellipsoidal routing geographic area, where the ellipsoid parameters are based on the origin and destination of the flight and the selected maximum flight trajectory length.

A method for reducing the number of flight segment performance calculations made during the flight trajectory optimization, proposed by Dancila & Botez (2018), constructs in advance, for each phase of the flight (climb, cruise, and descent) and cruise altitudes, the set of vertical path segments' performance data that cover the aircraft's flight envelope. The flight segment performance data are constructed based on the specific optimization problem: origin – destination pair, aircraft load, set of speeds, and a set of selected landing weights.

Franco & Rivas (2011) analyzed the optimal control problem for a minimum cost cruise at constant altitude, where the initial and final speeds are imposed. The authors study the singular arc section of the bang-singular-bang solution and the cost variation as function of flight time for three wind conditions and two cost index values, as well as for flights with RTA constraints. For flights with RTA constraints, the optimal flight corresponds to the CI value for which the minimum fuel profile yields the RTA.

Chamseddine, Zhang & Rabbath (2012) present a method for re-planning the flight trajectory for a formation of UAVs when one of the UAVs has failures. The objective is to identify the new flight trajectory and the control laws that take into account the limited capabilities of the faulty UAV (does not exceed the limitations imposed for the actuators), maintain the formation structure and the desired separation between vehicles, and minimizes the energy consumption.

A 3D trajectory planning method (Zhou et al., 2013) based on differential evolution uses a chaotic search, performed around the best solution identified for each generation, in order to improve the search results and to escape local optima solutions. A flight trajectory optimization method proposed by Patrón et al. (2015b) performs the optimization of a flight plan using a genetic algorithm. The lateral flight profiles are constructed by selecting nodes from a grid formed by five parallel tracks (the planned flight track and four parallel tracks). First, the vertical flight profile optimization for the climb phase is performed along the planned flight track by evaluating all the speed combinations considered for this phase. Next, for the cruise phase, five parallel tracks (two on each side of the original trajectory) are divided into n segments in order to form the routing grid for the cruise phase. An optimization using a genetic algorithm identifies the optimal cruise flight track for the planned vertical flight profile. An optimization of the vertical flight profile identifies the optimal vertical profile for the optimal flight track identified in the previous step. Finally, the descent phase is optimized by exhaustive evaluation of the descent speed combinations. The flight trajectory method proposed in Patrón & Botez (2015a) is similar to the one presented in Patrón et al. (2015b), with the difference that the lateral and the vertical flight profiles are optimized simultaneously.

The optimization method proposed by Murrieta-Mendoza et al. (2017b) defines the vertical flight trajectory optimization as a discrete combinatory problem (discrete values for the flight speed and altitude), modeled as a decision tree, and uses the Beam Search Algorithm to identify the optimal flight profile. Their method visits the nodes of the decision tree and, in each visited node, uses an optimistic cost evaluation heuristic to prune the decision tree in order to eliminate the non-optimal branches, and to reduce the number of profile calculations. In Murrieta-Mendoza, Ternisien, Beuze & Botez (2018a), a search space reduction method is applied before using the Beam Search Algorithm, which can reduce the search space by 50% and thus is reducing the execution time.

Murrieta-Mendoza, Botez & Bunel (2018b) present the results of a lateral and vertical flight trajectory optimization with RTA constraints using an Artificial Bee Optimization algorithm.

The lateral flight profiles generated during the optimization were constructed based on a dynamic routing grid. A Golden Search algorithm then optimizes the MACH speed for the optimal profile, identified by the bee optimization algorithm, in order to obtain a speed profile with values within a predetermined set. New constant speed segments are introduced in order to observe the RTA constraints.

The 4D flight trajectory optimization method proposed by Murrieta-Mendoza, Hamy & Botez (2017a) models the flight trajectory as a 3D grid (lat, lon, and alt), where the aircraft flies at the ECON speed and, at each node, the aircraft may advance only to neighboring grid nodes. The Mach speed profile is then optimized along the 3D profile using an Ant Colony Optimization algorithm, so that the RTA constraint is observed (4D).

This paper presents a flight trajectory optimization method based on Genetic Algorithms (GA). The proposed method is designed to determine the “best” flight trajectory for the selected origin – destination pair, aircraft model (performance characteristics) and load, atmospheric conditions, candidate flight profile characteristics, optimization criteria, and imposed constraints. This method is intended to be used by flight operators, in the planning phase (before a flight), or for flight plan update/change during a flight, on ground-based computers. The resulted optimal flight plans will be then uploaded to the aircraft.

4.2 Methodology

This section is structured as follows: The first sub-section (4.2.1) presents the concepts related to flight trajectory optimization. The next sub-sections describe the aircraft performance model used in this study (4.2.2), the atmospheric data model used in the flight trajectory performance calculations (4.2.3), and the elements of a flight trajectory (4.2.4) (i.e. the characteristics of the set of candidate flight trajectories evaluated in the optimization, and the methodology used to construct them). The following two sub-sections present the methodology used for computing the flight performance parameters for a flight trajectory through accelerated flight performance calculation (4.2.5), and the proposed optimization

method based on the genetic algorithm (4.2.6). Finally, the last sub-section (4.2.7) presents the flight data used for constructing the test cases and the reference flight plan (to evaluate the performance of the proposed method).

4.2.1 Flight trajectory optimization

The objective of a flight trajectory optimization process is to identify the optimal flight profile for a particular optimization problem defined by aircraft model (flight performance and envelope limitations), initial aircraft load and fuel quantity, initial and final trajectory points data and constraints (crossing time at the initial point, initial and final aircraft geographic locations, altitudes and speeds), navigation constraints, atmospheric conditions, and selected optimization criteria. The optimization criterion is, in general, the minimization of a cost function (e.g. minimization of fuel burn, total cost, flight time, etc.). However, it can also be a maximization of the cost function (e.g. maximum loitering time, etc.).

An aircraft flight trajectory can be decomposed into two components:

1. A lateral flight profile, represented by the projection of the flight trajectory on the Earth's surface; and
2. A vertical flight profile, defined by the evolution of the aircraft's flight parameters (e.g. altitude, speed, vertical speed/rate of climb or descent/angle of climb or descent, acceleration/deceleration, load factor, etc.) along the lateral flight profile.

In still air (no wind), International Standard Atmosphere (ISA) conditions, and in the absence of navigation constraints, the optimal lateral flight profile is the orthodromic route (the shortest route on the sphere/ellipsoid) between the initial and final point of the flight plan under optimization. The optimal vertical flight profile is specific for the aircraft model, aircraft weight, and the cost function selected as optimization criterion. When real atmospheric conditions are taken into account (i.e. wind and non-standard atmospheric temperature conditions), it may be advantageous to deviate from the orthodromic route, and

to perform altitude and speed changes in order to benefit from more advantageous wind and air temperature conditions.

A flight trajectory optimization process is conducted by successively evaluating flight trajectory profiles from a set of candidate flight profiles, and, in each step, by retaining as solution the “best” flight profile relative to the cost function and criterion set as objective for the optimization. The optimization process can be conducted for only one or for both components of the flight profile. In the former case, one of the components of the flight plan (lateral or vertical) is common for all the candidate flight plans, and the other component is different for each candidate flight plan. In the latter case, both of the flight plan components can change.

The methodologies used to generate the set of candidate flight plans, and select the flight plan to be evaluated at each step of the optimization process, are heuristic methods, selected as function of the specific optimization problem, selected cost function, constraints, etc.

For flight plans with navigation constraints (e.g. altitude, time, etc.), the constraints take precedence relative to the flight profile’s optimality. If the constraints are not satisfied, the flight plan is considered non-valid and rejected. Similarly, a flight plan is considered non-valid and is rejected if:

1. The flight profile generated based on the flight plan yields aircraft flight parameters that are beyond the aircraft’s flight envelope boundaries; or if
2. The flight along the resulted flight profile requires more fuel than is available.

The particular optimization problem considered in this paper is specific for the cases where:

1. The flight plans do not have navigation constraints;
2. Both the lateral and vertical components of the flight plan can be modified during the optimization; and
3. The objective is to minimize of the total cost for the flight.

The total cost for a flight is calculated as the sum of the fuel cost and the operational costs, which are proportional with the flight time, and are expressed as fuel quantity (kg of fuel). A detailed presentation of the total cost function, and the elements that contribute to it, can be found in Robertson (2007a), Robertson, Root & Adams (2007b), and DeJonge & Syblon (1984).

The total cost is calculated using the following formula:

$$TC = fuel\_burn + CI \times flight\_time \times 60 \quad (4.1)$$

where:

1. *TC* is the total cost, expressed in terms of fuel quantity [kg of fuel];
2. *fuel_burn* is the fuel burned for the flight along the evaluated flight profile [kg of fuel];
3. *flight_time* is the flight time for the flight along the evaluated flight profile [h]; and
4. *CI*, the Cost Index, is a constant (specific for each airline, aircraft type and route) that converts the flight time into operational costs expressed in terms of fuel quantity [kg of fuel / min].

The CI value adjusts the optimization in order to obtain a trade-off between the fuel consumption and the flight time; the larger the CI value the greater the weight that is attributed to the reduction of the flight time in the optimization process.

If *CI* = 0, the optimization criterion becomes the fuel burn minimization. When the *CI* value reaches a maximum value (e.g. 999), specific for a platform, the optimization criterion becomes the flight time minimization.

The flight performance and the aircraft dynamics (e.g. fuel burn, flight time, speeds, accelerations, traveled distances, etc.) parameters are calculated by performing an accelerated simulation of the flight along the evaluated flight profile. These calculations are performed

using an Aircraft Performance Model (APM) specific for the aircraft type, the atmospheric data along the flight profile (wind and air temperature), the aircraft's configuration parameters (mass, engine thrust setting, landing gear, flaps and speed brake positions, etc.), and the flight profile's data (speed, climb/descent angle, bank angle, load factor, etc.).

The method presented in this paper does not take into account any navigation constraints (such as restricted areas or airways, Required Time of Arrival - RTA, etc.), and adopts the TBO / "free flight" paradigm; the aircraft is thus free to fly along the trajectory that is best suited for the origin – destination pair, atmospheric conditions, aircraft performance, and load.

4.2.2 Aircraft Performance Model (APM)

The APM used in this study is the Base of Aircraft Data (BADA) version 4.0 (Eurocontrol, n.d.), developed and maintained by Eurocontrol. The APM provides specific aircraft type data (i.e. mathematical models and the related coefficients for the aircraft parameters, valid aircraft flight configurations, flight envelope limitations, etc.), a methodology for calculating the aero propulsive forces acting on the aircraft, the aircraft motion as a result of these forces (equations based on the Total Energy Model - TEM), and the associated fuel burn. An overview of the BADA APM can be found in Eurocontrol (n.d.) and Nuic et al. (2010a), Eurocontrol (2010) (for BADA version 3.7) and Nuic (2010b) (for BADA version 3.8). Specific information regarding the BADA version 4.0 APM can be obtained from Eurocontrol (n.d.) upon request, and is subjected to a license agreement.

The set of input parameters used in the calculation of the flight performance parameters, and in the aircraft's evolution along the flight path, their range of valid values and units of measurement, are specific for the APM. As an example, the input parameters can be:

1. Aircraft configuration parameters: aircraft mass, center of gravity position, landing gear position, flaps/slats position, spoilers/speed brakes position, etc.;

2. Engine parameters: These parameters are specific to the engine type. For a jet engine, they can be the Thrust Lever Angle (TLA), engine fan speeds, etc.;
3. Atmospheric conditions: air temperature and wind; and
4. Flight trajectory parameters: altitude, speed, acceleration/deceleration, bank angle, load factor, climb/descent angle, rate of climb/descent, etc.

A flight trajectory is composed of a succession of elementary flight profile types (e.g. constant speed cruise segment, acceleration/deceleration cruise segment, constant speed constant TLA climb/descent, constant TLA constant rate of climb accelerated climb segment, etc.). Function of the type of evaluated flight profile, some of the parameters presented above are input parameters and others are output parameters (resulted from the flight performance calculations). For example, for a cruise segment at constant altitude and constant speed, a selected speed (an input parameter) will require a specific engine thrust setting, and thus, a fuel burn rate (output parameters), to maintain the selected speed and altitude. Conversely, a selected engine thrust setting (an input parameter) will determine the speed and fuel burn rate (output parameters). The flight trajectory performance calculation model, developed using the APM, implements a specific performance calculation function for each elementary flight profile type and set of output parameter(s) of interest.

4.2.3 Atmospheric data

Atmospheric conditions have an important influence on aircraft flight performance characteristics and dynamics. The air temperature influences the engine performance and, as a result, it affects the available thrust, the maximum altitude for a selected speed, the minimum and maximum speeds at a selected altitude, the fuel burn rate, etc. The aircraft speed along the flight trajectory is defined in terms of Indicated Air Speed (IAS) or MACH number. The aircraft's aerodynamic characteristics are functions of the True Airspeed (TAS), which is the aircraft's speed relative to the mass of air. The aircraft's evolution along the flight trajectory is a function of the ground speed (GS), which is the aircraft's speed relative

to the ground. The TAS value, computed as function of the active speed value and its type (IAS or MACH), is affected by the air temperature and static pressure values.

For MACH speeds, the *TAS* is expressed only as function of the air temperature (Botez, 2006):

$$TAS = M\sqrt{\gamma RT} = M\sqrt{\gamma RT_0}\sqrt{\frac{T}{T_0}} = Ma_0\sqrt{\theta} \tag{4.2}$$

where:

1. M is the MACH number;
2. $\gamma = 1.4$ is the adiabatic index for air;
3. R = 287.05 J/kg/ºK is the universal gas constant for dry air;
4. T is the air temperature [ºK];
5. T_0 = 288.15 ºK is the standard air temperature at Sea Level Altitude (SLA), considered as 0 ft, in International Standard Atmosphere (ISA) conditions;
6. $a_0 = \sqrt{\gamma RT_0} = 340.29\ m/s$ is the speed of sound at SLA in ISA conditions;
7. $\theta = \frac{T}{T_0}$ is the air temperature ratio relative to the ISA SLA air temperature.

For a flight in the IAS speed mode, in the subsonic regime, when the air compressibility effects are neglected, the relationship between the *TAS* and the *IAS* is described in Botez (2006):

$$TAS = a_0\sqrt{5\theta\left[\left(\frac{q_c}{p_s} + 1\right)^{3.5} - 1\right]} \tag{4.3}$$

where q_c is the dynamic pressure computed for the *IAS* speed at the SLA in ISA conditions:

$$q_c = p_{s0}\left\{\left[1 + 0.2\left(\frac{IAS}{a_0}\right)^2\right]^{3.5} - 1\right\} \tag{4.4}$$

and:

1. a_0 is the speed of sound at SLA in ISA conditions;
2. θ is the air temperature ratio relative to the ISA SLA air temperature;
3. p_s is the static air pressure at the flight altitude (pressure altitude);
4. $p_{s0} = 101325\ Pa$ is the static air pressure at SLA (0 ft) in ISA conditions; and
5. *IAS* is the scheduled speed that is converted to TAS.

An aircraft flight trajectory is composed of segments defined by a set of fixed geographic points (Waypoints – WPTs) selected between the departure and destination points. In still air, in the absence of winds, the aircraft's heading is the segment heading at the aircraft location and the GS is equal to the TAS. In the presence of winds, for the aircraft's trajectory to follow the segment's track, the aircraft's heading must change (a process called "crabbing") so that the GS vector's direction, resulted from the vectorial summation between the TAS and wind vectors, is oriented along the segment's heading at that location. The GS value and the aircraft's crabbing angle (α_{CRB}) relative to the segment heading are computed using the wind triangle algorithm (Botez, 2006). Their expressions are:

$$\begin{cases} GS = \left(W_V\, cos\alpha_{Segm} + W_U\, sin\alpha_{Segm}\right) + \sqrt{\begin{matrix}(TAS\, cos\alpha_{CD})^2 - \\ \left(W_V\, sin\alpha_{Segm} - W_U\, cos\alpha_{Segm}\right)^2\end{matrix}} \\ \alpha_{CRB} = \dfrac{180}{\pi} arcsin\left(\dfrac{W_V\, sin\alpha_{Segm} - W_U\, cos\alpha_{Segm}}{TAS}\right) \end{cases} \tag{4.5}$$

where:

1. *GS* is the ground speed;
2. α_{CRB} is the aircraft's crabbing angle relative to the segment heading;
3. *TAS* is the true air speed;

4. W_V and W_U are the wind speed components along the geographic North and East axes;
5. α_{CD} is the aircraft's climb/descent angle; and
6. α_{Segm} is the flight trajectory segment's heading, relative to the geographic North, at the aircraft's location.

Equations (4.3), (4.4) and (4.5) show that the air temperature and the wind affect the *TAS* and the *GS* values. This influence, in turn, affects the flight performance (lift, drag, required thrust, etc.) and the flight trajectory/dynamics: the flight times along and/or the lengths (ground distances) of the segments composing the flight profile (climb/descent distances, climb/descent speeds, rate of climb/descent, etc.). For an accurate estimation of the aircraft's trajectory and flight performance parameters, it is therefore necessary to perform the calculations using atmospheric conditions that are as close as possible to the real conditions encountered during flight.

The atmospheric conditions (i.e. air temperature and wind) are constantly changing and, at each time instance, their values are different, function of the geographic location (latitude and longitude) and the altitude of the point where they are measured. The atmospheric data used in flight performance calculations are generated based on prediction data issued by meteorological agencies. Due to the chaotic nature of the atmosphere and to the limitations of the atmosphere models used in the prediction process, the atmospheric data predictions issued by the meteorological agencies may differ from the real atmospheric conditions occurring at the prediction location (latitude, longitude and altitude) and time. The magnitudes of the prediction errors vary as function of forecast type (global or regional) and resolution (forecast grid size), the time of the year, time of day (day or night), region, how far ahead in time is the prediction made for, etc. (Stohl, 1998; Cole et al. 2000; Schwartz et al, 2000; Lee et al., 2009; Vaddi et al., 2013).

The atmospheric data used in this study is a Global Deterministic Prediction System (GDPS) (Environment Canada, n.d.a) forecast issued by Environment Canada in GRIB2 (Environment Canada, n.d.g; NOAA, n.d.a) data file format. GDPS is a global level forecast,

issued twice a day, at 00h and 12h Coordinated Universal Time (UTC), that provides atmospheric data forecasts in the nodes of a 4D grid (latitude, longitude, pressure altitude and time) in the following format:

1. On a latitude-longitude map projection, available with two grid resolutions: 0.25x0.25 (Environment Canada, n.d.b) and 0.6x0.6 (Environment Canada, n.d.c) degrees;
2. At a fixed set of 27 isobaric levels (pressure altitudes); and
3. The forecasts are made at 3h intervals, for 240 hours for the 0.25x0.25 grid, and 144 hours for the 0.6x0.6 grid.

Therefore, each atmospheric parameter of interest (air temperature and wind) can be computed as a function $f(lat, lon, p_s, t)$ of the location of the point where they are evaluated (latitude, longitude, and pressure altitude), and the time instance for which it is evaluated.

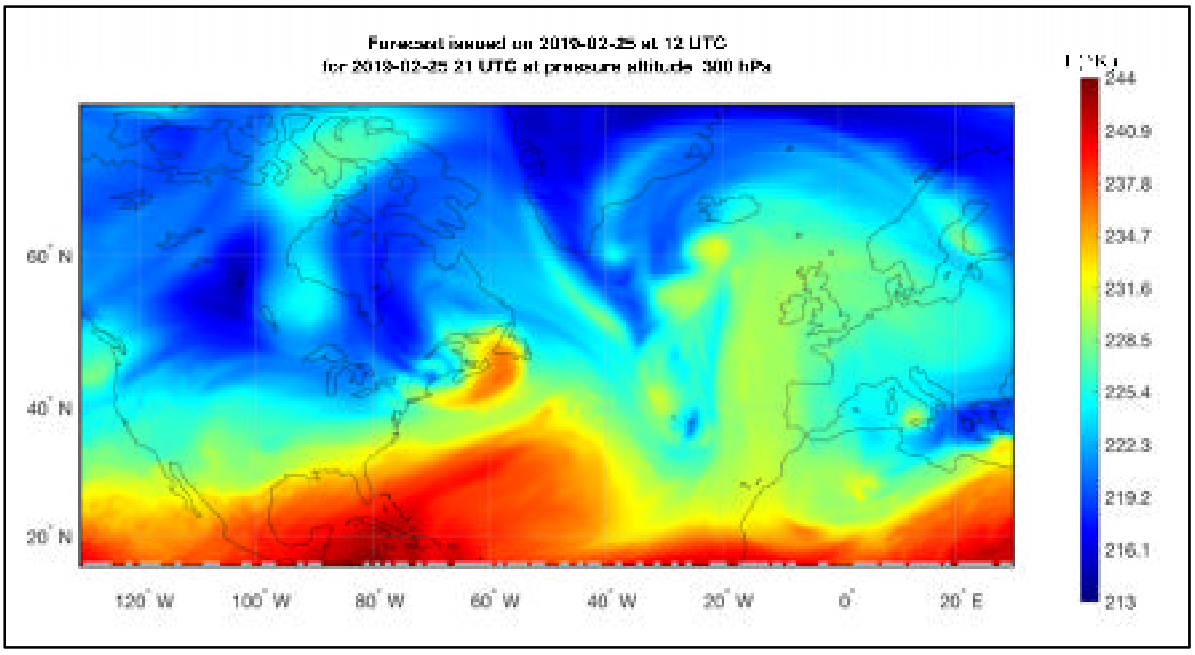

Figure 4.1 Example of air temperature forecast data issued by Environment Canada on Feb. 25th, 2019 at 12 UTC for Feb. 25th, 2019 at 21 UTC, at 300 hPa pressure altitude

Graphical illustrations of a GDPS atmospheric data forecast (air temperature and winds) on a 0.6x0.6 degrees grid, issued by Environment Canada, on February 25th, 2019, at 12:00 UTC, for February 25th, 2019, 03:00 UTC, at a pressure altitude of 300 hPa (30,065 ft), cropped to a geographic area delimited by the latitudes 10ºN and 75ºN and the longitudes 130ºW and 30ºE, are presented in Figure 4.1 and Figure 4.2.

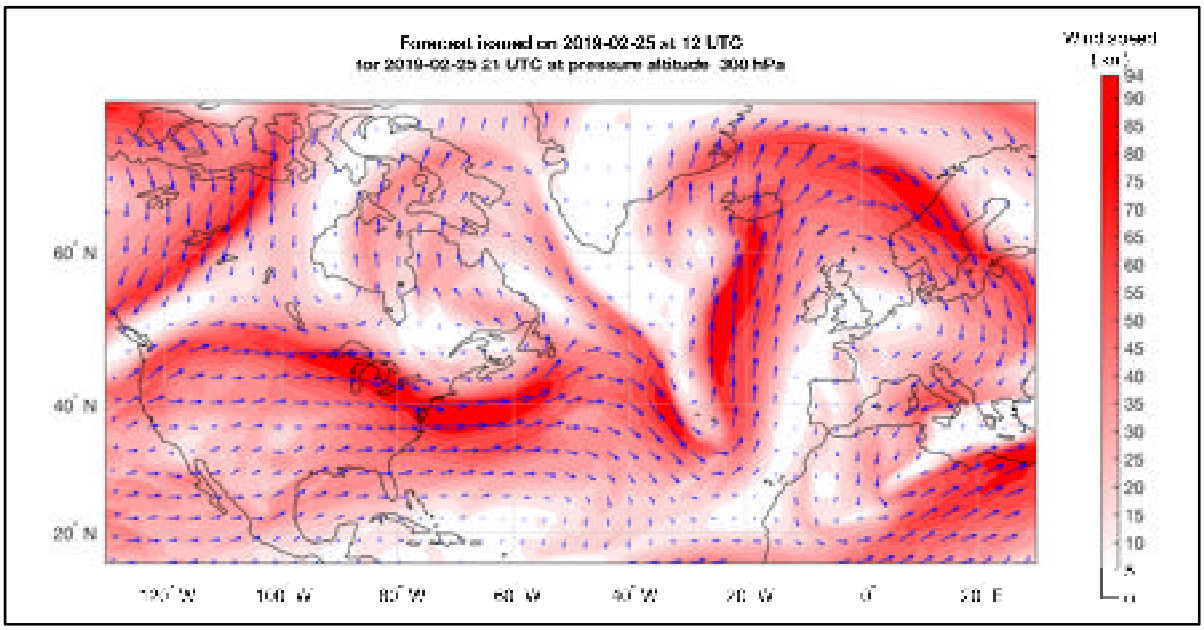

Figure 4.2 Example of wind forecast data issued by Environment Canada
on Feb. 25th, 2019 at 12 UTC for Feb. 25th, 2019 at 21 UTC,
at 300 hPa pressure altitude

The atmospheric parameters in a point other than a node of the forecast's 4D grid are computed by interpolation. The method selected in this study for atmospheric parameter interpolation is the "4D linear interpolation", predominantly used in flight trajectory optimization algorithms and flight trajectory performance calculations (Stohl et al. 1995; Stohl, 1998; Schwartz et al., 2000; Rubio & Kragelund, 2003; Zhang & McGovern, 2008; Wynnyk, 2012; Wickramasinghe et al., 2012; Jensen et al., 2015). More complex interpolation methods (such as quadratic, bicubic, spline, polynomial, etc.) are potentially more precise, but they are slower than the 4D linear interpolation. These interpolation methods have often been used in the literature (Soler-arnedo et al., 2010; Fukuda et al., 2010;

Soler et al., 2011; Soler et al., 2015), on ground-based platforms, in conjunction with regional atmospheric data forecasts and near horizon flight profile predictions such as the descent phase of a flight / CDO (Jin, Cao & Sun, 2013). Regional atmospheric data predictions, such as RDPS (Environment Canada, n.d.e) and RUC (Schwartz et al., 2000), are short time forecasts issued for a reduced geographic area, updated with a much higher rate, and are more precise.

4.2.4 Flight trajectory / flight plan

Generally, an aircraft flight trajectory can be very complex, limited only by the aircraft's performance capabilities (flight envelope limitations), pilot abilities and the required workload (if a maneuver is performed in manual mode), or the FMS/autopilot capabilities. Additional constraints are imposed by navigation and safety regulations, and passenger comfort.

In the fields of flight trajectory planning and optimization, ATM, and FMS, a flight trajectory is defined by a flight plan (Altus, 2009; FAA, n.d.a) that contains all the information regarding the intended evolution of the aircraft, in a concise and standard format. The flight plan contains all the information necessary to predict the precise space-time evolution of the aircraft. The flight trajectory description using a standard format is a result of the necessity to:

1. Reduce the complexity of flight profiles;
2. Easily construct the flight trajectory in the ATM and FMS platforms, based on the submitted/selected flight plan;
3. Implement the functionalities required for the calculation of the aircraft flight performance parameters and the aircraft flight dynamics, along a selected trajectory, through accelerated simulation, in order to:
    a. Compute flight performance parameters (e.g. fuel burn, flight time, etc.);
    b. Ensure that the flight parameters (e.g. altitude, speed, etc.) remain within the aircraft's flight envelope limits;

c. Evaluate the aircraft's position relative to the flight plan, and follow the planned trajectory (FMS);
d. Evaluate possible conflicts with other aircraft within the same airspace region (ATM); and
e. Validate the flight plan relative to imposed navigation constraints, fuel requirements, etc.

As mentioned in sub-section 4.2.1, an aircraft flight trajectory can be decomposed into two components:

1. A lateral flight profile, representing the projection of the flight trajectory on the Earth's surface; and
2. A vertical flight profile, defined by the evolution of the aircraft's flight parameters along the lateral flight profile.

Accordingly, a flight plan has a lateral and a vertical component, corresponding to the two components of the flight trajectory.

4.2.4.1 Lateral flight plan description and the resulting lateral flight profile

The lateral flight plan defines the segments composing the lateral flight profile:

1. The sequence of waypoints (WPTs) that define the lateral flight profile segments overflown by the aircraft (geographic locations defined by pairs of latitude and longitude coordinates); and
2. The lateral flight profile segment type(s): loxodromic or orthodromic (Lenart, 2017) – see Figure 4.3 below.

A loxodromic segment (represented by the red line in Figure 4.3) has the property that, in every point on the segment, the departure heading required to advance along the segment is constant. However, a loxodromic segment is not the shortest route between two points on a sphere or on an ellipsoid.

An orthodromic segment (represented by the yellow line in Figure 4.3) is the shortest route between two points on a sphere/ellipsoid (the geodesic or great circle that connects two geographic points). On an orthodromic route, the segment heading is not constant; it varies from the departure WPT (beginning of the segment) to the arrival WPT (end of the segment).

Although the orthodromic route between two geographic locations is the shortest flight distance between two points, aircraft do not necessarily follow an accurate orthodromic route due to air traffic constraints, atmospheric conditions (in order to avoid strong head winds and/or turbulence), navigation constraints, etc. The blue line in Figure 4.3 illustrates the lateral flight profile of a real flight, flight SWR40 between Zurich (ZHR) and Los Angeles (LAX), on Feb. 25th, 2019, retrieved from the FlightAware website (FlightAware, 2019a).

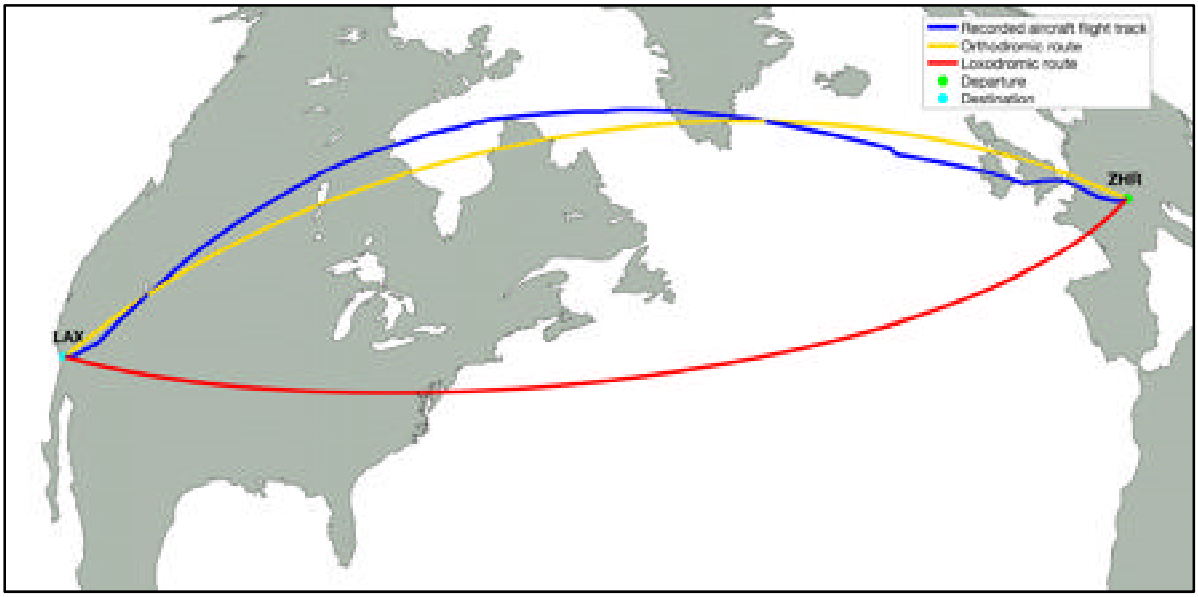

Figure 4.3 Illustration of orthodromic and loxodromic routes, and a recorded flight track (FlightAware, 2019a) between Zurich (ZHR) and Los Angeles (LAX)

Two consecutive WPTs from the lateral flight plan define a flight profile segment, and, together with the segment type information, determine the segment's SLA length, and the departure and arrival headings (the angle relative to the geographic North) in each point along the segment. Conversely, given the initial WPT of a segment and the segment type, the

departure heading from the initial WPT, and the SLA for a point of interest, it is possible to compute the geographic coordinates of the point of interest and the arrival heading at this point.

For a loxodromic segment, the calculations of various parameters (SLA length, the segment heading, the coordinates of a point situated at a given SLA distance, etc.) are performed using the rhumb line equations (Carlton-Wippern, 1992) for the Earth model (spherical or ellipsoid). For orthodromic segments, the calculations are performed differently as they are function of the Earth model used: spherical trigonometry for a spherical earth model, and Vincenty's formulas (Karney, 2013) for an ellipsoid Earth model.

The segment's length at the aircraft's flight altitude is obtained by multiplying the SLA distance with a correction factor calculated as:

$$c_{f\_dist} = \frac{R_{earth} + h_{geom} \times FT\_TO\_NM}{R_{earth}} \tag{4.6}$$

where:

1. c_{f_dist} is the segment length correction factor with altitude;
2. R_{earth} = 3,440.1 [n.m.] is the Earth radius;
3. h_{geom} is the aircraft geometric altitude relative to the sea level, in ft; and
4. FT_TO_NM = 16.457884 x 10^{-5} is the ft to n.m. conversion factor.

As an example, for a geometric altitude of 36,000 ft, c_{f_dist} = 1.0017222.

4.2.4.2 Vertical flight plan description and the resulting vertical flight profile

A vertical flight plan defines, in a succinct form, the aircraft's altitude - speed evolution along the lateral flight profile, and specifies the locations (WPTs) along the lateral flight plan segments where the planned vertical flight profile parameter changes occur (e.g. altitudes and

speeds), as well as the new values for the parameters that change. In this paper, it is assumed that the vertical flight plan defines the locations along the lateral flight plan where the changes are initiated (e.g. at the beginning of an acceleration/deceleration to a new speed, at the beginning of a climb/descent to a new flight altitude, etc.). A vertical flight plan (profile) can be decomposed into seven main phases: take-off, initial climb, climb, cruise, descent, approach, and landing. Each flight phase can include one segment or a succession of vertical flight plan segments.

The vertical flight profile, generated by the vertical flight plan, is obtained following the accelerated flight performance calculations (see sub-section 4.2.5). Each flight plan segment is decomposed in a succession of "standard" type segments, segments in which the control parameters and the mathematical models describing the aircraft's evolution (the dynamic and the status parameters) do not change (e.g. a constant altitude constant speed segment, a constant altitude acceleration segment, a climb segment at constant speed and constant climb angle, a climb segment at constant speed and rate of climb, etc.).

The set of parameters that define a vertical flight plan segment are specific for the flight segment type. The values of a vertical flight plan segment parameter can be specified:

1. Explicitly, provided as input;
2. Implicitly, when the parameter value:
    a. Is "inherited": does not change relative to the value it had at the end of the previous vertical flight plan segment; or
    b. It results from the flight performance parameter calculation (e.g. the geographic location where a constant altitude acceleration/deceleration segment ends, the geographic location where a climb segment ends, the altitude and geographic location where an accelerated climb segment ends, etc.).

The climb and descent sections are flown at "scheduled speed", defined as an [IAS, MACH] speed pair. The speed mode switch (between IAS and MACH) takes place at the crossover

altitude, defined as the altitude where the TAS computed from the IAS, described by Eq. (4.3), is equal to the TAS computed from the MACH speed, given by Eq. (4.2). The IAS speed is in effect below the crossover altitude, and the MACH speed is above the crossover altitude. The reason for the speed mode change at the crossover altitude is that a climb at constant IAS speed beyond the crossover altitude would result in a MACH speed beyond the maximum MACH operating speed limit (MMO); similarly, a descent at constant MACH below the crossover altitude would result in an IAS speed beyond the maximum operating speed limit (VMO). An example of a climb speed profile is presented in Figure 4.4, where the flight plan starts when the aircraft is at an altitude of 10,000 ft and a speed of 250 kn IAS, and defines a climb segment at [300 kn IAS, 0.80 MACH] to the cruise altitude (33,000 ft). Following the accelerated flight performance calculations, the resulting flight profile is composed of three segments:

1. An acceleration in climb, from 250 kn to the scheduled speed climb IAS (300 kn), which starts at 10,000 ft, and ends at an altitude that is a function of the aircraft performance parameters, such as weight, etc.;
2. Climb at constant IAS (300 kn) to the crossover altitude (30,594 ft); and
3. Climb at constant scheduled speed MACH (0.8) to the cruise altitude (33,000 ft).

It should be noted that the positions along the lateral flight plan segments (lateral flight profile) where the accelerated climb segment and the constant speed climb segments end are determined during the accelerated flight performance calculations. These positions are not only dependent of the flight plan speeds but also dependent of the aircraft flight performance characteristics, weight, and atmospheric conditions.

The structure of a descent altitude - speed profile is similar to that of a climb altitude - speed profile, except that the evolution along the profile is reversed.

The cruise phase is composed by a succession of constant altitude and climb (step climb) segments flown at MACH speed (constant speed, acceleration or deceleration segments). Generally, descent segments (step descents) are not employed, as the aircraft performance is

better at higher altitudes, and repeated sequences of step climbs and step descents result in an increased number of pressure change cycles on the airframe, and increase the maintenance costs.

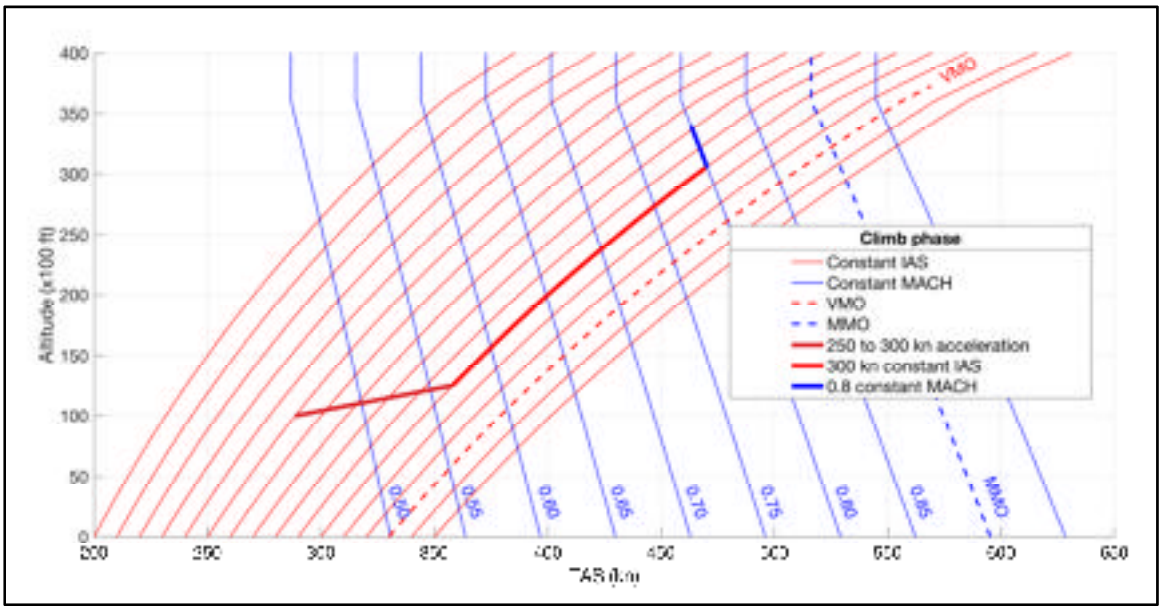

Figure 4.4 Example of altitude - speed profile for the climb phase of a flight

Figure 4.5 shows an example of an altitude profile for the climb, cruise, and descent phases of a real flight (flight Swiss SWR40, from Zurich to Los Angeles, flown on Feb. 25th, 2019), as retrieved from FlightAware (FlightAware, 2019a). The altitude profile data presented in Figure 4.5 have been selected to show the trajectory for altitudes above 10,000 ft.

The transition between the climb and the cruise sections of the flight trajectory occurs at the Top of Climb (TOC), the point where the aircraft reaches the cruise altitude. The transition between the cruise and the descent sections of the flight trajectory occurs at a point denoted as the Top of Descent (TOD), where the aircraft initiates the descent. Another important point along the vertical flight profile is the End of Cruise (EOC), situated in the cruise section of the vertical flight profile, at a preset sea level distance from the final point of the descent. The EOC is the point along the flight trajectory beyond which the accelerated flight

performance calculation function performs the calculations in “Descent” mode, which is a methodology specific for the descent phase of the flight. A more detailed presentation regarding the TOC, EOC and TOD positions along the lateral flight profile is provided in the next sub-section (4.2.5). Figure 4.6 illustrates the TOC, EOC, and EOD positions along the altitude flight profile.

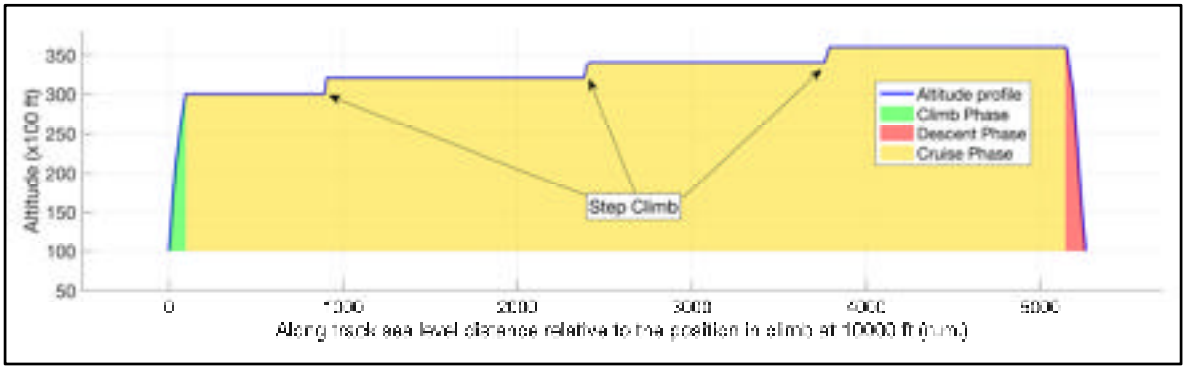

Figure 4.5 Example of altitude profile Flight SWR40, Zurich to Los Angeles, on Feb. 25th, 2019 Data for altitudes above 10,000 ft, as retrieved from FlightAware (FlightAware, 2019a)

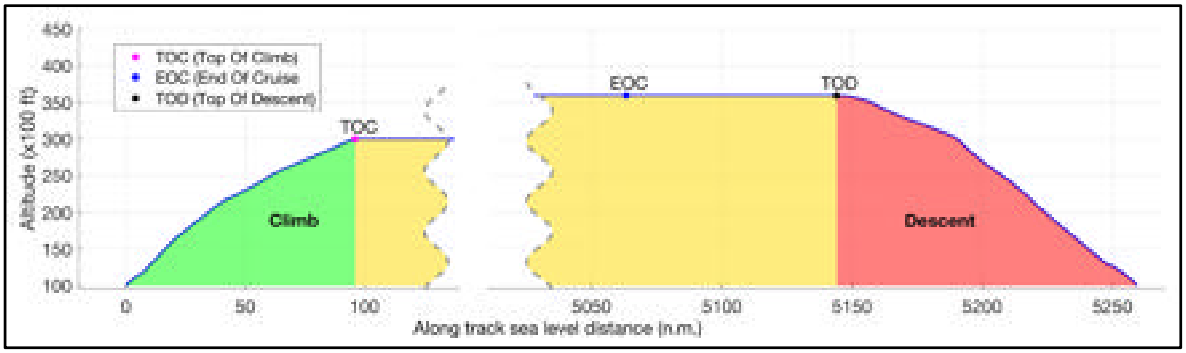

Figure 4.6 Illustration of the TOC, EOC and TOD positions along the altitude flight profile

4.2.5 Accelerated flight performance calculation

The aircraft model developed based on the APM provides a set of functions that compute the flight performance parameters and the aircraft dynamics for each "standard" flight profile segment type that can be used to construct a flight trajectory, as well as to evaluate the flight parameters relative to the aircraft's flight envelope.

The evolution of the aircraft along the selected flight trajectory, the flight performance and the aircraft status parameters are computed iteratively, segment by segment, starting from the initial point, by accelerated simulation:

1. The flight trajectory is constructed as a succession of "standard" segments;
2. Each segment of the flight trajectory is decomposed in sub-segments (integration steps);
3. The parameter along which a segment is decomposed into sub-segments (time, distance, altitude) depends upon the segment's type;
4. The integration step size (sub-segment decomposition step size) is chosen as a result of a tradeoff between the estimated result precision and computation time. Larger step sizes would result in a smaller number of sub-segments and, therefore in faster calculation. However, this would reduce the accuracy of the results;
5. For each sub-segment, the specific parameters are calculated in a point on the sub-segment (situated along the decomposing/integration parameter dimension) using the appropriate evaluation function, aircraft configuration, atmospheric conditions, etc.;
6. The performance parameters for the sub-segment are obtained by integration: the parameters returned by the function are multiplied by a factor computed based on the integration step size; and
7. The aircraft's state and configuration parameters, and its position along the lateral flight profile are updated. The new values become the input data for the trajectory performance calculation on the next sub-segment.

At each step, the aircraft performance parameters, its state, position and dynamics are validated relative to the flight envelope limitations (such as altitude and speed), fuel quantity on board, flight trajectory and navigation constraints, etc.

The methodology used for constructing the flight trajectory profile and computing the performance parameters is presented in Schreur (1995). The flight trajectory construction and the flight performance parameter calculation start from the initial point of the flight plan (initial geographic location and altitude), with the initial aircraft status parameter values (zero fuel weight, fuel quantity, center of gravity position, speed, climb angle, bank angle, etc.), and the time instance when the aircraft crosses the initial point of the flight plan. The climb phase is computed first, followed by the cruise phase. The TOC location, the point where the aircraft reaches the cruise altitude, is determined by the climb profile calculation module. The cruise phase calculations stop at a preset sea level distance from the final point of the flight plan (EOC), heuristically selected so that it is further away from the destination than the beginning of the descent flight profile (TOD). The aircraft weight and crossing time at the final point of the flight profile (flight plan) are then estimated using a heuristic, and the estimated values are used to construct the descent flight profile. The descent flight profile is constructed in reverse order (backwards integration), from the final point of the descent flight plan to the TOD, at the cruise altitude and speed. At this stage, the geographic location of the TOD and the aircraft crossing time at the TOD are known. Finally, the performance parameters are computed for last segment of the cruise flight profile, delimited by the EOC and the TOD. The validation of the estimated aircraft weight and crossing time at the end of the flight profile is performed by comparing their values obtained at the TOD: the values obtained from the descent profile calculations with the values obtained from the cruise profile calculations. If the aircraft weight and/or the crossing time difference are larger than selected threshold values, considered acceptable, then the estimated values at the end of the descent are corrected (based on the difference obtained for the parameter value) and the process is started again: a new decent profile computation, EOC to TOD profile calculation and comparison between the obtained values. The process stops when both the time

difference and the aircraft weight difference are smaller than the selected threshold values. Figure 4.7 shows a flowchart of the accelerated flight profile calculation process.

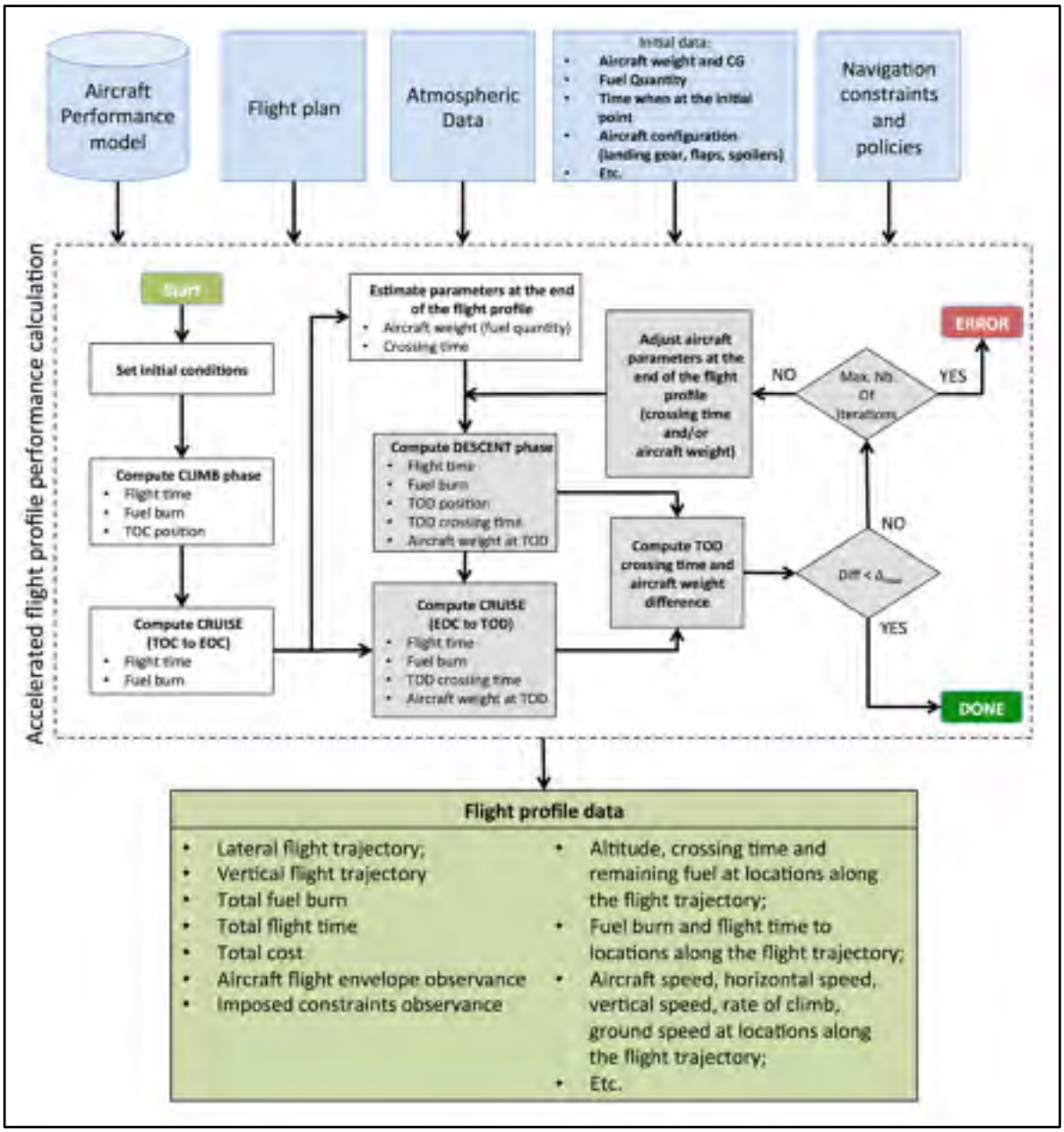

Figure 4.7 Accelerated flight profile calculation process flowchart

Navigation constraints (such as altitude, speed, RTA, etc.), assigned at different points along the flight path, are validated by comparison with their corresponding values resulting from the flight performance calculations.

4.2.6 Optimization method

The optimization method presented in this paper is intended for flight trajectory (sub-section 4.2.4) optimization, where both the lateral and vertical flight profiles modifications are considered. For a specific optimization problem, defined by:

1. Aircraft model (flight performance data), load (weight), and on-board fuel quantity;
2. Geographic locations of the initial and final points of the flight trajectory;
3. Aircraft flight altitude and speed at the beginning and at the end of the flight profile under optimization;
4. Navigation policies such as: climb at Maximum Climb (MCMB) TLA, IDLE descent, climb/descent mode (e.g. vertical speed, climb/descent angle, rate of climb/descent), etc.;
5. Selected values for the range of cruise altitudes, and the maximum deviation from the orthodromic route between the beginning and the end of the flight trajectory under optimization; and
6. Optimization criterion: minimization of fuel burn, flight time, or total cost.

the algorithm implementing the proposed optimization method identifies the “optimal” flight plan: the combination of lateral (sub-section 4.2.4.1) and vertical (sub-section 4.2.4.2) flight plans that minimizes the selected cost function.

The optimization problem presented in this paper considers a discrete / combinatorial optimization with a very large number of candidate solutions, determined by the characteristics of the family of candidate flight plan solutions (sub-section 4.2.6.1 and sub section 4.2.6.2). Some of the parameters that are used in the calculations (e.g. the atmospheric conditions, aircraft performance model) are defined by piecewise functions. The evolution of the aircraft is described by piecewise functions due to the decomposition in sub-

segments on which the mathematical model that describes the evolution of the aircraft and flight parameters do not change (please see sub-section 4.2.5 which describes the methodology used to compute the flight performance for a flight plan). Moreover, the total cost is expressed by a complex and non-linear function due to the relationship between the parameters that determine the total cost (fuel burn, flight time) and the input parameters: aircraft weight, flight plan parameters (altitude and speed flight profile), and atmospheric conditions. The total cost of a flight segment depends not only on its selected parameters but also on previous flight profile segments parameters. The aircraft weight, altitude, and crossing time at the beginning of a segment result from the fuel burn and flight time on previous segments (therefore, their flight profile characteristics). This fact affects the aircraft's performance characteristics and the atmospheric conditions encountered on the segment, which affect the fuel burn and the flight time and, therefore, the segment's total cost. This optimization problem might have multiple local minima and many ("near") optimal solutions. For these reasons, the optimization method described in this paper is based on genetic algorithms.

Due to the randomness characteristic for genetic algorithms, the optimality of the solution is not guaranteed; it is expected that the solution is a "near-optimal" flight plan. Multiple runs of the optimization algorithm, for an identical optimization problem, yield different "optimal" solutions.

The proposed optimization method starts by defining the families ("templates") of lateral and vertical flight plans from which the candidate flight plans (the combination of lateral and vertical flight plans) can be selected and evaluated in the optimization process. Then, a genetic algorithm iteratively selects random new candidate flight plans, from the candidate set or by applying genetic operators ("crossover" and "mutation") on pairs of selected candidates, and computes the flight performance parameters (through accelerated simulation), and the cost. The genetic operators are applied in such a way that the flight plans resulted after applying the genetic operators are themselves members of the candidates' set.

The first sub-section presents the methodology used for constructing the set of candidate lateral flight plans, and the configuration parameters that determine their characteristics. The next sub-section describes the methodology employed for constructing the family of vertical flight plans, and the configuration parameters that determine their characteristics. The last sub-section presents the implementation of the genetic algorithm used in the optimization.

4.2.6.1 Lateral flight profile routing grid and candidate lateral flight plan construction

This sub-section presents the methodology used for constructing the set of lateral flight plans that can be selected as components of the flight plans evaluated in the optimization. The definition of the set of lateral flight plans starts with the assumption that the lateral flight plan is composed by a succession of segments, where each segment is delimited by two geographic locations (WPTs), and is one of the two possible types: orthodromic or loxodromic. Another assumption made in this study is that the WPTs delimiting the lateral flight plan segments and, therefore, the aircraft's lateral flight trajectory, are restricted to a selected geographic area. It is also assumed that the set of WPTs that delimit the segments of a lateral flight plan are selected from a "grid" (routing grid), in which each segment is delimited by two adjacent WPTs from the grid.

The set of lateral flight plans is, therefore, defined by:

1. The geographic area within which the flight plan WPTs can be selected;
2. The methodology used to construct the routing grid, which defines the set of WPTs that delimit the flight plan segments;
3. The type of the segments (orthodromic or loxodromic) composing a lateral flight plan; and
4. The methodology used for selecting, from the routing grid, the set of WPTs that define the succession of segments of a lateral flight profile.

In this study, the lateral flight profile is composed of orthodromic segments. Each segment is characterized by:

1. An SLA length;
2. The headings required to advance along the segment: in the initial WPT of the segment (departure heading) and in points along the segment; and
3. The heading when arriving at the final WPT of the segment.

The segment's length, the departure and arrival headings, and the segment headings in a point along the segment are computed using the Vincenty's formulae (Karney, 2103), and the WGS84 ellipsoid Earth model (Janssen, 2009).

In this study, the routing grid, and thus, the geographic area to which the set of flight plans are restricted, is defined based on the orthodromic route (ORT) between the initial and the final WPTs of the trajectory under optimization. The routing grid is constructed as an "orthogonal" grid. First, a number of equidistant WPTs are generated along the ORT. Then, from each such WPT along the ORT, an orthodrome perpendicular to the ORT is constructed, and new routing grid WPTs are generated along this orthodrome. The new WPTs are equidistant, placed symmetrically, on both sides of the ORT, up to a maximum deviation relative to the ORT. An illustration of the routing grid construction is presented in Figure 4.8.

The first step in constructing the routing grid is to select the configuration parameters for the grid:

1. The maximum distance between the WPTs generated along the ORT;
2. The maximum deviation from the ORT; and
3. The distance between WPTs on the normal to the ORT.

It is assumed that the aircraft always moves to a new WPT situated at a (routing grid) step along the ORT track, and at a maximum number of grid steps across. The lengths of the segments along and across the orthodromic track, and the number of waypoint steps "across"

the ORT are chosen so that each segment, constructed as presented above, by waypoints selected from the grid, represents an integration step (has a maximum length that is below the maximum length of a computation step) for the flight performance estimation function.

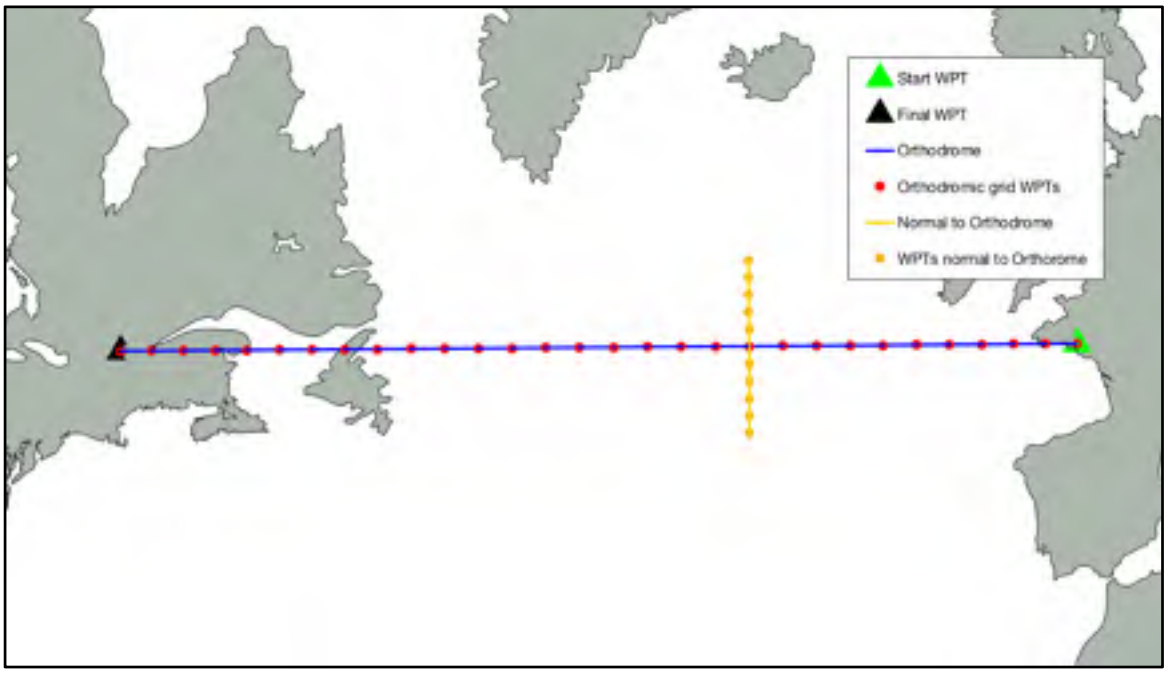

Figure 4.8 Example of routing grid construction

These parameters can also be used to refine the optimization process, as smaller distances produce a finer grid, which can yield profiles "better" adapted for the atmospheric conditions, but would result in a large increase in the number of "candidate" profiles to explore.

Given that at each step the aircraft moves to a new WPT situated at one grid step along the ORT and at a selected maximum number of steps across the ORT, the routing grid starts at the initial WPT, with no WPTs across the ORT. Then, at each step along the ORT, the number of WPTs across the ORT increases by the selected maximum number of lateral steps. The maximum number of steps across the ORT results from the selected maximum lateral deviation from the ORT and the lateral deviation step size. Similarly, at the other end, the

number of WPTs across the ORT decreases, at each step along the ORT, by the maximum number of lateral deviations steps, until it reaches the final point of the grid (the final WPT of the flight) with no WPTs across the ORT. Figure 4.9 presents an illustration of a routing grid.

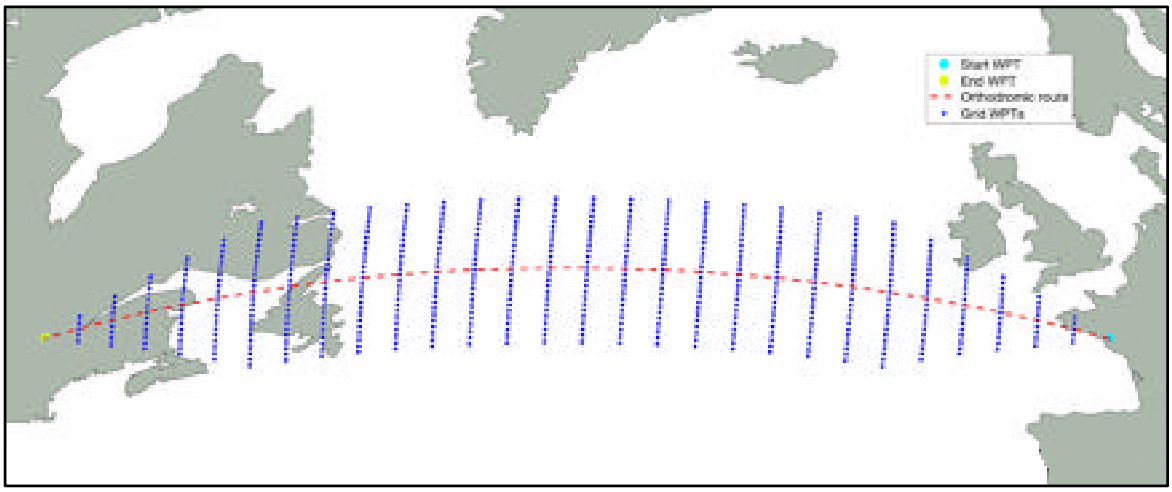

Figure 4.9 Example of a routing grid

The lateral flight plans, generated as candidates in the optimization, are random routes that traverse the routing grid, where the succession of WPTs must follow the rules set above. One method for generating the lateral flight plan is to select the set of WPTs successively, one step along the orthodromic route at a time (each new WPT is situated one step further along the orthodromic route). The domain of valid steps along the normal to the orthodromic route (the range of lateral steps that would end in a grid WPT) is determined, at each step, and the new WPT deviation is selected randomly, from the set of valid deviations. Tests showed that such a method yields zigzagged lateral flight plans (e.g. the red flight track in Figure 4.10), which result in flight trajectories that are not in accordance with normal operations/navigation.

This paper proposes a method to generate candidate lateral flight plans that observe standard flight operations by generating longer segments (longer steps along the orthodromic route), on which the lateral step value is maintained. For each new segment, the range of valid lateral step values (which can yield a grid WPT for at least one step along the orthodromic

route) is determined. The segment lateral step value is selected randomly from the range of valid values. The maximum number of valid steps along the orthodromic grid route is then calculated for the selected lateral step value: the maximum number of steps needed to reach the limit of the routing grid. The segment's length (the number of steps along the grid's orthodromic route) is selected randomly, within the set of valid values. Finally, the set of grid WPTs corresponding to the new segment, generated by advancing one orthodromic step at a time, and the selected lateral step size for the selected number of orthodromic steps are added to the generated lateral flight plan.

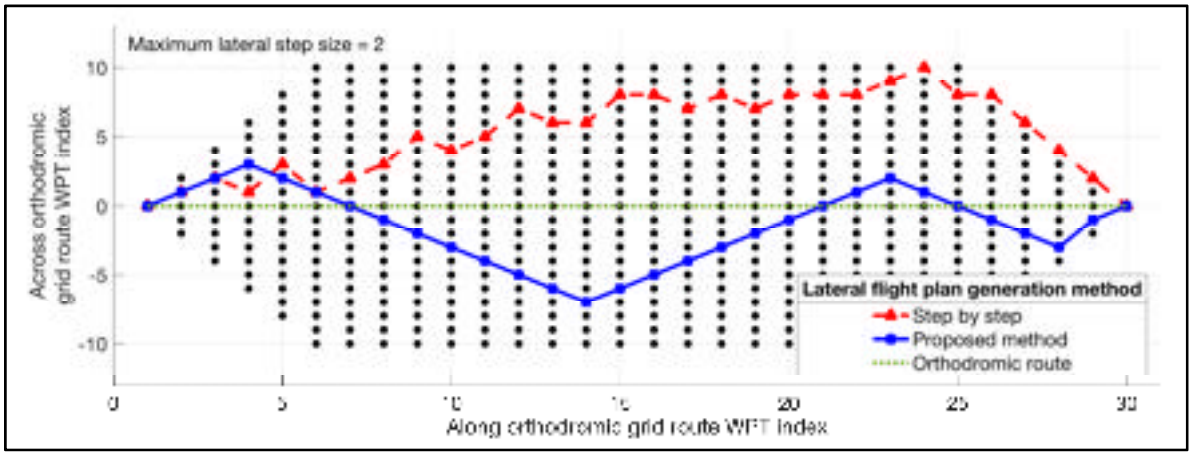

Figure 4.10 Example of random lateral flight plan generation using the "point by point" and "segment by segment" methods

4.2.6.2 Vertical flight plan candidates construction

A vertical flight plan has three main sections, corresponding to the three main phases of a flight: climb, cruise, and descent. Each phase of the vertical flight plan is composed of a succession of flight plan segments, for which the number of segments, the order in which they appear, and their type, are a function of the desired/selected aircraft evolution.

The set of vertical flight plan segment types considered in this paper, and their specific parameters, are:

1. Climb at constant speed schedule ([IAS, MACH]): initial altitude, final altitude, speed schedule, climb angle (as resulted from the equilibrium of forces and moments), and engine thrust set to Maximum Climb (MCMB). The initial point of the flight plan segment is the initial point of the flight trajectory;
2. Descent at constant speed schedule ([IAS, MACH]): initial altitude, final altitude, speed schedule, descent angle (as resulted from the equilibrium of forces and moments), and engine thrust set to IDLE. The final point of the flight plan segment is the final point of the flight trajectory; and
3. Cruise at constant speed: altitude, speed, initial position along the lateral flight plan, and the final position along the lateral flight plan or sea level segment length.

The flight profile corresponding to a selected flight plan will contain additional flight segments, which implement the transition phases between the flight segments defined in the flight plan:

1. Acceleration in climb/deceleration in descent phases: speed type, initial speed, final speed, initial altitude (initial altitude for climb/final altitude for descent), constant rate of climb/descent, and engine thrust setting (MCMB for climb and IDLE for descent);
2. Acceleration/deceleration in cruise phase: altitude, initial speed, final speed, acceleration/deceleration as resulted from the difference between thrust and drag, where the engine thrust is set to Maximum Cruise (MCRZ) thrust for acceleration and to IDLE for deceleration; and
3. Climb in cruise at constant speed: initial altitude, speed, final altitude, constant climb angle (as resulted from the equilibrium of forces and moments), and engine thrust set to MCMB.

The initial and final altitudes and speeds, at the beginning and at the end of the flight profile, are those defined by the optimization problem. The altitudes explored for the cruise phase are values multiple of 1,000 ft, selected between a minimum altitude (an input parameter for the

optimization problem), and the maximum operational altitude for the aircraft model. Similarly, the maximum IAS speed, and the maximum MACH speeds are VMO – 10 and MMO – 0.01, respectively. The minimum MACH speed value for the range of explored MACH speeds (for the climb, cruise, and descent) is an input parameter for the specific optimization problem.

The aircraft weight at locations along the flight trajectory (as well as other parameters that have an influence on the flight envelope limitations) can only be determined during the accelerated flight trajectory performance evaluation. Therefore, a valid flight plan segment parameters domain, from which valid segments can be selected, can only be determined during the accelerated flight trajectory performance evaluation. As a result, a valid flight plan can only be guaranteed if the parameters for each segment are selected based on the data obtained following a flight profile performance calculation from the initial point of the trajectory to the point where the segment parameters are generated.

For the optimization method presented in this paper, based on genetic algorithms, even if a flight plan is invalid due to one or more invalid flight plan segments, it can still contribute "genetic material" to the optimization process as a result of crossover and mutation genetic operations. In the optimization process, the lateral and the vertical flight plans are generated randomly. The vertical flight plans are generated based on minimum and maximum values for the altitude and speed parameters, provided as inputs.

The cruise altitude for the section immediately following the climb phase, is selected randomly from a range of valid initial altitudes, determined as follows:

1. The weight of the aircraft at the end of the climb flight profile (at the TOC), for each of the evaluated initial cruise altitudes, is estimated using a heuristic, based on the initial aircraft weight;
2. Then, for each evaluated initial cruise altitude and the corresponding aircraft weight for that altitude, the minimum and maximum valid cruise speeds (FAA, 2018) are determined using the aircraft performance model; and

3. The set of valid initial cruise altitudes comprises the initial cruise altitudes for which there are valid cruise MACH speeds (altitude – speed pairs that are within the aircraft's flight envelope given the aircraft's weight).

The vertical flight plan is constructed successively, starting with the climb section. First, the initial cruise altitude is randomly selected from the set of valid initial cruise altitudes. Next, the climb speed schedule values are selected at random, between initial speed and VMO – 10, for the IAS, and within the range of valid MACH speeds determined for the initial cruise altitude. These criteria ensure that the initial cruise segment is valid. Given that the position of the TOC along the lateral flight profile is a function of the selected climb profile, and in order to simplify the crossover and mutation operations, the climb section of the vertical flight plan is considered to end at a preset sea level distance from the initial WPT of the flight trajectory. Therefore, the climb flight plan ends with a cruise segment at constant altitude and speed.

The cruise section of the vertical flight plan is defined by a succession of constant altitude and speed segments. In this study, the set of cruise vertical flight plan segments were constructed so that they have an identical number of lateral flight plan segments (routing grid segments). The initial and final positions along the lateral flight plan are fixed, in order to simplify the crossover and mutation operations. The initial point for the first segment of the cruise vertical flight plan section, along the lateral flight plan, is the same as the final point for the last climb vertical flight plan section. The final point for the last segment of the cruise vertical flight plan section is situated at or before the EOC, i.e. the point selected as the limit between the cruise and the descent phases of the flight (see sub-sections 4.2.4.2 and 4.2.5).

The structure of the descent section of the vertical flight plan is similar to that of the climb phase, the difference being the order/succession of the vertical flight plan segments. The descent vertical flight plan section starts with the final descent segment (a descent at a constant [IAS, MACH] speed schedule from the cruise altitude), followed by constant speed and altitude cruise segment(s).

The flight profile for the selected flight plan (lateral and vertical flight plan components), atmospheric conditions, and aircraft configuration is obtained following the accelerated flight performance calculations. Figure 4.4 shows an example of a climb altitude – speed flight profile, while Figure 4.5 and Figure 4.6 show examples of an altitude profile, and the positions of the TOC, EOC and TOD, respectively.

4.2.6.3 Genetic algorithm

Genetic algorithms (Schmitt, 2001) are population based metaheuristic algorithms, inspired from the evolution theory presented by Darwin, which can be used for solving complex search problems for which the solution space is too large for an exhaustive exploration, in a timely manner, and/or are complex and nonlinear for other search techniques. In a genetic algorithm, the population, composed of a set of individuals (candidate solutions), evolves for a selected maximum number of generations or until a selected termination criterion is satisfied (the global optimum or an acceptable solution is found). Each generation has the same number of individuals, and all the individuals that are generated and evaluated in a genetic algorithm conform to a genetic structure template ("genotype"): they all have the same number of chromosomes, and each chromosome, situated at a given position in the genetic structure, has the same meaning (represents the same characteristic / parameter for the problem under optimization). For the initial population, the individuals are generated randomly or according to selected "values" that are deemed to conduct to optimal solutions. At each generation step, the fitness of each of the members of the population is evaluated. Then, the next generation (population) is selected/created through one or a combination of the following genetic operations:

1. "Elitism", where the best individuals are copied to the next generation; and
2. "Crossover" and "mutation" based on individual(s) selected from the current population.

In order to increase the population diversity, a number of individuals of a new generation may be generated randomly.

The individual selection for crossover and/or mutation operations can be made randomly or as a function of their fitness relative to the set of individuals in the current population. Some of the possible fitness-based selection methods are:

1. “Tournament”, where two individuals from the population are chosen at random, their fitness values are compared, and the best individual is retained;
2. “Roulette wheel” (proportional) selection, in which the selection is performed by generating a random number between 0 and 1, and by retrieving the individual that falls within the corresponding area of the roulette disk; and
3. “Stochastic acceptance” (Lipowski & Lipowska, 2012).

The crossover operation consists of exchanging “genetic” data (“chromosomes”) between two individuals (“parents”) selected from the candidate solution population. First, the position along the genome where the crossover will be performed is randomly selected. The new individual (“child”), member of the new generation population, is then constructed by concatenating the initial chromosome sequence (up to the crossover position) from one parent and the final sequence from the other parent.

A mutation changes the value of one chromosome, selected at random, to a new value among the range of values for the selected chromosome. This genetic operation can be applied independently, to a randomly selected individual from a population, or additionally to a crossover, to increase the diversity of the individuals from the new generation.

4.2.6.3.1 Candidate flight plan selection for mutation and crossover operations

The flight plan(s), on which the crossover or mutation operations are performed, are retrieved using the “roulette wheel” selection. The roulette wheel is created based on the list of total cost values for the population. For each element of the roulette wheel list (normalized values

with a total sum equal to one), the corresponding roulette wheel value is calculated as the quotient between:

1. The cost values for the population element; and
2. The sum for the entire population.

A random number between zero and one is used as a "pointer" to the list member (the population member) that will be selected for the genetic operation.

4.2.6.3.2 Lateral flight plan crossover and mutation

As presented in sub-section 4.2.6.1, the lateral flight plan is defined by a succession of segments delimited by the WPTs of the routing grid. For each lateral flight plan segment, the final WPT is situated one step further along the grid's orthodromic route direction, and up to a maximum number of steps across the orthodromic route, relative to the initial point. Therefore, in order to obtain a lateral flight plan that maintains this characteristic, the crossover between two lateral flight plans (as well as a mutation of a flight plan) can be only performed in the points of the lateral flight plan segment that are routing grid nodes. The flight plan WPT where the crossover or mutation is performed is identified by its grid position along the orthodromic route direction (N_M). Firstly, the crossover or mutation WPT is selected randomly, from the WPTs that define the flight plan, except for the initial and final WPTs (which would not yield any profile changes). Each lateral flight plan P_i can thus be divided into two sections: from the initial point to the crossover location (P_{i1}), and from the crossover location to the end of the lateral flight plan (P_{i2}).

The child lateral flight plan (C_{LFPL}), resulted from the crossover operation of two parent lateral flight plans (P_1 and P_2), will have its initial section (up to the crossover position) identical to that of the first parent (P_{11}). The final section (from the crossover position to the end) will be constructed based on the locations of the flight plan WPT offsets on the routing grid at the crossover position N_M, and on the structure of the final section from the other parent lateral flight plan (P_{22}).

The two parent lateral flight profiles can have different grid offsets at the points following the crossover position, relative to the orthodromic grid route, where the difference can be higher than the maximum step across the orthodromic grid route direction. Therefore, the final section of a child flight plan cannot be obtained by simply copying the final section from the other parent (P_{22} from P_2). A transition section, that starts at the crossover position, the final WPT of the initial section (P_{11}), and "intercepts" the new section (P_{22}) at a further WPT, has to be constructed along the orthodromic route direction, one step at a time. At each step S_j along the orthodromic grid route direction, the offset of the next lateral flight plan WPT, situated at step S_{j+1}, is selected based on:

1. The offset (along the direction normal to the orthodromic grid route) at the current location (S_j); and
2. The offset of the target flight plan section (P_{22}) WPT situated at step S_{j+1}.

This selection ensures the fastest convergence to the target flight plan section after the crossover (P_{22}). An example of child lateral flight plan resulted after a crossover between two parent flight plans is presented in Figure 4.11.

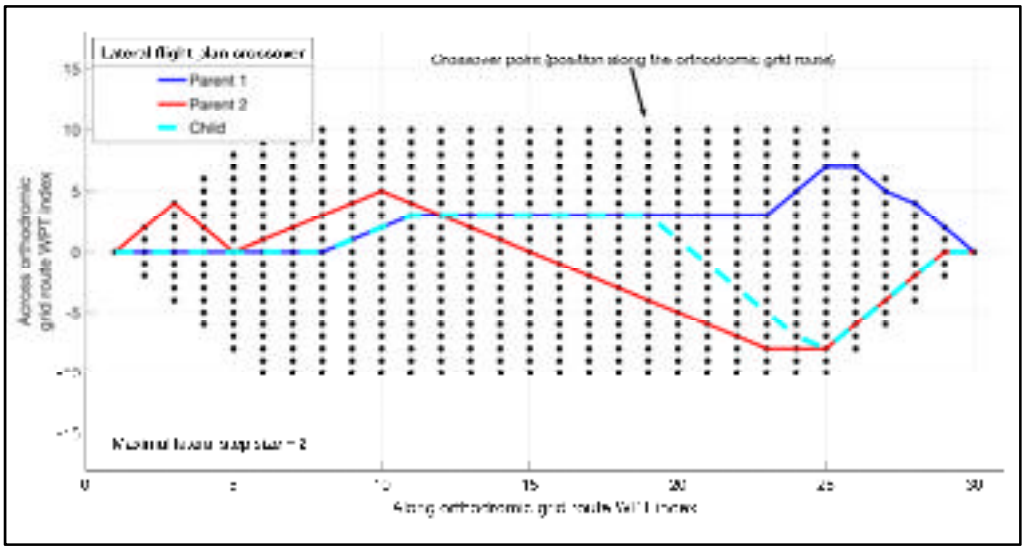

Figure 4.11 Example of lateral flight plan crossover

A lateral flight plan mutation consists in modifying the offset (relative to the routing grid's orthodromic route) of a lateral flight plan segment limit WPT (other than the first or the last WPT of the flight plan), randomly selected. The offset change is selected at random from a range of offsets that can be reached from the preceding WPT, with a step size within the imposed maximum range (sub-section 4.2.6.1). For the lateral flight plan section following the mutation location, the WPT's offsets are shifted with a value equal to the difference between the mutated and initial offset at the mutation position, and bounded to the routing grid. An example of lateral flight plan mutation is presented in Figure 4.12.

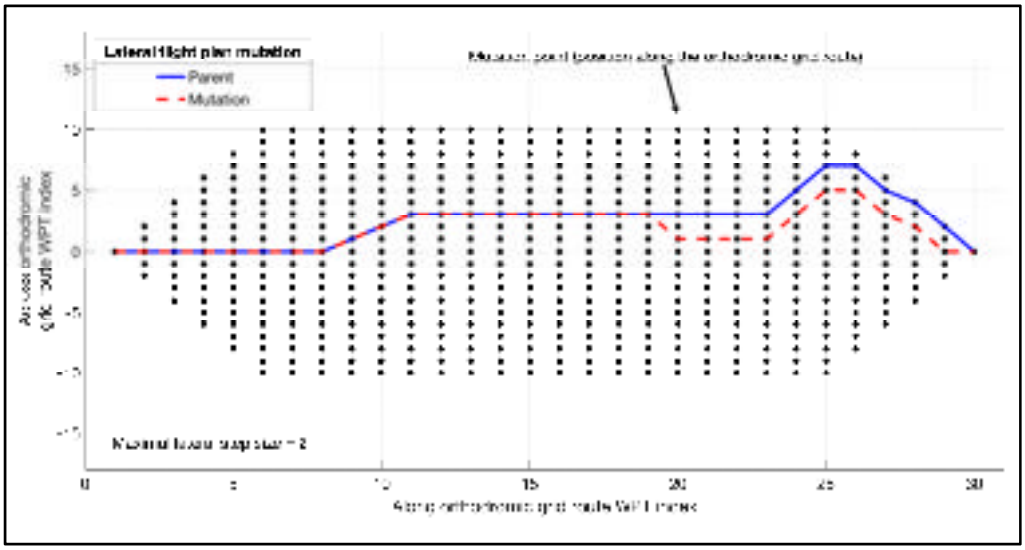

Figure 4.12 Example of lateral flight plan mutation

4.2.6.3.3 Vertical flight plan crossover and mutation

The vertical flight plan crossover operation is performed only on the cruise section of the flight plan, in the locations where the step altitude and speed changes are allowed (see sub-section 4.2.6.2), so that the resulting child vertical profiles conform to the vertical flight plan template selected for the family of candidate flight plans. Similarly to the flight plan crossover operation, the vertical flight plan operation starts by selecting, at random, the location where the crossover is performed. Next, the child vertical flight plans are

constructed by copying the initial section from one parent and the final section from the other parent (Figure 4.13).

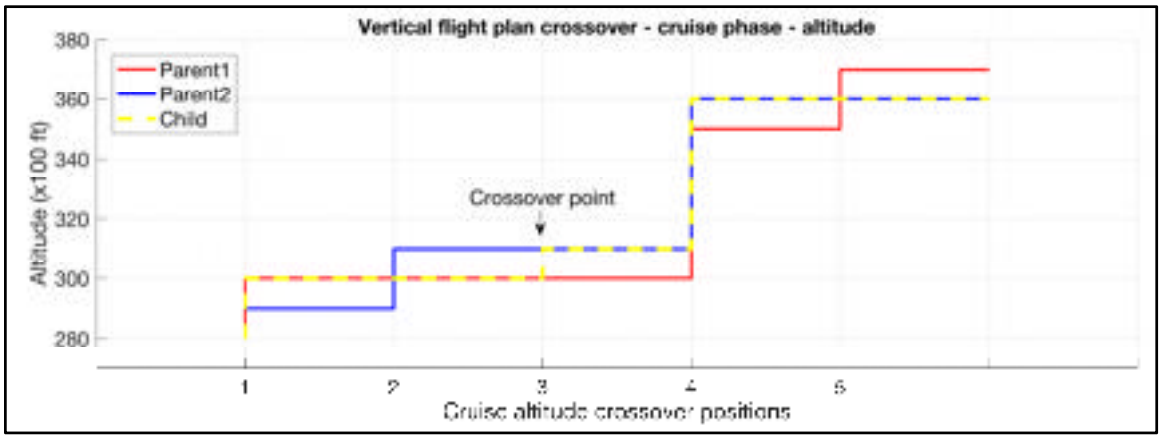

Figure 4.13 Example of altitude vertical flight plan crossover, where no altitude correction is necessary

Given that step descents are not allowed, the segment altitudes for the final sections of the child flight plans are adjusted, if needed, to values equal to or higher than the altitudes at the final point of the initial section (crossover position), as shown in Figure 4.14.

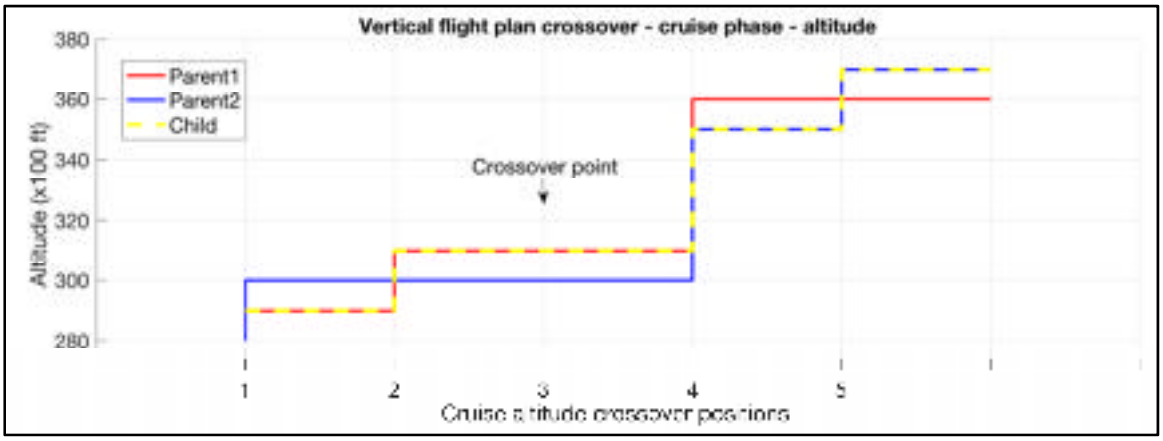

Figure 4.14 Example of altitude vertical flight plan crossover, where an altitude correction is necessary in order to avoid a step descent

For the mutation operation, firstly the section where the mutation is performed (climb, cruise or descent) is selected at random, and then the parameter to be changed:

1. The IAS, the MACH, or the target climb altitude (the initial cruise altitude) for the climb phase;
2. The cruise segment and the altitude or speed for the selected segment – for the cruise phase; or
3. The IAS or the MACH for the descent phase.

As mentioned for the crossover operation, if the mutation performs an altitude change for a cruise segment, the new selected altitude must be equal to or higher than the altitude on the previous cruise segment, or than the initial cruise altitude (if the selected segment is the first cruise segment).

4.2.7 Reference flight profile data (FlightAware)

For each specific flight planning/optimization problem, the lateral and vertical flight plans are built based on the actual data for the flight: initial and final geographic locations for the flight trajectory limits (departure and destination airports or flight trajectory section limits), navigation constraints, aircraft data (performance data, weight, fuel load) and atmospheric conditions.

In this paper, the set of candidate lateral and vertical flight plans, and the reference flight plan used for evaluating the performance of the optimization method, were constructed based on the flight track data of a real flight retrieved from the FlightAware (www.flightaware.com) website. This was done in order to generate a realistic optimization problem, and compare the optimal profile performance, identified by the proposed method, with the performance of a flight plan as close as possible to an “as flown” flight profile.

FlightAware is a company that retrieves real time aircraft flight data from various sources (ACARS, transponders, ADS-B, radar, etc.) and provides a platform to access this

information, at different levels of detail, function of the subscription type. Information about the area covered by the real time data providers, the types of data, and the specific regions covered for each of the specific data type, can be found in FlightAware (n.d.a). For aircraft without ADS-B transmitters, the position of the aircraft is determined, under certain circumstances, by multilateration based on transponder data reception (FlightAware, n.d.b). For areas not covered by the data feeders the real time aircraft positions are estimated based on the flight plans submitted to the FAA.

The flight track data used in this study were retrieved from FlightAware using Guest account privileges. The available flight track information is therefore a list of aircraft data points describing:

1. The flown flight track:
    a. A set of geographic location overflown by the aircraft;
    b. Aircraft flight parameters in the set of overflown geographic locations:
        i. The date and time of crossing;
        ii. Aircraft altitude;
        iii. Aircraft heading;
        iv. Ground speed; and
        v. Rate of climb/descent.
2. The submitted lateral flight plan data (flight route plan) is a list that enumerates:
    a. The name of the navigation point that defines a limit of a flight segment;
    b. The geographic location of the navigation point;
    c. The aircraft departure heading from that location (on the new segment);
    d. The distance to the next navigation point (the segment length);
    e. The distance remaining to the destination; and
    f. The distance flown from the initial point.

The flight track data retrieved from FlightAware via a Guest account has important limitations that make it impossible to perform an accelerated simulation along the flight trajectory and compute the performance parameters for the flight (such as fuel burn). The

flight track data lacks essential information, such as: aircraft configuration (weight and fuel load), atmospheric conditions encountered by the aircraft, unknown moments and locations where the flight profile changes are initiated or end (the data points can be considered "random" data points), etc.

An analysis of the flight track data showed that, for the flight track domains located in geographic areas not covered by the FlightAware data sources, the track data provides estimations of the geographic locations, crossing times and aircraft heading. However, the altitude, ground speed and rate of climb are set to zero.

It was observed that, occasionally, for data points along the flight track, the sequence of crossing times and/or geographic locations are not in the natural order for flight track data (probably due to particular cases of position estimation using multilocation):

1. A crossing time that is earlier that the crossing time at the previous location; and
2. A sequence of flight track geographic locations that generates a succession of lateral flight track segments with excessive heading changes, which are not consistent with a normal flight for passenger aircraft.

Given the facts presented above, the raw flight track data cannot be used as a reference flight profile. The reference flight profile must be created based on the filtered (corrected) flight track data, according to case-specific assumptions and criteria.

4.3 Results

This section presents the results obtained using an implementation of the proposed method in Matlab R2018a, on a PC based platform with a 2.3GHz AMD Phenom 9600B processor, 4GB of RAM, and Windows 7 Enterprise operating system. The aircraft flight performance parameters used in the calculations were computed using an in-house toolbox, developed in Matlab, that uses the BADA 4.0 APM published by Eurocontrol. The evaluation of the proposed method was conducted using a Boeing 777-300ER aircraft performance model, for

which the BADA APM was available at LARCASE. The results presented in this paper were obtained for an initial aircraft mass (at the beginning of the flight trajectory under optimization) corresponding to a payload equal to 50% of the maximum payload, and a fuel quantity equal to 80% of the maximum fuel load for the aircraft model.

The optimization scenario evaluated in this paper was the optimization of the flight trajectory (identification of the optimal flight plan) for a long flight. The optimized flight trajectory extends from a point in the climb phase, when the aircraft is at an altitude of 10,000 ft and a speed of 250 kn IAS (per FAA regulation 14 CFR Part 91.117 (FAA, n.d.b) the maximum speed at altitudes below 10,000 ft MSL), to a point in descent where the aircraft reaches an altitude of 10,000 ft at a speed of 250 kn IAS. The objective of the optimization was to identify the flight plan (the lateral and vertical components) that corresponds to a flight trajectory (flight track and altitude/speed profile) that minimizes the total cost for the flight. The total cost for the flight along the optimal flight plan, determined using the optimization method proposed in the paper, was compared with the total cost of a reference flight plan, where:

1. The candidate flight plans, evaluated in the optimization, and the reference flight plan:
    a. Started at identical locations (geographic locations and altitudes), speeds, and time; and
    b. Ended at identical locations (geographic locations and altitudes) and speeds.
2. The flight performance calculations were performed under identical conditions by: using the same aircraft model, initial aircraft configuration (fuel quantity and load), and climb/cruise/descent policies and strategies, etc.

Ideally, the reference flight plan should be a known global optimal flight plan (for the initial – final point combination, aircraft model and configuration, etc.), resulting from an exhaustive search of the ensemble of candidate flight plans. This option is prohibitive due to the large number of candidate flight plans and the amount of time required to evaluate them. Another option would have been to use an “as flown” flight plan: a flight plan corresponding

to a real flight, recorded by the crew or flight operator, where all the relevant information (aircraft load and fuel, speed and altitude profiles, etc.) are known. This option was not available to the authors.

The set of candidate flight plans evaluated in the optimization, and the reference flight plan used to evaluate the performance of the optimization method, were constructed based on the recorded flight track data of a real flight, retrieved from FlightAware. Specifically, the selected flight was Swiss 40 (SWR40), from Zurich (ZHR) to Los Angeles (LAX), flown on Feb 25th, 2019 (Figure 4.15 and Figure 4.16). This flight was selected based on aircraft type (matches the available APM aircraft model), and flight trajectory length (a very long flight).

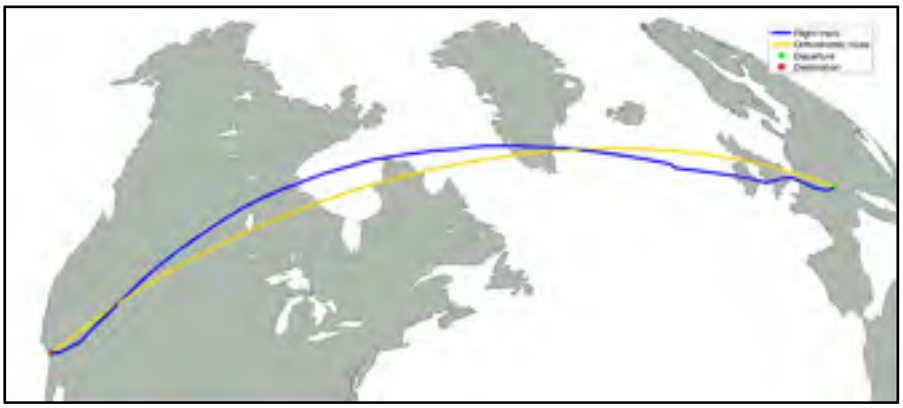

Figure 4.15 Recorded flight track for flight SWR40 (ZHR to LAX),
on Feb. 25th, 2019 (FlightAware, 2019a)

For three sections of the SWR40 reference track data (Figure 4.17), the FlightAware flight profile data contain only the estimated geographic locations and crossing times (possibly because the aircraft was beyond the range of the FlightAware ADS-B receivers); the ground speed, aircraft altitude and heading are set to 0. An analysis of the estimated aircraft track data showed that:

1. For two sections, the maximum distance between an estimated location and the orthodromic route constructed between the two valid ADS-B data encompassing that

section, are 5.57 and 4.04 n.m., respectively. For the third section, the maximum distance is 26.9 n.m.; and

2. The aircraft's altitudes at the valid data WPTs locations that delimit each of the three segments are identical, and equal to 32,000 ft. Since step descents in cruise are generally avoided during normal operations, it can be assumed that the three sections are constant altitude cruise segments, at 32,000 ft.

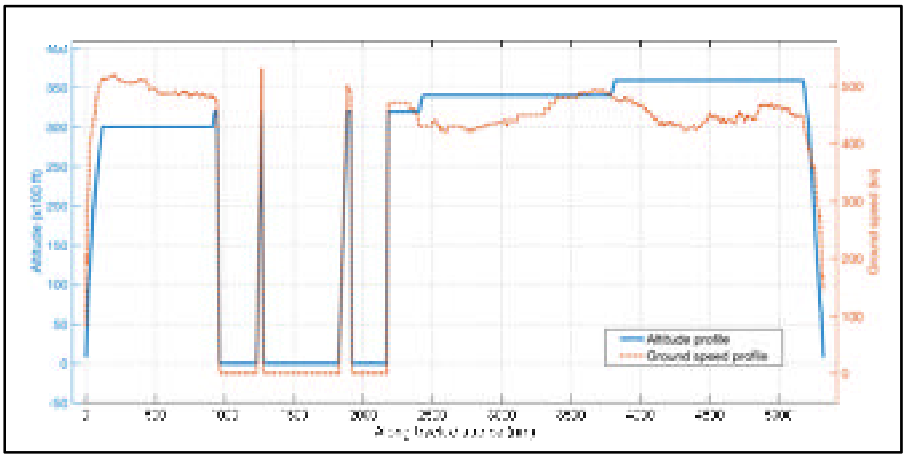

Figure 4.16 Recorded altitude and ground speed profiles for flight SWR40 (ZHR to LAX), on Feb. 25th, 2019 (FlightAware, 2019a)

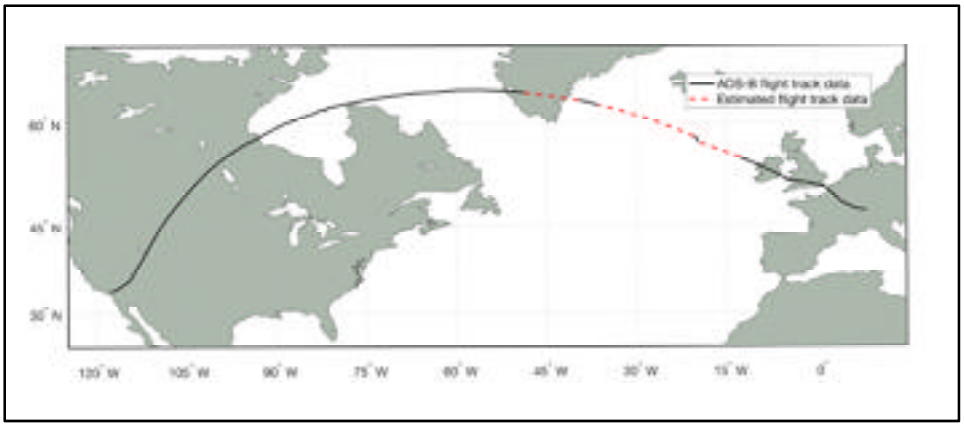

Figure 4.17 Illustration of the selected SWR40 flight profile section and the three domains containing estimated data

The SWR40 “recorded” flight data has been processed in order to identify and eliminate spurious flight track data (see sub-section 4.2.7). Only two track data WPTs were eliminated, WPTs 479 and 487, as they generated a succession of lateral flight track segments with excessive heading changes, which are not consistent with normal cruise flights. The reference flight track data for this study, denoted herein as “SWR40 reference track data”, was selected as the section of the processed SRW40 FlightAware track data between:

1. The track data WPT where the aircraft was in climb, at the highest altitude lower than or equal to 10,000 ft; and
2. The track data WPT where the aircraft was in descent, at the highest altitude lower than or equal to 10,000 ft.

The initial and final points of the SWR40 reference track data represent the initial and final WPTs of the flight trajectory under optimization. The aircraft altitudes in the initial and final WPTs of the SWR40 reference track data, as resulted following the selection process, have been modified, from 9,970 ft and 9,951 ft, respectively, to 10,000 ft in order to match the evaluated optimization scenario.

The flight performance calculations for the flight along a flight plan require information/predictions regarding the atmospheric conditions encountered by the aircraft during flight. The atmospheric data used in this study (air temperature and wind speeds along the geographic North and East axes) are GDPS forecasts issued by Environment Canada, on a longitude-latitude grid with a 0.6º x 0.6º resolution (see sub-section 4.2.3).

Before downloading the forecast data, the prediction date, time interval, geographic area, and altitude domain for the atmospheric data of interest had to be determined. As the date and time values corresponding to the downloaded SWR40 reference track data (FlightAware data) were referenced to the Eastern Standard Time (EST), and the atmospheric forecast data issued by Environment Canada was referenced to the Universal Coordinate Time (UTC), the SWR40 reference track time data were converted to UTC. The domain of interest for the downloaded GRIB forecast data was then determined as follows:

1. The “geographic area of interest” (the latitude – longitude domain) was selected as the smallest GRIB atmospheric forecast data grid domain that contains the routing grid WPTs from which the set of candidate lateral flight plans are generated (see sub-section 4.2.4.1);
2. The “altitude domain of interest” was taken to be the smallest GRIB forecast grid altitude domain that includes the altitude range between 10,000 ft and the maximum cruise altitude for the aircraft model; and
3. The GRIB time domain was taken as the “forecast grid time domain”, which includes:
    a. The aircraft crossing time at the initial WPT of the routing grid, as retrieved from the SWR40 reference track data; and
    b. The aircraft crossing time at the final WPT of the SWR40 reference track data, plus a “buffer interval” taken so that it covers the entire domain of flight times that can be obtained for the candidate flight plans. In this study, the time buffer interval has been chosen heuristically as six hours (approximately half the total flight time computed based on the FlightAware data).

The selected GRIB forecast data also covers the geographic domain/altitude domain/time domain necessary to conduct the flight performance calculations for the reference profiles, as they are within the respective domains of the optimization candidate profiles.

The lateral flight plan routing grid (Figure 4.18) between the initial and final WPTs, used in the flight plan optimization method, has been constructed using the methodology described in the sub-section 4.2.6.1. The characteristics of the routing grid considered in this study are:

1. The orthodromic route between the initial and final WPTs of the flight trajectory is decomposed in a set of equal length sub-segments. The number of sub-segments is calculated as the rounded value of the quotient of the orthodromic route’s sea level length by the maximum acceptable orthodromic route sub-segment sea level length (integration step length). In this study, this maximal length was selected to be 50 n.m.;
2. The maximum deviation from the orthodromic route was selected as 500 n.m.;

3. The size of the lateral step for the WPTs situated on the orthodrome normal to the orthodromic route was selected as 10 n.m.; and
4. At each flight trajectory step, the aircraft can advance to a WPT situated one step along the orthodromic route and a maximum of two steps (up or down) relative to the orthodromic route (see sub-section 4.2.6.1).

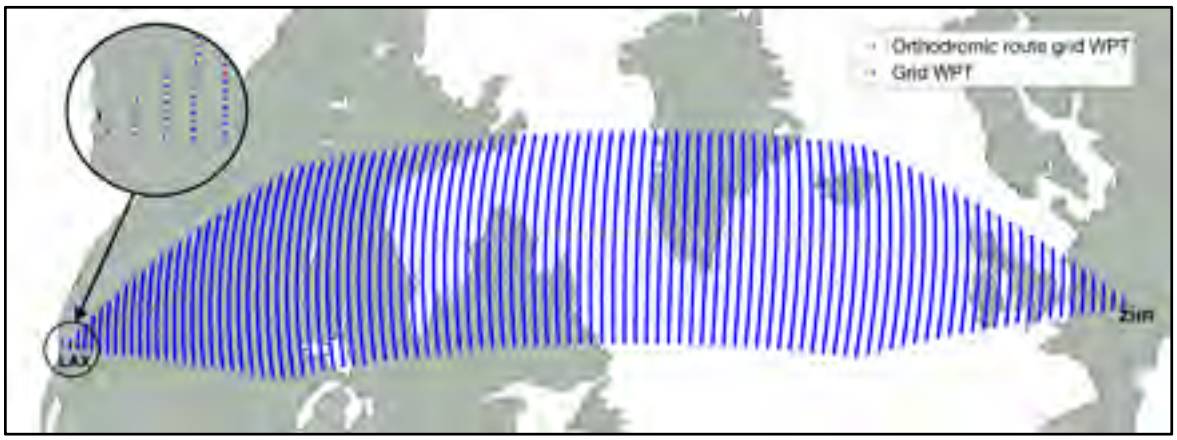

Figure 4.18 The routing grid used in the optimization of the Feb 25th, 2019 flight SWR40, from ZHR to LAX

The generated routing grid has 104 nodes (WPTs) along the orthodromic route axis, and up to 101 nodes along the axis normal to the orthodromic route. As a result, each candidate lateral flight plan is defined by a set of $N_{ORT} = 104$ adjacent WPTs selected from the routing grid; each WPT is a step further along the orthodromic route and up to two steps offset along the axis normal to the orthodromic route.

In order to speed up the accelerated flight performance calculations, and thus, the optimization process, the sea level segment lengths and departure/arrival headings for all possible routing grid segments were computed once, in advance, and stored in a data structure associated with the routing grid. For each node (WPT) of the routing grid, the data structure stores the sea level segment lengths and departure headings to all possible/valid advancing step WPTs. The time savings obtained from not having to compute the segment parameters come at the expense of an increased memory footprint. Similarly, the atmospheric

conditions in each of the routing grid WPTs were precompiled for the set of altitudes and time domains of interest, and stored in the corresponding routing grid WPT's data structure.

In this paper, the optimization method was applied for the case where the flight profile under optimization:

1. Starts in climb, at an altitude of 10,000 ft Above Sea Level (ASL) and an aircraft speed of 250 kn IAS;
2. Ends in descent, at 10,000 ft ASL and 250 kn IAS;
3. The climb and descent are performed at [IAS MACH] scheduled speeds, and the cruise at MACH speeds;
4. Climbs are performed at MCMB thrust setting;
5. Accelerations in cruise are performed at MCRZ thrust setting;
6. Descents, and decelerations in cruise, are performed at IDLE thrust setting;
7. The lateral and vertical flight plans conform to the templates presented in sub-sections 4.2.6.1 and 4.2.6.2;
8. In cruise, the aircraft can only perform step climbs (no step descents);
9. The ceiling cruise altitude (Young, 2018) for a selected cruise speed is considered as the maximum altitude, in multiples of 1,000 ft, at which the aircraft is still capable of performing a 300 fpm climb with the TLA set to MCRZ and at a load factor equal to 1.2; and
10. For a given cruise altitude, the range of cruise speeds is limited to the valid flight envelope speeds larger than the minimum drag speed (for speed stability (FAA, 2018)) at which the aircraft is still capable of performing a 300 fpm climb with the TLA set to MCRZ and at a load factor equal to 1.2.

The lateral flight plans generated randomly, as presented in sub-section 4.2.6.1, and those resulted from genetic operations most likely miss a set of lateral flight plans that might prove important relative to optimal flight profile exploration: the orthodromic route (the shortest route), and routes parallel to the orthodrome, at preset offset values on both sides of the

orthodromic route. Therefore, in the first generation, the lateral flight plans are generated as follows:

1. The orthodromic route;
2. Two lateral flight plans along the maximum deviation grid points (maximum offsets on each side of the orthodrome);
3. Twenty-six lateral flight plans parallel to the orthodrome, with offsets of a multiple of three steps relative to the orthodrome (on both sides of the orthodromic route); and
4. One random lateral flight plan.

The set of candidate vertical flight plans were constructed based on the following assumptions:

1. The evaluated cruise altitudes are multiples of 1,000 ft, between 28,000 ft and the maximum cruise altitude for the aircraft model;
2. The range of evaluated IAS speeds was taken to be between 250 kn and VMO – 10 kn, with a step of 1 kn;
3. The range of evaluated MACH speeds was taken to be between 0.6 and MMO – 0.01, with a step of 0.001;
4. The set of valid initial cruise altitudes, and the valid speed domain at each initial altitude (within the flight envelope limits), were determined based on the aircraft's weight at 28,000 ft, after a climb at 250 kn IAS constant speed from the altitude of 10,000 ft;
5. The climb MACH speed was selected from the valid initial speed domain, based on the selected initial cruise altitude;
6. The aircraft maintains the initial cruise altitude and speed until at least the 8th WPT of the lateral flight plan (approximately 400 n.m. from the initial point). The first WPT where step climbs and speed changes can occur is the 8th WPT of the lateral flight plan;
7. The aircraft enters DESCENT mode at the 96th WPT of the lateral flight plan (approximately 400 n.m. before reaching the final WPT). No step climb or cruise speed changes can occur beyond this WPT;

8. The cruise step climbs and speed changes can occur only at predetermined locations along the lateral flight plan: WPTs delimiting sections composed by five lateral profile segments (approximately 250 n.m.), starting at the 8th WPT (i.e. WPT8, WPT13, WPT18, WPT23, etc.). These are the locations where the step climb or speed changes can be initiated;
9. When both a step climb and a speed change occur at the same WPT, the aircraft first performs an acceleration/deceleration, at the initial altitude, and then the step climb; and
10. The genetic crossover operations can only occur in cruise, at the altitude and speed step WPTs;

A candidate flight plan can determine an invalid flight profile, where:

1. The flight can require more fuel than is available on board. This can occur for flight plans that generate:
    a. Very long flight tracks;
    b. Long flight times (low speeds); and
    c. High fuel burn rates (high speeds); or where
2. The altitude – speed flight profile is outside the aircraft's flight envelope for the aircraft weight at that point of the flight trajectory.

The approach used in the accelerated flight plan performance evaluation regarding invalid flight plans influences the evolution of the genetic algorithm optimization. For the case where the flight plan was invalid due to fuel constraints (requires more fuel than available) a very large penalty was assigned as the total cost (a fuel burn equal to twice the initial fuel quantity on board, and a 48-hours flight time). This cost is higher than any total cost that can be obtained for a valid flight plan.

For the case in which the flight plan was invalid due to flight envelope limitations, two approaches were studied. In the first approach, denoted as the Corrected Flight Plan (CFP), the flight plans resulted following the accelerated flight performance estimations were

always valid. During the accelerated flight performance calculations, any invalid altitude – speed profiles were corrected (set to the closest flight envelope domain limit combination). The priority was given to the selected altitude: if a valid speed existed for the selected altitude, then the flight plan speed was set to the valid speed value closest to the selected flight plan speed. Otherwise, the flight plan altitude was set to the highest valid altitude for the aircraft weight, and the speed was set to the valid value closest to the selected flight plan speed.

In the second approach, denoted as the Non Corrected Flight Plan (NCFP), the flight plan was not corrected, and a very large penalty total cost was assigned to it. Thus, although the flight plan had one or more invalid flight plan segments, it had a chance to be selected as a parent for crossover and/or mutation operations, and to propagate its "genetic information" to the next generation. The advantage of the former approach is that it better explores the flight envelope's limit region, and the new population is generated based on valid flight plans. The disadvantage is the reduction in population diversity (the invalid flight profiles are excluded from the candidate set and cannot contribute with genetic material – combinations of flight profile configurations).

The population size for the genetic optimization algorithm was selected to be 30 individuals (candidate flight plans), representing a trade-off between the computation time per population iteration and the diversity/exploration of the candidate set. The genetic algorithm was run for 500 population generations. Each new generation was constructed by copying the best two individuals (flight plans) from the previous generation, adding sixteen individuals generated by crossover (each parent selected by roulette wheel selection), generating six parents by the mutation of randomly selected parents, and adding six new random flight plans (to further add diversity).

The optimization was performed for six CI values: 0 (fuel burn minimization), 10, 30, 50, 100, and 999 (flight time minimization). Given the fact that the genetic algorithm optimization does not guarantee an optimum (as the results of the optimization are a function

of the randomly generated (initial) population/flight plan candidates, of random genetic operations such as crossover and mutation, and of the number of genetic algorithm iterations), the genetic algorithm optimization was performed 10 times for each CI value. This set of optimizations should give some information regarding the dispersion of the optimization algorithm's results.

The optimal profile total cost, obtained for the set of CI values, and test runs are presented in Table 4.1, for the case where the invalid vertical flight plans are corrected (CFPs) relative to the aircraft's flight envelope, and in Table 4.2, for the case when they are not corrected (NCFPs).

In these tables:

$$\Delta TC_{CI,i} = TC_{CI,i} - \min_i(TC_{CI}) \tag{4.7}$$

and

$$\Delta TC_{p_i}\big|_{CI} = 100 \times \frac{TC_{CI,i} - \min_i(TC_{CI})}{\min_i(TC_{CI})} \tag{4.8}$$

represent the absolute value and percentage (relative error) differences between the total cost obtained for a CI value optimization test run and the best total cost obtained for the set of optimization tests for the CI value. The elements marked with bold font in Table 4.1 and in Table 4.2 represent the minimum total cost (best flight profile optimization) results for the CI value and invalid flight plan correction strategy.

It can be observed that, for the optimization test runs conducted in this study, the maximum TC variation was smaller than 1%: 0.686% for CFPs (Table 4.1, test run 6 at CI = 0) and 0.634% for NCFPs (Table 4.2, test run 2 at CI = 0).

Table 4.1 Optimization results with Corrected Flight Plans (CFPs)

CI	Parameter Type	Optimization test run									
		1	2	3	4	5	6	7	8	9	10
0	TC [kg]	97,284.56	97,255.46	97,375.39	**96,794.84**	97,098.34	*97,459.08*	97,324.32	96,889.61	97,284.17	97,416.36
	ΔTC [kg]	489.72	460.61	580.55	**0**	303.5	*664.24*	529.48	94.77	489.33	621.51
	ΔTCp [%]	0.506	0.476	0.6	**0**	0.314	*0.686*	0.547	0.098	0.506	0.642
10	TC [kg]	103,932.06	104,235.63	104,326.76	104,445.75	**103,790.23**	104,159.03	103,965.91	104,138.53	104,319.06	104,060.24
	ΔTC [kg]	141.82	445.4	536.53	655.51	**0**	368.8	175.67	348.29	528.82	270
	ΔTCp [%]	0.137	0.429	0.517	0.632	**0**	0.355	0.169	0.336	0.51	0.26
30	TC [kg]	117,501.44	117,588.86	117,584.14	**117,228.6**	117,473.59	117,579.13	117,441.14	117,462.96	117,499.28	*117,693.34*
	ΔTC [kg]	272.83	360.25	355.54	**0**	244.99	350.53	212.53	234.36	270.67	*464.74*
	ΔTCp [%]	0.233	0.307	0.303	**0**	0.209	0.299	0.181	0.2	0.231	*0.396*
50	TC [kg]	131,261.96	131,098.73	130,942.43	131,054.45	131,053.38	131,346.16	130,909.73	*131,447.88*	131,118.3	**130,877.31**
	ΔTC [kg]	384.66	221.42	65.12	177.14	176.07	468.85	32.43	*570.57*	240.99	**0**
	ΔTCp [%]	0.294	0.169	0.05	0.135	0.135	0.358	0.025	*0.436*	0.184	**0**
100	TC [kg]	164,411.34	*164,748.05*	164,245.42	164,651.46	164,669.79	164,258.06	164,486.55	**163,942.14**	164,181.92	164,657.16
	ΔTC [kg]	469.2	*805.91*	303.28	709.32	727.65	315.92	544.41	**0**	239.78	715.02
	ΔTCp [%]	0.286	*0.492*	0.185	0.433	0.444	0.193	0.332	**0**	0.146	0.436
999	TC [kg]	**742,411.11**	742,762.18	744,984.08	*747,027.97*	745,462.78	743,679.02	744,526.92	744,791.69	743,401.48	743,525.06
	ΔTC [kg]	**0**	351.06	2,572.97	*4,616.85*	3,051.66	1,267.9	2,115.8	2,380.58	990.36	1,113.94
	ΔTCp [%]	**0**	0.047	0.347	*0.622*	0.411	0.171	0.285	0.321	0.133	0.15

Table 4.2 Optimization results with Non-Corrected Flight Plans (NCFPs)

CI	Parameter Type	Optimization test run									
		1	2	3	4	5	6	7	8	9	10
0	TC [kg]	97,167.92	*97,539.09*	97,211.42	97,099.68	97,268.38	97,364.14	97,182.57	97,236.88	**96,924.26**	96,937.47
	ΔTC [kg]	243.66	*614.83*	287.16	175.41	344.12	439.88	258.31	312.62	**0**	13.21
	ΔTCp [%]	0.251	*0.634*	0.296	0.181	0.355	0.454	0.267	0.323	**0**	0.014
10	TC [kg]	104,050.29	104,055.24	104,036.46	**103,664.28**	104,018.96	104,021.28	104,073.65	103,860.84	103,900.16	*104,133.61*
	ΔTC [kg]	386.01	390.96	372.17	**0**	354.67	357	409.37	196.56	235.88	*469.33*
	ΔTCp [%]	0.372	0.377	0.359	**0**	0.342	0.344	0.395	0.19	0.228	*0.453*
30	TC [kg]	117,256.72	117,431.76	117,198.77	117,306	117,138.52	**116,904.46**	117,491.92	117,465.64	*117,503.34*	117,453.59
	ΔTC [kg]	352.26	527.3	294.31	401.55	234.07	**0**	587.46	561.18	*598.88*	549.14
	ΔTCp [%]	0.301	0.451	0.252	0.344	0.2	**0**	0.503	0.48	*0.512*	0.47
50	TC [kg]	*131,142.84*	130,748.98	**130,518.34**	131,031.24	130,891.63	130,923.48	130,794.07	131,097.4	130,928.26	130,929.18
	ΔTC [kg]	*624.5*	230.64	**0**	512.9	373.29	405.14	275.73	579.06	409.91	410.84
	ΔTCp [%]	*0.479*	0.177	**0**	0.393	0.286	0.31	0.211	0.444	0.314	0.315
100	TC [kg]	164,372.44	164,318.54	164,311.78	**163,445.1**	*164,438.76*	164,426.9	164,127.93	164,139.71	164,435.83	163,887.5
	ΔTC [kg]	927.34	873.43	866.67	**0**	*993.65*	981.8	682.82	694.6	990.72	442.39
	ΔTCp [%]	0.567	0.534	0.53	**0**	*0.608*	0.601	0.418	0.425	0.606	0.271
999	TC [kg]	*742,299.57*	742,234.21	741,906.71	740,670.7	**740,129.31**	741,468.03	740,791.68	740,609.28	740,443.96	740,350.8
	ΔTC [kg]	*2,170.25*	2,104.89	1,777.39	541.39	**0**	1,338.72	662.36	479.97	314.64	221.49
	ΔTCp [%]	*0.293*	0.284	0.24	0.073	**0**	0.181	0.09	0.065	0.043	0.03

A comparison between the best and worst optimization results for the two approaches (corrected vertical flight plans versus not corrected) presented in Table 4.3, obtained based on the data from Table 4.1 and Table 4.2, shows that the results obtained for NCFPs are better than those for CFPs (except for CI = 0). When the best optimization results (CFPs vs. NCFPs) are compared (TC_{Min}), the maximum TC difference is 0.308% (obtained for CI = 999). For the worst-case optimization results (TC_{Max}), the maximum difference is 0.673%.

Table 4.3 Comparison between the minimum and maximum optimized TC for the cases where the vertical flight plan is corrected vs. not corrected

CI	TC_{Min}				TC_{Max}			
	TC_{CFP}[kg]	TC_{NCFP}[kg]	ΔTC [kg] $(TC_{CFP} - TC_{NCFP})$	ΔTCp [%] $100 * \frac{(TC_{CFP} - TC_{NCFP})}{TC_{NCFP}}$	TC_{CFP}[kg]	TC_{NCFP}[kg]	ΔTC [kg] $(TC_{CFP} - TC_{NCFP})$	ΔTCp [%] $100 * \frac{(TC_{CFP} - TC_{NCFP})}{TC_{NCFP}}$
0	96,794.84	96,924.26	-129.42	-0.134	97,459.08	97,539.09	-80.01	-0.082
10	103,790.23	103,664.28	125.95	0.121	104,445.75	104,133.61	312.14	0.3
30	117,228.6	116,904.46	324.14	0.277	117,693.34	117,503.34	190	0.162
50	130,877.31	130,518.34	358.97	0.275	131,447.88	131,142.84	305.04	0.233
100	163,942.14	163,445.1	497.04	0.304	164,748.05	164,438.76	309.29	0.188
999	742,411.11	740,129.31	2,281.8	0.308	747,027.97	742,299.57	4,728.4	0.637

The execution times for the optimization method and the two approaches relative to the invalid flight plans are presented in Table 4.4. It can be noted that the execution time for the case where the invalid flight plans are corrected (CFP) is more than twice longer than for the case where they are not corrected (NCFP). This is due to the fact that, when CFP is employed, for each segment, before computing the flight performance for a sub-segment, the altitude-speed combination is validated relative to the flight envelope. If the altitude – speed combination is not valid, the appropriate valid combination must be determined. In both cases, the long execution time can be attributed, in part, to the long flight, the complexity and implementation of the accelerated segment performance calculations, by using an aero-propulsive aircraft performance model, and the large number of sub-segments (integration steps) determined by the lateral flight plan (routing grid) and the vertical flight plan.

The flight plan used as the reference for comparing the performance of the proposed optimization method was generated based on the SWR40 reference track data. The limitations of the FlightAware flight track data are presented in sub-section 4.2.7 (i.e. unknown aircraft configuration, unknown atmospheric conditions encountered by the aircraft, unknown precise times and locations where the flight profile changes occur, etc.). An optimal flight plan (lateral path and altitude-speed flight profile) is specific for an

aircraft's configuration and atmospheric conditions. Therefore, a realistic reference flight plan cannot be constructed by retrieving data from the recorded data.

Table 4.4 Optimization execution times

	CI	Execution time (h)													
		Optimization test run										Min	Max	Avg.	Standard deviation
		1	2	3	4	5	6	7	8	9	10				
CFP	0	3.15	3.20	3.13	3.08	3.16	3.10	3.05	3.07	3.13	3.13	3.05	3.20	3.12	0.045
	10	3.10	3.12	3.13	3.04	3.12	3.07	3.10	3.10	3.10	3.14	3.04	3.14	3.10	0.028
	30	3.15	3.14	3.08	2.98	3.13	3.11	3.10	3.09	3.15	3.11	2.98	3.15	3.11	0.049
	50	3.15	3.15	3.12	3.06	3.15	3.10	3.11	3.10	3.10	3.13	3.06	3.15	3.12	0.030
	100	3.12	3.16	3.14	3.03	3.15	3.07	3.07	3.10	3.08	3.09	3.03	3.16	3.10	0.043
	999	3.19	3.10	3.19	3.05	3.20	3.10	3.12	3.08	3.15	3.15	3.05	3.20	3.13	0.052
NCFP	0	1.49	1.19	1.31	1.24	1.14	1.22	1.45	1.27	1.43	1.44	1.14	1.49	1.32	0.125
	10	1.27	1.22	1.31	1.31	1.45	1.41	1.36	1.31	1.39	1.48	1.22	1.48	1.35	0.083
	30	1.29	1.50	1.27	1.23	1.40	1.26	1.31	1.37	1.49	1.47	1.23	1.50	1.36	0.100
	50	1.24	1.33	1.43	1.28	1.34	1.67	1.28	1.30	1.57	1.41	1.24	1.67	1.39	0.138
	100	1.19	1.38	1.33	1.17	1.09	1.40	1.19	1.28	1.36	1.36	1.09	1.40	1.28	0.107
	999	1.27	1.25	1.41	1.22	1.23	1.33	1.28	1.28	1.50	1.17	1.17	1.50	1.29	0.097

The reference lateral flight plan was constructed by retaining, from the SWR40 reference track data, a subset of WPTs that best approximate the lateral flight trajectory using the minimum number of orthodromic segments. The selection of the WPTs that define the reference lateral flight plan starts with the initial WPT of the SWR40 reference track. At each step, a new WPT is selected such that it results in the longest orthodromic segment for which the distance from the orthodromic segment to each of the SWR40 reference track data WPTs, situated in-between the two selected WPTs that delimit the orthodromic segment, is smaller than 5 n.m. Two more WPTs, denoted as WPTV1 and WPTV2, were added at locations where the vertical flight profile changes occur:

1. The location of the End of Climb phase/beginning of the Cruise phase, selected at 300 n.m. from the initial WPT; and
2. The location of the End of Cruise phase/beginning of the Descent phase, selected at 300 n.m. before the final WPT.

If such a location was already among those selected as a lateral flight plan WPT, then there is no need to add it to the reference flight plan.

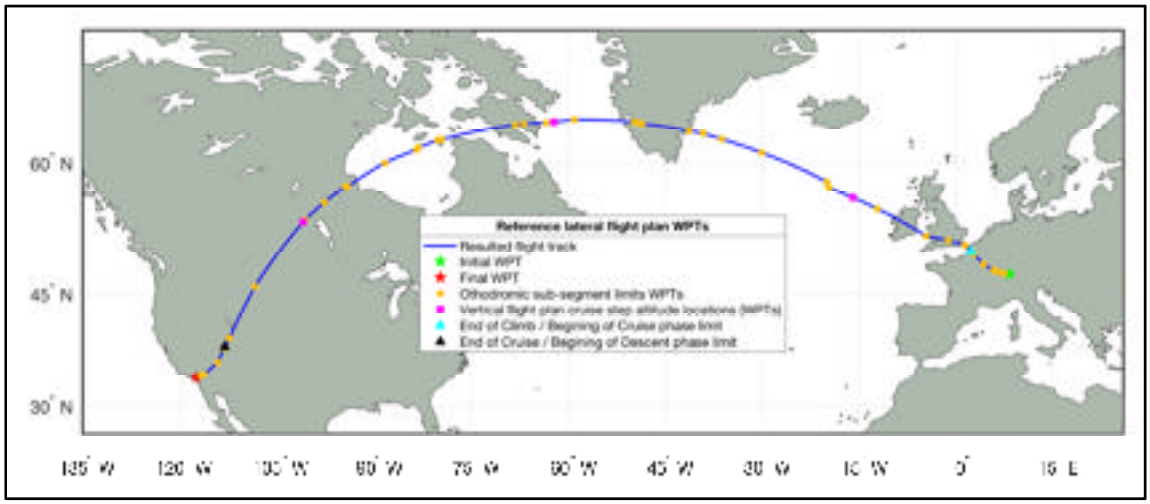

Figure 4.19 The significant WPTs of the reference lateral flight plan

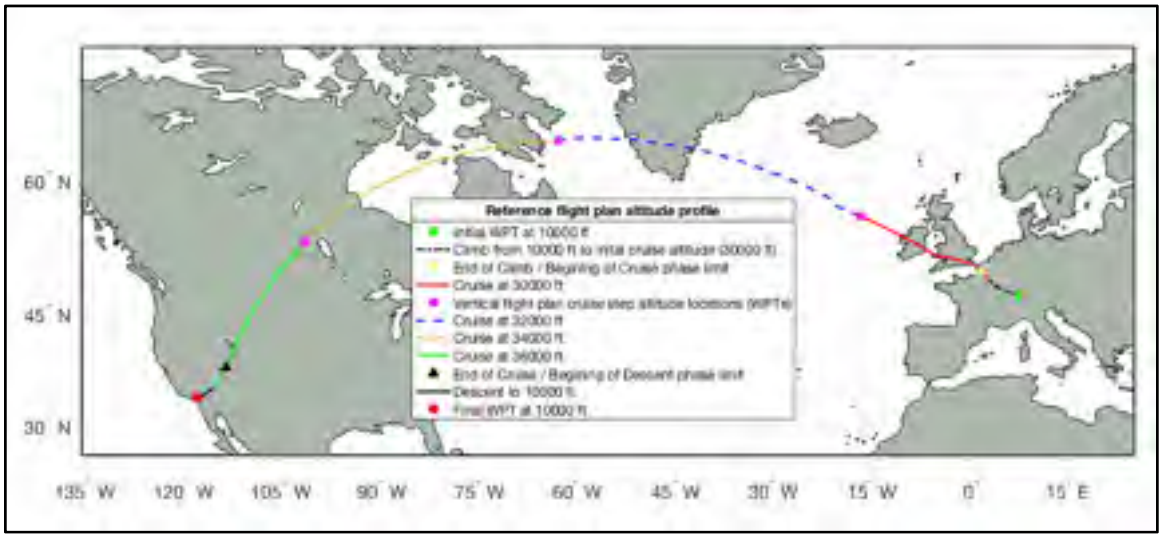

Figure 4.20 Altitude profile for the reference profile

The lateral component of the reference flight trajectory and the selected significant WPTs, corresponding to the reference flight plan, resulted by following the process described above, are presented in Figure 4.19. During the accelerated flight simulation each segment was decomposed into sub-segments (integration steps) with a maximum sea-level length of 50 n.m., on which the same laws of variation describe the aircraft performance parameters and evolution. These WPTs are not represented in Figure 4.19 because they are specific for the

selected flight plan parameters, and they are determined during the accelerated flight performance calculations.

The altitude component of the reference vertical flight plan, the initial, final and cruise flight altitudes, as well as the points where the cruise altitude changes occur along the flight track, were all obtained from the SWR40 reference track data (Figure 4.20).

Given the limitations of the FlightAware flight track data, and in order to obtain a good reference profile, the speed component of the reference flight plan was obtained following an optimization for the aircraft weight (the same value as used in the proposed method evaluation), atmospheric conditions, reference lateral flight plan and altitude flight plan. The structure of the candidate reference plan speed profile is constructed as follows:

1. A climb and descent at [IAS, MACH] speed schedule pairs; and
2. It was assumed that the constant altitude cruise sections are flown at constant speed. Thus, the cruise section contains four constant speed cruise segments, corresponding to the four constant altitude cruise segments.

The structure of the speed profile is consistent with the employed aircraft climb/descent speed profiles, and the current navigation paradigm (long cruise segments at constant speed) on busy airways, such as oceanic routes and congested airspace.

The speed optimization was performed using a genetic algorithm, similar to the one used in the proposed method (in this case only the speed changes were considered). The speed optimization was performed five times for each CI value. The population size for the genetic algorithm was selected to be 30 and the number of generations was set at 300. As in the case of the proposed optimization method, when a profile speed candidate was invalid, the reference speed flight plan optimization was conducted using two approaches: Corrected Speed Flight Plan (CFP) and Non-Corrected Speed Flight Plan (NCFP).

Table 4.5 Reference profile optimization results

	CI	Parameter Type	Reference flight plan optimization run					TC_{RSmin} [kg]	TC_{RSmax} [kg]
			1	2	3	4	5		
CFP	0	TC_{RS} [kg]	98,364.37	98,369.11	98,361.17	98,353.25	98,372.26	98,353.25	98,372.26
		ΔTC_{RS} [kg] (TC_{RS}-TC_{RSmin})	11.12	15.86	7.92	0	19.015	0	19.015
		ΔTC_{RSp} [%] $(100 * \frac{\Delta TC_{RS}}{TC_{RSmin}})$	0.0113	0.0161	0.0081	0	0.0193	0	0.0193
	10	TC_{RS} [kg]	105,311.0	105,320.56	105,330.45	105,322.44	105,313.86	105,311.09	105,330.45
		ΔTC_{RS} [kg] (TC_{RS}-TC_{RSmin})	0	9.46	19.35	11.34	2.77	0	19.35
		ΔTC_{RSp} [%] $(100 * \frac{\Delta TC_{RS}}{TC_{RSmin}})$	0	0.009	0.0184	0.0108	0.0026	0	0.0184
	30	TC_{RS} [kg]	119,192.5637	119,123.9429	119,227.1199	119,207.9352	119,185.7595	119,123.9429	119,227.11
		ΔTC_{RS} [kg] (TC_{RS}-TC_{RSmin})	68.6208	0	103.177	83.9923	61.8165	0	103.17
		ΔTC_{RSp} [%] $(100 * \frac{\Delta TC_{RS}}{TC_{RSmin}})$	0.0576	0	0.0866	0.0705	0.0519	0	0.0866
	50	TC_{RS} [kg]	132,980.1012	133,060.4954	132,896.1737	132,921.6528	132,981.7899	132,896.1737	133,060.49
		ΔTC_{RS} [kg] (TC_{RS}-TC_{RSmin})	83.9275	164.3216	0	25.4791	85.6162	0	164.32
		ΔTC_{RSp} [%] $(100 * \frac{\Delta TC_{RS}}{TC_{RSmin}})$	0.0632	0.1236	0	0.0192	0.0644	0	0.1236
	100	TC_{RS} [kg]	167,298.4173	167,238.4737	167,349.724	167,301.4764	167,345.7783	167,238.4737	167,349.72
		ΔTC_{RS} [kg] (TC_{RS}-TC_{RSmin})	59.9436	0	111.2503	63.0027	107.3046	0	111.25
		ΔTC_{RSp} [%] $(100 * \frac{\Delta TC_{RS}}{TC_{RSmin}})$	0.0358	0	0.0665	0.0377	0.0642	0	0.0665
	999	TC_{RS} [kg]	765,706.5453	768,088.8428	767,239.7605	766,411.3878	766,658.9698	765,706.5453	768,088.84
		ΔTC_{RS} [kg] (TC_{RS}-TC_{RSmin})	0	2,382.2975	1,533.2152	704.8425	952.4245	0	2,382.29
		ΔTC_{RSp} [%] $(100 * \frac{\Delta TC_{RS}}{TC_{RSmin}})$	0	0.3111	0.2002	0.0921	0.1244	0	0.3111
NCFP	0	TC_{RS} [kg]	99,653.146	99,123.4788	99,420.2238	99,154.2192	100,492.4391	99,123.4788	100,492.43
		ΔTC_{RS} [kg] (TC_{RS}-TC_{RSmin})	529.6673	0	296.745	30.7404	1,368.9604	0	1,368.96
		ΔTC_{RSp} [%] $(100 * \frac{\Delta TC_{RS}}{TC_{RSmin}})$	0.5344	0	0.2994	0.031	1.3811	0	1.3811
	10	TC_{RS} [kg]	106,292.7885	106,042.2328	106,052.2285	105,936.0668	106,943.0873	105,936.06	106,943.08
		ΔTC_{RS} [kg] (TC_{RS}-TC_{RSmin})	356.7217	106.166	116.1617	0	1,007.0205	0	1,007.0205
		ΔTC_{RSp} [%] $(100 * \frac{\Delta TC_{RS}}{TC_{RSmin}})$	0.3367	0.1002	0.1097	0	0.9506	0	0.9506
	30	TC_{RS} [kg]	119,803.3294	119,753.1844	119,792.4048	120,329.545	119,698.7655	119,698.76	120,329.54
		ΔTC_{RS} [kg] (TC_{RS}-TC_{RSmin})	104.5639	54.4189	93.6394	630.7795	0	0	630.77
		ΔTC_{RSp} [%] $(100 * \frac{\Delta TC_{RS}}{TC_{RSmin}})$	0.0874	0.0455	0.0782	0.527	0	0	0.527
	50	TC_{RS} [kg]	133,569.0875	133,982.639	133,451.4108	133,578.9475	133,900.8273	133,451.41	133,982.63
		ΔTC_{RS} [kg] (TC_{RS}-TC_{RSmin})	117.6766	531.2281	0	127.5367	449.4165	0	531.22
		ΔTC_{RSp} [%] $(100 * \frac{\Delta TC_{RS}}{TC_{RSmin}})$	0.0882	0.3981	0	0.0956	0.3368	0	0.3981
	100	TC_{RS} [kg]	167,922.7594	167,984.945	167,975.5775	168,099.6192	167,832.6943	167,832.69	168,099.61
		ΔTC_{RS} [kg] (TC_{RS}-TC_{RSmin})	90.0651	152.2508	142.8833	266.925	0	0	266.925
		ΔTC_{RSp} [%] $(100 * \frac{\Delta TC_{RS}}{TC_{RSmin}})$	0.0537	0.0907	0.0851	0.159	0	0	0.159
	999	TC_{RS} [kg]	774,492.9721	772,589.8084	771,007.7656	770,817.4302	770,727.5163	770,727.51	774,492.97
		ΔTC_{RS} [kg] (TC_{RS}-TC_{RSmin})	3,765.4558	1,862.2922	280.2493	89.9139	0	0	3,765.45
		ΔTC_{RSp} [%] $(100 * \frac{\Delta TC_{RS}}{TC_{RSmin}})$	0.4886	0.2416	0.0364	0.0117	0	0	0.4886

Table 4.5 presents the results obtained for the reference flight plan speed optimization for each of the five CI test runs. The flight plan that yielded the best total cost among the five test runs (marked by the column TC_{RSmin}) was retained as the speed component of the reference vertical flight plan.

A comparison between the best/worst flight plan optimization results obtained using the proposed method, and the best reference flight plans is shown in Table 4.6. The TC_{RSmin} in Table 4.6 represents the best total cost (best flight optimization results) obtained for the reference flight profile, cost index and invalid flight profile correction strategy. The other two columns ("Best case optimization results" and "Worst case optimization results") represent the best and worst optimizations results obtained using the proposed methodology (minimum and maximum total costs) and the comparison with the best reference profile performance.

Table 4.6 Flight plan optimization results: comparison between the best and worst optimization results versus the best reference flight plan

	CI	TC_{RSmin} [kg]	Best case optimization results			Worst case optimization results		
			$TC_{Optimal}$ [kg]	ΔTC_{RS} [kg] ($TC_{Optimal}$ - TC_{RSmin})	ΔTC_{RSp} [%] $100 * \frac{\Delta TC_{RS}}{TC_{RSmin}}$	$TC_{Optimal}$ [kg]	ΔTC_{RS} [kg] ($TC_{Optimal}$ - TC_{RSmin})	ΔTC_{RSp} [%] $100 * \frac{\Delta TC_{RS}}{TC_{RSmin}}$
CFP	0	98,353.25	96,794.84	-1,558.41	-1.585	97,459.08	-894.17	-0.909
	10	105,311.09	103,790.23	-1,520.86	-1.444	104,445.75	-865.34	-0.822
	30	119,123.94	117,228.6	-1,895.34	-1.591	117,693.34	-1,430.6	-1.201
	50	132896.17	130,877.31	-2,018.86	-1.519	131,447.88	-1,448.29	-1.09
	100	167238.47	163,942.14	-3,296.33	-1.971	164,748.05	-2,490.42	-1.489
	999	765706.55	742,411.11	-23,295.44	-3.042	747,027.97	-18,678.58	-2.439
NCFP	0	99,123.48	96,924.26	-2,199.22	-2.219	97,539.09	-1,584.39	-1.598
	10	105,936.07	103,664.28	-2,271.79	-2.144	104,133.61	-1,802.46	-1.701
	30	119,698.77	116,904.46	-2,794.31	-2.334	117,503.34	-2,195.43	-1.834
	50	133,451.41	130,518.34	-2,933.07	-2.198	131,142.84	-2,308.57	-1.73
	100	167,832.69	163,445.1	-4,387.59	-2.614	164,438.76	-3,393.93	-2.022
	999	770,727.52	740,129.31	-30,598.21	-3.97	742,299.57	-28,427.95	-3.688

It can be observed that, for the case where the invalid flight plans are corrected (CFP), the best optimization results (optimal flight plan obtained using the proposed method vs. the reference flight plan) gave a reduction of the total cost of between 1.585% and 3.042%. In the worst case, the reduction was found to be between 0.909% and 2.439%.

When the invalid flight plans were not corrected (NCFP), the results were found to be better: in the best case the total cost reduction was between 2.144% and 3.97%, and the in worst case the total cost reduction was between 1.598% and 3.688%.

For the evaluated test cases, the best results (in terms of both optimization performance and execution time) were obtained when the invalid candidate flight plans were not corrected relative to the aircraft's flight envelope limitations (NCFP).

4.4 Conclusions

This paper presents a new optimization method for flight trajectory optimization, in which the candidate flight trajectories, and thus the optimal flight trajectory, are defined as flight plans decomposed into two elements: a lateral flight plan and a vertical flight plan. The proposed method uses a genetic algorithm to search for the "optimum" flight plan among the set of candidate flight plans that minimizes the total cost for the flight. The accelerated flight performance calculations, which construct the flight trajectory resulted from executing a candidate flight plan, and compute the flight performance parameters, were conducted using an in-house aircraft performance model that uses the BADA 4.0 APM. The test scenario employed for the evaluation of the proposed method was constructed based on the recorded flight trajectory of a real flight, retrieved from FlightAware, performed with the same aircraft model as the one used in the calculations.

As expected for optimizations performed using genetic algorithms, for an identical optimization problem (identical input data), the optimal solution varied from test run to test run. However, for the tests performed in this study, for each of the evaluated test scenarios the difference between the optimum flight plan total costs obtained for the ten runs was less than 1%. It can be observed that, the case where the candidate flight plans are "corrected" (CFP) produces the worst results, both in terms of total cost and total execution time, relative to the case where the invalid flight plan is assigned a large penalty total cost (NCFP). The authors believe that, for the cases where the candidate flight plans are "corrected", even though in each new generation all the child flight plans are valid relative to the aircraft's flight envelope, there is a loss of optimality because of the fact that, overall, the populations are "less diverse". The increase in execution time is due to the fact that for each invalid altitude/speed flight plan segment additional (complex) computations are required to identify

the appropriate flight envelope limit combination. For the NCFP approach and the set of CI values considered as test cases, the total cost reduction for the optimal flight plan relative to the best obtained reference flight plan was found to be between 2.144% and 3.97%, and the worst case gave cost reductions between 1.598% and 3.688%. The authors therefore estimate that the longer execution time renders the method more appropriate for flight planning rather that real time/online optimization. The longer execution time is due to the large number of flight plans evaluated during the optimization, the very long flight (5,130.3 n.m sea level distance along the orthodromic route), with its large number of integration steps/flight performance calculation steps, and partially due to the flight performance calculations using a dynamic atmosphere model and the aero propulsive/Total Energy Model aircraft performance model.

For any optimal flight plan (local or global), there is a correlation between the lateral and vertical flight plans. Changing/imposing one component of a flight plan could result in a different optimal solution, with a different total cost, and different configuration for the other components of the flight plan.

Future work could investigate the performance of a more computationally expensive optimization approach, where at each step of the genetic algorithm:

1. The new population is generated using the genetic operations applied on the lateral flight plan (the vertical flight plan is retained from a parent); and then,
2. For each member of the new population a new search (e.g. branch and bound, annealing, etc.) identifies the optimal vertical flight plan.

Another direction of investigation could evaluate the execution time performance of the proposed method when the accelerated flight performance calculations are performed using a simplified aircraft performance model, based on interpolation tables, mainly used in FMS platforms.

CHAPTER 5

NEW FIGHT PLAN OPTIMIZATION METHOD UTILIZING A SET OF ALTERNATIVE FINAL POINT ARRIVAL TIME TARGETS (RTA CONSTRAINTS)

Radu Ioan Dancila[a] and Ruxandra Mihaela Botez[b]

[a,b]École de Technologie Supérieure, Université du Québec
LARCASE Laboratory of Research in Active Controls, Aeroservoelasticity and Avionics
1100 rue Notre Dame Ouest, Montréal, H3C1K3, Québec, Canada

This article was submitted to The Aeronautical Journal, in November 2020

Résumé

Cet article propose une nouvelle méthode pour l'optimisation des trajectoires de vol, dérivée de la méthode Non-dominated Sorting Genetic Algorithm II utilisée dans les optimisations multi-objectives. La nouvelle méthode trouve, en parallèle, un ensemble des plans de vol optimaux pour un segment de trajectoire de vol. Chacune des solutions est la solution optimale (consommation minimale) pour une des contraintes d'heure d'arrivée requise de l'ensemble des contraintes de temps imposées pour le point final de la trajectoire de vol. L'ensemble de contraintes de temps sont choisis en tant que leurs limites sont contiguës, c.a.d. elles couvrent entièrement un domaine de temps sélectionné. La méthode d'optimisation proposée peut être appliquée dans de futures paradigmes opérationnelles, comme Trajectory Based Operations/free flight, où les avions ne doivent pas suivre des routes prédéterminées. La méthode proposée est destinée à aider les décisionnaires, dans la phase de planification du vol quand il existe une contrainte de temps ou un temps de passage préféré pour le point final de la trajectoire de vol à optimiser. Les décideurs peuvent choisir, parmi l'ensemble des profils de vol optimaux, celui qui remplit mieux leur critères (consommation minimale ou temps de passage). Si le plan de vol est rejeté par le système de gestion du trafic aérien, ils peuvent choisir le suivant meilleur plan de vol parmi l'ensemble des solutions (plans de vol), sans être obliges d'effectuer une autre optimisation. Cette méthode peut être appliquée quand l'optimisation est réalisée sur la composante latérale ou la composante verticale du plan de vol, ou sur les deux composantes. Sept versions de cette

méthode ont été évaluées, et 10 essais ont été effectués pour chaque version. Pour cinq de ces versions, les pires résultats ont mené à une consommation de combustible inférieure à 90 kg (0.14 %) au-dessus des optimums «globaux». La version de méthode la moins performante a produit une consommation de combustible avec 321 kg (0.56 %) au-dessus des optimums «globaux».

Abstract

This study investigates a new aircraft flight trajectory optimization method, derived from the Non-dominated Sorting Genetic Algorithm II method used for multi-objective optimizations. The new method determines, in parallel, a set of optimal flight plan solutions for a flight. Each solution is optimal (requires minimum fuel) for a Required Time of Arrival constraint from a set of candidate time constrains selected for the final waypoint of the flight section under optimization. The set of candidate time constraints are chosen so that their bounds are contiguous (they completely cover a selected time domain). The proposed flight trajectory optimization method may be applied in future operational paradigms, such as Trajectory Based Operations / free flight, where aircraft do not need to follow predetermined routes. The intended application of the proposed method is to support Decision Makers in the planning phase when there is a time constraint or a preferred crossing time at the final point of the flight section under optimization. The Decision Makers can select, from the set of optimal flight plans, the one that best fits their criteria (minimum fuel burn or observes a selected time constraint). If the Air Traffic Management rejects the flight plan, then they can choose the next best solution from the set without having to perform another optimization. The method applies for optimizations performed on lateral and/or vertical flight plan components. Seven proposed method variants were evaluated, and 10 test runs were performed for each variant. For five variants, the worst results yielded a fuel burn less than 90 kg (0.14%) over the “global” optimum. The worst variant yielded a maximum of 321 kg (0.56%) over the “global” optimum.

5.1 Introduction

This paper presents a new optimization method designed to support Decision Makers in the planning phase of flights with a Required Time of Arrival (RTA) constraint at the final waypoint (WPT_{final}). The proposed flight trajectory optimization method may be applied in future operational paradigms, such as Trajectory Based Operations / free flight, where aircraft do not need to follow predetermined routes.

Aircraft flight trajectories are the result of two levels of planning, optimization and validation: local (aircraft), and global (airspace). At the aircraft level, the flight trajectory planning, optimization, and validation are performed by aircraft operators / the Flight Management System (FMS) / an aircrew (Ng, Sridhar & Grabbe, 2012; Ballin, Williams, Allen & Palmer, 2008; Patrick & Sheridan, 1998), based on specific flight data (aircraft performance data and limitations, load, departure/destination pair, atmospheric conditions, navigation constraints, etc.). The result is a flight profile that minimizes a preselected cost function (fuel burn, total costs, flight time, etc.), and satisfies all constraints and regulations (FAA, n.d.d). At the global level, the Air Traffic Management System (ATM) (Fanti, Pedroncelli, Stecco & Ukovich, 2012; Ballin, Wing, Hughes & Conway, 1999; Rodionova et al., 2012; Torres & Delpome, 2012; Cate, 2013) performs the optimization and validation. The objective is to ensure safe operations for all aircraft in that airspace (aircraft separation, compliance with navigation rules, regulations and policies, etc.) and to maximize the airspace throughput. The optimal flight trajectory selected by the flight operator is defined as a Flight Plan (FPL) (FAA, n.d.a; Altus, 2009). A FPL is a standard, structured format, flight trajectory description, and is submitted to ATM for validation and approval. If the FPL is rejected, the flight planning sequence is repeated. In the future, upon the implementation of time-based metering operation in the US airspace (Underwood et al., 2020), at certain points in the airspace (geographic locations and altitudes) where the traffic demand is high, a time constraint (RTA constraint), negotiated between the flight planner and the ATM, will be assigned to each aircraft, which will have to cross the location within its assigned time window.

An aircraft can fly at any altitude – speed combination within its flight envelope. Although this is the case, the FPL segments have discrete speed and altitude values. The discrete speed values (multiples of 1 knot (kn) for Calibrated Air Speed (CAS), and 0.001 for MACH) are a result of the limitations regarding their selectable values in the FMS and the Flight Control Unit (FCU). Cruise altitudes are multiples of 1,000 feet (ft), as imposed by navigation regulations.

Some examples of flight trajectory optimization problems treated in the literature as a flight-planning problem are: Di Vito et al. (2009), Chaimatanan et al. (2012), Qu et al. (2014), Wickramasinghe et al. (2012), Rodionova et al. (2014), Chamseddine et al. (2012), Woods et al. (2013), Woods, Vivona, Wing & Burke (2016). The Aircraft's Performance Model (APM), the Atmospheric Data Model (ADM), the specific optimization problem (initial aircraft position and speed, weight, fuel quantity, etc.) and the method/approach, etc., influence the results of the optimization: the flight trajectories/flight plans identified as solutions and their qualities.

The type of APM used in flight performance calculations differs as a function of the context and platform on which they are conducted. In ATM platforms, the flight performance calculations are performed on ground-based computers, using an aero-propulsive aircraft model (BADA: Nuic et al., 2010a; Eurocontrol, n.d.; Nuic, 2010b; Eurocontrol, 2010) that is more complex and more accurate than other models. In current FMS platforms, on-board systems with a limited computational power, the flight performance calculations are performed using an APM based on interpolation tables (Performance Database – PDB) (Murrieta-Mendoza & Botez, 2015a; Sibin et al., 2010), less accurate and less complex. Ramasamy et al. (2014) and Ramasamy, Sabatini, Gardi & Liu (2013) presented concepts for a New Generation Flight Management System (NG-FMS) architecture and flight trajectory optimization algorithms. The APM can be provided either by the aircraft manufacturer, or could be generated/estimated based on flight test data. Ghazi presented a method to generate an APM (Ghazi & Botez, 2015b), and an engine model (Ghazi et al., 2015a), based on test flight data. Murietta-Mendoza et al. (2015b) devised a method for generating a cruise phase

PDB from flight test data generated with a level D flight simulator. Ghazi, Botez & Tudor (2015c) presented a method to generate a climb phase PDB from an aero-propulsive aircraft model created from flight test data obtained using a level D flight simulator for Cessna Citation X. Dancila et al. (2013) developed a new method that estimates, faster and more precisely, the fuel burn for a cruise segment at constant altitude and the time required to burn a specified quantity of fuel.

The atmospheric data (air temperature and wind predictions) are issued by national meteorological service agencies in a gridded format (GRIB2) (NOAA, n.d.a; Environment Canada, n.d.g), and in various forecast models. Atmospheric data are defined in the nodes of a 4D grid (latitude, longitude, pressure altitude, and time). The differences between the forecast models refer to the area covered by the forecast (global (Environment Canada, n.d.a; Buehner et al., 2015) or regional (Environment Canada, n.d.e; Caron et al., 2015)), the grid resolution, map projection type (latitude-longitude or polar-stereographic), forecast timespan, and update interval. Various studies evaluated the forecast data accuracy relative to the real atmospheric conditions encountered by aircraft (Cole et al., 2000; Wynnyk, 2012; Bronsvoort et al., 2011), and interpolation methods (Stohl et al., 1995; Stohl, 1998). The atmospheric conditions (wind and air temperature) along the flight trajectory have an important effect on the aircraft's flight performance (flight envelope limitations, fuel burn rate, etc.) and its global performance (fuel burn and flight time). Therefore, the atmospheric data used in calculations should be as close as possible to the real atmospheric conditions encountered by the aircraft. A review of the available atmospheric data, their sources, and their integration in a prototype route optimization tool developed by NASA, called the Traffic Aware Planner (TAP) application, is presented in Lewis, Burke, Underwood & Wing (2019).

Similarly with the APM, ADMs vary as a function of the optimization context/platform, timespan, and area delimiting the flight trajectory. In FMS platforms, given their limited computational power and memory, the atmospheric data are considered stationary, defined in a selected set of points along the flight trajectory, at a limited set of altitudes (Bronsvoort et al., 2011). The atmospheric conditions in a point of interest, other than where the data was

defined, are computed by multi-linear interpolations (Stell, 2010a; Stell, 2010b; De Smedt & Berz, 2007). In online ATM platforms, the atmospheric data are computed from forecast data (Wynnyk, 2012; Wickramasinghe et al., 2012) by linear interpolations, as a tradeoff between precision and computation time. Dancila & Botez (2020a) (the investigation presented in Chapter 3) developed a new ADM that defines the time-varying atmospheric data in the nodes of a routing grid (RGRID). The model computes the atmospheric parameter values in a grid node on average six times faster and with the same accuracy as when calculated by 4D interpolations from GRIB2 data.

In flight performance prediction and fight planning/optimization applications, an aircraft flight trajectory is determined by performing an accelerated simulation of the FPL. The methodology for performing the accelerated simulation and the performance data calculation is described in Schreur (1995) and Karr, Vivona, Woods & Wing (2017). The optimal solution to a flight planning/trajectory optimization problem is the result of a search. The search identifies, as a function of the optimization objective, the lateral flight trajectory (Lateral Flight Plan – LFPL), the vertical flight trajectory (Vertical Flight Plan – VFPL – the speed and altitude profile), or both, that minimize a selected cost function and satisfy the imposed constraints. The search is performed within a candidate solution set, selected as a function of the optimization scenario. Dancila & Botez (2014) proposed a method to construct a family of vertical flight profiles, that cover the aircraft's flight envelope, appropriate for use in FMS flight trajectory computation and optimization. Geometrical approaches to vertical flight trajectory optimization are presented in Dancila, Beulze & Botez (2016b) and Dancila, Beulze & Botez (2019). Yu & Zhang (2015) presented a survey on Unmanned Aerial Systems (UAS) flight planning approaches. Ceruti & Mazorca (2017) modeled the docking maneuver of an airship by Bezier curves and proposed an optimization method using Particle Swarm Optimization (PSO) to determine the optimal Bezier curve parameters that minimize the energy necessary for the maneuver. For constrained optimization problems, some constraints apply to the candidate profile set (e.g. altitudes, speeds, WPTs, etc.), and others refer to solution attributes (e.g. time constraint(s), etc.). Liden (1992) showed that when a flight trajectory is defined by an LFPL and a VFPL that

contains a set of segments flown at a set of constant speeds and altitudes, the flight time as a function of speed might contain discontinuities (there are no FPL segment speed and altitude combinations that yield a flight time within a time domain).

Hagelauer & Mora-Camino (1998) proposed a Dynamic Programming (DP) optimization method for 4D trajectories with multiple RTA constraints along the route, defined as a control problem, where the search space was reduced using a heuristic. Other authors used an approach based on evolutionary algorithms for solving the optimization problem of a flight trajectory with an RTA constraint. Murrieta Mendoza, Bunel & Botez (2016) used an Artificial Bee Colony optimization algorithm to determine the optimum vertical flight profile for a cruise segment with RTA constraint. The vertical flight profile was then processed to obtain a vertical flight profile with a minimum number of speed changes. Gardi et al. (2016) presented a review of the multi-objective 4D flight trajectory optimization methods, in which the cost functions incorporate operational costs, as well as other cost elements such as noise, polluting emissions, contrails, airspace congestion, etc. Flight guidance and control concepts (Ballin et al., 2008; Diaz-Mercado, Lee, Egerstedt & Young, 2013) were developed to generate optimal 4D trajectories with a set of RTA constraints assigned at WPTs along the flight trajectory.

Ceruti et al.(2014) presented a multidisciplinary optimization approach that uses heuristic optimization strategies, appropriate for the case where the optimization involves multiple independent parameters. Another multidisciplinary optimization method presented by Ceruti et al. (2018) assigns the fitness value for a candidate solution based on two extreme solutions (an ideal best and an ideal worst solutions) determined for each iteration of the algorithm.
Multi-Objective Optimization (MOO) algorithms are extensively used to solve problems where the solution must satisfy multiple competing and contradictory objectives. Marler & Arora (2004) conducted a survey of the MOO methods used in engineering. Miettinen (2001) presented the concepts related to MOO and described a series of approaches and methods to conduct the optimization. Fonseca & Fleming (1993) presented an analysis of MOO methods based on genetic algorithms. Murata and Ishibuchi presented examples of MOO methods

based on genetic algorithms: an outline for conducting MOO using genetic algorithms (MOGA – (Murata & Ishibuchi, 1995)), and local search methods (Ishibuchi & Murata, 1996; Ishibuchi & Murata, 1998). Fonseca and Fleming proposed a MOO method for optimization problems with multiple constraints, based on evolutionary algorithms (Fonseca & Fleming, 1998a; Fonseca & Fleming, 1998b). Deb et al. (2002) presented an elitist MOO algorithm based on genetic algorithms and non-dominated population sorting (NSGA-II). Jensen (2003) proposed a new non-dominated sorting method that reduces the number of comparisons between the population members, thus reduces the computation time.

5.2 Problem statement

The optimization problem considered in this paper is defined as follows:

1. Given an:
    a. Aircraft model that performs the flight (aircraft flight envelope, APM);
    b. Initial conditions: aircraft location WPT_{init} (latitude, longitude, altitude) and time, weight, quantity of fuel on-board, and speed;
    c. The final location WPT_{final} (latitude, longitude, and altitude) to be reached by the aircraft, and the speed at the final location;
    d. The selected range of flight altitudes and speeds, and the geographic area through which the aircraft trajectory can be routed;
    e. The atmospheric conditions for the geographic area, range of altitudes and times that cover all the candidate flight trajectories; and
    f. A set of N adjacent RTA constraints, defined by a set RTA_n of constraint values bounded by ΔRTA, which cover a selected time domain, imposed at WPT_{final}.
2. Identify the set of FPLs (each FPL corresponds to a particular RTA constraint [RTA_n - ΔRTA / 2, RTA_n + ΔRTA / 2]), where each FPL requires the minimum fuel burn relative ro FPLs that yield a flight time within the particular RTA constraint bounds. It is assumed that the FPLs have the standard format presented in sub-section 5.3.1.

5.3 Methodology

A flight trajectory optimization for a flight section with an imposed/chosen RTA constraint could pose two problems: the optimized FPL may be rejected by the ATM, or there may be another RTA constraint value acceptable for the DM and ATM for which the optimal FPL yields a better fuel burn/performance.

To the best of the authors' knowledge, the method proposed in this paper has not been considered before. The proposed optimization method, based on an Evolutionary Algorithm, derived from the Non-dominated Sorted Genetic Algorithm II (NSGA-II) (Deb et al., 2002), solves these problems by conducting, in parallel, a search for optimal FPLs for a set of adjacent RTA constraint values that cover a flight time domain of interest. The optimization is conducted in the objective space (fuel burn – flight time). Following the optimization, a DM is presented with a set of optimal FPL solutions, one for each RTA constraint. The FPL that best suits the optimization criteria (minimum fuel burn, flight time, or a tradeoff between the two) can be selected and filed for approval by the ATM. If rejected, the next-best FPL could be selected from the solution set.

This section is structured as follows: The first sub-section (5.3.1) presents concepts regarding flight trajectories and flight plans. The next sub-section (5.3.2) presents the APM used in this study, followed by the ADM, in sub-section 5.3.3. Sub-section 5.3.4 describes the methodology used for computing the flight trajectory and the flight performance (flight time and fuel burn) for a candidate flight plan. Finally, sub-section 5.3.5 presents the proposed methodology.

5.3.1 Flight trajectory/flight plan

An FPL (FAA, n.d.a; Altus, 2009) is a description of an aircraft's flight trajectory (the space-time evolution), in a standard and compact format. It contains all the information necessary for:

1. The onboard automation (FMS) to perform predictive calculations and flight performance parameter validations (flight envelope limitations, available fuel, navigation constraints, etc.), and to execute the flight along the flight trajectory; and
2. The ATM to validate the flight trajectory relative to conflicts with other aircraft trajectories along the route, restricted airspace incursions, adverse/dangerous atmospheric conditions (icing, severe turbulence, convective activity, etc.), navigation constraints, regulations, regulations, etc.

An FPL has two components: a lateral flight plan (LFPL) that defines the lateral flight trajectory component (the flight trajectory's projection on the earth's surface), and a vertical flight plan (VFPL), which defines the altitude – speed profile along the LFPL.

5.3.1.1 Lateral flight plan

An LFPL describes the lateral flight trajectory component as a succession of WPTs (geographic locations) that define flight trajectory segments. A LFPL segment type (Lenart, 2017) can be either loxodromic (the aircraft maintains a constant heading along the segment) or orthodromic (the shortest distance between the two WPTs and the heading changes along the segment). The lateral segment parameters' calculations (Sea Level Length - SLL, departure and arrival headings, the aircraft's heading in a point along the segment, etc.) are performed differently, as a function of the segment's type and the Earth model employed (spherical or WGS84 ellipsoid (Janssen, 2009)). The loxodromic segment parameters are computed using the rhumb line equations (Carlton-Wippern, 1992). The orthodromic segment parameters are computed using spherical trigonometry for orthodromic segments on a spherical Earth, and Vincenty's formulas (Karney, 2013) for orthodromic segments on an ellipsoidal Earth.

The set of LFPL candidates evaluated in the optimization are constructed by selecting, successively, from an RGRID, the WPTs that delimit each FPL segment. First, the RGRID is

constructed similarly to the method presented in Dancila & Botez (2020a) (the investigation presented in Chapter 3) and in a flight trajectory optimization study conducted by the authors (Dancila & Botez (2020b) – Chapter 4). An Orthodromic Route (ORT) is constructed between WPT_{init} and WPT_{final} and then divided into the minimum number of equal segments with an SLL smaller than or equal to a selected value (step size). In each ORT segment limit WPT a new orthodrome is constructed, perpendicular to the ORT (P-ORT), and new WPTs are created at locations that generate segments with a selected SLL, up to a selected maximum deviation from the ORT. The RGRID is constructed step by step, starting from WPT_{init}. Relative to its location, the aircraft can advance to a new RGRID WPT situated one step ahead along the ORT, and a maximum number of steps (Nw) along the P-ORT, on either side. Therefore, the RGRID starts with a single WPT (WPT_{init}) and increases, at each step along the ORT, with $2 \times N_W$ (Nw on each side of the ORT), until it reaches the maximum deviation (number of transversal WPTs). At the other end, starting at a certain position along the ORT, the number of WPTs across the ORT starts to decrease by $2 \times N_W$ WPTs, until it reaches the final WPT (WPT_{final}), where there is a single WPT. The candidate LFPL construction is performed step by step, starting from WPT_{init}. For each LFPL segment, the RGRID WPTs that define the segment are selected by choosing the lateral deviation step and the number of WPTs on the segment (steps along the ORT). An illustration of an RGRID and a LFPL are presented in Figure 5.1.

To accelerate the flight performance evaluations, the SLL and the departure headings are computed ahead of time for each possible segment starting at a RGRID node (a maximum of $2 \times N_W + 1$, which is the maximum number of lateral deviation choices), and stored in a RGRID node data structure. During the flight performance calculations the segment SLL and the departure heading are readily available. The distance flown by the aircraft along an LFPL segment is calculated by multiplying the segment's SLL with a correction factor, computed based on the Earth's radius and the aircraft's altitude.

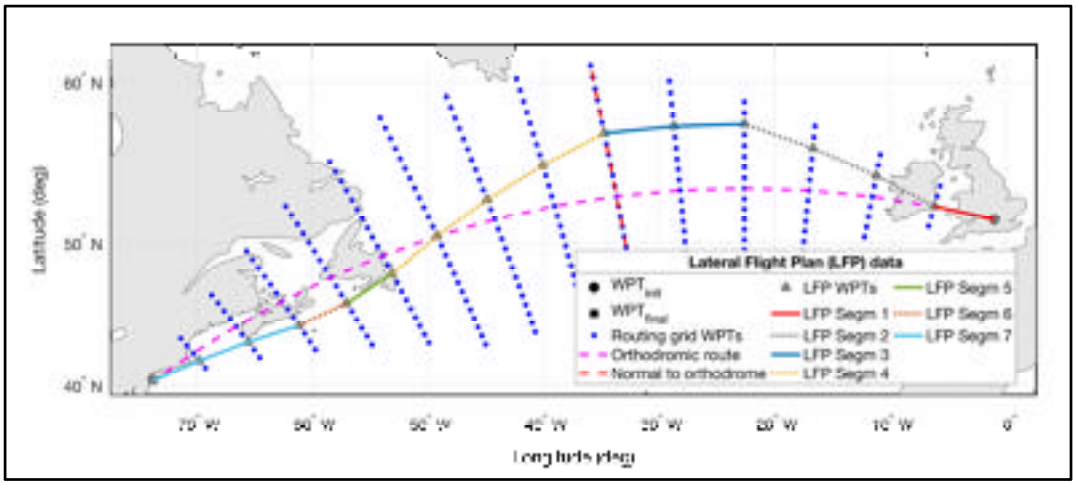

Figure 5.1 Example of a Routing Grid and a Lateral Flight Plan component constructed based on the Routing Grid

5.3.1.2 Vertical flight plan

The VFPL describes, in a concise, standardized form, the aircraft's altitude and speed evolution along the LFPL. A VFPL can be decomposed in seven sections (flight phases): takeoff, initial climb, climb, cruise, descent, approach, and landing. Each VFPL section is composed by a set of segments, defined by a set of specific parameters for each segment type (e.g. the segment type, altitude, speed, position along the LFPL, etc.). Not every vertical flight trajectory segment is explicitly defined in the VFPL. There are vertical flight trajectory segments (e.g. constant altitude acceleration/deceleration, climb in cruise, etc.) that are transition segments between segments defined in the VFPL, and they are generated during the FPL accelerated flight performance calculations. In this paper, it was assumed that the WPT that demarcates two VFPL segments defines the geographic location (WPT) where the altitude/speed change is initiated (starts), and not the geographic location where the aircraft reaches the new speed and/or altitude.

Some VFPL segment parameters are implicit, "inherited" from the previous segment (e.g. constant speed climb segment start altitude), or defined by the FPL (e.g. geographic location/WPT where a constant altitude and speed cruise segment ends). Other parameters

are dependent on the specific context (aircraft performance, weight, atmospheric conditions, etc.) and can be only determined during the accelerated flight performance calculations (e.g. the distance necessary/geographic location where the aircraft reaches the cruise altitude).

In this study, a VFPL is considered to have three phases/sections (climb, cruise, and descent) and the structure described below, similar to that used by the authors in a previous flight trajectory optimization study (Dancila & Botez, 2020b – the study presented in Chapter 4.), and can contain some or all of the listed elements. The number of sections, segments, the segment types and the order in which they appear, are specific for the FPL. It is assumed that:

1. The climb is flown at [CAS_{CLIMB}, $MACH_{CLIMB}$] from the initial aircraft position WPT_{init}, at alt_{INIT} (initial aircraft altitude) to the Top of Climb (the point where the aircraft reaches the initial cruise altitude alt_{CRZ_INIT}), executed at Maximum Climb (MCMB) Thrust Lever Angle (TLA). The transition between CAS and MACH occurs at the crossover altitude;
2. The cruise phase is composed of a succession of constant speed cruise segments:
    a. A constant altitude (alt_{CRZ_INIT}) and speed ($MACH_{CRZ\_INIT}$) cruise segment from TOC to a selected location along the lateral flight trajectory (LFPL segment);
    b. A set of constant altitude and speed cruise segments ([alt_{CRZi}, $MACH_{CRZi}$]) where each segment can have a different cruise altitude and/or speed value and are delimited by selected LFPL WPTs. The set's last segment ends at the End of Cruise (EOC – a point in cruise beyond which the aircraft is considered in descent mode, therefore no more step climbs are executed). The EOC location is selected so that the Top of Descent (TOD), the point where the aircraft starts the descent, is located after the EOC; and
    c. A final constant altitude (alt_{CRZ_FINAL} – same as the altitude of the previous segment ending in EOC) and speed ($MACH_{CRZ\_FINAL}$) segment, from the EOC to the TOD.

3. The aircraft does not perform descents in cruise, the altitude for a cruise VFPL segment is always equal to or higher than that of a previous segment;
4. The descent is flown at constant scheduled speed ([$MACH_{DESCENT}$, $CAS_{DESCENT}$]), starting from TOD, from the final cruise altitude (alt_{CRZ_FINAL}) to the final descent altitude (alt_{FINAL}) at WPT_{final}, and executed at idle (IDLE) TLA. The transition from MACH to CAS speed occurs at the crossover altitude; and
5. The speeds (CAS and MACH) and altitudes have discrete values, multiples of 1 kn for CAS, 0.001 for MACH, and 1,000 ft for altitude.

The TOC and TOD locations along the LFPL are specific for the FPL data (LFPL and VFPL), aircraft performance and weight, atmospheric conditions, etc.

5.3.2 The aircraft performance model

The accelerated flight performance calculations were performed using a toolbox, developed in-house, and based on the Base of Aircraft Data (BADA) (Nuic et al., 2010a; Eurocontrol, n.d.; Nuic, 2010b; Eurocontrol, 2010) version 4.0 APM developed by Eurocontrol. The BADA APM provides aircraft specific parameters and data models (flight envelope limitations, aerodynamic and engine performance, valid aircraft configurations, etc.), and the methodology to compute the flight performance parameters of interest and the aircraft dynamics using equations based on the Total Energy Model (TEM). Specific information regarding BADA 4.0 can be obtained from Eurocontrol (n.d.) and is subject to a license agreement.

The flight performance calculation toolbox contains a set of functions specific for each type of vertical flight trajectory segment generated for a flight along a profile defined by an FPL.

5.3.3 Atmospheric data model

The Atmospheric Data Model (ADM) used in this study was that presented in Dancila & Botez (2020a) (the investigation presented in Chapter 3). The model defines the atmospheric data, as a function of time, in RGRID nodes (see sub-section 5.3.1) and at a set of selected altitudes. The geographic area covered by the RGRID, the range of altitudes selected for the vertical flight profile, and the time domain estimated to cover the possible flight times between the initial and final WPTs determine the atmospheric data prediction files to be retrieved from the meteorological service agency. This ADM has the advantage that, in a large majority of the cases, the atmospheric parameters used in the flight segment performance calculations only require 1D linear interpolations to compute their values in an RGRID node, at the altitude and time instance of interest. The ADM was shown (Dancila & Botez, 2020a - presented in Chapter 3) to be on average six times faster, and as accurate as when computed by linear interpolations from the GDPS GRIB2 data. Atmospheric data at points other than the RGRID nodes, a reduced number of instances during the flight performance calculations (e.g. at the final points of climb/descent and acceleration/deceleration segments), can be computed through linear interpolation based on the atmospheric data in the grid nodes. Depending on the specific case, a smaller number of interpolations may be required than when the GRIB2 data is used.

5.3.4 Accelerated flight simulation and flight performance parameters calculations

The accelerated flight simulation performs a step-by-step simulation of the aircraft's evolution along the flight trajectory determined by the selected FPL. The specific methodology employed for performing the accelerated flight simulation, used for flight trajectory prediction and optimization, is described in Schreur (1995) and illustrated in Figure 5.2.

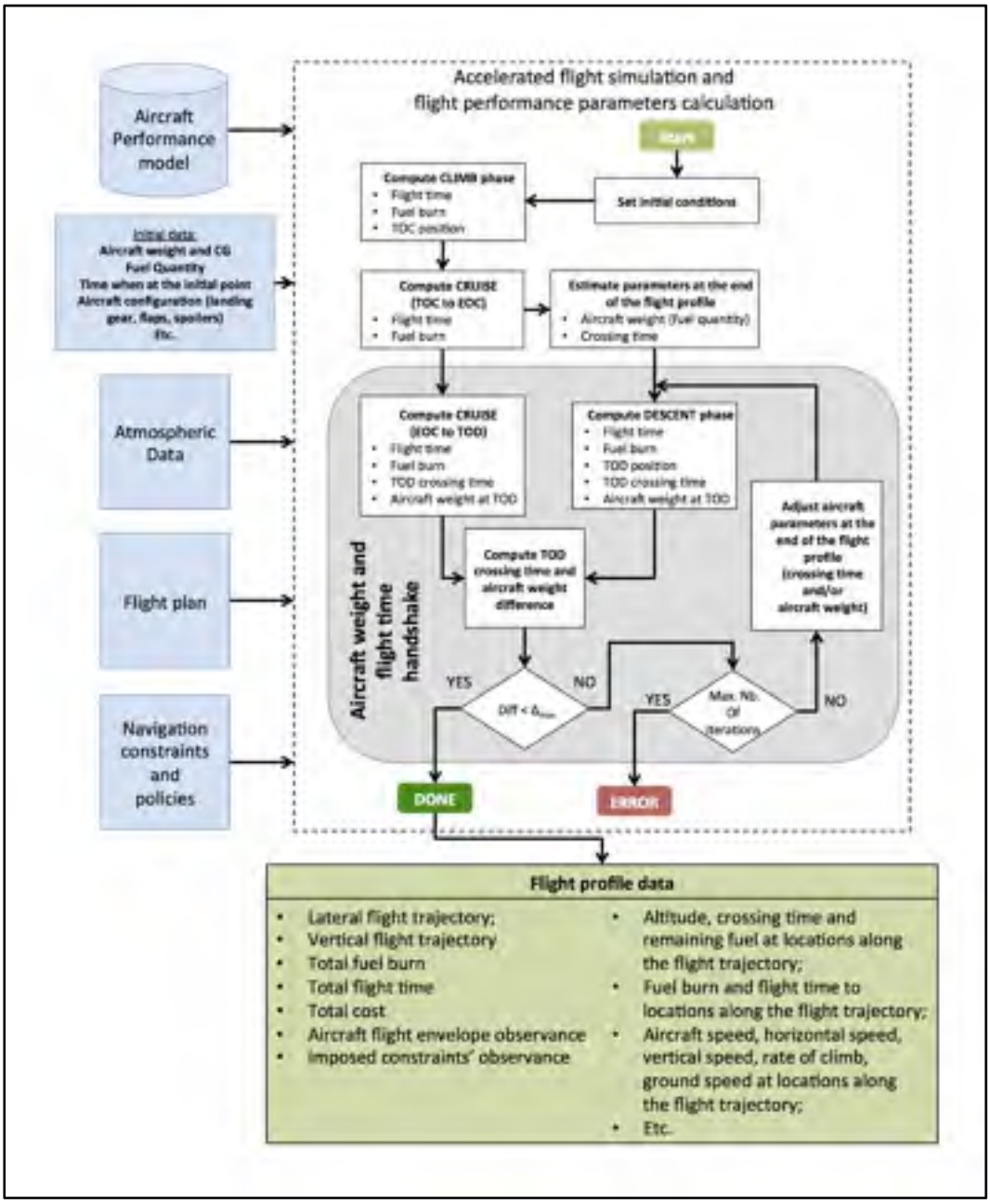

Figure 5.2 Accelerated flight simulation and
flight performance parameters calculations

The simulation is performed phase by phase, starting from the initial aircraft position (geographic location, altitude, and time), attitude (banking angle, climb/descent angle, etc.), speed, and aircraft configuration (weight, fuel quantity, etc.). For each flight phase, the

accelerated simulation successively estimates the aircraft's evolution along each VFPL section and LFPL segment. Each VFPL segment is decomposed into a set of sub-segments, chosen so that the mathematical model that describes the aircraft and the performance parameters' evolution does not change, and is then divided into smaller sub-segments (integration steps). The parameter along which the decomposition is made (altitude, distance, time) is a function of the segment's type. The integration step size is chosen as a tradeoff between computation time and precision. Small integration steps increase the results' accuracy, but the computation time may become prohibitive.

For each sub-segment, the flight performance parameters are computed by multiplying the parameter values computed in a point on the sub-segment with the integration step size. The computed data are then used to determine the aircraft's weight, position along the LFPL, altitude, speed, etc., at the segment's end. These data are the initial conditions for the next sub-segment's accelerated simulation. During the accelerated flight simulation, new flight trajectory segments are created that do not have their correspondent in the VFPL segments. They are transitions between VFPL segments, such as acceleration/deceleration segments between two consecutive constant speed segments or climb/descent segments between two constant altitude cruise segments.

The simulation starts by performing the climb phase accelerated simulation, from WPT_{init} to the TOC, followed by the cruise phase simulation, from the TOC to the EOC. Next, the descent phase accelerated simulation is conducted backwards (backward integration), from WPT_{final} to the TOD. The aircraft weight and crossing time at WPT_{final} are estimated heuristically, based on the aircraft's weight and crossing time at the EOC. After the descent phase simulation, the estimated aircraft position, weight, and crossing time at the TOD are known. Finally, the cruise segment between EOC and TOC is simulated, and the aircraft weight and crossing time at the TOD are known, based on the forward simulation from the initial waypoint. The heuristic estimation of the aircraft weight and crossing time at WPT_{final} is validated by comparing the differences between the aircraft weight and crossing time at the TOD, computed forward, from the cruise phase, and those computed backwards, from the

descent phase. If the difference(s) is (are) larger than selected threshold(s), they are applied as corrections to the estimated values at WPT_{final}. The simulation from the EOC to WPT_{final} and the validation are repeated until the simulation converges (the differences are smaller than the thresholds) or the number of iterations surpasses a selected maximum value (simulation error).

During the simulation, for each sub-segment, the flight parameters are validated relative to the flight envelope limitations and fuel requirements (if the flight requires more fuel than available). An accelerated flight simulation module option allows, if desired, the correction of FPL segments that would result in flight parameters outside the aircraft's flight envelope (invalid altitude – speed profiles). The corrected FPL (with valid altitude – speed profiles) is returned by the accelerated flight simulation function for future use in the optimization.

5.3.5 The proposed optimization method

The proposed optimization method uses a new evolutionary search method, derived from the NSGA-II. The first sub-section (5.3.5.1) presents the general considerations and observations regarding the optimization problem. Sub-section 5.3.5.2 presents the characteristics of the candidate FPLs solutions selected and evaluated during the optimization. Next, sub-section 5.3.5.3 presents the genetic operations applied to candidate FPLs (crossover and mutation) and, finally, sub-section 5.3.5.4 details the proposed method.

5.3.5.1 General considerations

For a selected FPL, a change in total flight time can be obtained by changing one or more FPL parameters, for one or multiple segments. Given that the candidate FPL parameters (speeds, altitudes, WPT locations) have discrete values, the set of obtainable flight times are also discrete values. The complex and nonlinear relationship between (lateral and vertical) FPL parameters, atmospheric conditions and the flight parameters of interest (total flight time and total fuel burn), as well as the atmospheric conditions which vary as a function of the

selected altitude, route, and the time when the aircraft crosses each trajectory point, makes it possible that for each RTA value the optimal solution is located in a different search space region.

The proposed method is based on the following observations:

1. The fuel burn variation versus flight time cannot be estimated a priori. Depending on the specific optimization problem, the fuel burn variation in general, and specifically for the optimal (minimum fuel) solution set, could increase or decrease with the flight time, or it may not have a monotonous variation;
2. The optimization problem can be seen as a constrained MOO with a two-dimensional objective space (fuel burn versus flight time); however, this is not a classical MOO problem since the set of optimal FPL solutions might not form a Pareto front (see the first observation). The solutions sought here do not constitute a tradeoff between fuel burn and flight time, but they are the FPLs that yield the minimum fuel burn for the set of RTA constraints;
3. Techniques and elements from the MOO methods can be adopted for solving the optimization problem: population-based search methods (evolutionary algorithms), tentative solution set, ranking and fitness assignment for the evaluated solutions at a search iteration, searches performed in the objective space, etc.; and
4. The differences relative to classic MOO methods would have to address the population elements' ranking and their fitness value assignment, which guides the selection of population elements for the genetic operations and, therefore, the search.

5.3.5.2 The set of candidate flight plans

The RGRID and the set of candidate FPLs (composed of LFPLs and VFPLs) conform to the models presented in sub-section 5.3.1. Ideally, the range of altitudes and speeds from which the altitude/speed pairs that define the VFPL segments are chosen to cover the entire flight envelope, without extending beyond it. FPLs that have segment parameters outside the aircraft's flight envelope or require more fuel than available reduce the search efficiency, as

they spend computational resources without adding information that could guide the search. Given the complexity/impossibility to determine a priori, at waypoints along the flight trajectory, the parameters (aircraft's weight, atmospheric conditions, etc.) that determine the aircraft's flight envelope limitations, and to ensure that the entire flight envelope is covered, the range of speeds and altitudes for the VFPL segments were chosen as follows:

1. CAS for climb (descent): CAS_{INIT} (CAS_{FINAL}) to VMO – 10 kn;
2. Climb (decent) MACH: MACH equivalent for CAS_{INIT} at alt_{INIT} (CAS_{FINAL} at alt_{FINAL}) to MMO – 0.01;
3. Cruise altitudes are multiples of 1,000 ft, between a selected minimum cruise altitude and the service ceiling for the aircraft model; and
4. Cruise speeds are multiples of 0.001 MACH, between a minimum selected value and MMO – 0.01.

At the beginning of the flight, when the aircraft is heavier, the range of valid cruise altitude and speed combinations are smaller than for the other flight segments. Therefore, the set of alt_{CRZ_INIT} and $MACH_{CRZ\_INIT}$ combinations are determined heuristically, as the valid combinations of altitudes multiples of 1,000 ft and speeds multiples of 0.001 MACH for an aircraft weight resulted after a climb at 250 kn, from alt_{INIT} to the minimum initial cruise altitude.

5.3.5.3 Flight plan genetic operations

Due to their different structures, the LFPL and the VFPL genetic operations are different. The first sub-section presents the genetic operation applied to LFPLs, and the second sub-section presents the genetic operations applied to VFPLs.

5.3.5.3.1 Lateral flight plan genetic operations

The LFPL genetic operations are applied in an LFPL WPT selected at random, between the second and the last but one WPT. Performing a crossover at the first or last WPT would not

yield new FPLs, and mutations cannot be performed at these locations. If, at the location where the crossover must be performed, the difference between the lateral deviations for the two LFPL WPTs is larger than the maximum lateral deviation step, the crossover cannot be obtained just by swapping the final LFPL sections. A transition section is constructed, so that at each step along the ORT the lateral deviation relative to the previous WPT is less than or equal to the maximum lateral deviation step size. An LFPL mutation changes the lateral deviation for the WPT situated at the selected location, relative to the previous WPT, to a new value within the range of possible relative lateral deviations. For the following WPTs, the deviation relative to their preceding WPT is maintained, and limited to the routing grid.

5.3.5.3.2 Vertical flight plan genetic operations

The crossover between two VFPLs is applied in the cruise section, at points that delimit cruise segments, between the WPT at the end of the initial cruise segment and the EOC. The crossover can be performed on the speed component, the altitude component, or on both. The VFPL speed component crossover is obtained by swapping the final sections of the VFPL speed component (between the crossover position and the end of the VFPL). A VFPL speed component mutation can be performed on any segment by changing the selected segment's speed with a value within the range allowed for the segment (see sub-section 5.3.5.2). If at the point where the VFPL altitude component crossover is performed the altitudes are identical, the crossover swaps the final sections (from the crossover position to the end of the VFPL) between the two VFPLs. If the altitudes are different, given that the descent in cruise is not accepted, for the VFPL with the higher altitude at the crossover position the swap is performed at a further location, where the altitude on the other parent profile is equal or higher (if it exists). For the FPL with a lower altitude, the swap is performed at the crossover location. The mutation is obtained by modifying the cruise altitude of a randomly selected cruise segment. The new altitude is selected from the range of altitudes considered for that segment. The altitudes for the cruise segments that follow are modified, if necessary, to be equal to or higher than the selected new altitude (no descent in cruise).

5.3.5.4 Search method description

The proposed method uses an Evolutionary Algorithm, based on genetic algorithms, derived from the NSGA-II algorithm (Deb et al., 2002). The differences between the proposed method and the NSGA-II method presented in (Deb et al., 2002) consist in the methods used for non-dominance/ranking determination, the fitness assignment for crossover element selection, the tentative solution set construction and update, and its propagation to the extended population. In the proposed method the tentative set size is equal to the number of RTA constraints, and is initially empty. Each tentative solution set member is associated with an RTA constraint. In each iteration, a population member that yields a flight time within an RTA constraint bounds will replace the tentative solution element for that RTA if the fuel burn is lower, and will not affect the other tentative solution set members. A high-level block diagram representation of the proposed search methods is presented in Figure 5.3. The detailed description is presented in the text that follows.

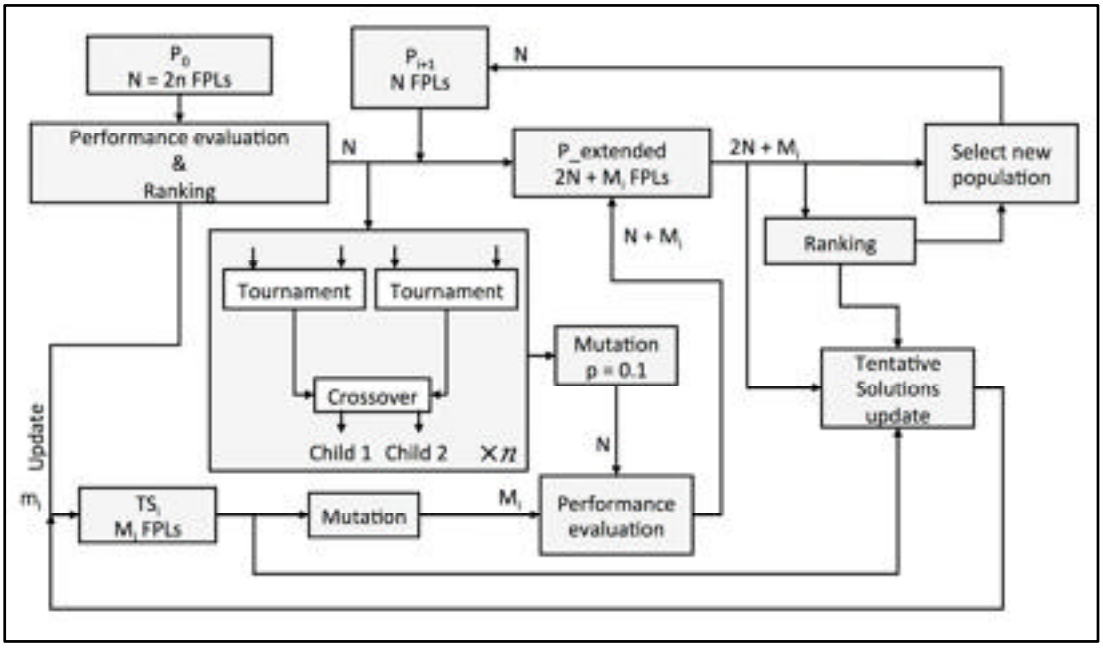

Figure 5.3 Proposed search method block diagram

An initial population (P0), with *N* elements, is randomly created according to the RGRID, LFPL and VFPL templates, and the parameter value ranges for each FPL component. The initial population FPLs are evaluated, and the fuel burn and flight times are calculated. During the accelerated flight simulation of the first population, the FPLs that are invalid relative to the aircraft's flight envelope are corrected and updated in the population, so that the search starts with the largest number of valid candidate solutions and therefore, better information to guide the search. For invalid FPLs (caused in the first population by FPLs that require more fuel than available and, for the next populations also due to aircraft envelope limits violation), the fuel burn and flight time are assigned penalty values, larger than for any valid FPL. The range of flight times between the initial and final points that cover the entire set of possible flight times along the set of candidate FPLs are estimated heuristically. In the next step the population elements are evaluated relative to the RTA values and fuel burn, and assigned ranking and fitness. Similar to the method proposed by Jensen (2003), the population elements ranking is performed by first sorting the population based on the two cost function components (first by flight time, and then by fuel burn), and then assigning them to optimal fronts (sets of population elements with the same ranking/level of optimality). The elements of the ordered list that have a flight time within the RTA constraint bounds of an RTA value are successively retrieved, ordered as a function of fuel burn, and then ranked. The element with the lowest fuel burn is assigned rank 1 (assigned to front 1), the next is assigned rank 2 (assigned to front 2), and so on. The best element for the RTA constraint value (the element having rank 1) is copied to the tentative solution (TS) set. The uniform distribution of the solutions along the optimal front results from the rank assigning method. The non-valid population elements (those that have a flight time outside the RTA constraint set bounds or are invalid) are assigned the lowest rank (highest rank value), and form the last/least optimal front.

An example of fronts (solutions with the same "level of optimality") for an FPL population is presented in Figure 5.4 (the last front, corresponding to non-valid flight plans, are not represented). It can be noted that, for the case represented in Figure 5.4, the tentative optimal solutions are present for every RTA constraint. However, the number of non-optimal

solutions and their quality (fuel burn value relative to the optimal solution for the RTA constraint) differs for each RTA. In general, the presence in a population of an optimal solution for an RTA constraint, its performance relative to the global optimum, and the number of non-optimal solutions, is a function of the evolution of the search process.

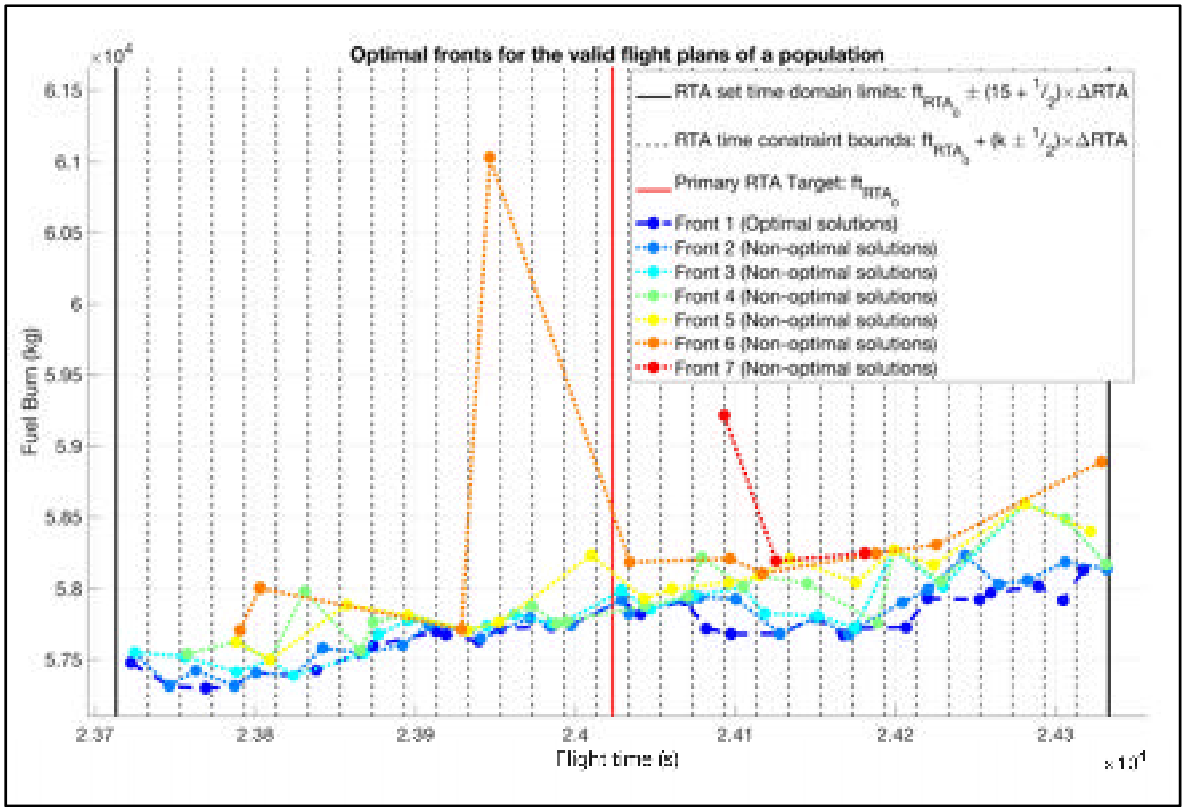

Figure 5.4 Example of solution fronts for a population (the image does not show the last front: the non-valid FPLs)

Figure 5.5 presents a detailed view of the three adjacent RTA constraints represented in Figure 5.4 and delimited by the time interval (24073 24133] seconds. It can be noted that some solutions from adjacent fronts could be very close - e.g. the tentative optimal solution (front 1) and the next, near best, solution (front 2) for the RTA constraint bounded by the time domain (24113 24133] seconds. The choice to assign different sizes for the dots that represent solutions from different fronts was determined by the fact that in such cases dots of identical size would overlap rendering some solutions not visible.

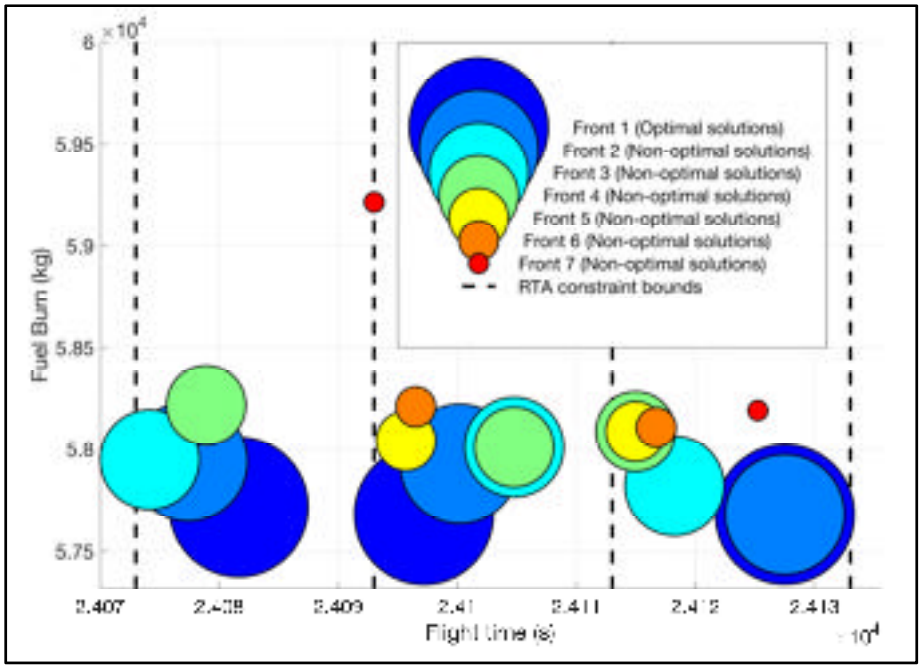

Figure 5.5 Example of valid solutions in a population:
detail view for the RTA constraints from Figure 3
delimited by the interval (24073 24133] seconds

In the next step, an extended population (P_extended) is created by copying the current population's *N* elements, adding *N* elements generated by *N*/2 crossover operations, followed by a mutation with probability $p = 0.1$ – in a similar manner to the NSGA-II method. The difference is that, in the proposed method, the M_i non-empty tentative solution set members are mutated and added to the extended population (a local search).

The selection of population elements for crossover is performed at random. Four different elements are selected and compared two by two. If the two elements have different ranks, then the element with the lowest rank (highest fitness) is selected as a "parent". If the elements have the same rank and are valid flight plans, then the element with the smallest number of elements within the RTA constraint bounds is selected. If they both have an identical number of elements within the RTA bounds, the FPL with the lowest fuel burn is selected. If the fuel burn is also identical, the FPL with a flight time closer to the RTA constraint is selected. If the FPLs also have the same flight time difference relative to their

respective RTA constraints, the parent is randomly selected among the two. If the two elements have the same rank and are non-valid, the parent is selected based on the Euclidian distance, in the normalized objective space, between the element's projection on the normalized objective space, and a reference point with coordinates corresponding to the minimum fuel burn obtained for the population and the central RTA constraint (RTA_0). The element with the smallest distance to the reference point is selected as a parent. If both elements have the same distance, then the element with the lowest fuel burn is selected. If the fuel burn is also identical, the parent is selected at random between the two elements. An illustration of the fitness values for non-valid FPLs, expressed as the Euclidian distance to a reference point in the normalized objective space, is presented in Figure 5.6. Here also the number of invalid flight plans and their fitness are a function of the evolution of the search process. In the example presented in Figure 5.6 the best fit invalid flight plan (the dark brown dot) is located near the minimum RTA constraint set bound and has a low (normalized) fuel burn. The least fit flight plan is the dark blue dot, located in the upper right corner of Figure 5.6, which has the largest fuel burn and flight time, and is the farthest from the reference point. The children elements, the new extended population members, are generated by crossover between the two winning parents, where the crossover is performed on the lateral or vertical FPL component, selected at random.

The subsequent step is similar to that of the NSGA-II method. The new elements in the extended population are evaluated, the extended population is ranked and assigned to optimal fronts. If the extended population contains m_i elements that are new solutions (for RTA constraints with empty Tentative Solutions element) or better solutions (lower fuel burn than the Tentative Solutions element), then m_i solutions update the Tentative Solutions set. The new population (P1), for the next iteration, is composed of the best N elements from the extended population – as in the NSGA-II method. The copied elements are retrieved, successively, from the optimal fronts associated with the "extended population", starting with the optimal front elements (rank 1), and continuing with the elements from the subsequent, less optimal fronts (higher ranks), until N elements are retrieved. If the remaining number of elements to be retrieved, N_R, is less than the number of elements in the current front, then the

first N_R elements are copied from the front. The steps listed above are repeated until the selected number of iterations is reached. The tentative solution set at the end of the optimization is the set of optimal solutions. Given the randomness associated with genetic algorithms and the flight trajectory optimization problem characteristics, the solution set could contain solutions for all RTA constraints, for some, or for none, and the solutions may be optimal, near optimal or not optimal.

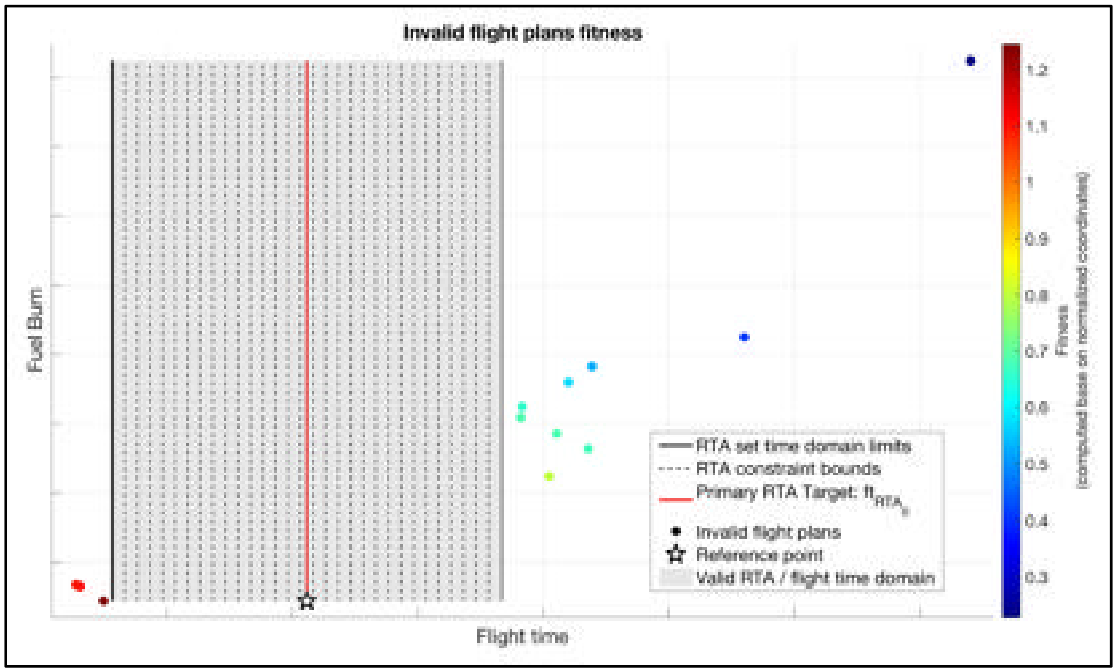

Figure 5.6 Example of fitness for the non-valid flight plans of a population, calculated based on the Euclidian distance, in the normalized objective space, between the flight plan's projection and the reference point

The impacts of different possible changes in the proposed method are evaluated using seven method variants. The first variant is the one described above. The other six variants differ as follows:

1. Non-valid FPLs' fitness assigned based on the absolute time difference to the central RTA constraint (RTA_0) – not the Euclidian distance to the reference point;
2. The extended population does not include mutated tentative solution set versions (local search);

3. Non-valid FPLs' fitness assigned based on the absolute time difference to the central RTA value (RTA_0), and the extended population does not include mutated tentative solution set versions (local search);
4. The extended population is created by crossover applied on both LFPL and VFPL;
5. The initial population FPLs are not corrected relative to the aircraft flight envelope; and
6. Different number of iterations used in the optimization.

5.4 Results

This section presents the results of tests performed to evaluate the performance of the proposed flight plan optimization method. First, sub-section (5.4.1) presents the test environment used in the evaluation. Then, sub-section 5.4.2 describes the test scenario used to perform the evaluation. Sub-sections 5.4.3 and 5.4.4 present the research questions investigated in this study and the test cases devised for this purpose. Finally, sub-section 5.4.5 presents and discusses the results.

5.4.1 Simulation environment

The proposed method was evaluated on a PC-based platform with a 2.8GHz AMD Phenom II X4 B93 processor, 8GB of RAM, and Windows 10 Enterprise, using code developed in Matlab (R2108a). The flight performance parameters for candidate FPLs were calculated using a module developed in-house, in Matlab, based on the Boeing 777-300ER BADA 4.0 Aircraft Performance Model (APM) published by Eurocontrol.

5.4.2 Test scenario

The test scenario was the optimization of a flight section that starts in climb, at 10,000 ft and 250 kn CAS, and ends in descent, at 10,000 ft and 250 kn CAS. The aircraft was considered to be in normal operation (no malfunctions) and in clean configuration (retracted landing

gear, flaps and spoilers). The aircraft weight and fuel at the initial point were taken to be 0.5 and 0.7, respectively, of their maximum allowed values for the aircraft model. For a "realistic" evaluation (attainable constraint times for the selected flight section, atmospheric conditions, and aircraft model), the initial and final FPL points and their crossing times were recovered from a real flight track data, retrieved from the FlightAware website (www.flightaware.com). The selected flight was American Airlines AAL107 (FlightAware, 2109b), between London Heathrow (LHR) and New York JFK (JFK), flown on February 25, 2019, chosen at random from the flights performed that day with the same aircraft model as the APM available to the authors.

Currently the North Atlantic traffic observes specific navigation policies, and the aircraft follow predetermined tracks: the North Atlantic Organized Track System (NAT_OAS). This study / proposed method assumes possible future navigation paradigms, such as TBO or free flight, where the aircraft can fly along the flight plan/trajectory that is best suited for the mission (aircraft type, load, atmospheric conditions, and departure-destination pair).

The reference points and the crossing times were selected as the track data points, in climb and descent, where the aircraft was closest to the altitude of 10,000 ft:

1. Initial point (WPT_{init}): Lat. 51.5144 N, Lon. 1.0188 W, Time 12:27:50 EDT; and
2. Final point (WPT_{final}): Lat. 40.3386 N, Lon. 73.8018 W, Time 19:07:28 EDT.

The set of N adjacent RTA constraints were calculated based on the aircraft's crossing time at WPT_{final}, considered as the primary RTA constraint (RTA_0), defined by RTA values within a range of $RTA_0 \pm 5$ min ($RTA = RTA_0 + k \times \Delta RTA$, with $k \in \mathbb{Z}, -15 \leq k \leq 15$), and window width ΔRTA = 20s. This produced 31 RTA constraints, and therefore, the optimization was expected to produce 31 optimal FPLs, one for each RTA value. The RTA constraint bounds were selected as follows:

$$\begin{cases} \left[RTA_0 + \left(k - \frac{1}{2}\right) \times \Delta RTA \quad , \quad RTA_0 + \left(k + \frac{1}{2}\right) \times \Delta RTA\right) & k < 0 \\ \left[RTA_0 - \frac{1}{2} \times \Delta RTA \quad , \quad RTA_0 + \frac{1}{2} \times \Delta RTA\right] & k = 0 \\ \left(RTA_0 + \left(k - \frac{1}{2}\right) \times \Delta RTA \quad , \quad RTA_0 + \left(k + \frac{1}{2}\right) \times \Delta RTA\right] & k > 0 \end{cases} \tag{5.1}$$

The set of RTA values at WPT_{final} were transformed into total flight time constraints, calculated as a difference, in seconds, between the RTA at WPT_{final} and the aircraft crossing time at WPT_{init}:

$$ft_{RTA_n} = \left(RTA_n - t_{WPT_{init}}\right) \times 3600 \tag{5.2}$$

where:

1. ft_{RTA_n} is the total flight time constraint for the nth RTA (RTA_n); and
2. $t_{WPT_{init}}$ is the aircraft crossing time at WPT_{init}.

The value obtained for ft_{RTA_0} was:

$$\begin{aligned} ft_{RTA_0} &= RTA_0 - t_{WPT_{init}} = t_{WPT_{final}} - t_{WPT_{init}} \\ &= 19h07min28s - 12h27min50s \\ &= 6h39min38s \\ &= 24023s \end{aligned} \tag{5.3}$$

The set of flight time constraints were obtained by replacing RTA_0 with ft_{RTA_0} in Eq. (5.1)

The selected RGRID parameters were: a maximum ORT sub-segment SLL of 50 n.m., a maximum lateral deviation of 500 n.m. from the ORT, a lateral deviation step of 10 n.m., and a maximum of two lateral deviation steps can be performed at one time. The resulted RGRID (Figure 5.7) has the ORT divided into 60 equal sub-segments with an SLL of 49.71 n.m., and a maximum of 50 deviations (WPTs) on each side of the orthodrome.

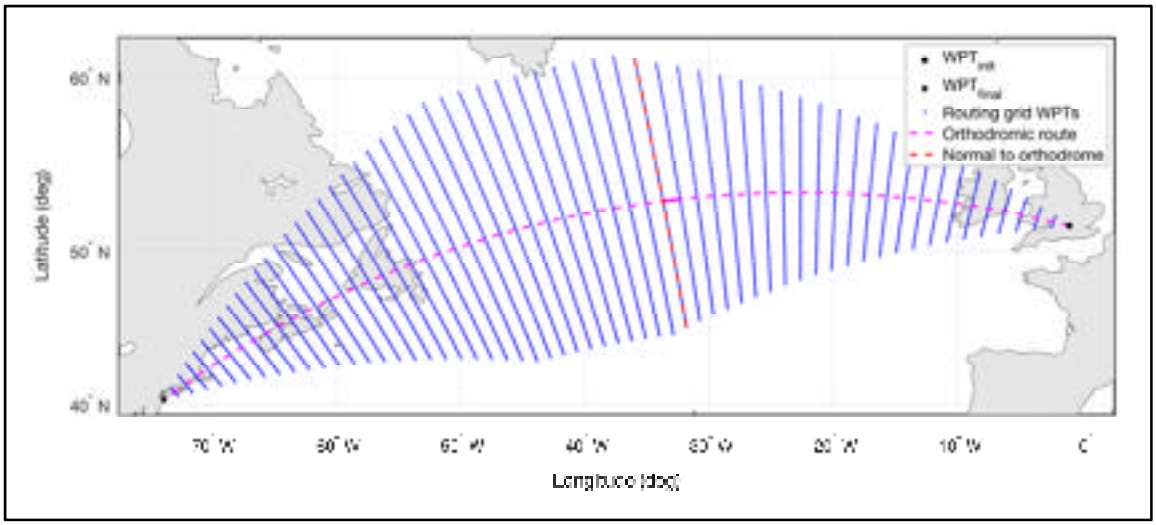

Figure 5.7 The routing grid for the set of lateral flight plans evaluated for the flight AAL107 (FlightAware, 2019b) optimization

The parameters selected for the candidate VFPLs were:

1. Climbs at constant [CAS, MACH] and MCMB TLA: [250 to VMO – 10] kn CAS, and [0.452 (250 kn CAS at 10,000 ft) to MMO – 0.01] MACH;
2. Descents at constant [CAS, MACH] and IDLE TLA. Speed ranges as for climb;
3. Climb in cruise performed at constant MACH, MCMB TLA, and 500 fpm climb rate;
4. Accelerations in cruise performed at MCRZ TLA and decelerations at IDLE TLA;
5. The sets of valid initial cruise altitude and valid cruise speeds are determined heuristically (see sub-section 5.3.5.2);
6. A constant altitude (initial cruise altitude) and MACH speed (initial cruise MACH speed) from the TOC to the 8th LFPL WPT (approx. 400 n.m. from WPT_{init});
7. EOC is placed at the 53rd LFPL WPT (approx. 400 n.m. before WPT_{final});
8. From the 8th LFPL WPT to the EOC, the cruise section defines constant altitude and speed segments with a length of approximately 250 n.m. (five LFPL segments). The cruise altitude and/or speed changes can occur at the LFPL WPTs [8 13 18 23 28 33 38 43 48]; and

9. The cruise phase altitude and speed values and the MACH speed for the final cruise segment (from WPT 53 to TOD) are selected at random: altitudes between 28,000 ft and 43,000 ft, and speeds between 0.68 and 0.9 MACH.

Next, the ADM was constructed based on the RGRID, the range of VFPL altitudes, and the time domain that covered all flights along the candidate FPLs. The maximum flight time for a flight between WPT_{init} and WPT_{final} was assumed to be 10h 00' 34" ($1.5 \times ft_{RTA_0}$). Therefore, the time domain of interest for the atmospheric data is:

$$\begin{aligned} ft_{domain} &= \left[t_{WPT_{init}}, t_{WPT_{init}} + 1.5 \times ft_{RTA_0}\right] \\ &= [12{:}27{:}50, 22{:}28{:}24]\ EDT \end{aligned} \tag{5.4}$$

The population size for the algorithm implementing the proposed method was selected to be 62, twice the number of searched FPL solutions. Given the proposed method's stochastic nature, 10 test runs were conducted for each optimization method variant.

5.4.3 Research questions

The research questions evaluated in this study are:

1. Does the optimization method identify solutions for all RTA constraints?
2. How fast (in what generation) does the first tentative solution for an RTA value appear?
3. What is the fuel burn difference between a "random" FPL that satisfies the RTA constraint (the first identified tentative solution) and the final solution?
4. How many iterations are necessary until a tentative solution reaches a fuel burn that is 1%, 0.1%, 100 kg, and 50 kg over the final solution, or the final solution?
5. How different are the solutions identified in the 10 test runs of a test case?
6. Does adding mutated tentative solutions to the extended population (local search) improve the results?

7. Does an FPL correction relative to the flight envelope, in the initial population, improve the results?
8. How does the method's performance change if the extended population is generated by crossover solely on the LFPL or VFPL (chosen at random), or on both?
9. What is the effect of assigning the fitness value for non-valid FPLs as a function of: Euclidian distance to a reference point versus the absolute time difference relative to the primary flight time constraint ft_{RTA_0}?
10. Does an increase of the number of iterations (generations) improve the results?
11. What are the differences between an optimization performed for 300 generations versus one performed for 1,000 generations?

5.4.4 Test cases

A test case configuration synopsis of the optimization method variants is presented in Table 5.1.

Table 5.1 Test case configurations synopsis

Test case	Add mutated tentative solutions to the extended population	Non RTA compliant FPL fitness assignment criteria		Extended population generated by crossover on both LFPL and VFPL	Correct initial population FPLs – bring flight/altitude combinations within the flight envelope limits	Number of generations	Number of test runs
		Euclidian distance to the reference point	Absolute difference between the flight time and the reference time				
1	✓	✓			✓	300	10
2	✓		✓		✓		
3		✓			✓		
4			✓		✓		
5	✓	✓		✓	✓		
6	✓	✓					
7	✓	✓			✓	1,000	

For an invalid FPL, the flight time and fuel burn were assigned penalty values: $3 \times ft_{RTA_0}$ for the flight time, and 1.5 times the initial fuel quantity for fuel burn (see Figure 5.8 below).

In the first population, where all the FPLs are generated at random, one, multiple, or all FPLs may be non-valid. Since all invalid FPLs have the same values for fuel burn and flight time, this could affect the algorithm's ability to properly guide the search. For test cases 1-5 and 7, the invalid FPLs in the initial population were corrected (see sub-section 5.3.4). For test case 6 the invalid FPLs in the initial population were not corrected, in order to evaluate their influence on results.

5.4.5 Results and discussions

The number of invalid profiles in the initial generation when the FPLs were corrected (test cases 1 – 5 and 7) was between 0 and 3 (4.84 %). For the test case 6, the number of invalid FPLs was between 19 and 24 (30.65% to 38.71%). However, over the entire set of 70 test runs, the first population (G0) contained tentative solutions for a minimum of two and a maximum of 20 RTA values (mean 11.27, median 12, and a standard deviation 3.937). Moreover, for all test cases, test runs, and RTA values, the first tentative solution appeared after a maximum of eight generations (see Table 5.2). Therefore, in all test cases, by the 8th generation a complete tentative solution set was found and, as a result, the final solution contained optimal FPLs for all RTAs. Table 5.2 presents the statistical data for the first RTA value tentative solution occurrence.

The results show that the invalid FPLs generated in the first population do not have a large impact on the ability to obtain, within the first few iterations, tentative FPL solutions for all the RTA values.

An illustration of the FPLs generated in the first population for test case 1 - test run 1, represented in the objective space (fuel burn versus flight time) is presented in Figure 5.8. Among the 62 randomly generated initial FPLs, 16 were valid (the blue dots in Figure 5.8),

and 46 were non-valid (the red dots in Figure 5.8). Among the 46 non-valid FPLs, one required more fuel than available (the red dot in the upper right corner of Figure 5.8). A more detailed illustration, for FPLs with parameters within the aircraft's flight envelope, is presented in Figure 5.9.

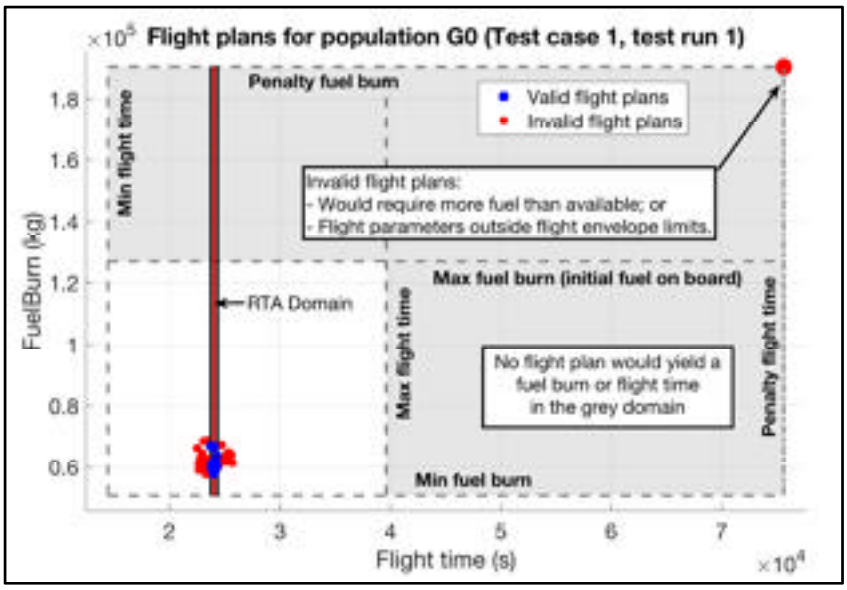

Figure 5.8 Initial population (G0) represented in the objective space (fuel burn – flight time) for Test case 1, test run 1

Table 5.2 Flight plan solution occurrence for an RTA constraint value

Test case	Number of RTA constraint values for which no solution was found	Number of generations until first tentative optimal flight plan for an RTA constraint value was found				
		Min	Max	Mean	Median	Standard deviation
1	0	0	6	1.032258	1	1.122984
2			5	0.9903226		1.116181
3			7	1.254839		1.373428
4			7	1.387097		1.422824
5			5	1.074194		1.063203
6			8	2.335484	2	1.456055
7			5	0.9032258	1	1.009817

Figure 5.10 presents an example of global optimization evolution obtained for test case 1 - test run1. The initial population (G0) yielded only 11 tentative solutions, with a fuel burn difference relative to the final solutions (optimal solutions for the same RTA values at G300)

between 10,192.47 kg (17.961%), for RTA $ft_{RTA_0} - 15 \times \Delta RTA$, and 887.45 kg (1.559%), for RTA $ft_{RTA_0} - 2 \times \Delta RTA$. At the 50th generation (G50), the differences were found to be between 262.56 kg (0.462%), for RTA $ft_{RTA_0} - 13 \times \Delta RTA$, and 167.84 kg (0.295%), for RTA $ft_{RTA_0} - 5 \times \Delta RTA$.

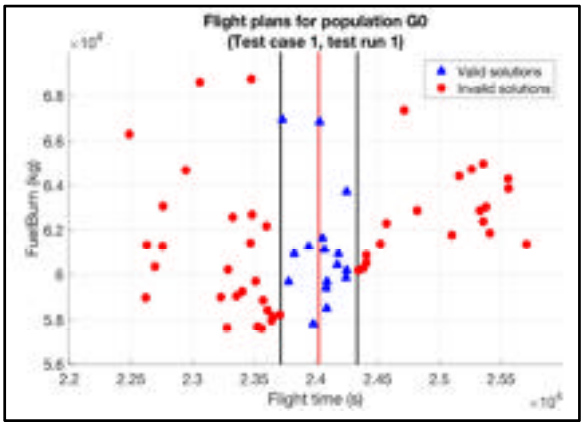

Figure 5.9 Initial population (G0) flight plans represented in the objective space, (flight parameters within the aircraft's flight envelope) for test case 1, test run 1

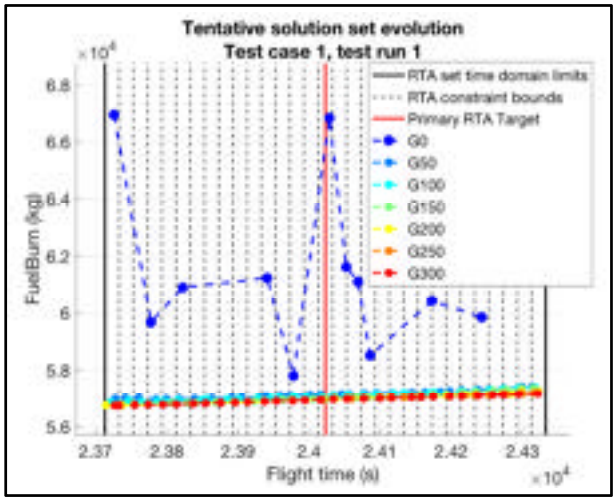

Figure 5.10 Example of global tentative solution set evolution for Test case 1, test run 1

Table 5.3 Synopsis for the optimization results obtained using the proposed method

Test case		A		B		C	
		Fuel burn reduction for a test run and RTA value (final solution vs. initial solution)		Optimal solution fuel burn variation for an RTA value over the 10 test runs		Fuel burn difference: final solution for a test run and RTA value vs. a "global" min. fuel burn solution for the RTA value (over the entire set of tests)	
		kg	%	kg	%	kg	%
1	Min	518.11	0.91	0.00	0.00	0.00	0.00
	Max	12,343.47	21.70	65.79	0.12	69.95	0.12
	Mean	3,597.01	6.32	18.80	0.03	22.34	0.04
	Median	3,072.48	5.40	15.19	0.03	19.16	0.03
	Standard deviation	1,989.75	3.49	16.75	0.03	16.75	0.03
2	Min	589.95	1.04	0.00	0.00	1.50	0.00
	Max	13,584.85	23.83	95.23	0.17	105.46	0.19
	Mean	3,596.52	6.31	24.54	0.04	35.07	0.06
	Median	3,233.15	5.68	19.42	0.03	31.82	0.06
	Standard deviation	2,021.86	3.55	21.67	0.04	21.80	0.04
3	Min	537.94	0.95	0.00	0.00	20.19	0.04
	Max	12,909.97	22.64	185.38	0.33	321.81	0.56
	Mean	3,945.01	6.92	61.08	0.11	110.79	0.19
	Median	3,770.00	6.60	47.64	0.08	105.50	0.19
	Standard deviation	1,950.29	3.42	48.62	0.09	61.07	0.11
4	Min	628.53	1.11	0.00	0.00	3.77	0.01
	Max	14,218.05	24.91	264.33	0.46	290.68	0.51
	Mean	3,702.58	6.49	60.80	0.11	90.55	0.16
	Median	3,270.22	5.74	39.83	0.07	66.75	0.12
	Standard deviation	1,927.02	3.38	61.48	0.11	65.56	0.11
5	Min	646.20	1.13	0.00	0.00	0.00	0.00
	Max	13,699.90	24.10	77.47	0.14	82.12	0.14
	Mean	3,480.00	6.11	29.25	0.05	35.10	0.06
	Median	3,158.54	5.54	29.09	0.05	35.30	0.06
	Standard deviation	1,792.86	3.15	17.68	0.03	17.63	0.03
6	Min	407.12	0.72	0.00	0.00	0.00	0.00
	Max	14,104.33	24.83	88.31	0.16	89.83	0.16
	Mean	3,386.59	5.95	24.19	0.04	29.11	0.05
	Median	2,869.56	5.03	12.80	0.02	17.04	0.03
	Standard deviation	2,174.58	3.82	24.80	0.04	24.79	0.04
7	Min	631.49	1.11	0.00	0.00	0.00	0.00
	Max	12,455.23	21.87	62.12	0.11	62.54	0.11
	Mean	3,438.50	6.04	21.63	0.04	22.05	0.04
	Median	2,911.92	5.12	15.32	0.03	15.66	0.03
	Standard deviation	1,990.90	3.49	18.73	0.03	18.70	0.03

The results presented in Table 5.3, column A, show a synopsis of the fuel burn reduction between the initial, random, tentative solutions, and the optimal FPLs at the end of the optimization. The seven method variants (test cases) yielded similar results. These results are influenced by how far the random initial population (G0) candidate FPLs are from the optimal solutions. Column B of Table 5.3 shows how close (in terms of fuel burn) are the optimal solutions found for 10 runs of an identical test case and RTA value. The worst results (the maximum difference between test run results, and the maximum variance) were obtained for the test cases 3 and 4, where no local search was performed. The best results were

obtained for the optimization method variants 1 and 7, where the initial population's invalid FPLs were corrected, a local search was performed, and the fitness for the non-valid FPLs were computed using the Euclidian distance to the reference point. Among the two (test cases 1 and 7), the best results were obtained for test case 7, when the optimization was performed for 1,000 iterations. Column C of Table 5.3 shows the results of a comparison between the optimal FPL fuel burn for an RTA value and a test run, with the "global optimum" for the RTA value (the best fuel burn for the RTA value obtained from the 70 test runs – the 10 test runs for each of the seven test cases). Once again, the best results were obtained for the test cases 7 and 1, with maximum fuel burn differences relative to the "global optimum" of 62.54 kg (0.11%) and 69.95 kg (0.12%), respectively. The worst results were obtained for test cases 3 and 4, with maximum fuel burn differences of 321.81 kg (0.56%) and 290.68 kg (0.51%), respectively. It can be concluded that the local search significantly improves the optimization results. The improvement is obtained at the expense of computation time; the extended population increases by up to 31 elements, and therefore, a higher number of flight performance calculations must be conducted.

Comparing the results obtained for test cases 1 and 3, where the only difference between the two test cases is the fitness assignment method for the non-valid FPLs, it can be seen that test case 1 yields better results. The maximum fuel burn difference relative to the global optimum for an RTA constraint for test case 3 is larger with 35.51 kg (0.07%) than that obtained for test case 1. It can be concluded that the non-valid FPL fitness calculation based on the time difference to a reference point, although easier to implement and less computationally expensive, degrades the optimization results. A comparison between the results obtained for test cases 1 and 5 shows that the results obtained for test case 1 (crossover is performed on only one component of the FPL) are better both in terms of maximum difference between the results for 10 identical test runs, and the maximum fuel burn difference relative to the "global optimum". A comparison of the results obtained for test case 6 and test case 1 shows that correcting the invalid initial candidate FPLs, generated randomly for population G0, improves the optimization results.

An illustration of a tentative solution evolution for an RTA value (test case 1, test run 1, $ft_{RTA_0} - 13 \times \Delta RTA$) is presented in Figure 5.11:

1. The first tentative FPL solution appeared in the second generation (G2);
2. A fuel burn value equal to 1% higher than the final solution (G300) was achieved at G10;
3. Less than 0.1% over the fuel burn for G300 was reached at G145;
4. Less than 100 kg over fuel burn at G300 was reached at G119;
5. Less than 50 kg over fuel burn at G300 was reached at G145; and
6. The final solution was reached at G161.

The final solution uses 1,435.40 kg (2.466%) less fuel than the initial tentative FPL solution.

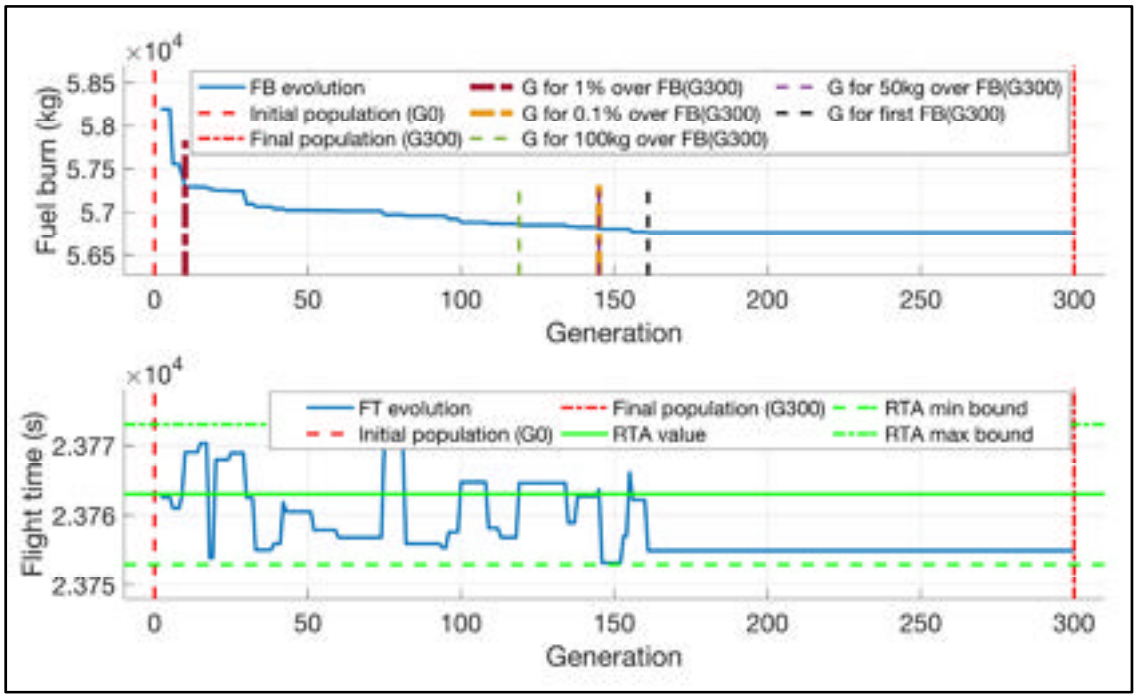

Figure 5.11 Example of tentative FPL solution evolution for test case 1, test run1, and RTA constraint value $ft_{RTA_0} - 13 \times \Delta RTA$

Table 5.4 presents the number of iterations until the tentative FPL solutions reached a selected threshold relative to the final solution fuel burn. For each test case, the analysis is

performed over the 10 test runs and for the entire set of RTA values. In this case too, the optimization method versions 3 and 4 (test cases 3 and 4) yield the worst results among test cases 1 to 6, in which the optimization was performed for 300 generations.

Table 5.4 Number of algorithm iterations until the tentative solution reaches a fuel burn (FB) below a threshold value relative to the final solution (FBfinal)

Test case		The test run generation where the first occurrence of a tentative solution: for the RTA value, over the final, optimal solution fuel burn value:				
		$FB \leq 1.1\ FB_{final}$	$FB \leq 1.01\ FB_{final}$	$FB \leq FB_{final} + 100$ kg	$FB \leq FB_{final} + 50$ kg	$FB = FB_{final}$
1	Min	0	18	16	18	58
	Max	58	219	206	219	300
	Mean	17.73	94.17	66.17	99.51	246.16
	Median	16	83	55	85.50	260
	Standard deviation	7.86	49.29	35.71	50.84	48.98
2	Min	2	23	20	26	76
	Max	41	290	155	290	300
	Mean	15.72	84.59	62.00	91.41	237.37
	Median	14	70	55	77	251
	Standard deviation	7.60	46.00	30.59	50.02	50.60
3	Min	0	63	49	77	104
	Max	97	295	276	295	300
	Mean	27.17	151.11	119.08	157.14	255.29
	Median	19	150	114.50	155	278
	Standard deviation	21.82	50.53	44.44	50.38	49.18
4	Min	5	40	33	41	104
	Max	80	299	299	299	300
	Mean	25.79	143.29	121.20	149.63	256.56
	Median	22	123.50	99.50	131.50	268
	Standard deviation	14.79	63.90	59.83	64.31	38.63
5	Min	4	22	14	23	61
	Max	53	239	145	239	300
	Mean	14.76	73.98	53.71	78.40	230.64
	Median	12	72	47.50	74	236.50
	Standard deviation	8.77	36.19	25.90	37.76	50.05
6	Min	3	20	9	20	72
	Max	46	247	137	247	300
	Mean	20.75	94.66	72.80	98.55	233.45
	Median	20	89	68.50	92	245.50
	Standard deviation	8.40	35.54	28.29	37.56	52.28
7	Min	2	35	22	35	116
	Max	36	260	207	269	1000
	Mean	15.80	91.57	63.44	99.09	660.91
	Median	15	88	59	95.50	708.50
	Standard deviation	5.79	41.43	27.93	44.14	242.57

The results suggest that the case 7 yields the worst results (converges after a large number of iterations). However, the optimization was performed for 1,000 iterations (3.3 times more than for test cases 1 to 6) and, therefore, new tentative solutions appear late in the optimization, beyond the 300th iteration. A comparison of the results in column C, between test cases 1 and 7, reveals that the maximum fuel burn reduction relative to the general optimum (7.41 kg, or 0.01%) may not justify the additional 700 iterations. The results obtained for test cases 1, 2, 5, and 6 are close, and suggest that test case 1 converges faster to the selected threshold fuel burn values (except for 100 kg over the final solution fuel burn, where it performed the worst).

Table 5.5 shows the fuel burn reduction, relative to the "global" optimum, at different points (iterations) during the optimization. Test cases 1 and 7 have identical optimization method configurations, except for the number of iterations. For an FPL solution at the 300th iteration the maximum fuel burn differences relative to the "global" optimum for an RTA value are different (a difference of 12.28 kg or 0.02%), due to the optimization method's stochastic nature (due to the randomness characteristic for the evolutionary algorithms).

Together, the results for test cases 1 and 7, at the 300th iteration, are equivalent to running test case 1 for 20 times. As such, relative to the "global" optimal solutions, variant 1 of the optimization method found solutions that had a higher fuel burn: between 0 kg and 82.23 kg (0.14%), with a mean of 27 kg (0.04 %), a median of 23.58 kg (0.04%) and a standard deviation of 19.37 kg (0.03%). These results confirm that test case 1 still produced the best results, however, they are just marginally better relative to results obtained for test cases 5 and 6.

The execution times for the tests performed in this paper are presented in Table 5.6. These are total execution times, from the start of the optimization (initializations), and include: loading the aircraft performance model and the reference track data, processing the reference track data, routing grid construction, loading the atmospheric data, and storing the large amounts of data needed to analyze the evolution and the performance of each test run.

Table 5.5 Synopsis of the fuel burn improvement for the tentative flight plan solution for the set of RTA constraints, relative to the "global" optimal solutions, at a set of points (iterations / generations) during the optimization

Test case	Generation	G50		G100		G150		G200		G250		G300		G500		G1000	
	Fuel burn over the "global" optimum	kg	%	kg	%	kg	%	kg	%	kg	%	kg	%	kg	%	kg	%
1	Min	7.30	0.01	4.99	0.01	3.39	0.01	0.00	0.00	0.00	0.00	0.00	0.00				
	Max	688.18	1.21	257.58	0.45	239.12	0.42	140.55	0.25	110.71	0.19	69.95	0.12				
	Mean	164.08	0.29	75.29	0.13	49.81	0.09	34.88	0.06	26.30	0.05	22.34	0.04				
	Median	147.11	0.26	59.47	0.10	35.72	0.06	25.79	0.05	21.64	0.04	19.16	0.03				
	Standard deviation	112.30	0.20	57.06	0.10	43.06	0.08	29.75	0.05	19.34	0.03	16.75	0.03				
2	Min	16.61	0.03	8.22	0.01	7.51	0.01	3.75	0.01	1.50	0.00	1.50	0.00				
	Max	569.99	1.00	284.95	0.50	186.13	0.33	165.21	0.29	155.85	0.27	105.46	0.19				
	Mean	178.35	0.31	81.27	0.14	55.99	0.10	45.21	0.08	40.49	0.07	35.07	0.06				
	Median	140.79	0.25	64.19	0.11	43.11	0.08	37.46	0.07	33.65	0.06	31.82	0.06				
	Standard deviation	118.98	0.21	58.51	0.10	38.82	0.07	33.44	0.06	30.20	0.05	21.80	0.04				
3	Min	158.87	0.28	70.28	0.12	23.51	0.04	20.19	0.04	20.19	0.04	20.19	0.04				
	Max	1683.88	2.95	819.21	1.43	489.72	0.86	367.16	0.64	354.81	0.62	321.81	0.56				
	Mean	472.24	0.83	267.17	0.47	179.63	0.32	138.33	0.24	124.32	0.22	110.79	0.19				
	Median	373.00	0.66	220.71	0.39	158.93	0.28	131.55	0.23	123.80	0.22	105.50	0.19				
	Standard deviation	307.06	0.54	155.14	0.27	88.68	0.16	73.32	0.13	67.00	0.12	61.07	0.11				
4	Min	62.52	0.11	30.62	0.05	23.97	0.04	20.01	0.04	20.01	0.04	3.77	0.01				
	Max	924.57	1.62	707.42	1.24	707.42	1.24	492.70	0.86	370.53	0.65	290.68	0.51				
	Mean	386.56	0.68	227.90	0.40	171.42	0.30	133.10	0.23	104.08	0.18	90.55	0.16				
	Median	351.02	0.62	189.46	0.33	141.87	0.25	114.15	0.20	82.99	0.15	66.75	0.12				
	Standard deviation	202.73	0.36	151.15	0.26	126.78	0.22	85.61	0.15	71.16	0.12	65.56	0.11				
5	Min	52.33	0.09	6.68	0.01	5.17	0.01	2.60	0.00	0.00	0.00	0.00	0.00				
	Max	715.41	1.25	192.51	0.34	129.69	0.23	121.90	0.21	96.32	0.17	82.12	0.14				
	Mean	158.95	0.28	67.54	0.12	49.73	0.09	44.08	0.08	38.18	0.07	35.10	0.06				
	Median	121.80	0.21	63.38	0.11	50.26	0.09	44.80	0.08	37.11	0.07	35.30	0.06				
	Standard deviation	111.26	0.20	34.31	0.06	23.13	0.04	22.08	0.04	19.27	0.03	17.63	0.03				
6	Min	28.89	0.05	5.73	0.01	1.52	0.00	1.52	0.00	0.00	0.00	0.00	0.00				
	Max	587.78	1.03	222.09	0.39	113.42	0.20	113.42	0.20	94.70	0.17	89.83	0.16				
	Mean	219.11	0.38	84.76	0.15	46.27	0.08	35.52	0.06	31.32	0.06	29.11	0.05				
	Median	212.74	0.37	77.62	0.14	44.41	0.08	26.11	0.05	18.53	0.03	17.04	0.03				
	Standard deviation	109.85	0.19	49.79	0.09	27.93	0.05	25.43	0.04	24.94	0.04	24.79	0.04				
7	Min	41.77	0.07	4.82	0.01	1.41	0.00	1.21	0.00	1.21	0.00	0.63	0.00	0.00	0.00	0.00	0.00
	Max	443.57	0.78	204.28	0.36	163.04	0.29	140.41	0.25	92.64	0.16	82.23	0.14	78.18	0.14	62.54	0.11
	Mean	153.44	0.27	69.82	0.12	49.18	0.09	40.46	0.07	33.95	0.06	31.75	0.06	26.04	0.05	22.05	0.04
	Median	149.51	0.26	61.72	0.11	45.55	0.08	40.16	0.07	34.42	0.06	32.92	0.06	19.29	0.03	15.66	0.03
	Standard deviation	72.56	0.13	38.44	0.07	25.86	0.05	24.87	0.04	21.07	0.04	20.67	0.04	20.98	0.04	18.70	0.03

The execution times are affected by the fact that the code was written in Matlab (interpreted code) in a Windows environment (the processor time for a task is allocated by the operating system according to its own priorities), with large data structures stored in the memory.

Table 5.6 Execution times obtained for the 7 variants (test cases) of the proposed optimization method

Execution time	Test case						
	1	2	3	4	5	6	7
Min (s)	4,992.59	5,041.32	3,420.88	3,449.43	4,976.35	4,785.86	16,117.74
Max (s)	5,133.54	5,172.87	3,557.71	3,604.48	5,069.75	4,873.95	16,430.31
Mean (s)	5,047.47	5,096.34	3,490.67	3,525.96	5,034.87	4,812.08	16,303.89
Median (s)	5,038.60	5,095.38	3,478.28	3,537.66	5,042.21	4,799.44	16,324.68
Standard deviation (s)	48.78	38.64	45.64	66.53	30.42	31.36	100.70

A comparison of the execution times between test cases 1 and 3, and 2 and 4, shows that the local search performed during the optimization increased the execution time by approximately 1,568.39 to 1,591.89 seconds (an increase of close to 30%), which was expected. As more tentative FPL solutions for the RTA constraint set are identified, mutated, and added to the extended population set, more FPL performance calculations must be performed (93 FPL evaluations in every iteration, in comparison with 62 FPL evaluations if the local search is not performed). The local search produced a maximum reduction in fuel consumption of between 250 kg (test case 1 versus test case 3) and 185 kg (test case 2 versus test case 4) – see Table 5.3 column C. The effect of generating the extended population FPLs through crossover on both lateral and vertical flight plans (test case 5) was an increase in execution time by a maximum of 36 seconds, and did not yield better results. This result could be due to the specifics of the FPL components' crossover, and to the fact that performing a crossover on both the LFPL and VFPL components produces child FPLs that are too different than the parents, and thus results in a loss of good genetic information. The invalid FPL parameters' correction (test cases 1 versus 6) resulted in a maximum increase in execution time of 260 seconds and reduced the maximum fuel burn difference with respect to the reference profile by 20 kg. Finally, increasing the number of optimization iterations beyond 300 (test case 7 versus test case 1) did not produce significantly better solutions; however, for the 1,000 iterations performed for test case 7, the execution time increase was approximately 11,300 seconds, or 220% more than for test case 1.

5.5 Conclusion

This paper presents a new optimization method that addresses a flight planning problem where the flight planner/decision maker has a preferred time domain for an aircraft crossing time at a WPT or they must include an RTA constraint. The proposed method was able to quickly identify, within the first eight iterations, tentative solutions for the entire set of 31 selected RTA values. These initial tentative solutions are not optimal; they are random FPLs that satisfy the optimization objective's time constraint (not the minimum fuel requirement). Seventy test runs were conducted for the same optimization problem (10 runs for each

optimization method variant). The best solutions (FPLs that yield the minimum fuel burn) for each of the 31 RTA values were considered the “global” optimums and were used as references, to evaluate the performance of the proposed method and its variants (i.e. the influence of various techniques applied during the optimization, such as adding a local search).

The tests showed that, relative to the initial, random, tentative FPL solutions, the optimization method can yield a fuel burn reduction of up to 14,000 kg, depending on how far from the optimum profile the initial FPL is. Although a local search performed in each iteration increases the execution time by 30%, it also increases the solution’s quality, both in terms of reduction of the maximum fuel burn variation between FPL solutions for two runs of the optimization, and in a reduction of the maximum fuel burn difference relative to the “global” optimum, from 321 kg to 69 kg (a better convergence to a “global” optimum). Performing a correction of the invalid FPLs in the initial population improves the solution quality, with a relative minimal increase in execution time (200 seconds).

The proposed optimization method successfully identified optimal FPL solutions for the entire set of RTA constraint values and had a good convergence: solutions of 0 to 82 kg (0.14%) fuel burn over the “global” optimum. Given the long execution time, and the solution randomness (in the parameter space), the optimization method is found to be appropriate for the flight-planning phase, as it can provide the decision maker with a set of optimal FPLs from which to choose, according to specific criteria. If the ATM rejects the selected FPL, the decision maker can select the next-best FPL/RTA value, without having to perform a new optimization.

Future work could investigate an optimization method that can determine the set of optimal FPLs for a set of RTA constraints that are not clustered (non-contiguous RTA constraint bounds). Another direction of research would be to investigate if other methods, derived from other MOO techniques, can be successfully applied for the optimization of flight trajectories with RTA constraints. A third direction of investigation would be to apply the

proposed optimization approach for flight trajectories with multiple RTA constraints, at points along the flight trajectory, where each time constraint would add another dimension to the objective space. A fourth study could investigate the implementation of avoidance area by assigning time (and possible altitude) dependent crossing restrictions for the nodes of the routing grid.

CHAPTER 6

DISCUSSION OF THE RESULTS

The research presented in this thesis relates to the field of flight trajectory optimization and investigates a new method to model and compute the atmospheric data in points (locations) along the flight trajectory, for a constant altitude section of the cruise phase, and two new flight trajectory optimization methods.

The first investigation, presented in Chapter 3, analyzed a new atmospheric data model to be used in flight trajectory optimization calculations for constant altitude cruise segments. This new model defines the atmospheric parameters variation as a function of time, at a selected altitude, in the nodes of a routing grid constructed based on the orthodromic route between the geographical points that define the segment under optimization. The parameters defining the routing grid are: along and across the orthodromic route step size at sea level (SLL), the maximum number of steps across the orthodromic route that can be taken by the aircraft at a step along the orthodromic route, and the maximum deviation from the orthodromic route. These parameters were selected so that the maximum distance of a cruise flight sub-segment (integration step), between adjacent grid nodes, would be less or equal to the maximum integration step used in the flight trajectory performance calculations, and the grid covers the geographic area intended for aircraft routing.

The first hypothesis was that the proposed method would yield an atmospheric parameter value (air temperature or wind) in a grid definition point (geographical location), at the selected cruise altitude, for a selected time instance, with the same precision and faster than when computed using a 4D interpolation from the forecast data (GRIB data) provided by the meteorological agencies. The second hypothesis was that, given that the cruise phase is the longest phase of the flight, and that the flight performance calculations for the constant altitude and constant speed segments are performed by integration over the segment distance, the proposed model would conduct to important reductions of the flight trajectory simulation / flight performance parameters computation time.

First, the geographic locations of the initial and final points for the cruise phase of a real flight (the initial and final points of the routing grid) were taken from the FlightAware website (flight TSC601 of 14 June 2016, between Nantes and Montréal). Then, four grids were constructed based on two maximum deviations from the orthodromic route (250 n.m. and 500 n.m.), two lateral deviation settings (maximum one step of 20 n.m. and maximum two steps of 10 n.m.), a maximum segment SLL along the orthodromic route of 50 n.m, and a cruise altitude of 30,000 ft. These grids were used for evaluating the proposed model's performance: the time necessary to generate the atmospheric data, the memory requirements for different grid sizes (number of nodes), the time necessary to compute the atmospheric parameters in a grid node at a selected time instance, and the time necessary to perform a flight trajectory simulation / flight performance calculations. Finally, the Global Deterministic Prediction System (GDPS) atmospheric forecast data for the period that covered the time domain of interest, for which the Atmospheric Data Model (ADM) would be created (14 June, 2016, between 12:00 and 24:00 UTC), and the pressure altitudes that encompass the cruse altitude of 30,000 ft (i.e. 350 hPa and 300 hPa) were downloaded from the Environment Canada website. The data corresponding to a geographic area that covers the four grids was selected and subsequently used for the evaluation.

The results showed that the time necessary to generate the ADM using the proposed method is significantly reduced (relative to 4D interpolations using the GRIB data): between 28.95% and 58.47%. For the cases where a low grid resolution was used (e.g. one step of 20 n.m. lateral deviation) the memory requirement was less than that for the GRIB data covering the same geographic area, altitude, and time interval of interest. Tests performed in each node of the routing grid for time instances covering the entire timespan for which the model was created, showed that the atmospheric parameters computed based on the ADM were obtained on average six time faster than when they were computed using the GRIB data. The atmospheric data values were identical; the differences between their values were of the order of 10^{-14}. These results validated the first hypothesis, that the ADM computes the atmospheric parameters faster and with the same precision as a 4D interpolation from GRIB data.

Another set of tests evaluated the ADM's performance in the context of flight trajectory simulation / flight performance parameters calculations. Flight trajectory simulations were performed for two trajectories constructed based on a grid having a maximum deviation of 500 n.m. from the orthodrome and a maximum of two lateral steps of 10 n.m. The results showed a computation time reduction higher than 10%. Since the atmospheric parameters computed based on the ADM were "identical" with those created using the GRIB data, the results of the flight trajectory simulation using the ADM were "identical" with those computed using the GRIB data. Therefore, the second hypothesis was validated.

The second research, presented in Chapter 4, proposed a new flight trajectory optimization method based on genetic algorithms, where the candidate flight trajectories were defined as "flight plans", with their lateral components defined by selecting WPTs from an orthogonal routing grid (similar to that used in the first research) and the vertical components have a structure conforming to a proposed template. For each node of the grid, the segment SLL and heading for each possible segment starting in that node are calculated and stored for use in the flight trajectory accelerated simulation / flight performance calculations. The objective of the optimization is the minimization of the total cost for the flight. In this research it was assumed that:

1. The lateral flight plan component is constructed by selecting grid nodes that are one step further along the orthodromic route direction, and up to a selected maximum number of routing grid steps across the orthodromic route direction (grid axis);
2. The vertical component of the flight plan:
    a. The climb and descent sections are performed at constant [CAS, MACH] speeds;
    b. The cruise section is composed of constant altitude and speed sub-segments, according to a proposed template;
    c. The climb and descent sections do not contain constant altitude segments;
    d. In the cruise phase, only step climbs are allowed (the cruise altitude of a cruise segment is always equal or higher than the altitude of the preceding cruise segment.

The proposed crossover and mutation methodologies for the lateral and vertical components of the flight plan ensure that the "child" flight plans, resulted from the crossover between two candidate flight plans or their mutation, are themselves members of the set of candidate flight plans (they conform with the templates selected for the flight plan components).

The candidate flight plans evaluated during the optimization, generated randomly or resulted from a genetic operation, could be invalid: they could generate aircraft flight parameters (altitude – speed combinations) outside the aircraft's flight envelope or they could require more fuel than available onboard. Two strategies were evaluated regarding the invalid flight plans with parameters outside the flight envelope limits. The first strategy consisted in assigning them penalty fuel burn and flight time values (estimated heuristically to be larger than for any possible valid flight plan). This is equivalent to assigning the lowest fitness value and, therefore, they could contribute with genetic material to the next generation, however, the probability is very low. The second strategy was that, during the accelerated simulation of the flight along the evaluated flight plan, if the altitude - speed parameters of a segment were invalid relative to the aircraft's flight envelope then the segment's speed – altitude settings were corrected to values within the aircraft's envelope limits (with preference for the pre-planned altitude). For invalid flight plans due to fuel burn larger than the available fuel, penalty values were assigned as fuel burn and flight time (identical with the values assigned for the case when the flight plans resulted in flight parameters outside the aircraft's flight envelope).

The routing grid used for the construction of the flight plan components and the atmospheric data model used in the performance calculations, as well as the flight profiles used as reference, were generated based on the flight track data corresponding to a real flight (Swiss Air flight SWR40 of 25 February, 2019) segment retrieved from FlightAware. The reference profiles were obtained by a speed optimization along the lateral and altitude profiles constructed based on the SWR40 track data. Each reference profile was obtained for identical conditions (e.g. initial aircraft weight, crossing time at the initial point, and CI value).

Ten test runs were performed for each of the six CI values used in the method's performance evaluation. Five reference profile optimization test runs were performed for each CI value. The best reference profiles obtained for each CI value were used as reference for the optimization method and CI value tests.

The first hypothesis was that the flight plan solutions yielded by the proposed optimization method would be better (would have a smaller total cost) than the reference profile. The results have shown that for both method variants (corrected and non-corrected flight plans) and for all CI values this is true. The second hypothesis was that correcting the invalid flight plans relative to aircraft's flight envelope would yield better results than if they were not corrected, and would increase the computation time. This hypothesis was partially disproved. Except the case when CI = 0 (fuel burn minimization), the flight plan corrections increased the total cost. A comparison between the execution times for CFP and NCFP variants of the optimization method have shown that the flight plan corrections more than double the optimization's execution time. The loss of performance when the flight plan corrections were performed during the optimization might be due to the loss of population diversity. The invalid profiles might contain characteristics (chromosomes) that might be useful in future generations of the population. Even for the case where CI = 0, when the CFP variant yielded better results, it might be possible that the same optimal results, or even better, could be obtained with a smaller execution time increase by increasing the number of optimization iterations (generations).

The third research investigated a new optimization method, derived from the NSGA-II algorithm, which identifies, in "parallel", optimal flight plans for a set of contiguous RTA constraints at the end of the segment under optimization. The routing grid, candidate flight plans, and atmospheric data were constructed similarly with the method presented in the previous research investigations, based on the initial and final points (geographical locations, altitudes, and crossing times) of the segment under optimization, retrieved from a real flight track data. The central RTA constraint value (RTA_0) was considered to correspond to the aircraft crossing time at the selected final point, as retrieved from the flight track data. Seven

variants of the proposed optimization method were evaluated. Given the stochastic nature of the optimization method, 10 test runs were conducted for each variant of the method in order to better characterize the performances of the optimization method and its variants. The set of contiguous RTA constraints were taken as the 31 contiguous time windows with a width of 20 s, with their central values spanning the interval $RTA_0 \pm 5$ min. For each of the 31 RTA constraint values the optimum flight plan (the minimum fuel burn) over the 70 test runs (10 test runs for each method variant) were considered the "global" optimum and used as reference to determine the performance of the method and its variants.

The first hypothesis stated that the method is capable to identify solutions for the entire set of RTA constraints. The tests showed that all the method variants identified tentative solutions for all the RTA constraint domains within the first eight iterations. Therefore, this hypothesis was validated. The second hypothesis stated that by performing invalid flight plan corrections for the first generation population more tentative solutions would be identified in the first iterations of the optimization. The tests confirmed this hypothesis, however, the difference in number of tentative flight plan solutions identified within the first iterations was small: for the case when the initial population invalid flight plans were corrected, the tentative solutions for all RTA constraints were identified in maximum seven iterations, whereas if the invalid flight plans were not corrected, the tentative solutions were identified in maximum eight iterations.

The flight plan solutions improved when a local search was performed in every iteration of the optimization, which confirms the third hypothesis

For the considered test scenario, the best results were obtained for the case when: the invalid first generation flight plans were corrected, a local search is performed in each generation, the crossover is performed only on one of the flight plan components, and the flight plan fitness for non-valid flight plans (flight time does not satisfy any RTA constraint) is assigned based on the Euclidian distance to a reference point. For five optimization method variants,

for each RTA value the solution converged to fuel burn value within 90 kg of the “global” optimum for that particular RTA value.

The tests also showed that, performing the optimization beyond a certain number of iterations does not improve significantly the solution. The solutions obtained after 1000 iterations resulted in an improvement of the fuel burn by 20 kg. However, the computation time increased by 220%.

The advantage of the proposed method is that provides a set of optimal flight plans for a range of RTA values of interest for the flight planner, that can be used in the negotiation with the ATM system, without having to perform new optimizations.

CONCLUSION AND RECOMMENDATIONS

This thesis proposed three new methods related to flight trajectory optimization, viewed as a flight-planning problem. The first proposed method generated an atmospheric data model that provided the values of atmospheric parameters as a function of time, in a set of geographic locations, at a selected altitude. The second proposed method was an optimization method based on genetic algorithms, were the lateral and vertical components of the candidate flight plans conform to proposed models (templates). The methodologies to perform the crossover and mutation operations were adapted to the lateral and vertical flight plan structures. The third proposed method was a new optimization method that identified, in parallel, the optimal flight plans for a set of contiguous RTA constraints.

The originality of the work presented in this thesis consists in:

1. The study presented in Chapter 3 proposed a new method and data model to define atmospheric parameters (air temperature and wind) in a selected location (fixed latitude, longitude, and altitude) as a function of time. This study also proposed a new method to construct a routing grid, appropriate for use in flight trajectory optimization algorithms. Each node of the routing grid holds the precomputed atmospheric data for that geographic location and for a selected set of altitudes, and the flight segment information (sea level segment length and segment heading) for all "allowed" flight segments starting in that node;
2. The study presented in Chapter 4 proposed a new flight trajectory optimization method using a genetic algorithm, in which the lateral and vertical components of the candidate flight plans were constructed based on the routing grid proposed in Chapter 3. New methodologies were proposed for the construction of the candidate flight plan components and for performing the crossover and mutation operations;
3. The study presented in Chapter 5 proposed a new flight trajectory optimization method capable of identifying, in parallel, the optimal flight plans for flight segment with a set of contiguous RTA constraints at the final point. The new optimization method was derived from the NSGA-II multi-objective optimization method, and

adapted for the specific characteristics of the flight trajectory optimization problem. The construction of the routing grid and of the candidate flight plans, as well as the crossover and mutation operations, were similar with those presented in Chapter 4.

The advantage of the ADM proposed in the first research is that, for a cruise section flown at constant altitude, it provides the atmospheric parameter values as a function of time (compared with stationary data currently used on FMS platforms) much faster and with the same precision as when computed from GRIB data. When the ADM defines the atmospheric data in points along a selected lateral flight plan, and for lower resolution routing grids, the memory required to store the atmospheric data is smaller than when using GRIB data. In flight trajectory optimization algorithms, where a large number of candidate flight plans are evaluated iteratively, and a large number of atmospheric parameter calculations are performed for each candidate flight plan evaluation, the faster atmospheric parameter calculations using the ADM can significantly reduce the computation time.

The disadvantage of the ADM model is that, when extended for a set of N altitudes, the required memory increases by a factor of N.

The optimization method based on genetic algorithms, proposed in CHAPTER 4, was able to converge to solutions that are better than those for the reference flight plan, when the optimization was conducted only for the speed profile (imposed lateral flight plan component and altitude profile). For 10 identical test runs the maximum total cost variation obtained for the solutions was 0.686% for the CFP, and 0.634% for the NCFP. Except for the case where CI = 0, the NCFP method variant yielded better results, probably due to the loss in population diversity when the flight plan corrections (CFP) were performed.

The disadvantages of the optimization method proposed in CHAPTER 4 are:

1. For successive optimization runs, under identical initial conditions and optimization problem, the optimal flight plan solutions are different – typical for optimizations based on genetic algorithms;

2. Long execution times, due to the large number of candidate flight plans evaluated during the optimization. For the tests performed with the CFP method variant, the execution time more than doubled relative to the tests with the NCFP variant;
3. Not appropriate for on-board (FMS), or online optimization.

The optimization method proposed in CHAPTER 5, derived from the NSGA-II multi-objective optimization, was able to identify optimal solutions for all the RTA constraints in the target RTA constraints set. For five of the proposed method variants, the optimal solutions were found to be within 82 kg of fuel (0.14%) over the "global" optimum solution (the best solution over the entire set of tests for the RTA constraint value). The local search, performed in each iteration, reduced the maximum fuel burn difference relative to the global optimum from 321 kg to 69 kg, with an execution time increase of approximately 30%. For the test performed in this study, an increase of the number of optimization algorithm iterations, from 300 to 500, yielded a maximum fuel burn reduction of 9 kg, and from 300 to 1000 iteration a reduction of 20 kg and a 220% increase in execution time. The disadvantages of the proposed optimization method are the long execution time and the fact that the solutions are different for each run of the same optimization problem.

Based on the research and the results presented in this thesis, the following recommendations are made for future research:

1. Perform a comparison of the ADM model's precision relative to the atmospheric parameters obtained using other data models and interpolation methods, more complex and more computing intensive. Compare the differences between the atmospheric parameters generated using the ADM and those generated using other data models/interpolation methods with the precision of the atmospheric prediction data issued by the meteorological agencies;
2. Compare the atmospheric parameters computed using 4D linear interpolation, ADM, and other (more complex) interpolation methods with the real atmospheric data (recorded during flight);
3. Relative to the optimization method proposed in CHAPTER 4:

a. Investigation of a more computationally expensive optimization approach, where in each step of the genetic algorithm:
    i. The new population will be generated using the genetic operations applied on the lateral flight plan (the vertical flight plan would be retained from a parent); and then,
    ii. For each member of the new population, a new search (e.g. branch and bound, annealing, etc.) identifies the optimal vertical flight plan.
b. Investigate the execution time improvements when the accelerated flight performance calculations are performed using a simplified aircraft performance model, based on interpolation tables, mainly used in FMS platforms.

4. Relative to the optimization method proposed in CHAPTER 5:
    a. Investigation of an optimization method that can determine the set of optimal flight plans for a set of RTA constraints that are not clustered (non adjacent RTA constraints);
    b. Investigate if the proposed optimization approach can be successfully extended for flight trajectories with multiple RTA constraints, at various points along the flight trajectory, where each time constraint would add another dimension in the objective space.

LIST OF REFERENCES

Altus, S. (2009). Effective Flight Plans Can Help Airlines Economize, *Boeing AERO Magazine*, *35*(03), 27-30.

Ballin, M., Wing, D., Hughes, M., & Conway, S. (1999, August). *Airborne Separation Assurance and Traffic Management: Research of Concepts and Technology*, Paper presented at Guidance, Navigation, and Control Conference and Exhibit, Portland, OR (pp. 3989). DOI: 10.2514/6.1999-3989

Ballin, M. G., Williams, D. H., Allen, B. D., & Palmer, M. T. (2008, October). *Prototype flight management capabilities to explore temporal RNP concepts*. Paper presented at 2008 IEEE/AIAA 27th Digital Avionics Systems Conference, St. Paul, MN (pp. 3.A.6-1-3.A.6-12). DOI: 10.1109/DASC.2008.4702797

Bonami, P., Olivares, A., Soler, M., & Staffetti, E. (2013). Multiphase Mixed-Integer Optimal Control Approach to Aircraft Trajectory Optimization. *Journal of Guidance, Control, and Dynamics*, *36*(5), 1267-1277. DOI: 10.2514/1.60492

Botez, R. (2006). GPA-745: Introduction à l'avionique: notes de laboratoire GPA-745. École de Technologie Supérieure.

Bronsvoort, J., McDonald, G., Potts, R., & Gutt, E. (2011, June). *Enhanced descent wind forecast for aircraft*. Paper presented at the 9th USA/Europe Air Traffic Management Research and Development seminar (ATM2011), Berlin, Germany.

Buehner, M., McTaggart-Cowan, R., Beaulne, A., Charette, C., Garand, L., Heilliette, S,. … Zadra, A. (2015). Implementation of deterministic weather forecasting systems based on ensemble variational data assimilation at Environment Canada. Part I: The global system. *Monthly Weather Review*, *143* (7): 2532–2559, DOI: 10.1175/MWR-D-14-00354.1

Carlton-Wippern, K. C. (1992). On loxodromic navigation. *The Journal of Navigation*, *45*(2), 292-297. DOI: 10.1017/s0373463300010791

Caron, J.F., Milewski, T., Buehner, M., Fillion, L., Reszka, M., Macpherson, S., & St-James, J. (2015) Implementation of Deterministic Weather Forecasting Systems Based on Ensemble–Variational Data Assimilation at Environment Canada. Part II: The Regional System. *Monthly Weather Review*, *143*(7): 2560–2580, DOI: 10.1175/MWR-D-14-00353.1

Casado, E., Vilaplana, M., & Goodchild, C. (2013, August). *Sensitivity of Trajectory Prediction Accuracy to Aircraft Performance Uncertainty*. Paper presented at AIAA Infotech@ Aerospace (I@ A) Conference, Boston, MA (pp. 5045). DOI: 10.2514/6.2013-5045

Cate, K. (2013, January). *Challenges in achieving trajectory-based operations*. Paper presented at 51st AIAA Aerospace Sciences Meeting including the New Horizons Forum and Aerospace Exposition, Grapevine (Dallas/Ft. Worth), TX (pp. 443). DOI: 10.2514/6.2013-443

Ceruti, A., Voloshin, V., & Marzocca, P. (2014). Heuristic algorithms applied to multidisciplinary design optimization of unconventional airship configuration. *Journal of Aircraft*, *51*(6), 1758-1772. DOI: 10.2514/1.C032439

Ceruti, A., & Marzocca, P. (2017). Heuristic optimization of Bezier curves based trajectories for unconventional airships docking. *Aircraft Engineering and Aerospace Technology*, *89*(1), 76-86. DOI: 10.1108/AEAT-11-2014-0200

Ceruti, A., Fiorini, T., Boggi, S., & Mischi, L. (2018). Engineering optimization based on dynamic technique for order preference by similarity to ideal solution fitness: Application to unmanned aerial vehicle wing airfoil geometry definition. *Journal of Multi-Criteria Decision Analysis*, *25*(3-4), 88-100. DOI: 10.1002/mcda.1637

Chaimatanan, S., Delahaye, D., & Mongeau, M. (2012, June). *A methodology for strategic planning of aircraft trajectories using simulated annealing*. Paper presented at ISIATM 2012, 1st International Conference on Interdisciplinary Science for Air traffic Management, Daytona Beach, FL.

Chamseddine, A., Zhang, Y., & Rabbath, C.A. (2012, June). *Trajectory planning and re-planning for fault tolerant formation flight control of quadrotor unmanned aerial vehicles*. Paper presented at 2012 American Control Conference (ACC), Montreal, QC (pp. 3291-3296). DOI: 10.1109/ACC.2012.6315363

Cole, R. E., Green, S., Jardin, M., Schwartz, B., & Benjamin, S. (2000, June). *Wind prediction accuracy for air traffic management decision support tools*. Paper presented at 3rd USA/Europe Air Traffic Management R&D seminar, Napoli, Italy

Dancila, B. D., Botez, R., & Labour, D. (2013). Fuel burn prediction algorithm for cruise, constant speed and level flight segments. *The Aeronautical Journal*, *117*(1191), 491-504. DOI: 10.1017/S0001924000008149

Dancila, B. D., & Botez, R. (2014, June). *Construction of an aircraft's VNAV flight envelope for in-FMS flight trajectory computation and optimization*. Paper presented at 14th AIAA Aviation Technology, Integration, and Operations Conference, Atlanta, GA (pp. 2291). DOI: 10.2514/6.2014-2291

Dancila, B. D., & Botez, R. M. (2016a). Geographical area selection and construction of a corresponding routing grid used for in-flight management system flight trajectory optimization. *Proceedings of the Institution of Mechanical Engineers, Part G: Journal of Aerospace Engineering*, *231*(5), 809 – 822. DOI: 10.1177/0954410016643104

Dancila, B. D., Beulze, B., & Botez, R. M. (2016b). Geometrical Vertical Trajectory Optimization – Comparative Performance Evaluation of Phase versus Phase and Altitude-Dependent Preferred Gradient Selection. *IFAC-PapersOnLine*, *49*(17), 17-22. DOI: 10.1016/j.ifacol.2016.09.004.

Dancila, B. D., & Botez, R. M. (2018). Vertical flight path segments sets for aircraft flight plan prediction and optimization. *The Aeronautical Journal*, *122*(1255), 1371-1424. DOI: 10.1017/aer.2018.67

Dancila, B. D., Beulze, B., & Botez, R. M. (2019). Flight phase and altitude-dependent geometrical vertical flight plan optimization minimizing the total number of vertical plan segments. *Proceedings of the Institution of Mechanical Engineers, Part G: Journal of Aerospace Engineering*, *233*(13), 4825–4838. DOI: 10.1177/0954410019832127

Dancila, R. I., & Botez, R. M. (2020a). New atmospheric data model for constant altitude accelerated flight performance prediction calculations and flight trajectory optimization algorithms. *Proceedings of the Institution of Mechanical Engineers Part G: Journal of Aerospace Engineering*. DOI: 10.1177/0954410020945555

Dancila, R. I., & Botez, R. M. (2020b). *New Flight Trajectory Optimization Method using Genetic Algorithms*. Manuscript submitted for publication

De Smedt, D., & Berz, G. (2007, October). *Study of the required time of arrival function of current FMS in an ATM context*. Paper presented at 2007 IEEE/AIAA 26th Digital Avionics Systems Conference, Dallas, TX (pp.1.D.5-1-1.D.5-10). DOI: 10.1109/DASC.2007.4391837

Deb, K., Pratap, A., Agarwal, S., & Meyarivan, T. (2002). A fast and elitist multiobjective genetic algorithm: NSGA-II. *IEEE Transactions on Evolutionary Computation*, *6*(2), 182-197. DOI: 10.1109/4235.996017

DeJonge, M.K., & Syblon, W.H. (1984, June). *Application of cost index to fleet hub operation*, Paper presented at 1984 American Control Conference. San Diego, CA (pp.179-183). DOI: 10.23919/ACC.1984.4788373

Di Vito, V., Corraro, F., Ciniglio, U., & Verde, L. (2009). An Overview on Systems and Algorithms for On-Board 3D/4D Trajectory Management. *Recent Patents on Engineering*, *3*(3), 149-169. DOI: 10.2174/187221209789117744

Diaz-Mercado, Y., Lee, S.G., Egerstedt, M., & Young, S. (2013, October). *Optimal trajectory generation for next generation flight management systems*. Paper presented at 2013 IEEE/AIAA 32nd Digital Avionics Systems Conference (DASC), East Syracuse, NY (pp. 3C5-1-3C5-10). DOI: 10.1109/DASC.2013.6712566

Environment Canada. (n.d.a). Global Deterministic Prediction System. Retrieved from http://data.ec.gc.ca/data/weather/products/global-deterministic-prediction-system/?lang=en

Environment Canada. (n.d.b). GDPS data in GRIB2 format: 25 km. Retrieved from https://weather.gc.ca/grib/grib2_glb_25km_e.html

Environment Canada. (n.d.c) GDPS data in GRIB2 format: 66 km. Retrieved from https://weather.gc.ca/grib/grib2_glb_66km_e.html

Environment Canada. (n.d.d). RDPS data in GRIB2 format: 10 km. Retrieved from https://weather.gc.ca/grib/grib2_reg_10km_e.html

Environment Canada. (n.d.e). Regional Deterministic Prediction System. Retrieved from http://data.ec.gc.ca/data/weather/products/regional-deterministic-prediction-system/?lang=en

Environment Canada. (n.d.f). Using wget with the Datamart data in GRIB format. Retrieved from https://weather.gc.ca/grib/usage_tips_e.html

Environment Canada. (n.d.g). What is GRIB? Retrieved from https://weather.gc.ca/grib/what_is_GRIB_e.html

Eurocontrol. (2010). Documents for BADA Version 3.7. Retrieved from https://www.eurocontrol.int/eec/public/standard_page/proj_BADA_documents_37.html

Eurocontrol. (2020). Free route airspace. Retrieved from https://www.eurocontrol.int/concept/free-route-airspace

Eurocontrol. (n.d.). BADA: aircraft performance model. Retrieved from https://simulations.eurocontrol.int/solutions/bada-aircraft-performance-model/

European Commission. (2020). Welcome to the SESAR project. Retrieved from https://ec.europa.eu/transport/modes/air/sesar_en

European Environment Agency. (2018). *Transport and environment reporting mechanism (TERM): progress of EU transport sector towards its environment and climate objectives* (EEA Briefing 15/2018). DOI: 10.2800/139739

Fanti, M. P., Pedroncelli, G., Stecco, G., & Ukovich, W. (2012, July). *Modeling and Optimization of Aircraft Trajectories: A review*. Paper presented at 2012 7th International Conference on System of Systems Engineering (SoSE), Genova, Italy (pp. 235-240). DOI: 10.1109/SYSoSE.2012.6384209

Federal Aviation Administration. (2018). Airplane Upset Recovery High Altitude Operations Rev.2 [pdf]. Retrieved from https://www.faa.gov/other_visit/aviation_industry/airline_operators/training/media/Appendix_3-E_HighAltOperations.pdf

Federal Aviation Administration. (2020). What is NextGen? Retrieved from https://www.faa.gov/nextgen/what_is_nextgen/

Federal Aviation Administration. (n.d.a). FAA Flight Planning Information. Retrieved from https://www.faa.gov/about/office_org/headquarters_offices/ato/service_units/air_traffic_services/flight_plan_filing/

Federal Aviation Administration. (n.d.b). Part 91 – General Operating And Flight Rules, Electronic Code of Federal Regulations, Title14: Aeronautics and Space. Retrieved from https://www.ecfr.gov/cgi-bin/text-idx?c=ecfr&sid=3efaad1b0a259d4e48f1150a34d1aa77&rgn=div5&view=text&node=14:2.0.1.3.10&idno=14#se14.2.91_1117

Federal Aviation Administration. (n.d.c). Subpart B—Flight Rules, PART 91—GENERAL OPERATING AND FLIGHT RULES, Electronic Code of Federal Regulations, Title14: Aeronautics and Space. Retrieved from https://www.ecfr.gov/cgi-bin/text-idx?c=ecfr&sid=3efaad1b0a259d4e48f1150a34d1aa77&rgn=div5&view=text&node=14:2.0.1.3.10&idno=14#sp14.2.91.b

Federal Aviation Administration. (n.d.d). Title 14 – Chapter 1 – Subchapter F - AIR TRAFFIC AND GENERAL OPERATING RULES, Electronic Code of Federal Regulations, Title14: Aeronautics and Space. Retrieved from https://www.ecfr.gov/cgi-bin/text-idx?SID=d478b198bb6aac8e070a37a06181eeec&mc=true&tpl=/ecfrbrowse/Title14/14CIsubchapF.tpl

FlightAware. (2016). Air Transat 601. Retrieved from https://flightaware.com/live/flight/TSC601/history/20160614/1145ZZ/LFRS/CYUL

FlightAware. (2019a). Swiss 40. Retrieved from https://flightaware.com/live/flight/SWR40/history/20190225/1220Z/LSZH/KLAX

FlightAware. (2019b). American Airlines 107. Retrieved from https://flightaware.com/live/flight/AAL107/history/20190225/1715ZZ/EGLL/KJFK

FlightAware. (n.d.a). FlightAware ADS-B Coverage Map. Retrieved from https://flightaware.com/adsb/coverage#data-coverage

FlightAware. (n.d.b). Multilateration (MLAT) Overview, Retrieved from https://flightaware.com/adsb/mlat/

Fonseca, C.M., & Fleming, P.J. (1993). Genetic Algorithms for Multiobjective Optimization: Formulation, Discussion and Generalization. *Proceedings of the 5th International Conference on Genetic Algorithms*, *93*(), 416-423. DOI: 10.5555/645513.657757

Fonseca, C. M., & Fleming, P. J. (1998a). Multiobjective optimization and multiple constraint handling with evolutionary algorithms. I. A unified formulation. *IEEE Transactions on Systems, Man, and Cybernetics - Part A: Systems and Humans*, *28*(1), 26-37. DOI: 10.1109/3468.650319

Fonseca, C. M., & Fleming, P. J. (1998b). Multiobjective optimization and multiple constraint handling with evolutionary algorithms. II. Application example. *IEEE Transactions on Systems, Man, and Cybernetics - Part A: Systems and Humans*, *28*(1), 38-47. DOI: 10.1109/3468.650320

Franco, A., & Rivas, D. (2011). Minimum-cost cruise at constant altitude of commercial aircraft including wind effects. *Journal of Guidance, Control, and Dynamics*, *34*(4), 1253-1260. DOI: 10.2514/1.53255

Fukuda, Y., Shirakawa, M., & Senoguchi, A. (2010, September). *Development and evaluation of trajectory prediction model*. Paper presented at 27th international congress of the aeronautical sciences, NICE, France

Gardi, A., Sabatini, R., & Ramasamy, S. (2016). Multi-objective optimisation of aircraft flight trajectories in the ATM and avionics context. *Progress in Aerospace Sciences*, *83*(), 1-36. DOI: 10.1016/j.paerosci.2015.11.006

Ghazi, G., Botez, R., & Achigui, J.M. (2015a). Cessna citation X engine model identification from flight tests. *SAE International Journal of Aerospace*, *8*(2), 203-213. DOI: 10.4271/2015-01-2390

Ghazi, G., & Botez, R. (2015b). *Development of a high-fidelity simulation model for a research environment* (SAE Technical Paper 2015-01-2569). DOI: 10.4271/ 2015-01-2569

Ghazi, G., Botez, R. M., & Tudor, M. (2015c, September). *Performance database creation for Cessna Citation X aircraft in climb regime using an aero-propulsive model developed from flight tests*. Paper presented at Sustainability 2015: Environmental Sustainability in Design and Operations of Aircraft, Montreal, QC, Canada, American Helicopter Society.

Gillet, S., Nuic, A., & Mouillet, V. (2010, October). *Enhancement in realism of ATC simulations by improving aircraft behaviour models*. Paper presented at 29th Digital Avionics Systems Conference. Salt Lake City, UT (pp. 2.D.4-1-2.D.4-13). DOI: 10.1109/DASC.2010.5655482

Grigorie, L., Botez, R. M., & Popov, A. V. (2016, January). *Self-adaptive morphing wing model, smart actuated and controlled by using a multiloop controller based on a laminar flow real time optimizer*. Paper presented at 24th AIAA/AHS adaptive structures conference, San Diego, CA (pp. 1082). DOI: 10.2514/6.2016-1082

Herndon, A. A., Cramer, M., & Nicholson, T. (2009, October). *Analysis of advanced flight management systems (FMS), flight management computer (FMC) field observations, trials; lateral and vertical path integration*. Paper presented at 2009 IEEE/AIAA 28th digital avionics systems conference, Orlando, FL (pp.1.C.2-1–1.C.2-16). DOI: 10.1109/DASC.2009.5347572

Hagelauer, P., & Mora-Camino, F. (1998). A soft dynamic programming approach for on-line aircraft 4D-trajectory optimization. *European Journal of Operational Research*, *107*(1), 87-95. DOI: 10.1016/S0377-2217(97)00221-X

International Air Transport Association. (2018). IATA Forecasts Predicts 8.2 billion Air Travelers in 2037, Retrieved from https://www.iata.org/en/pressroom/pr/2018-10-24-02

International Civil Aviation Organization. (2018). ICAO Long-Term Traffic Forcasts [pdf], Retreived from https://www.icao.int/sustainability/Documents/LTF_Charts-Results_2018edition.pdf

International Civil Aviation Organization. (n.d.a). Forecasts of Scheduled Passenger and Freight Traffic, Retreived from https://www.icao.int/sustainability/Pages/eap-fp-forecast-scheduled-passenger-traffic.aspx

Ishibuchi, H., & Murata, T. (1996). Multi-objective genetic local search algorithm, *Proceedings of IEEE International Conference on Evolutionary Computation*, 119-124. DOI: 10.1109/ICEC.1996.542345

Ishibuchi, H., & Murata, T. (1998). A multi-objective genetic local search algorithm and its application to flowshop scheduling. *IEEE Transactions on Systems, Man, and Cybernetics, Part C (Applications and Reviews)*, *28*(3), 392-403. DOI: 10.1109/5326.704576

Janssen, V. (2009). Understanding coordinate reference systems, datums and transformations. *International Journal of Geoinformatics*, *5*(4), 41-53. Retrieved from: https://eprints.utas.edu.au/9575/

Jardin, M. R., & Bryson Jr, A. E. (2012). Methods for computing minimum-time paths in strong winds. *Journal of Guidance, Control, and Dynamics*, *35*(1), 165-171. DOI: 10.2514/1.53614

Jensen, M. T. (2003). Reducing the run-time complexity of multiobjective EAs: The NSGA-II and other algorithms. *IEEE Transactions on Evolutionary Computation*, *7*(5), 503-515. DOI: 10.1109/TEVC.2003.817234

Jensen, L., Tran, H., & Hansman, J.R. (2015, June). *Cruise Fuel Reduction Potential from Altitude and Speed Optimization in Global Airline Operations*. Paper presented at Eleventh USA/Europe Air Traffic Management Research and Development Seminar (ATM2015), Lisbon, Portugal

Jin, L., Cao, Y., & Sun, D. (2013). Investigation of potential fuel savings due to continuous-descent approach. *Journal of aircraft*, *50*(3), 807-816. DOI: 10.2514/1.C032000

Karney, C. F. (2013). Algorithms for geodesics. *Journal of Geodesy*, *87*(1), 43-55. DOI: 10.1007/s00190-012-0578-z

Karr, D. A., Vivona, R. A., Woods, S., & Wing, D. J. (2017, June). Point-Mass Aircraft Trajectory Prediction Using a Hierarchical, Highly-Adaptable Software Design. Paper presented in AIAA Modeling and Simulation Technologies Conference, Denver, CO (pp. 3336). DOI. 10.2514/6.2017-3336

Koreanschi, A., Sugar Gabor, O., Acotto, J., Botez, R., Mamou, M., & Mebarki, Y. (2016a, June). *A Genetic Algorithm Optimization Method for a Morphing Wing Tip Demonstrator Validated Using Infra Red Experimental Data*. Paper presented at 34th AIAA applied aerodynamics conference, Washington, D.C. (pp. 4037). DOI: 10.2514/ 6.2016-4037

Koreanschi, A., Sugar-Gabor ,O., & Botez, R. M. (2016b). Drag optimisation of a wing equipped with a morphing upper surface. *The Aeronautical Journal*, *120*(1225), 473–493. DOI: 10.1017/aer.2016.6

Koreanschi, A., Sugar Gabor, O., Ayrault, T., Botez, R., Mamou, M, & Mebarki, Y. (2016c, January). *Numerical optimization and experimental testing of a morphing wing with aileron system*. Paper presented at 24th AIAA/ AHS adaptive structures conference, San Diego, CA (pp. 1083). DOI: 10.2514/6.2016-1083

Lee, A., Weygandt, S., Schwartz, B., & Murphy, J. (2009, August). *Performance of trajectory models with wind uncertainty*. Paper presented at AIAA modeling and simulation technologies conference, Chicago, Illinois, (pp. 5834). DOI: 10.2514/6.2009-5834

Lenart, A. S. (2017). Orthodrome and Loxodromes in Marine Navigation. *Journal of Navigation*, *70*(2), 432-439. DOI: 10.1017/s0373463316000552

Lewis, T. A., Burke, K. A., Underwood, M. C, & Wing, D. J. (2019, June). *Weather Design Considerations for the TASAR Traffic Aware Planner*. Paper presented in AIAA Aviation 2019 Forum, Dallas, TX (pp. 3616). DOI. 10.2514/6.2019-3616

Li, J., & Heap, A.D., (2008). A review of spatial interpolation methods for environmental scientists. *Geoscience Australia, Record 2008/23*. Retrieved from www.ga.gov.au/webtemp/image_cache/GA12526.pdf

Liden, S. (1992, October). *Optimum 4D guidance for long flights*. Paper presented at IEEE/AIAA 11th Digital Avionics Systems Conference, Seattle, WA (pp. 262-267). DOI: 10.1109/DASC.1992.282146

Lipowski, A., & Lipowska, D. (2012) Roulette-wheel Selection via Stochastic Acceptance. *Physica A: Statistical Mechanics and its Applications*, *391*(6), 2193-2196. DOI: 10.1016/j.physa.2011.12.004

Marler, R., & Arora, J. (2004). Survey of multi-objective optimization methods for engineering. *Structural and Multidisciplinary Optimization*, *26*(), 369–395. DOI: 10.1007/s00158-003-0368-6

Matsuno, Y., & Tsuchiya, T. (2014, March) *Stochastic 4D Trajectory Optimization for Aircraft Conflict Resolution*. Paper presented at 2014 IEEE Aerospace Conference. Big Sky, MT (pp. 1-10). DOI: 10.1109/AERO.2014.6836275

Miettinen, K. (2001). Some Methods for Nonlinear Multi-objective Optimization. In: Zitzler, E., Thiele, L., Deb, K., Coello Coello, C.A., & Corne, D. (Eds), *Evolutionary Multi-Criterion Optimization. EMO 2001. Lecture Notes in Computer Science* (Vol 1993, pp. 1-20). DOI: 10.1007/3-540-44719-9_1

Murata, T., & Ishibuchi, H. (1995). MOGA: multi-objective genetic algorithms. *Proceedings of IEEE International Conference on Evolutionary Computation*, *1*(), 289-294. DOI: 10.1109/ICEC.1995.489161

Murrieta-Mendoza, A, & Botez, R. (2015a). *Aircraft Vertical Route Optimization Deterministic Algorithm for a Flight Management System* (SAE Technical Paper 2015-01-2541). DOI: 10.4271/2015-01-2541

Murrieta-Mendoza, A., Demange, S., George, F., & Botez, R. (2015b, February). *Performance DataBase creation using a level D simulator for Cessna Citation X aircraft in cruise regime*. Paper presented at IASTED Modeling, Identification and Control Conference, Innsbruck, Austria. DOI: 10.2316/P.2015.826-028

Murrieta Mendoza, A., Bunel, A., & Botez, R.M. (2016, June). *Aircraft vertical reference trajectory optimization with a RTA constraint using the ABC algorithm*. Paper presented at 16th AIAA Aviation Technology, Integration, and Operations Conference, Washington, D.C. (pp. 4208). DOI: 10.2514/6.2016-4208

Murrieta-Mendoza, A., Hamy, A., & Botez, R. M. (2017a). Four- and Three-Dimensional Aircraft Reference Trajectory Optimization Inspired by Ant Colony Optimization. *Journal of Aerospace Information Systems*, *14*(11), 597-616. DOI: 10.2514/1.I010540

Murrieta-Mendoza, A., Beuze, B., Ternisien, L., & Botez, R. M. (2017b) New reference trajectory optimization algorithm for a flight management system inspired in beam search. *Chinese Journal of Aeronautics*, *30*(4), 1459-1472. DOI: 10.1016/j.cja.2017.06.006

Murrieta-Mendoza, A., Ternisien, L., Beuze, B., & Botez, R. M. (2018a). Aircraft vertical route optimization by beam search and initial search space reduction, *Journal of Aerospace Information Systems*, *15*(3), 157-171. DOI: 10.2514/1.I010561

Murrieta-Mendoza, A., Botez, R. M., & Bunel, A. (2018b). Four-Dimensional Aircraft En Route Optimization Algorithm Using the Artificial Bee Colony. *Journal of Aerospace Information Systems*, *15*(6), 307-334. DOI: 10.2514/1.I010523

National Oceanic and Atmospheric Administration, National Weather Service. (n.d.a). NCEP WMO GRIB2 Documentation. Retrieved from http:// www.nco.ncep.noaa.gov/pmb/docs/grib2/grib2_doc/

National Oceanic and Atmospheric Administration, National Weather Service. (n.d.b). wgrib2: wgrib for GRIB-2 Utility to read and write grib2 files. Retrieved from https://www.cpc.ncep.noaa.gov/pro- ducts/wesley/wgrib2/

Ng, H. K., Sridhar, B., & Grabbe, S. (2012, October). *A practical approach for optimizing aircraft trajectories in winds*. Paper presented at 2012 IEEE/AIAA 31st Digital Avionics Systems Conference (DASC), Williamsburg, VA (pp. 3D6-1-3D6-14). DOI: 10.1109/DASC.2012.6382319

Nuic, A., Poles, D., & Mouillet, V. (2010a). BADA: An advanced aircraft performance model for present and future ATM systems. *International journal of adaptive control and signal processing*, *24*(10), 850-866. DOI: 10.1002/acs.1176

Nuic, A. (2010b). *User Manual For Base Of Aircraft Data (BADA) Revision 3.8, Eurocontrol Experimental Centre*, (EEC Technical/Scientific Report No. 2010-003). Retreived from https://www.eurocontrol.int/sites/default/files/library/007_BADA_User_Manual.pdf

Park, S. G., & Clarke, J. P. B. (2012, October). *Fixed RTA fuel optimal profile descent based on analysis of trajectory performance bound*. Paper presented at 2012 IEEE/AIAA 31st Digital Avionics Systems Conference (DASC), Williamsburg, VA (pp. 3D3-1-3D3-13). DOI: 10.1109/DASC.2012.6382316

Patrick, N. J. M., & Sheridan, T. B. (1998). Modeling decision-making for vertical navigation of long-haul aircraft. *SMC'98 Conference Proceedings. 1998 IEEE International Conference on Systems, Man, and Cybernetics (Cat. No.98CH36218)*, *1*(), 885-890. DOI: 10.1109/ICSMC.1998.725527

Patrón, R. S. F., & Botez, R. M. (2015a). Flight trajectory optimization through genetic algorithms for lateral and vertical integrated navigation. *Journal of Aerospace Information System*, *12*(8), 533-544. DOI: 10.2514/1.I010348

Patrón, R. S. F., Berrou, Y., & Botez, R. M. (2015b). New methods of optimization of the flight profiles for performance database-modeled aircraft. *Proceedings of the Institution of Mechanical Engineering, Part G: J Aerospace Engineering*, *229*(10), 1853-1867. DOI: 10.1177/0954410014561772

Qu, Y., Zhang, Y., & Zhang, Y., (2014, May). *Optimal flight path planning for UAVs in 3-D threat environment*. Paper presented at 2014 International Conference on Unmanned Aircraft Systems (ICUAS), Orlando, FL (pp. 149-155). DOI: 10.1109/ICUAS.2014.6842250

Ramasamy, S., Sabatini, R., Gardi, A., & Liu, Y. (2013, August). *Novel Flight Management System for Real-Time 4-Dimensional Trajectory Based Operations*. Paper presented at AIAA Guidance, Navigation, and Control Conference (GNC 2013), Boston, MA, USA. DOI: 10.2514/6.2013-4763

Ramasamy, S., Sabatini, R., Gardi, A., & Kistan, T. (2014). Next Generation Flight Management System for Real-Time Trajectory Based Operations. *Applied Mechanics and Materials*, *629*(), 344-349. DOI: 10.4028/www.scientific.net/AMM.629.344.

Robertson, B. (2007a). Fuel Conservation Strategies: Cost Index Explained. *Boeing Aero Magazine*, *26*(2), 26-28.

Robertson, W., Root, R., & Adams, D. (2007b). Fuel Conservation Strategy: Cruise Flight. *Boeing Aero Magazine*, *28*(4), 22-27.

Rodionova, O., Sibihi, M., Delahaye, D., & Mongeau, M. (2012, May). *Optimization of aircraft trajectories in North Atlantic oceanic airspace*. Paper presented at ICRAT 2012, 5th International Conference on Research in Air Transportation. Berkley, CA.

Rodionova, O., Delahaye, D., Sbihi, M., & Mongeau, M. (2014, October). *Trajectory prediction in North Atlantic oceanic airspace by wind networking*. Paper presented at 2014 IEEE/AIAA 33rd digital avionics systems conference (DASC). Colorado Springs, CO (pp.7A3-1-7A3-15). DOI: 10.1109/ DASC.2014.6979511

Rubio, J.C., & Kragelund, S. (2003, October). *The trans-pacific crossing: long range adaptive path planning for UAVs through variable wind fields*. Paper presented at the 22nd digital avionics systems conference, DASC '03. Indianapolis, IN (pp. 8.B.4-81-12). DOI: 10.1109/DASC.2003.1245898

Schmitt, L. M. (2001). Theory of genetic algorithms. *Theoretical Computer Science*, *259*(1-2), 1-61. doi: 10.1016/s0304-3975(00)00406-0

Schreur, J. M. (1995). B737 Flight management computer flight plan trajectory computation and analysis. *In Proceedings of American Control Conference ACC'95*, *5*(), 3419-3424. DOI: 10.1109/ACC.1995.532246

Schwartz, B. E., Benjamin, S.G., Green, S.M., & Jardin, M. R. (2000). Accuracy of RUC-1 and RUC-2 Wind and Aircraft Trajectory Forecasts by Comparison with ACARS Observations. *Weather and Forecasting*, *15*(3), 313-326. DOI: 10.1175/1520-0434(2000)015<0313:AORARW>2.0.CO;2

Sibin, Z., Guixian, L., & Junwei, H. (2010, March). *Research and modelling on performance database of flight management system*. Paper presented at 2010 2nd International Asia Conference on Informatics in Control, Automation and Robotics (CAR). Wuhan, China (pp. 295-298). DOI: 10.1109/CAR.2010.5456841

Soler, M., Olivares, A., & Staffetti, E. (2010). Hybrid optimal control approach to commercial aircraft trajectory planning. *Journal of Guidance, Control, and Dynamics*, *33*(3), 985-991. DOI: 10.2514/1.47458

Soler, M., Olivares, A., Staffetti, E., & Bonami, P. (2011, June). *En-route optimal flight planning constrained to pass through waypoints using MINLP*. Paper presented at Ninth USA/Europe Air Traffic Management Research and Development Seminar (ATM2011), Berlin, Germany.

Soler, M., Olivares, A., & Staffetti, E. (2015). Multiphase optimal control framework for commercial aircraft four-dimensional flight-planning problems. *Journal of Aircraft*, *52*(1), 274-286. DOI: 10.2514/1.C032697

Soler-arnedo, M., Olivares A., & Staffetti, E. (2010, August). *Hybrid optimal control approach to commercial aircrafts 3D multiphase trajectory optimization*. Paper presented at AIAA Guidance, Navigation and Control Conference, Toronto, ON (pp. 8453). DOI: 10.2514/6.2010-8453

Stell, L. (2010a, October). *Analysis of flight management system predictions of idle-thrust descents*. Paper presented at 29th Digital Avionics Systems Conference, Salt Lake City, UT (pp.1.E.2-1- 1.E.2-13). DOI: 10.1109/DASC.2010.5655506

Stell, L. (2010b, September). *Predictability of top of descent location for operational idle-thrust descents*. Paper presented at 10th AIAA Aviation Technology, Integration, and Operations (ATIO) Conference, Fort Worth, TX (pp. 9116). DOI: 10.2514/6.2010-9116

Stohl, A., Wotawa, G., Seibert, P., & Kromp-Kolb, H. (1995). Interpolation errors in wind fields as a function of spatial and temporal resolution and their impact on different types of kinematic trajectories. *Journal of Applied Meteorology*, *34*(10), 2149-2165. DOI: 10.1175/1520-0450(1995)034<2149:IEIWFA>2.0.CO;2

Stohl A. (1998). Computation, accuracy and applications of trajectories – a review and bibliography. *Atmospheric Environment*, *32*(6), 947-966. DOI: 10.1016/S1352-2310(97)00457-3

Torres, S., & Delpome, K. L. (2012, October). *An integrated approach to air traffic management to achieve trajectory based operations*. Paper presented at 2012 IEEE/AIAA 31st Digital Avionics Systems Conference (DASC), Williamsburg, VA (pp. 3E6-1-3E6-16). DOI: 10.1109/DASC.2012.6382325

Underwood, M. C., Cotton, W. B., Hubbs, C. E., Vincent, M. J., KC, S., & Karr, D. A. (2020). *Incorporation of Time of Arrival Constraints in a Trajectory Optimization Technology*. (Report No. NASA/TM-2020-5005117), Hampton VA, NASA Langley Research Center

Vaddi, V., Tandale, M., & Cheng, V. (2011, August). *Robustness analysis of terminal area scheduling operations using a queuing framework*. Paper presented at AIAA guidance, navigation, and control conference, Portland, OR (pp. 6532). DOI:10.2514/6.2011-6532

Vaddi, V., Sweriduk, D., Tandale, M., & Cate, K. (2012, September). *Design and Evaluation of Guidance Algorithms for 4D- Trajectory- Based Terminal Airspace Operations*. Paper presented at 12th AIAA Aviation Technology, Integration, and Operations (ATIO) Conference and 14th AIAA/ISSMO Multidisciplinary Analysis and Optimization Conference. Indianapolis, IN (pp. 5619). DOI: 10.2514/6.2012-5619

Vaddi, V.V., Tandale, M.D., & Lin, S. (2013, August). *Spatio-Temporally Correlated Wind Uncertainty Model for Simulation of Terminal Airspace Operations*. Paper presented at 2013 Aviation Technology Integration and Operations Conference, Los Angeles, CA (pp. 4404). DOI: 10.2514/6.2013-4404

Villaroel, J., & Rodrigues, L. (2016). Optimal control framework for cruise economy mode of flight management systems. *Journal of Guidance, Control, and Dynamics*, *39*(5), 1022-1033. DOI: 10.2514/1.G001373

Wickramasinghe, N.K., Harada, A., & Miyazawa, J. (2012, December). *Flight trajectory optimization for an efficient air transportation system*. Paper presented at 28th International Congress of the Aeronautical Science (ICAS 2012). Birsbane, Australia.

Woods, S., Vivona, R. A., Roscoe, R., LeFebvre, B. C., Wing, D. J., & Ballin, M. G. (2013, August). *A Cockpit-base Application for Traffic Aware Trajectory Optimization*. Paper presented in AIAA Guidance, Navigation, and Control (GNC) Conference, Boston, MA (pp. 4967). DOI: 10.2514/6.2013-4967

Woods, S., Vivona, R. A., Wing, D. J., & Burke, K. A. (2016, June). *Traffic Aware Planner for Cockpit-based Trajectory Optimization*. Paper presented in 16th AIAA Aviation Technology, Integration, and Operation Conference, Washington, DC (pp. 4067). DOI: 10.2514/6.2016-4067

Wynnyk, C.M. (2012, October). *Wind analysis in aviation applications*. Paper presented at 2012 IEEE/AIAA 31st Digital Avionics Systems Conference (DASC), Williamsburg, VA (pp. 5C2-1-5C2-10). DOI: 10.1109/DASC.2012.6382366

Young, T. M. (2018). *Performance of the Jet Transport Airplane: Analysis Methods, Flight Operations, and Regulations*. Hoboken, NJ: John Wiley &Sons Inc.

Yu, X., & Zhang, Y. (2015). Sense and avoid technologies with applications to unmanned aircraft systems: Review and prospects. *Progress in Aerospace Sciences*, *74*(), 152-166. DOI: 10.1016/j.paerosci.2015.01.001

Zhang, Y., & McGovern, S. (2008). Application of the rapid update cycle (RUC) to aircraft flight simulation. *Proceedings of the ASME 2008 International Mechanical Engineering Congress and Exposition*. *14*(), 45-53. DOI: 10.1115/ IMECE2008-66518

Zhou, Z., Duan, H., Li, P., & Di, B. (2013, June). *Chaotic differential evolution approach for 3D trajectory planning of unmanned aerial vehicle*. Paper presented at 2013 10th IEEE International Conference on Control and Automation (ICCA), Hangzhou, China (pp. 368-372). DOI: 10.1109/ICCA.2013.6565043

Zillies, J., Kuenz, A., Schmitt, A., Schwoch, G., Mollwitz, V., & Edinger, C. (2014, April). *Wind optimized routing: an opportunity to improve European flight efficiency?*. Paper presented at 2014 Integrated Communications, Navigation and Surveillance Conference (ICNS) Conference Proceedings. Herndon, VA (pp. X3-1-X3-9). DOI: 10.1109/ICNSurv.2014.6820029